MODELING UNSATURATED SOIL RESPONSE UNDER SUCTION-CONTROLLED MULTI-AXIAL STRESS STATES

by

ARTHIT LAIKRAM

Presented to the Faculty of the Graduate School of

The University of Texas at Arlington in Partial Fulfillment

of the Requirements

for the Degree of

DOCTOR OF PHILOSOPHY

THE UNIVERSITY OF TEXAS AT ARLINGTON

DECEMBER 2007

ACKNOWLEDGMENTS

The author would like to thank his supervising professor, Dr. Laureano R. Hoyos, for his guidance and support throughout the course of this research effort.

Thanks are also extended to the other members of his dissertation committee, Dr. Ali Abolmaali, Anand J. Puppala, Chien-Pai Han, and MD Sahadat Hossain, for their valuable advice and review of this manuscript. In addition, the author would like to thank the faculty and staff of the Department of Civil and Environmental Engineering at The University of Texas at Arlington for their valuable assistance during his academic studies.

The author also would like to thank all Geotechnical Engineering graduate students in this institution for their help and support, specially Thornchaya Wejrungsikul. Special thanks are also extended to Mr. Paul Shover and Napat Intharasombat.

This work was supported by the US National Science Foundation under grant No. 0216545. This support is gratefully acknowledged.

Finally, and most of all, the author would like to thank his family for their love, encouragement and great support. It is the best thing in his life to be a part of this family.

November 26, 2007

ABSTRACT

MODELING UNSATURATED SOIL RESPONSE UNDER SUCTION-CONTROLLED MULTI-AXIAL STRESS STATES

Publication No._____

Arthit Laikram, Ph.D.

The University of Texas at Arlington, 2007

Supervising Professor: Laureano R. Hoyos

In this research work, a novel suction-controlled true triaxial testing apparatus has been developed to test 3-in (7.5-cm) side, cubical specimens of unsaturated soil under controlled-suction states for a wide range of stress paths that are not easily achievable in a conventional cylindrical apparatus. The equipment is a mixed-boundary type of device, with the specimen seated on top of a high-air-entry ceramic disk and between five flexible (latex) membranes on the remaining sides of the cube. The new cell is an upgraded, more elaborate version of the one previously reported by Hoyos (1998), featuring two independent pore-air and pore-water pressure control systems via a PCP-5000-UNSAT pressure panel. Matric suction states in the specimens are induced during testing via the axis-translation technique. The technique is implemented by utilizing the $s = u_a$ testing concept ($u_w = 0$). The paper outlines the full development of the new cell, including details of its main components and the step-by-step assembling process. Results from a series of constant-suction hydrostatic compression (HC), conventional triaxial compression (CTC), triaxial compression (TC), and

triaxial extension (TE) tests on lightly compacted silty sand are presented. An attempt was made to calibrate and validate the Barcelona model (Alonso et al. 1990) using results from CTC and TC tests. The operational true triaxial apparatus will play a fundamental role in the complete characterization of unsaturated soil behavior under multiaxial stress paths that are likely to be experienced in the field.

TABLE OF CONTENTS

LIST OF FIGURES

LIST OF TABLES

CHAPTER 1

INTRODUCTION

1.1 Background and Importance

In nature, subgrade and shallow foundation soils above the ground water table are subjected to three-dimensional stress gradients due to changes in the stress variables $(\sigma_{ij} - u_a\delta_{ij})$ and $(u_a - u_w)\delta_{ij}$, as shown in Figure 1.1. Moreover, most natural/compacted soils have a tendency to behave as cross-anisotropic rather than isotropic materials. In boundary value problems involving soils with negative pore water pressures, accurate predictions of the stress-strain response of the geosystem require that all the constitutive relations be valid for all major stress paths likely to be experienced in the field.

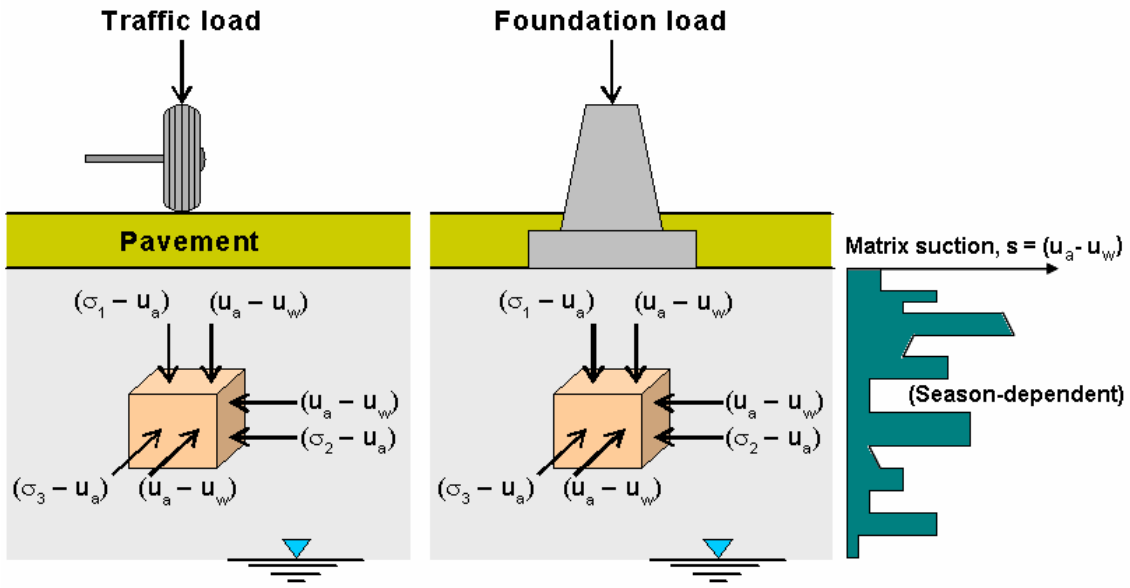

Figure 1.1 Unsaturated Subgrade/Foundation Soils

Over the last few decades, the description of the stress-strain-strength behavior of unsaturated soils has been closely linked with efforts to isolate the relevant effective stress fields governing the soil's mechanical response. The adoption of matric suction, $s = (u_a - u_w)$, and the excess of total stress over air-pressure, $(\sigma - u_a)$, as the relevant stress state variables has allowed the modeling of various key features of unsaturated soil behavior via suction-controlled oedometer, triaxial, and direct shear testing (Alonso et al. 1990, Wheeler and Sivakumar 1992, Fredlund and Rahardjo 1993). However, those devices allow for the application of loading along limited paths and modes of deformation, such as one-dimensional, hydrostatic, or axisymmetric loading.

Several studies, including Kjellman (1936), Ko and Scott (1967), Atkinson (1972), Lade and Duncan (1973), Sture (1979), Suture and Desai (1979), Arthur (1988), Reddy et al. (1992), and Callisto and Calabresi (1998), among many others, have been conducted on the use of true triaxial devices for characterization of soil, rock, and cemented materials. These studies have outlined the benefits of the true triaxial (cubical) apparatus over the cylindrical triaxial cell for testing stress-strain-strength behavior of soils, and have contributed to the mechanical characterization of dry and saturated soils for multiaxial stress states under drained or undrained conditions.

Moreover, matric suction (the effect of negative pore water pressure) has been shown to play a paramount role in the mechanical response of unsaturated soil under one-dimensional, isotropic and axisymmetric loading conditions. Hence, suction is also expected to play as critical a role in unsaturated soil response under multiaxial stress states (Figure

1.1). However, none of the previous efforts listed above have dealt directly with the behavior of unsaturated soil under suction-controlled multi-axial stress conditions.

It is in this context that a true triaxial (cubical) test cell, capable of inducing in the test specimens a wide range of simple-to-complex multiaxial stress paths under controlled-suction states, plays a fundamental role in a thorough stress-strain-strength characterization of this type of materials.

Only a few attempts in this area have been recently reported in the literature (Hoyos and Macari 2001, Matsuoka et al. 2002), but the outcomes from these previous efforts are far from conclusive. The present work is an attempt to build upon these previous efforts any gain further insight into the response of unsaturated soils under general stress states.

1.2 Objective and Scope

The main objective of the present research work is to advance the knowledge and understanding of the mechanical behavior of unsaturated soils under different stress states and matric suction conditions in order to facilitate more elaborate analytical solutions in geotechnical boundary problems involving soils that remains partially saturated throughout any given year.

To accomplish this goal, a comprehensive series of drained, suction-controlled true triaxial tests on compacted silty sand specimens, were preformed on a newly developed true triaxial (cubical) apparatus. Results are used to assess the ability of a previously proposed elasto-plastic model (Barcelona model) to reproduce, quantitatively, observed behavior of unsaturated silty sand under isotropic and axisymmetric stress states.

Four types of stress paths are followed: hydrostatic compression (HC), conventional triaxial compression (CTC), triaxial compression (TC), and triaxial extension (TE). Simple shear (SS) testing was out of the scope of this work due to time constraints and limitations. The soil was artificially prepared by mixing 20% silt (from south Arlington, Texas) and 80% clean sand (commercially supplied from a local source).

The novel cubical cell is used to investigate stress-strain response of unsaturated soils under controlled suction states and for various stress paths that are not easily achievable and instrumented in a conventional (cylindrical) triaxial cell. The cubical testing device is capable of controlling pore-air and pore-water pressures independently in 3-in cubical soil specimens. Matric suction states in soil specimens (50 kPa, 100 kPa, 200 kPa, 300 kPa, and 400 kPa matric suction) are induced and maintained constant during application of isotropic/shear stress paths via the axis translation technique (Fredlund and Rahardjo 1993).

Experimental results form the series of suction-controlled TC and TE tests are used to assess the size and position of the failure envelopes in octahedral and principal stress planes. Test data from suction-controlled CTC and TC tests are used for calibration and fine-tuning of the Barcelona model in compacted silty sand. The incipient critical state condition in all tests was defined at a total shear strain of approximately 12%.

1.3 Organization

A brief summary of the chapters included in this dissertation is presented in the following.

Chapter 2 describes the fundamental concepts of unsaturated soil mechanics. Considerable attention is given to the concept of soil suction and the definition of the

relevant stress state variables governing the mechanical response of soils under unsaturated conditions.

Chapter 3 summarizes the previously reported attempts at suction-controlled multiaxial testing in unsaturated soils. In addition, the chapter summarizes the results from a series of calibration and check-out verification tests preformed with the new true triaxial apparatus developed in this work. These tests were performed on pluviated silty sand at different initial moisture contents and along a wide range of multiaxial stress paths, with no control of suction states during testing (Park 2005).

Chapter 4 is devoted to describing the main features of the suction-controlled true triaxial device developed in this work, including the step-by-step assembly process. Description of the pore-air and pore-water pressure control/monitoring systems is also presented in detail. The fundamentals of true triaxial testing schemes, the saturation process of high-air-entry ceramic disks, and the specimen preparation method are also described in this chapter.

Chapter 5 describes the experimental program and procedure followed in this research work, including a comprehensive analysis of all suction-controlled true triaxial test results on unsaturated silty sand.

Chapter 6 summarizes the conceptual framework of the critical-state based Barcelona model (Alonso et al. 1990). Results from suction-controlled HC, TC and CTC tests on silty sand are then used for calibration and validation of the model for this type of soil.

Chapter 7 includes the summary and conclusions of this research work, as well as some key recommendations for future work.

CHAPTER 2

FUNDAMENTAL CONCEPTS OF UNSATURATED SOIL MECHANICS

2.1 Introduction

The engineering behavior of saturated soils has long been investigated by a considerable number of researchers using a variety of laboratory and field testing techniques. It is now widely accepted that most problems involving the mechanical behavior of saturated soils have a counter problem of interest in unsaturated soils. In order to understand the key features of unsaturated soil behavior, it is necessary to review the fundamental engineering properties and physics of this type of soils. This chapter describes the basic concepts of unsaturated soil mechanics that are relevant to the present research work.

The first describes basic principles of unsaturated soil mechanics, including the concepts of surface tension, capillarity and suction stress. The second part describes the method of measurement of negative pore-water pressure using a high-air-entry porous ceramic disk. The third part presents the volumetric and stress state variables of unsaturated soil mechanics. The fourth part is devoted to describing the axis-translation technique to reach higher levels of matric suction in unsaturated soil specimens in the laboratory. The fifth part describes the phenomenon of soil-water characteristic curve and its hysteresis effects in unsaturated soils. Finally, a brief review of unsaturated shear strength parameters is presented.

2.2 Fundamental Principles

2.2.1 Surface Tension

Unsaturated soil is a multiphase system comprised of three phases of matter: gas, liquid and solid. The geometry of the interface between any two fluids is governed by the balance of forces existing on both sides of the interface. Surface tension is often defined as the maximum energy level a fluid can store without breaking apart. In a gas-liquid system, such as the air-water interface in unsaturated soil, the surface tension of the air phase can be practically ignored, leading to only three components necessary for mechanical equilibrium: air pressure, water pressure and the *surface tension* of the water phase (Lu and Likos 2004).

In more specific terms, surface tension may be defined as the energy required either opening or closing a unit area at a phase interface. At an air-water interface, the water molecules located some finite distance away from the interface do not experience equal cohesive force in all directions. These forces are different from those acting on molecules in the interior of the water. Rather, surface tension is the resultant of a distributed stress that acts not only at the interface, but also to some depth within the water phase, as shown in Figure 2.1.

A molecule in the interior of the water experiences equal forces in all directions, which means there is balanced force. A water molecule within the contractile skin experiences an unbalanced force towards the interior of water. In the order for the contractile skin to be in equilibrium, a tensile pull is generated along the air-water interface. The resultant of the stress increase within the boundary layer, conveniently called surface tension T_s, may therefore be defined mathematically as :

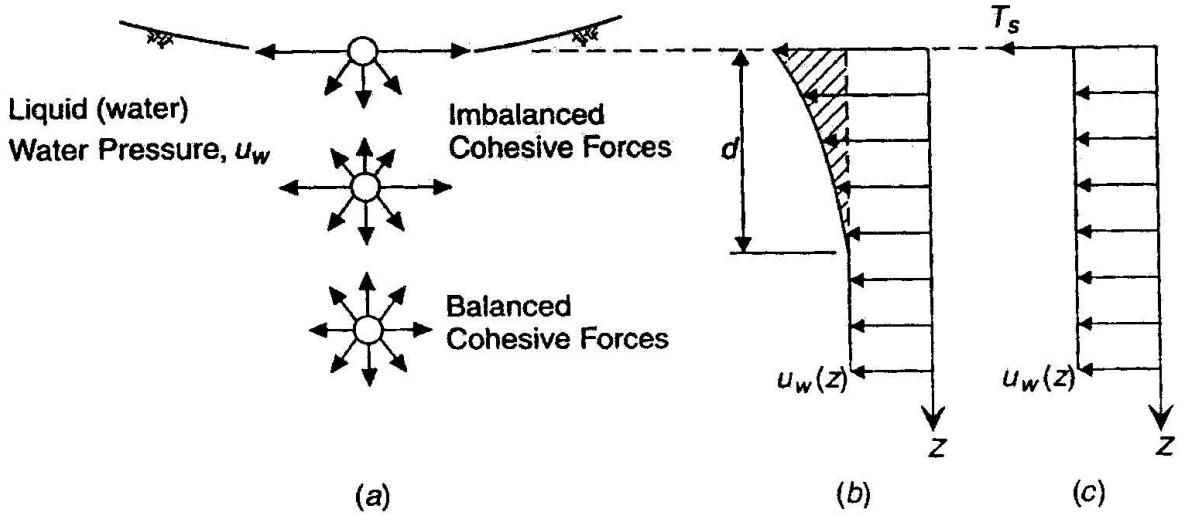

Figure 2.1 Surface tension at air-water interface: (a) intermolecular cohesive forces among water molecules near the interface; (b) conceptual pressure distribution with depth from the interface; (c) surface tension model showing T_s as the resultant of imbalanced intermolecular forces acting along interface (Lu and Likos 2004)

$$T_s = \int_0^d (\sigma - u_w)\delta z \tag{2.4}$$

where σ is the total stress in the water phase and d is the thickness of the boundary layer where the stress increase occurs. The surface tension of water is dependent on temperature, generally decreasing as temperature increases. Weast (1981) had defined surface tension of air-water interface as function of temperature, as shown in Figure 2.2.

The existence of a curved air-water interface is a direct indication of a pressure difference existing between the air and water phases. In a three-phase unsaturated soil systems whether the concave side of the interface corresponds to the water or air phase depends on the properties of the soil solid, the air pressure, and the location of the pore water in the system. The pressure difference across the curved surface can be related to the surface

tension, T_s, and the radius of curvature of surface, R, by considering equilibrium across a spherical phase interface. In the analysis that follows, the equations presented can be applied to any general air-water interface. Figure 2.3a shows a free-body diagram for a two-dimensional curved interface. The interface is analogous to meniscus in a capillary tube, where phase y would represent water and phase x would represent the overlying air. Referring to Figure 2.3b, the projection of the incremental force due to pressure on both sides of the interface over an area δA in the vertical direction is as:

$$\delta F_v \downarrow = -(u_x - u_y)\delta A \cos\alpha = -(u_x - u_y)\delta A' \tag{2.5}$$

where $\delta A'$ is the projection of δA in the horizontal axis. The total vertical force due to pressure difference acts over the area of the interface as:

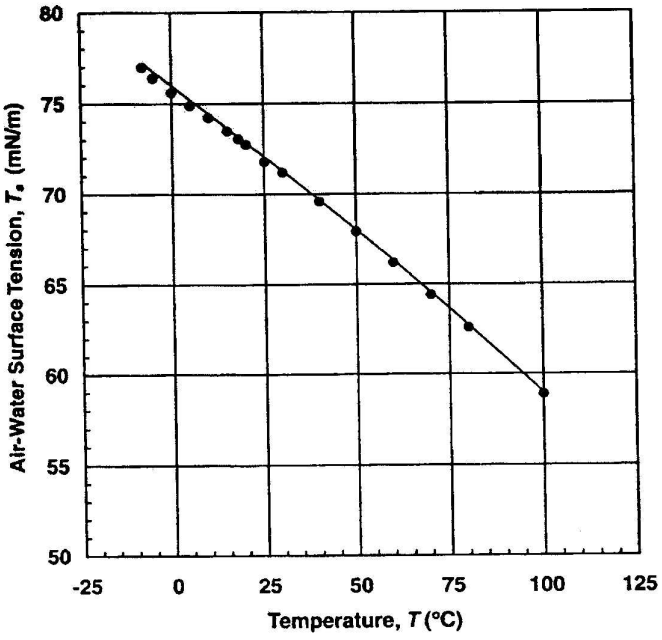

Figure 2.2 Surface tension of air-water interface as a function of temperature (Weast et al. 1981)

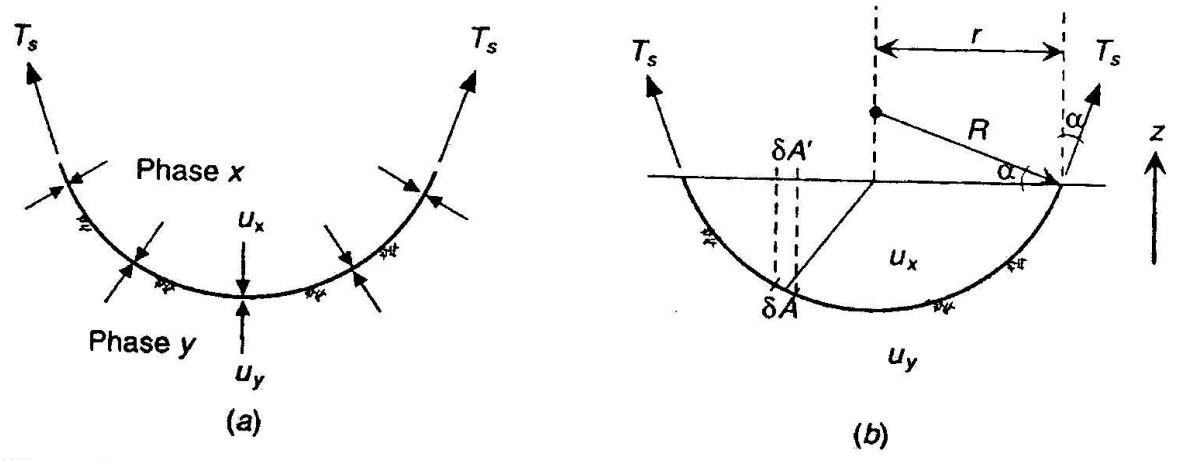

Figure 2.3 Free-body diagrams for pressure and surface tension across a spherical phase interface (Lu and Likos 2004)

$$F_v \downarrow = -(u_x - u_y)\pi r^2 \tag{2.6}$$

the projection of the surface tension around the circumference of the cut in the vertical direction is :

$$F_v \uparrow = 2\pi t T_s \cos\alpha \tag{2.7}$$

applying force equilibrium leads to the following :

$$2\pi r T_s \cos\alpha - (u_x - u_y)\pi r^2 = 0 \tag{2.8}$$

or

$$(u_x - u_y) = \frac{2T_s}{r/\cos\alpha} = \frac{2T_s}{R} \tag{2.9}$$

This simple equation describes the interrelation among surface tension, pressure change, and surface curvature. When $R \rightarrow \infty$, equation (2.9) leads to $u_x = u_y$, indicating a null pressure difference and flat interface. When $u_x > u_y$, $R > 0$, whereas when $u_x < u_y$, $R < 0$.

With respect to water rising in a capillary tube, equation (2.9) can be written more specifically as :

$$(u_a - u_w) = \frac{2T_s}{R} \tag{2.10}$$

where u_a is positive or zero air pressure, u_w is negative water pressure, and R is the radius of curvature of the capillary meniscus. With respect to unsaturated soil, the difference u_a-u_w is referred to as matric suction (Lu and Likos 2004).

2.2.2 Soil Suction

Suction is defined as the water potential in a soil-water system (Richards 1974). Retention and movement of soil water, and the mechanical behavior of unsaturated soils described in terms of strength and deformation characteristics, all depend strongly on the soil water potential (Brady 1974). Generally in the geotechnical engineering, the soil water potential is referred to as negative pore water pressure or suction. This approach provides a more mechanistic view of the state of the soil water in the soil environment (Wan et al. 1995). The suction in an unsaturated soil is controlled by three components. Richards (1974) had been referred to capillarity, adsorption of water on the surface of clay minerals, and osmotic phenomena. The first component, capillary is the dominating component of soil water potential, especially in soils composed of minerals with low surface activity. The second component is due to surface charges on mineral surface. The third component is a function of the chemistry of the soil water and is affected by surface-reaction minerals.

However, in an unsaturated porous media the pore water pressure, u_w is lower than the atmospheric pressure, pat, i.e., u_w is negative when $u_a = 0$ (atmospheric air pressure). This

negative pore water pressure, as quantified in term of the relative humidity in soil, is commonly call total suction, ψ. In engineering studies, total suction is generally taken as having two major components, the matric suction, $(u_a\text{-}u_w)$, (generated by capillarity) and the osmotic suction, π (generated by pore fluid chemistry and water adsorption) (Wan et al. 1995). In an equation form, this can be written as follows:

$$\psi = (u_a - u_w) + \pi \tag{2.1}$$

Matric Suction

Matric suction is generally the dominant component of total suction. In studies where the pore fluid does not change, the matric suction is usually taken as the constant osmotic suction subtracted from the total suction component. Matric suction is defined as the difference between pore water pressure, u_w and the pore air pressure, u_a acting on the air-water interface, as follows:

$$\psi_m = (u_a - u_w) \tag{2.2}$$

In highly active clay soils, capillarity and adsorption of water on the surface of clay minerals both contribute to the matric suction (Richards 1974). For inert materials such as sands and silts, the matric suction is generally due to only the capillarity.

The capillary model which was developed to determine the suction based on the pore size distribution of materials is given by Fredlund and Rahardjo (1993). The total pressure change in matric suction, $u_a\text{-}u_w$, across a curved air-water interface in capillary tube or idealized soil pore with radius, r and contact angle, α was derived :

$$(u_a - u_w) = \frac{2T_s \cos\alpha}{r} \tag{2.3}$$

where T_s is the surface tension of the air-water interface.

Using this information, suction can be related to the pore size distribution of the material. The structure of the soil influences suction as a function of the particle packing, with smaller pore sizes producing larger suctions. Estimation of matric suction in surface inert materials can be made using a model based on capillarity (Fredlund and Xing 1994).

Osmotic Suction

Osmotic suction represents the ionic potential of the pore fluid in a soil system (Fredlund 1995). Osmotic pressure in soil can be calculated using thermodynamic principles. Since osmotic suction is a function of ionic concentration in the pore fluid, it can be present in both saturated and unsaturated soils (Robinson and Stokes 1968).

Osmotic solution can be altered by either changing the mass of the water or the amount of ions in solution. Wan et al. (1995) showed that osmotic suction in buffer material varied only slightly under changes in water content with a constant ionic concentration. If pore fluid chemistry is altered, osmotic suction will be altered accordingly.

Researchers have shown that osmotic suction can have an impact on the mechanical behavior of active clay materials. The influence of osmotic suction on mechanical behavior of soils comes through alteration of effective stresses by osmotic processes (Graham et al. 1988, Barbour and Fredlund 1989). Negatively charged clay particles possess a charge distribution that extends away from their surface. This is frequently termed the diffuse double layer. More recent discussions regarding double layer theory have been presented by Mitchell (1976).

In the most of geotechnical discussions the influence of osmotic suction is commonly neglected, and therefore the change in total suction is equal to the change in matric suction (Fredlund 1989, Fredlund 1991). In the following sections and chapters, only the component referred to as matric suction, (u_a-u_w), will be used to describe the influence of negative pore water pressure on the physical/mechanical response of an unsaturated soil.

2.2.3 Capillarity

In the soil pores, the geometry of the pores and fluid menisci are far more complicated, particularly at scale greater than the largest pore dimension. A double-curvature model may be developed on the basis of analytical geometry and mechanical equilibrium to represent the complicated geometry of the air-water-solid interface. Laplace first derived double-curvature concept in 1806 on the basis of potential theory, not surface tension. T. Young introduced the concept of macroscopic surface tension in 1805. The surface tension approach provides an extremely useful means to interpret many interface phenomena.

Consider mechanical equilibrium near a point *O* on any arbitrary air-water interface as shown in Figure 2.4. Cut an infinitesimal circular elements having radius ρ with an axis at point *O*. The segments *AA'* and *BB'* are pairs of any orthogonal lines on the element that pass through point *O*. the small segments *ds* at points *A*, *A'*, *B*, and *B'* are subjected to a force arising from surface tension equal to $T_s ds$ with projection along the vertical direction (*z*) equal to 2 T_s *ds* sin ø at points *A* and *A'* and $2T_s ds$ sin β at points *B* and *B'*. Since ρ is small, ø is also small. The Young-Laplace equation may be written as :

$$(u_a - u_w) = T_s \left(\frac{1}{R_1} + \frac{1}{R_2} \right) \tag{2.11}$$

where u_a and u_w are the air and water phase pressure, respectively, the difference $u_a - u_w$ is the matric suction, T_s is the surface tension of the water phase, and R_1 and R_2 are the two principal radii of curvature of the interface near the area of interest.

The values of r_1 and r_2 generally vary from any one pair of lines *AA'* and *BB'* to any other pair but can be uniquely linked to principal radii of curvature R_1 and R_2 by theorem of Euler as:

$$\frac{1}{R_1}+\frac{1}{R_2}=\frac{1}{r_1}+\frac{1}{r_2} \tag{2.12}$$

By introducing the "mean" meniscus curvature R_m, the Young-Lapalce equation can be considered a generalized from of the mechanical equilibrium equation for a capillary tube containing a perfectly wetting material. For a three-dimension meniscus, the mean curvature is as follows:

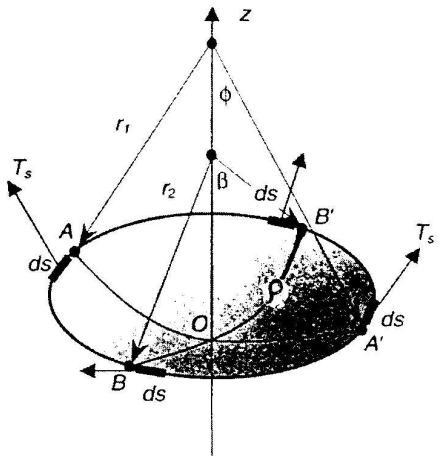

Figure 2.4 Mechanical equilibrium of three-dimensional double-curvature air-water interface (Lu and Likos 2004)

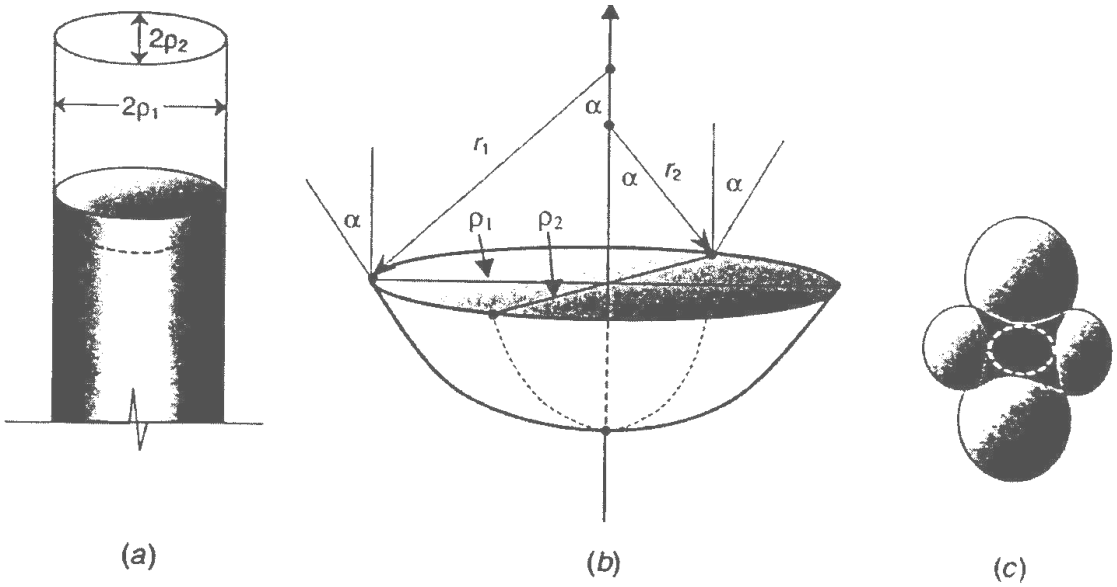

Figure 2.5 Representation of air-water-solid interface by an ellipsoid geometry: (a) in a cylindrical tube; (b) finite ellipsoid interface; (c) an example in soil pores (Lu and Likos 2004)

$$\frac{1}{R_m} = \frac{1}{2}\left(\frac{1}{R_1} + \frac{1}{R_2}\right) \tag{2.13}$$

which allows equation (2.11) to be simplified to the form introduced in the previous:

$$(u_a - u_w) = \frac{2T_s}{R_m} \tag{2.14}$$

Thus, if the geometry of the air-water-solid interface in an unsaturated soil-water system can be represented by an ellipsoidal shape with principal radii ρ_1 and ρ_2, it can be shown (as illustrated in Figure2.5) as:

$$r_1 \cos\alpha = \rho_1 \qquad r_2 \cos\alpha = \rho_2 \tag{2.15}$$

Substituting equation (2.12) and (2.15) into equation (2.11) results in:

$$(u_a - u_w) = T_s \cos\alpha \left(\frac{1}{r_1} + \frac{1}{r_2}\right) \tag{2.16}$$

The negative pore water pressure resulting form interfacial surface tension leads to the redistribution of water in a capillary tube or unsaturated soil. Figure 2.6 demonstrates this *capillary rise* phenomenon for a series of different sized capillary tubes at hydrostatic equilibrium. Capillary rise in soil describes the upward movement of water above the water table resulting form the gradient in the water potential across the air-water interface at the wetting front. At mechanical equilibrium, the pore water pressure at the air-water interface, u_{wi}, is equal to the unit weight of the water, γ_w, multiplied by the height of the capillary rise, h_i:

$$u_{wi} = u_a - \frac{2T_s \cos\alpha}{r_i} = u_{w0} - \frac{2T_s \cos\alpha}{r_i} = -h_i\gamma_w \tag{2.17}$$

or

$$h_i = \frac{2T_s \cos\alpha}{r_i\gamma_w} \tag{2.18}$$

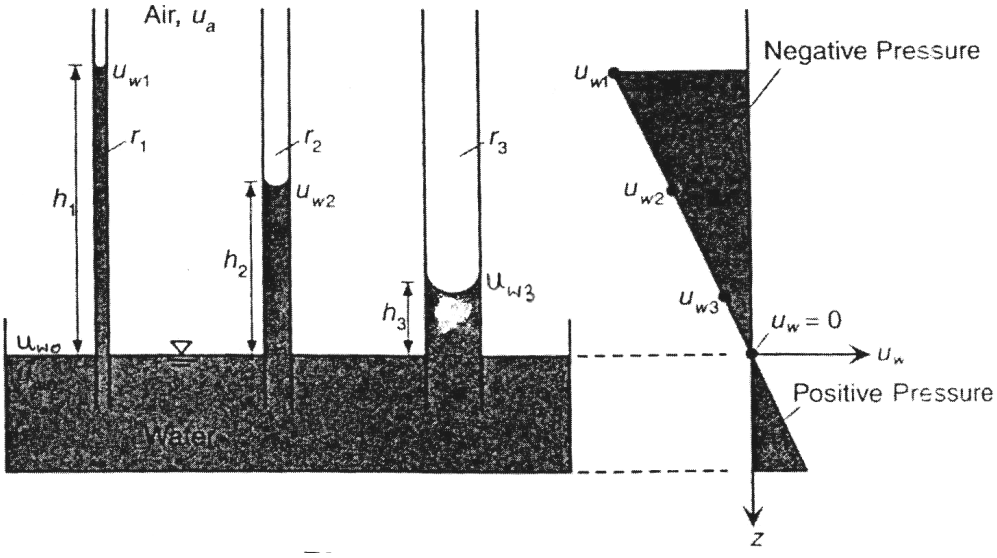

Figure 2.6 Rise of water in capillary tubes of various sizes at hydrostatic equilibrium (Lu and Likos 2004)

In the unsaturated soil, the hydrostatic equilibrium position can be inferred from equation (2.18) if the principal radii of curvature are estimated (Lu and Likos 2004). The ultimate height of capillary rise, h_c, can be evaluated by considering mechanical equilibrium in the area of the large dashed circle in figure 2.7. Here, the total weight of the water column under the influence of gravity is balanced by surface tension along the water-solid interface. In an ideal cylindrical capillary tube with a diameter d, $r_1 = r_2 = d/2$ equation (2.16) becomes:

$$h_c \rho_w g \frac{\pi}{4} d^2 = T_s \pi d \cos\alpha \tag{2.19}$$

or

$$h_c = \frac{4T_s \cos\alpha}{d \rho_w g} \tag{2.20}$$

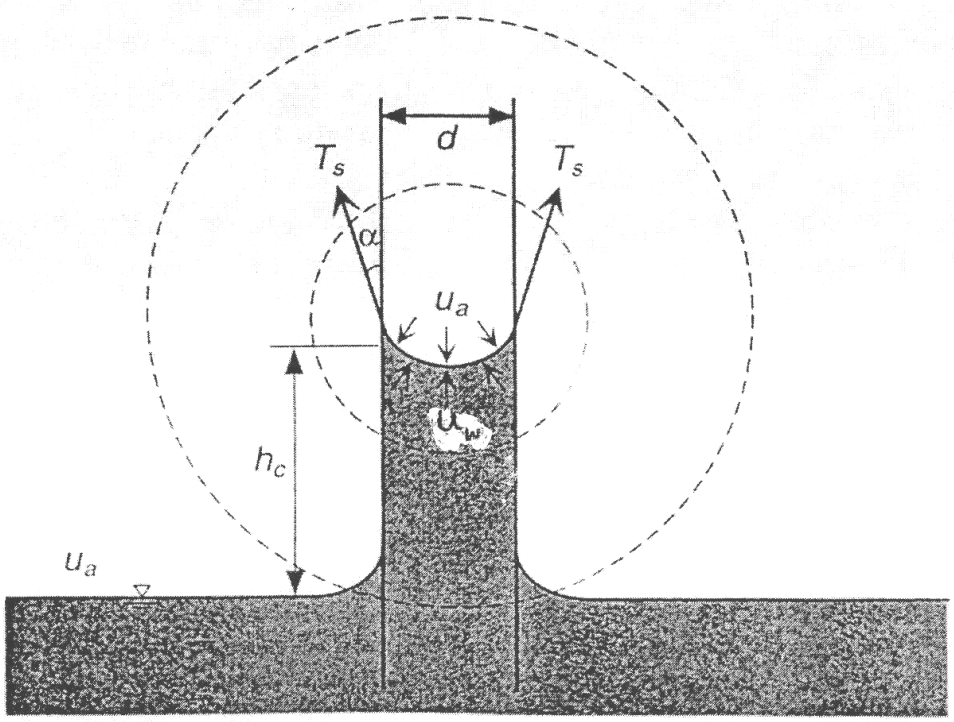

Figure 2.7 Mechanical equilibrium for capillary rise in small-diameter tube (Lu and Likos 2004)

The above explanation has demonstrated the ability of surface tension to support a column of water, h_c, in a capillary tube. The surface tension associated with the contractile skin results in a reaction force on the wall of the capillary tube, as shown in figure 2.8. The vertical component of this reaction force produces compressive stresses on the wall of the tube. The weight of the water column is transferred to the tube through the contractile skin. If a soil has a capillary zone, the contractile skin results in an increased compression of the soil structure. Thus the presence of matric suction in an unsaturated soil increases the shear strength of the soil (Fredlund and Rahardjo 1993).

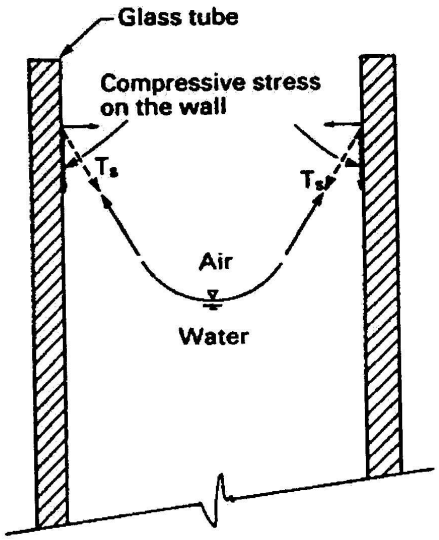

Figure 2.8 Forces acting on a capillary tube (Fredlund and Rahardjo 1993)

Because real soil is comprised of range of different particle sizes falling within some size distribution and complex packing geometry, analytical evaluation of the height of capillary rise is extremely difficult. Perhaps the most reliable method to determine the height of capillary rise is by direct measurement through open-tube capillary rise tests conducted in the laboratory. Numerous experiment programs in this regard have been described in the

literature (e.g., Lane and Washburn 1946, Malik et al. 1989, Kumar and Malik 1990). A summary of results from laboratory capillary rise experiments for several different type of soil is shown in Table 2.1. The data in Table 2.1 support the notion of an empirical relationship between air-entry head and the maximum height of capillary rise. As a result, if the air-entry head is estimated from independent measurements of grain size distribution or the soil-water characteristic curve, it appears that the upper and lower limits for maximum height of capillary rise may be reasonably estimated (Lu and Likos 2004).

2.2.4 Suction Stress

Lu and Likos (2004) suggested that suction stress refers to the net interparticle force generated within a matrix of unsaturated granular particles (e.g., silt or sand) due to the combined effects of negative pore water pressure and surface tension, and the macroscopic consequence of suction stress is a force that tends to pull the soil grains toward one another, similar in effect and sign convention to an overburden stress or surcharge loading. According to them, consideration of the micro scale forces acting between and among idealized assemblies of spherical unsaturated soil particles is one of approaches to evaluating the magnitude of suction stress. Besides, interparticle forces arise from the presence of the air-water-solid interface defining the pore water menisci between the particles at low degrees of pore water saturation. Two particles system is shown in figure 2.9. Figure 2.9 shows that the water meniscus formed between particles may be described by two radii r_1 and r_2, the particle radius R, and a filling angle Θ. A free-body diagram for the relevant system forces, which involves contribution from air pressure u_a, pore water u_w, surface tension T_s, and applied external force of overburden F_e, is shown in figure 2.9 (Lu and Likos 2004).

Table 2.1 Experimental capillary rise parameter for several different soils

Test No	Soil	Gravel (%)	Sand (%)	Silt/Clay (%)	Clay (%)	Void ratio	h_a (cm)	h_c (cm)	$\frac{h_c}{h_a}$
1	Class 5	25.0	68.0	7.0	-	0.27	41	82	2.0
2	Class 6	0.0	47.0	53.0	-	0.66	175	239.6	1.4
3	Class 7	20.0	60.0	20.0	-	0.36	39	165.5	4.1
4	Class 8	0.0	5.0	95.0	-	0.93	140	359.2	2.6
5	Ludas sand	-	-	-	-	-	29.1	72.1	2.5
6	Rawalwas sand	-	-	-	-	-	29.6	77.5	2.6
7	Rewari sand	-	-	-	-	-	29.4	60.9	2.1
8	Bhiwani sand	-	-	-	-	-	27.6	65.6	2.4
9	Tohana loamy sand1	-	-	-	-	-	37.4	117.0	3.1
10	Hissar loamy sand 1	-	-	-	-	-	37.5	149.4	4.0
11	Barwala sandy loam1	-	-	-	-	-	41.2	158.4	3.8
12	Rohtak sandy loam 1	-	-	-	-	-	48.2	155.7	3.2
13	Hisar sandy loam 1	-	-	-	-	-	47.7	173.5	3.7
14	Pehwa sandy clay loam	-	-	-	-	-	44.5	154.6	3.5
15	Hansi clayey loam 1	-	-	-	-	-	29.6	127.5	4.3
16	Ambala silty clay loam1	-	-	-	-	-	15	141.5	9.4
17	Tohana loamy sand 2	-	89.0	6.0	6.0	0.92	66.7	117	1.8
18	Hissar loamy sand 2	-	82.5	11.5	6.0	0.90	72.9	149.4	2.0
19	Barwala sandy loam2	-	75.0	13.5	11.5	0.94	47.3	158.4	3.3
20	Rohtak sandy loam 2	-	63.0	23.0	14.0	1.01	44	155.7	3.5
21	Hissar sandy loam 2	-	63.0	24.0	13.0	0.99	66	174.5	2.6
22	Pehowa sandy clay loam	-	55.0	27.0	18.0	1.06	59.6	154.6	2.6
23	Hansi clayey loam 2	-	30.2	26.5	43.3	1.27	16.3	127.5	7.8
24	Ambala silty clay loam 2	-	15.0	49.0	36.0	1.49	16.9	141.5	8.4

1-4 (Lane and Washburn 1946), 5-16 (Malik et al. 1989), and 17-24 (Kumar and Malik 1990)

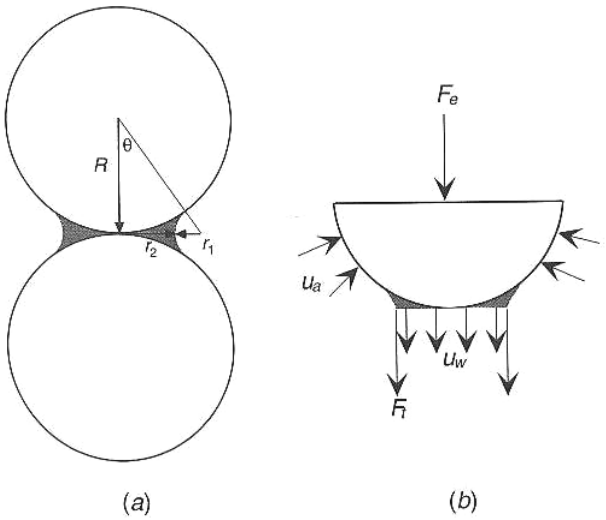

Figure 2.9 Air-water-solid interaction for two spherical particles and water meniscus (Lu and Likos, 2004)

A free-body diagram for the relevant system forces, which involves contribution from air pressure u_a, pore water u_w, surface tension T_s, and applied external force of overburden F_e, is shown in figure 2.9 (Lu and Likos, 2004).

A compressive force on the soil skeleton will be exerted by positive and isotropic air pressure u_a. The total force due to air pressure (F_a) is expressed as:

$$F_a = u_a(\pi R^2 - \pi r_2^2) \tag{2.21}$$

F_a is equal to the product of the magnitude of the air pressure and the area of the air-solid interface over which it acts.

The total force due to surface tension (F_t) is given by:

$$F_t = -T_S 2\pi r_2 \tag{2.22}$$

F_t acts along the perimeter of the water meniscus.

The projection of total force due to water pressure (F_w) is given in the following manner :

$$F_W = u_W \pi r_2^2 \tag{2.23}$$

F_w acts on the water-solid interface in the vertical direction.

The sum of all three of the above forces (F_{sum}) is expressed as:

$$F_{sum} = u_a \pi R^2 - u_a \pi r_2^2 - T_S 2 \pi r_2 + u_W \pi r_2^2 \tag{2.24}$$

F_{sum} is the resultant capillary force.

The net interparticle force due to the interfacial interaction (F_e) is given by:

$$F_a = u_a \pi R^2 - (u_a - u_W) \pi r_2^2 - T_S 2 \pi r_2 \tag{2.25}$$

The above eq. (2.25) is based on the assumption that the air pressure is the only contribution to external force. F_e exerts a tensile stress on the soil skeleton as long as the following condition met :

$$(u_a - u_W) r_2^2 + T_S 2 r_2 > u_a R^2 \tag{2.26}$$

2.3 Soil-Water Characteristic Curve

Previous sections reviewed the two principal components of suction and showed the relative importance of the individual physical and physicochemical mechanisms responsible for soil suction depend on the water content of the unsaturated soil-water-air system. The relationship between water content, w (or degree of saturation, S_r), and the soil matric suction, (u_a-u_w), can be establish by monitoring both, the amount of drained water and the pore water pressure changes in drying process, as shown in figure2.10. The relationship between water content and the soil matric suction is called the *soil water characteristic*

curve, SWCC (Fredlund and Rahardjo 1993). Figure 2.10 shows the development of an unsaturated soil by withdrawal of the air-water interface in the drying process at different stages of matric suction, (u_a-u_w), or degree of saturation, S_r. As the soil becomes unsaturated (i.e., stages 1-5), the air-water inter face is drawn closer to the soil particles, reducing the water content of the soil and in turn its degree of saturation. The curvature of the contractile skin in air-water interface depends on the amount of drained water. As the drying process continues, the meniscus becomes sharper, resulting in higher matric suction due to surface tension effects. If the wetting process is considered, the pores will be successively re-filled with water, the meniscus radii increase (i.e., stages 6-7), and the matric suction decreases until finally reaching a value close to zero at full saturation (Childs 1969, Fredlund and Rahardjo 1993, Oberg 1997).

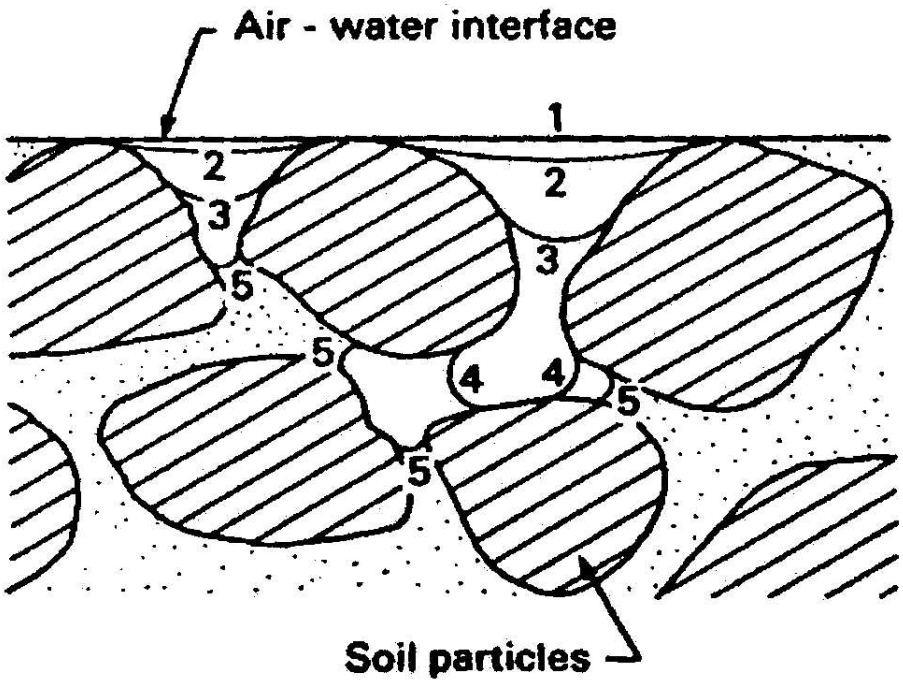

Figure 2.10 Development of an unsaturated soil (i.e., stages 1-5) (Childs 1969)

The general shape of the SWCC is a reverse S-shape. McQueen and Miller (1974) developed an instructive conceptual model based on empirical evidence for describing the general shape and behavior of the SWCC. As illustrated graphically in Figure 2.11, it was suggested that any SWCC could be approximated as a composite of three straight line segments on a semi log plot of suction versus moisture content ranging form zero to saturation. The general shape of the SWCC for various soils reflects the dominating influence of material properties including pore size distribution, gain size distribution, density, organic material content, clay content, and mineralogy on the pore water retention behavior, as depicted schematically in Figure 2.12 (Lu and Likos 2004). In the other hand, there is a unique relationship between total soil suction, ψ, and initial water content, w_o, for a particular compacted soil, regardless of the soil's dry density, γ_d (Krahn and Fredlund 1972). The in-situ suction of the same compacted soil in the field can then be inferred from this type of relationship by measuring its water content.

The SWCC can be either a desorption (drying process) or an adsorption (wetting process) curve. Hysteresis behavior has been attributed to several mechanisms that act on both a relatively microscopic (partical) scale and a relatively macroscopic (interparticle) scale and the most outstanding example of hystertic behavior is that between wetting and drying paths of the SWCC. Figure 2.13 shows a conceptualization of hysteresis in the suction water content relationship for a typical coarse-grained unsaturated porous material. The non-uniform pore size distributions in a soil, as well as the presence of entrapped air in the pore water, are considered to be the main causes for hysteresis in the SWCC.

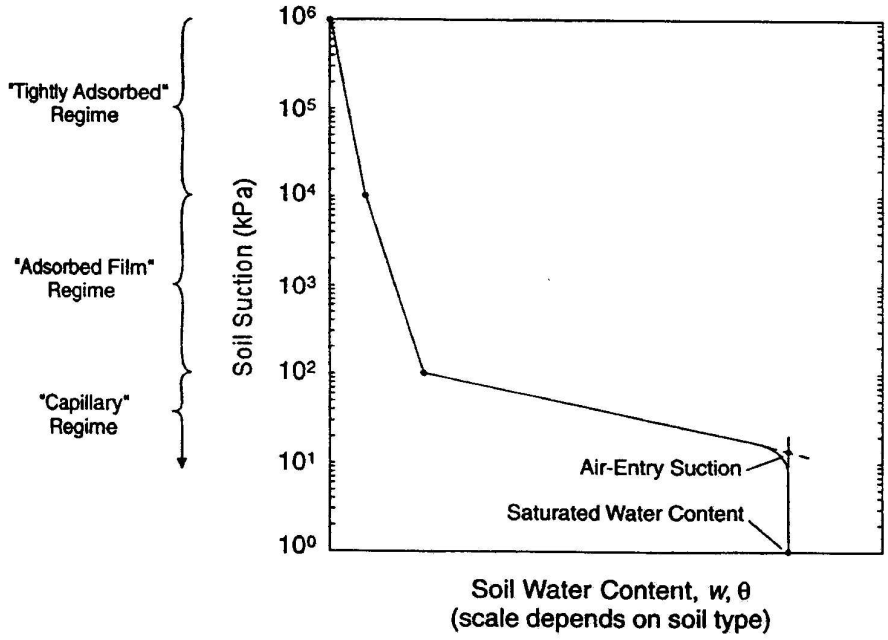

Figure 2.11 Illustration of McQueen and Miller's (1974) conceptual model

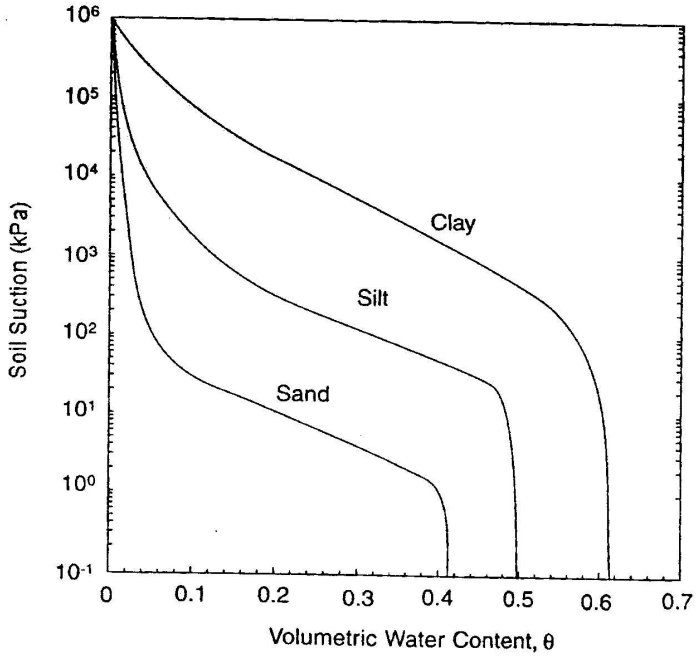

Figure 2.12 Representative soil-water characteristic curves for sand, silt, and clay (Lu and Likos 2004)

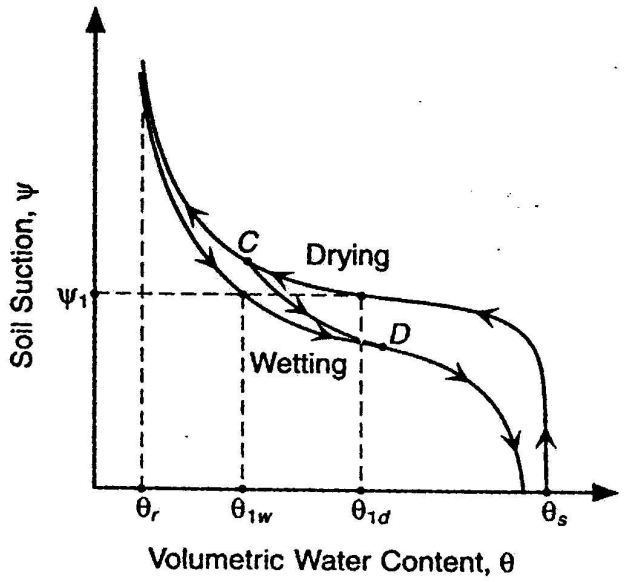

Figure 2.13 Conceptual illustration of hysteresis in soil-water characteristic curve (Lu and Likos 2004)

In addition, the contact angle between a soil particle and the advancing air-water interface during the wetting process is different from that between the same soil particle and the receding air-water interface during the dry process, and viceversa. This phenomenon is called the *rain-drop effect* (Bear 1979). Moreover, a local increase in pressure is required when water re-enters narrow channels, resulting in an unstable condition that does not allow the water front to further enter the pores until the surrounding pores are completely filled with water. This phenomenon is called the *ink-bottle* effect (Bear 1979).

Determination of the SWCC in the laboratory is generally performed by increasing/decreasing the soil matric suction in different steps and measuring the resulting soil water content after equilibrium is reached at each step. The most suitable procedure uses the axis-translation technique in a setup to the null type pressure plate apparatus (Fredlund and Rahardjo 1993, Oberg 1997). Flushing lines are connected to the water compartment for

elimination of diffused air bubbles. A burette pipe (or a differential pressure transducer) is also connected to the water compartment to register the amount of drained water after each suction increase.

2.4 Concept of Axis Translation Technique

The general term *axis translation* refers to the practice of the elevation pore air pressure in unsaturated soil while maintaining the pore water pressure at a measurable reference value, typically atmospheric. As such, the matric suction variable, u_a-u_w, may be controlled over a range far greater that he cavitation limit for water under negative pressure. As described in early section, cavitation in free water under negative pressure occurs as the magnitude of the pressure approaches -1 atm. As cavitation occurs, the water phase in both the soil and measurement system becomes discontinuous, making the measurements unreliable or impossible (Brennen 1997).

The origin of reference, or "axis," for the matric suction variable is "translated" from the condition of atmospheric air pressure and negative water pressure to the condition of atmospheric water pressure and positive air pressure. Matric suction may be accurately controlled in this manner because positive air pressure may be easily controlled and measured. This technique has been successfully applied to the volume change and shear strength testing of an unsaturated soil (Hilf 1956, Bishop and Donald 1961, Gibbs and Coffey 1969, Fredlund 1973, Ho and Fredlund 1982a, Gen et al. 1988, Fredlund and Rahardjo 1993).

The axis translation technique forms the basis for the laboratory testing of unsaturated soils. The soil specimen is placed on top of a saturated 10 kPa air-entry value porous disk, and a U-tube is connected to the water compartment below the disk for direct measurement

of pore water relative to atmospheric air pressure conditions, as show in figure 2.14. Consider an unsaturated soil specimen with matric suction of 50 kPa. The U-tube is moved up and down until there is no tendency for flow in or out of the specimen. The pore water pressure in specimen is being measured relative to atmospheric air pressure as -50 kPa. An air-entry value of porous disk is lower than the soil matric suction. At this point, air enters the water compartment. The measuring system then becomes filled with air bubbles as illustrated in Figure 2.14a.

Another limitation of the direct measurement arises from the fact that water cavitates as a gauge pressure of -1 atm is approached (i.e.,-101 kPa). Figure 2.15a illustrates that water phase of the unsaturated soil specimen undergoes a tension of 101 kPa (i.e., u_w = -101 kPa), under equilibrium conditions. The unsaturated soil specimen experiences the matric suction, (u_a-u_w), of 101 kPa. A saturated high-air-enter value porous disk with an air entry value of 2 bar (202 kPa) is suitable since it is higher than the soil matric suction (i.e., 101 kPa). Nevertheless, the water in the compartment below the disk starts to cavitate when the gauge water pressure approaches -1 atm. As a result, occluded air bubbles accumulate below the disk in the water compartment, as shown in Figure 2.15b. This causes an error in the pore-water pressure measurements.

The axis translation technique is particularly useful when testing an unsaturated soil with high matric suction. Basiclly, both the pore air and pore water pressure are translated into the positive pressure range. The translation of pore air pressure can be considered as an artificial increase in the atmospheric pressure under which the test is preformed (Bishop et al. 1960). As a result, the negative gauge pore water pressure is also raised by an equal amount

to positive gauge pressure. Thus, the matric suction of the unsaturated soil specimen remains constant regardless of the magnitude of the pore air pressure.

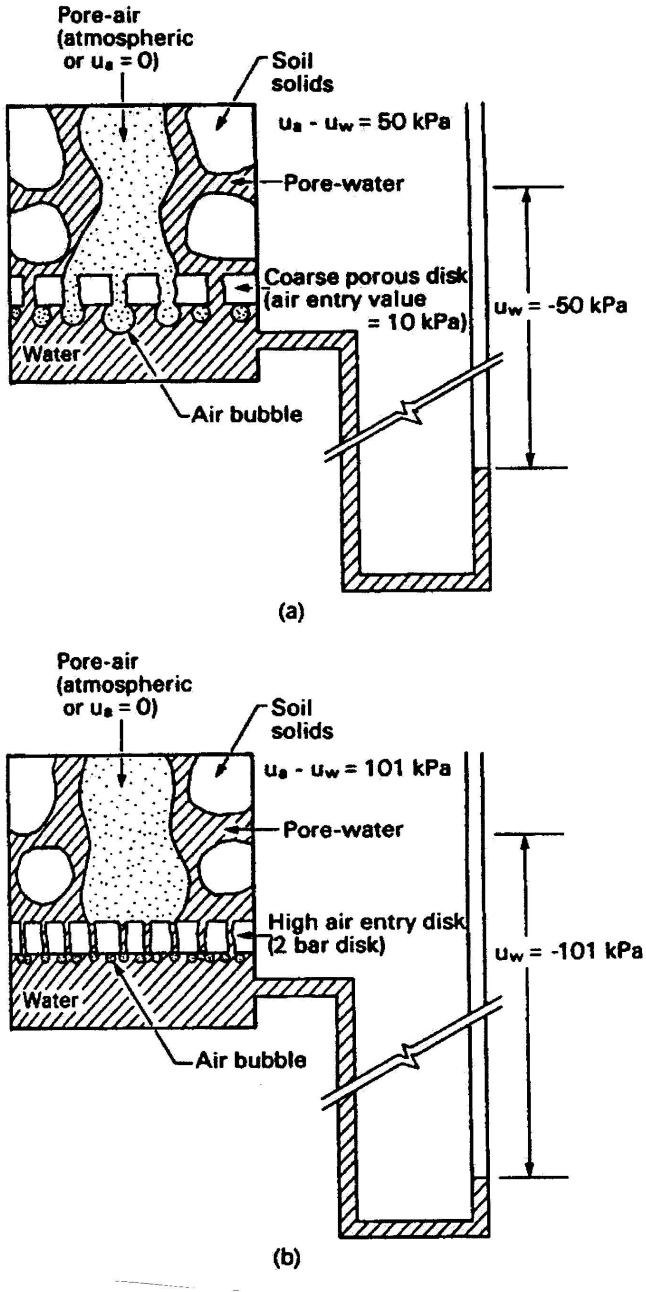

Figure 2.14 Direct measurement of pore water pressure in an unsaturated soil specimen (not to scale): (a) air movement through the porous disk when its air entry value is exceeded; (b) air diffusion through the high air entry disk and water cavitation in the measuring system (Fredlund and Rahardjo 1993)

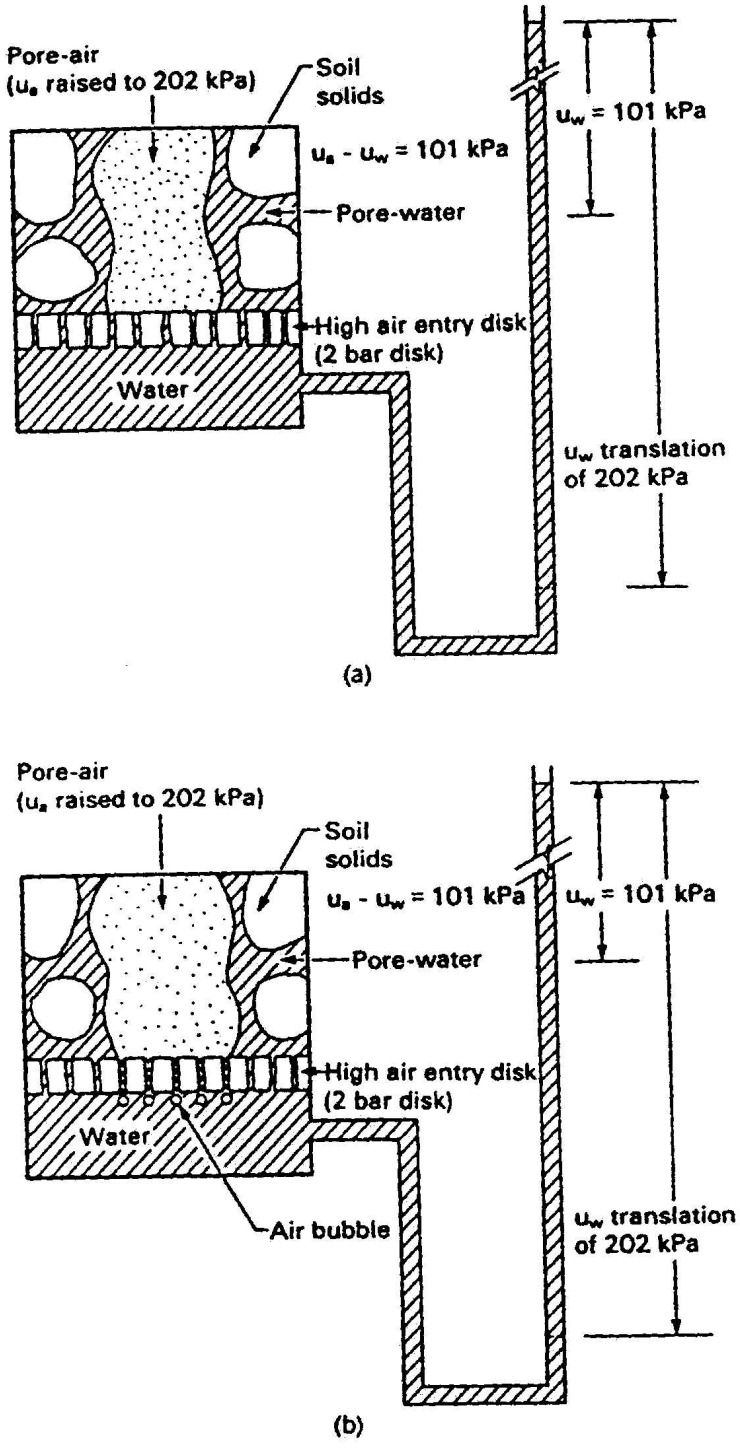

Figure 2.15 Measurement of pore water pressure in an unsaturated soil specimen using the axis translation technique (not to scale): (a) the axis translation of 101 kPa; (b) air diffusion through the high air entry disk (Fredlund and Rahardjo 1993)

A long period of the axis translation technique testing does not guarantee that the water pressure measuring system (i.e., compartment) will remain free of air bubble. Figure 2.15a illustrates the application of the axis translation technique to an unsaturated soil specimen with a matric suction of 101 kPa. The pore water pressure is measured below a saturated 2 bar (202 kPa) porous disk. The water phase of the specimen was originally under 101 kPa tension. An air pressure of 202 kPa is then applied directly to the specimen in order to raise the pore air pressure. The pore air pressure is raised to 202 kPa. As a result, the pore water pressure is increased by equal amount, which is now at a positive value of 101 kPa. Throughout the axis translation procedure, the pore air pressure has been translated from 0 to 202 kPa. The matric suction of the soil remains constant at 101 kPa, and there is no problem associated with the cavitation of water in measuring system as shown in Figure 2.15a. As the test progress, pore air diffuses through the water in the high-air-entry disk and appears as air bubbles beneath the disk, as shown in Figure 2.15b. Periodic flushing of the diffused air is then necessary to ensure continuity between the pore-water in the soil and the water in the measuring system (Fredlund and Rahardjo 1993).

2.5 Properties of High-Air-Entry Materials

Matric suction may be considered an important variable in defining the state of stress in unsaturated soil. Control or measurement of matric suction, therefore, becomes necessary in order to evaluate the physical behavior of unsaturated soil under changing stress conditions. Experimental techniques for measuring soil suction and corresponding soil-water characteristic curves can be generally categorized as either laboratory or field methods and differentiated by the component of suction (matric or total) that is measured.

Tensiometer is used to directly measure negative pore water pressure. Axis translation techniques rely on controlling the difference between the pore air pressure and pore water pressure and measuring the corresponding water content of soil in equilibrium with the applied matric suction. Electrical or thermal conductivity sensors, gypsum block, are used to indirectly relate matric suction to the electrical or thermal conductivity of porous medium embedded in mass of unsaturated soil.

Tensiometer and axis translation techniques rely on the unique properties of high-air-entry (HAE) materials. HAE materials are characterized by microscopic pores of relatively uniform size and size distribution. When an HAE material is saturated with water, the surface tension maintained at the gas-liquid interface formed in the material's pores allows a pressure difference to be sustained between gas and liquid phases located on either side. Physically, surface tension acts as a membrane for separation the two phases, thus allowing negative water pressure and air pressure to be directly controlled, as in axis translation (Lu and Likos 2004).

The phrase "high-air-entry" refers to the fact that relatively high pressure is required for air to break through the membrane formed by surface tension. Figure 2.16 shows an enlarged schematic cross section of a saturated HAE ceramic disk. The maximum sustainable difference between the air pressure above the disk and the water pressure within and below the disk is inversely proportional to the maximum pore size of the material, which is captured by the Young-Leplace equation as :

$$(u_a - u_w)_b = \frac{2T_s}{R_s} \tag{2.27}$$

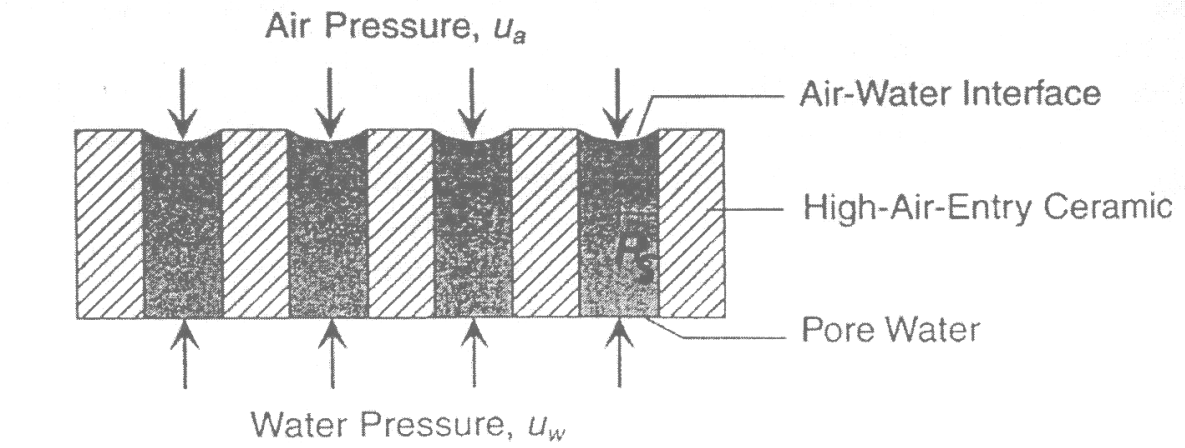

Figure 2.16 Operating principle of the high-air-entry ceramic disk (Lu and Likos 2004)

where $(u_a\text{-}u_w)_b$ is the air-entry, or "bubbling," value of HAE ceramic disk, T_s is the surface tension of the air-water interface, and R_s is the effective radius of the maximum pore size of the HAE material.

Surface tension, T_s, changes slightly with temperature (Kaye and Laby 1973). The air-entry value of HAE ceramic disk, $(u_a\text{-}u_w)_b$, is then largely controlled by the radius of curvature, R_s, of the largest pore in the disk. Equation (2.27) shows that the smaller the pore size in a disk, $2R_s$, the greater will be its air-entry value, $(u_a\text{-}u_w)_b$.

The separation of the air and water across a high-air-entry disk can be achieved only as long as the matric suction in the soil, $(u_a\text{-}u_w)$, does not exceed the air-entry value, $(u_a\text{-}u_w)_b$, of HAE ceramic disk. Once the air-entry value of HAE ceramic disk is exceeded, air will pass through the disk and enter the measuring system, causing erroneous measurements of the pore-water pressure, u_w, in a closed system.

An idealized characteristic curve for the ceramic porous disk with a uniform pore size distribution would follow the simple path show in Figure 2.17. The saturated water content

and air-entry value, AEV for the HAE disk, $\theta_{s(\mathrm{HAE})}$ and $\mathrm{AEV}_{\mathrm{HAE}}$, respectively are defined by two straight-line segment of characteristic curve. Table 2.2 lists the characteristics of several commercially available types of porous ceramics in terms of their approximate average pore diameter, saturated hydraulic conductivity, and air-entry value manufactured by Soilmoisture Equipment Corporation. Note that hydraulic conductivity decreases with increasing air-entry value, a reflection of the increasingly smaller pore sizes of the material.

2.6 Stress Phenomena

2.6.1 Proposed Effective Stress Equations

The effective stress concept, as the only single valued state stress variable required to describe the mechanical behavior of a saturated soil, has been well accepted, studied, and experimentally verified (Terzaghi 1936, Skempton 1961), and is commonly expressed in the form of an equation as:

$$\sigma' = \sigma - u_w \tag{2.28}$$

where σ' is effective normal stress, σ is total normal stress, and u_w is pore water pressure.

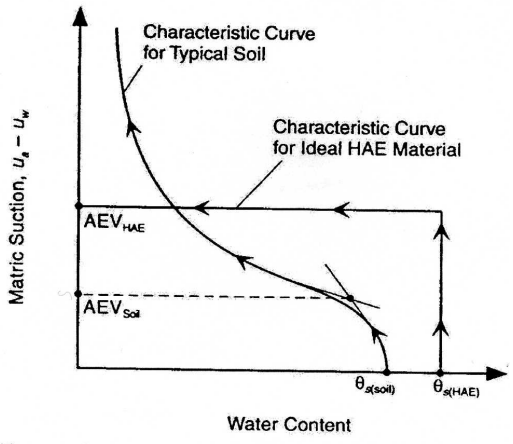

Figure 2.17 Characteristic curves for idealized high-air-entry material and typical coarse-grained soil (Lu and Likos 2004)

Table 2.2 Air-entry pressure and hydraulic conductivity of several commercially available HAE ceramics (Soilmoisture Equipment Corporation 2003)

Type of HAE Ceramic	Approximate Pore Diameter ($\times 10^{-3}$ mm)	Saturated Hydraulic Conductivity (m/s)	Air-Entry Value (kPa)
½ bar high flow	6.00	3.11×10^{-7}	48-62
1 bar	1.70	7.56×10^{-9}	138-207
1 bar high flow	2.50	8.60×10^{-8}	131-193
2 bar	1.10	6.30×10^{-9}	262-310
3 bar	0.70	2.50×10^{-9}	317-483
5 bar	0.50	1.21×10^{-9}	550
15 bar	0.16	2.59×10^{-11}	1520

Satisfactory stress state variables for an unsaturated soil have been considerably more difficult to establish. Since it is desirable that the concept of effective stress, σ', for saturated soil be extended to unsaturated soils, all pro posed effective stress equations for an unsaturated soil have attempted to provide a single value stress state variable. Difficulties arise from the inclusion of soil parameters in all the proposed equation (Fung 1977). In the early 40's, Biot (1941) proposed a general theory of the consolidation for an unsaturated soil with occluded air bubbles. The constitutive equations were formulated in terms of the effective stress, $\sigma' = \sigma - u_w$, and the pore water pressure, u_w, suggesting the need for separating the effects of total stress, σ, and pore water pressure, u_w.

Croney et al. (1958), proposed the following form of an effective stress equation for an unsaturated soil:

$$\sigma' = \sigma - \beta' u_w \tag{2.29}$$

where σ' is effective normal stress, σ is total normal stress, and u_w is pore water pressure. Croney added β' in an effective stress equation as bonding factor, which is measure of the number of bonds under tension (effective in contributing to shear strength, τ, of the soil).

Bishop (1959), suggested am expression for effective stress which gained widespread acceptance:

$$\sigma' = (\sigma - u_a) + \chi(u_a - u_w) \tag{2.30}$$

where χ is parameter related to degree of saturation, S_r, of the soil. The magnitude of the χ parameter is unity for a saturated soil (i.e., χ =1 for S_r = 100%), and zero for a dry soil (i.e., χ =0 for S_r = 0%). The relationship between the χ parameter and the degree of saturation was obtained experimentally (Blight 1961, Donald 1961).

Aitchison (1961), proposed the following form of an effective stress equation for an unsaturated soil:

$$\sigma' = \sigma - \psi p'' \tag{2.31}$$

where ψ is parameter with values ranging from 0 to 1 and p'' is pore water pressure deficiency.

Jennings (1961), suggested an expression for effective stress similar to that presented by Aitchison (1961):

$$\sigma' = \sigma + \beta p'' \tag{2.32}$$

where β is experimentally measured statistical of the same type as the contact area, and p'' is negative pore water pressure taken as a positive value.

Further investigations conducted by Jennings and Burland (1962), Coleman (1962), Bishop and Blight (1963), Blight (1965), and finally Burland (1964, 1965), questioned the validity of the proposed effective stress equation (2.29) to (2.32), suggesting that the mechanical behavior of an unsaturated soil should be independently related to the stress variables, $(\sigma - u_a)$ and $(\sigma - u_w)$, whenever is possible. Blight (1965), concluded that the proposed effective stress equations depend on the type of process to which the soil was subjected.

Richards (1966), incorporated a solute suction component into the effective stress equation:

$$\sigma' = \sigma - u_a + \chi_m (h_m + u_a) + \chi_s (h_s + u_a) \tag{2.33}$$

where χ_m is effective stress parameter for matric suction, h_m is matric suction, χ_s is effective stress parameter for solute suction, and h_s is solute suction.

The complexity associated with the χ parameter was pointed out by Aitchison (1967), who stated that a specific value of χ many only relate to a single combination of (σ) and $(u_a - u_w)$ for a particular stress path. It was also suggested that the terms (σ) and $(u_a - u_w)$ be separated in analyzing the behavior of an unsaturated soil. Further research on volume change behavior of unsaturated soils conducted by Aitchison and Woodburn (1969), Matyas and Radhakrishna (1968), Barden et al. (1969), and Brackley (1971), suggested that the volume change of an unsaturated soil be analyzed in terms of the separate components of applied stress, $(\sigma - u_a)$, and matric suction, $(u_a - u_w)$.

Aitchison (1973), proposed an effective stress equation slightly modified from that presented by Richards (1966):

$$\sigma' = \sigma + \chi_m p''_m + \chi_s p''_s \tag{2.34}$$

where p''_m is matric suction, $(u_a\text{-}u_w)$, p''_s is solute suction, and χ_m and χ_s are soil parameter ranging from 0 to 1, and dependent upon the stress path.

The brief literature review present above shows that considerable effort has been extended in the establishment of a single-valued effective stress equation for an unsaturated soil. Nevertheless, experiments have demonstrated that the effective stress, as the only stress state variable, is not single values for an unsaturated soil. Rather, there is a dependence on the stress path followed, and the soil parameters and constants proposed appear to be difficult to evaluate. Difficulties also arise in justifying the use of soil properties in the description of a stress state (Morgenstern 1979, Fredlund and Rahardjo 1993).

2.6.2 Stress State Variables

The theoretical stress analysis of an unsaturated soil on the basis of multiphase continuum mechanics concluded that two independent sets of stress variable, $(\sigma - u_a)$ and $(u_a - u_w)$, may be used to describe the shear strength behavior and the volume change behavior of an unsaturated soil (Fredlund and Morgenstern 1977). This eliminates the need to find a single valued effective stress equation that is applicable to both shear strength and volume change problems. The two independent stress state variable are expressed in terms of physically measurable quantities, i.e., the total stress, σ, the pore water pressure, u_a, and pore air pressure, u_w; and they also been experimentally tested (Fredlund 1973).

If the soil particles and the water phase are assumed to be incompressible, and the soil is treated as though it were chemically inert, the complete from of the stress state for an unsaturated soil can be written as two independent stress tensor:

$$(\sigma_{ij} - u_a)\delta_{ij} = \begin{pmatrix} (\sigma_x - u_a) & \tau_{yx} & \tau_{zx} \\ \tau_{xy} & (\sigma_y - u_a) & \tau_{zy} \\ \tau_{xz} & \tau_{yz} & (\sigma_z - u_a) \end{pmatrix} \tag{2.35}$$

and,

$$(u_a - u_w)\delta_{ij} = \begin{pmatrix} (u_a - u_w) & 0 & 0 \\ 0 & (u_a - u_w) & 0 \\ 0 & 0 & (u_a - u_w) \end{pmatrix} \tag{2.36}$$

where, δ_{ij} = Kronecker delta, i.e.:

$$\delta_{ij} = \begin{cases} 1 & for, i = j \\ 0 & for, i \neq j \end{cases} \tag{2.37}$$

Figure 2.18a illustrates the two independent stress tensors acting at a point in an unsaturated soil. As an unsaturated soil approaches saturation, the degrees of saturation, S_r, approaches 100%, the pore water pressure approaches the pore air pressure and matric suction term goes towards zero. Therefore, a saturated soil can be viewed as a special case of an unsaturated soil. Only the first stress tensor is retained for a saturated soil when considering this special case,

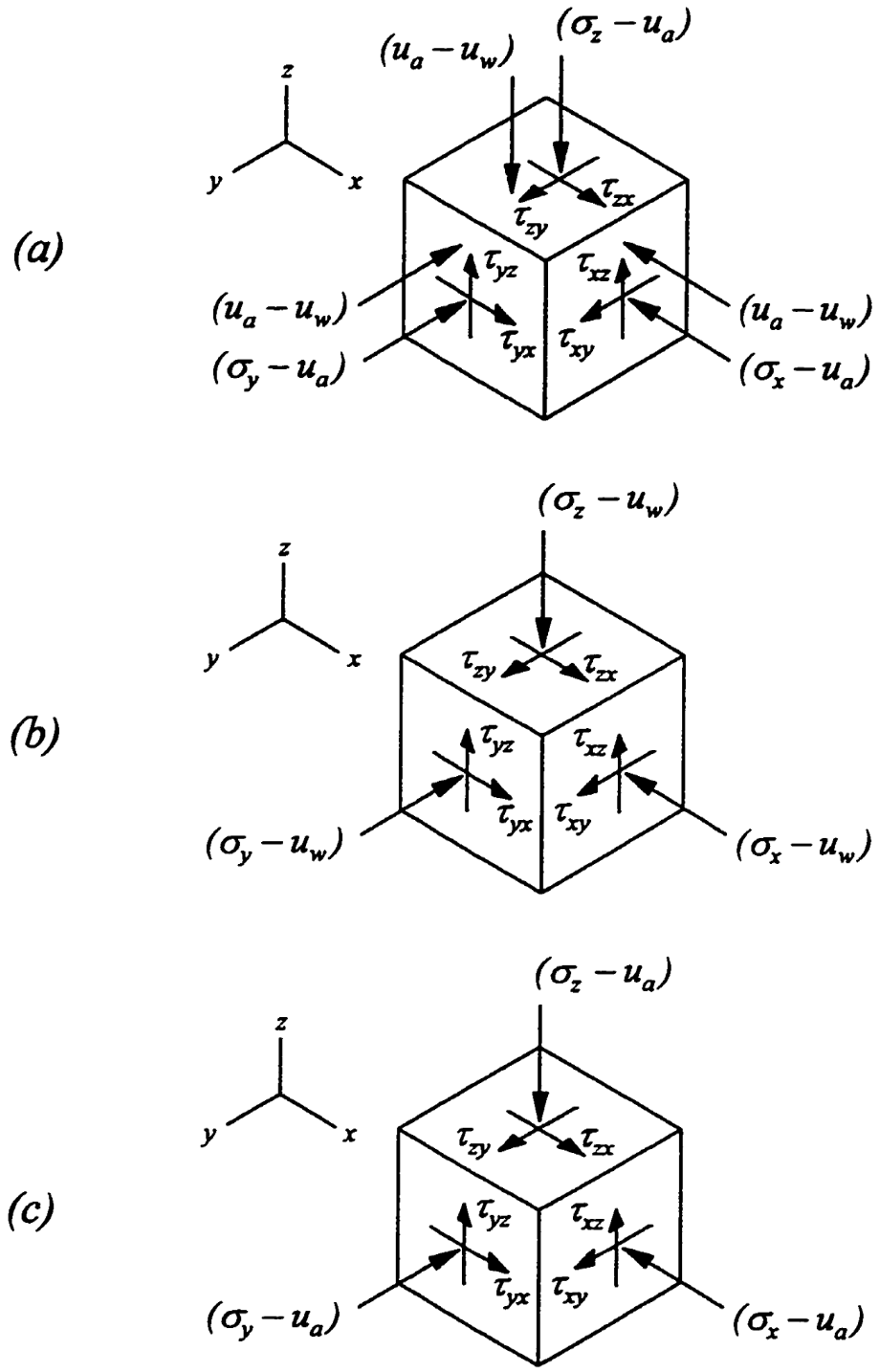

Figure 2.18 Stress state variables suitable : (a) partially saturated soils; (b) fully saturated soil; (c) dry soil (Fredlund and Rahardjo 1993)

$$(\sigma_{ij} - u_w\delta_{ij}) = \begin{pmatrix} (\sigma_x - u_w) & \tau_{yx} & \tau_{zx} \\ \tau_{xy} & (\sigma_y - u_w) & \tau_{zy} \\ \tau_{xz} & \tau_{yz} & (\sigma_z - u_w) \end{pmatrix} \tag{2.38}$$

The second stress tensor, $(u_a - u_w)\delta_{ij}$, disappears because the matric suction, $(u_a - u_w)$, goes toward zero. Figure 2.18b illustrates the stress tensor acting at a point in a saturated soil. The stress state variable, $(\sigma - u_w)$, is commonly referred to as effective stress (Terzaghi 1936).

The above rationale demonstrates the smooth transition in stress state description when going from an unsaturated soil to a saturated soil, and vice versa.

Water evaporation from a soil, or air drying a soil, will increase the matric suction. The relationship between the water content and the matric suction of a soil is commonly referred to as the soil water characteristic curve, which is presented previously in this chapter. As a soil become extremely dry (shrinkage limit), the effects of a change in matric suction on the mechanical behavior of the soil may become negligible. In other words, a change in matric suction on a dry soil may not produce any significant change in the volume or shear strength of the soil (Fredlund and Rahardjo 1993).

Although matric suction, $(u_a - u_w)$, remains a stress state variable, it may not be required for describing the behavior of a dry soil. Only the first stress tensor may be retained for a dry soil when considering this special case:

$$(\sigma_{ij} - u_a\delta_{ij}) = \begin{pmatrix} (\sigma_x - u_a) & \tau_{yx} & \tau_{zx} \\ \tau_{xy} & (\sigma_y - u_a) & \tau_{zy} \\ \tau_{xz} & \tau_{yz} & (\sigma_z - u_a) \end{pmatrix} \tag{2.39}$$

Nevertheless, it may be necessary to consider matric suction, $(u_a - u_w)$, as a stress state variable when examining the volume increase or swelling of a dry soil. Figure 2.18c illustrates the stress tensor acting at a point in a dry soil.

There are three possible combinations of stress state variables that can be used to describe the stress state relevant to the soil structure and contractile skin in an unsaturated soil. There are tabulated in table 2.3. Using the pore water pressure as the reference pressure is only relevant for soils with compressible soil particles. On the other hand, the stress variable, (σ), when using the total normal stress, σ, as a reference, can be ignored when the soil particles are assumed to be incompressible. Referencing the stress state to the pore air pressure would appear to produce the most reasonable and simple combination of stress state variables (Fredlund and Rahardjo 1993).

The stress state represented by $(\sigma - u_a)$ and $(u_a - u_w)$ combination seems to be the most satisfactory for use in engineering practice. This pair of the independent stress state variables is advantageous because the effects of a change in the pore water pressure. In addition, the pore air pressure is atmospheric (i.e., zero gage pressure) for most practical engineering problems (Fredlund and Rahardjo 1993).

Table 2.3 Possible combinations of stress state variable for an unsaturated soil (Fredlund and Rahardjo 1993)

Reference pressure (1)	Symbol (2)	Stress State Variables (3)
Pore air pressure	u_a	$(\sigma - u_a)$, and $(u_a - u_w)$
Pore water pressure	u_w	$(\sigma - u_w)$, and $(u_a - u_w)$
Total pressure	σ	$(\sigma - u_a)$, and $(\sigma - u_w)$

Fredlund and Morgenstern (1977), presented null type test data to experimentally validate the proposed stress state variables, $(\sigma - u_a)$ and $(u_a - u_w)$, using the so called axis translation technique. The $(\sigma - u_a)$ and $(u_a - u_w)$ combination is used throughout the present research work. These stress variables are referred to as the net normal stress, $(\sigma - u_a)$, and the matric suction, $(u_a - u_w)$.

2.7 Shear Strength Parameters

Measuring, modeling, and predicting the shear strength of soil are hallmarks of the soil mechanics and geotechnical engineering. The shear strength of soil, whether saturated or unsaturated, may be defined as the maximum inter resistance per unit area the soil is capable of sustaining along the failure plane under external or internal stress loading.

2.7.1 Saturated Soil

The shear strength is commonly described by the Mohr-Coulomb failure criterion, which defines shear strength in term of the material variables ϕ' and c' and the stress variable effective stress as:

$$\tau_f = c' + \sigma'_f \tan\phi' = c' + (\sigma - u_w)_f \tan\phi' \qquad (2.40)$$

where τ_f is the shear stress on the failure plane at failure, c' is the effective cohesion, $(\sigma\text{-}u_w)_f$ is effective normal stress on the failure plane at failure, and ϕ' is the effective angle of internal friction.

Mohr's circles can be drawn to represent the state of normal and shear stress acting on any plane in a soil element. Consider the states of stress defined by circles *A* and *B* in Figure 2.19. The minor and major effective principal stress in condition *A*, $(\sigma_3\text{-}u_w)_A$ and $(\sigma_1\text{-}$

$u_w)_A$, are lower than failure envelop which the soil element remains stable. However, the major principal stress, $(\sigma_1\text{-}u_w)_B$, is increased to reach the failure envelop in condition *B*, then failure occurs under normal and shear stress conditions, $(\sigma\text{-}u_w)_f$, and τ_f.

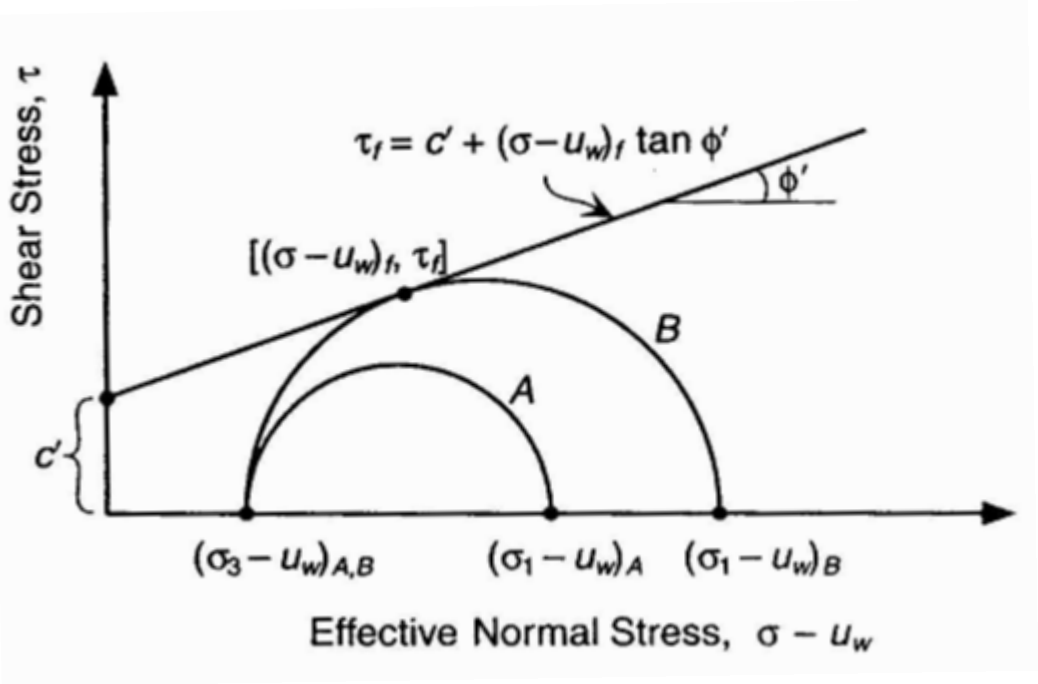

Figure 2.19 Mohr-Coulomb for saturated soil

2.7.2 Unsaturated Soil

The accurate understanding shear strength on soil necessarily is required for analyzing and solving geotechnical problems at which a certain load is applied on the soil. Terzaghi(1936) initially developed the concept of effective stress to interpret soil's strength. However, Bishop (1959) had found that the effective stress equation suggested by Terzaghi hasn't effectively reflected the strength of unsaturated soil since unsaturated soil generally showed higher strength than saturated soil. Bishop introduced new terms which are the pore

air pressure, u_a and the pore water pressure, u_w, and effective stress parameter, χ to modify Terzaghi' effective stress equation for unsaturated soil as following:

$$\sigma_n = (\sigma - u_a) + \chi(u_a - u_w) \tag{2.41}$$

This equation was used to determine effective stress in an unsaturated soil and the shear strength of unsaturated soils can be obtained from using the Mohr-Coulomb' shear strength formulation. The χ-parameter, significantly affected by degree of pore water saturation, is a material property that changes between zero and unity. However, experimental programs which found χ greater than unity indicated that χ parameter was inconsistent in predicting the effective stress of unsaturated soils. This is attributed to χ parameter is essentially material variable and therefore should not be employed in the definition of stress state. The effective stress equation including this material variable becomes the form of constitutive model rather than the definition of a stress state.

Jennings and Burland (1962) and Coleman (1962) proposed that separating the stress state variables for unsaturated soil was more adequate than incorporating them into new effective stress equation and therefore, the stress variables had to be treated independently. A null experiment performed by Fredlund and Morgenstern (1977) showed that the independent stress state variables $(\sigma - u_a)$ and $(u_a - u_w)$ could be valuably employed for describing the shear strength and volume change of unsaturated soils. Fredlund et al. (1978) developed new equation in terms of independent stress variables for the shear strength of unsaturated soil as following:

$$\tau_f = c' + (\sigma_f - u_a)_f \tan\phi' + (u_a - u_w)_f \tan\phi^b \tag{2.42}$$

Where:

c' = intercept of the "extended" Mohr-Coulomb failure envelope on the shear stress axis where the net normal stress and the matric suction at failure are equal to zero; it is also referred to as "effective cohesion"

$(u_a - u_w)_f$ = net normal stress state on the failure plane at failure

u_{af} = pore air pressure on the failure plane at failure

ϕ' = angle of internal friction associated with the net normal stress state variable, $(u_a - u_w)_f$

$(u_a - u_w)_f$ = matric suction on the failure plane at failure

ϕ^b = angle indicating the rate of increase in shear strength relative to the matric suction, $(u_a - u_w)_f$.

The first two terms on the right-hand side e.q. (2.1) present the conventional M-C criterion for the strength of saturated soil. The third term is representing the increase in shear strength along with increasing matric suction in unsaturated soil. The extended M-C criterion is illustrated in three-dimensional space as shown in figure 2.20.

In describing a projection of the failure surface to the shear stress versus net normal stress plane, the extended M-C criterion can be written as:

$$\tau_f = c_1' + (\sigma - u_a)_f \tan\phi' \tag{2.43}$$

where:

$$c_1' = \tau_{f|(\sigma - u_a)=0} = c' + (u_a - u_w)_f \tan\phi^b \tag{2.44}$$

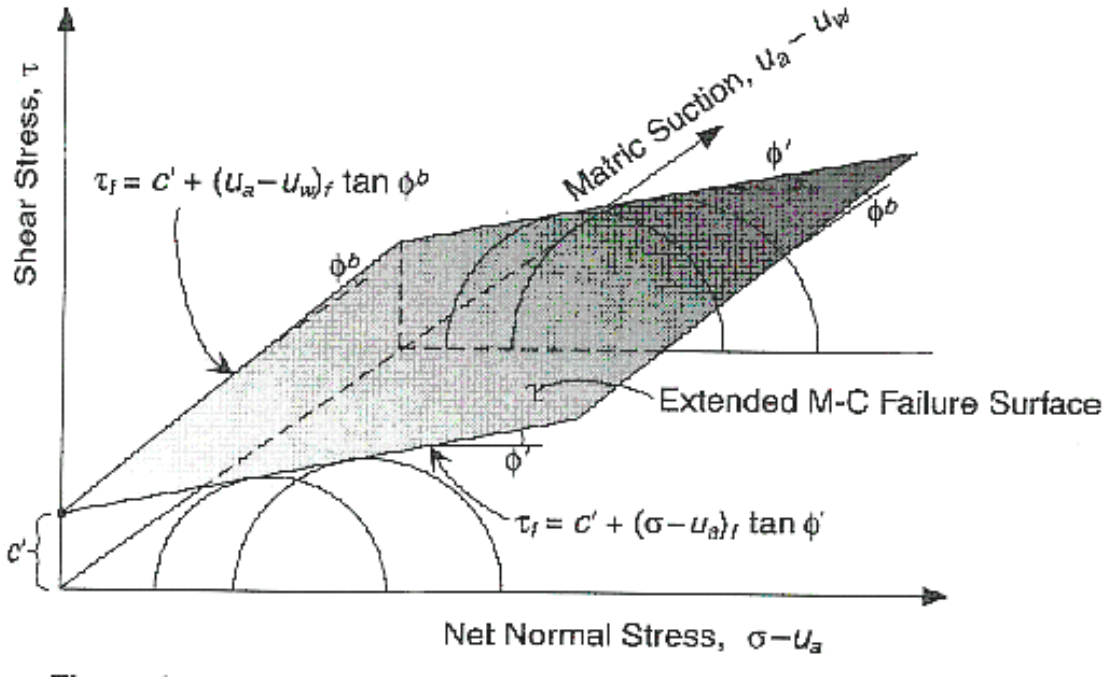

Figure 2.20 Extended mohr-coulomb failure surface for unsaturated soil (Fredlund and Rahardjo, 1993)

In the same way, in describing a projection of the failure surface to the shear stress versus matric suction plane, the extended M-C criterion can be expressed in the following manner:

$$\tau_f = c_2' + (u_a - u_w)_f \tan \phi^b \tag{2.45}$$

where:

$$c_2' = \tau_{f|(u_a - u_w)=0} = c' + (\sigma - u_a)_f \tan \phi' \tag{2.46}$$

The next chapter describes some previous work and the check-out verification testing of the new cubical apparatus developed in this present research work.

CHAPTER 3

PREVIOUS WORK AND CELL PERFORMANCE TESTING

3.1 Introduction

The conventional (cylindrical) triaxial apparatus is well known laboratory equipment for testing shearing resistance and deformation characteristics of soils. The effect of the intermediate stress, however, cannot be examined in the conventional triaxial apparatus since the intermediate principal stress has to be equal to at least one of the other principal stresses in the apparatus. Thus, only axisymmetric stress states $\left(\sigma_2 = \sigma_3\right)$ are achievable in the conventional triaxial apparatus, while true triaxial stress states $\left(\sigma_1 \neq \sigma_2 \neq \sigma_3\right)$ are unachievable. The true triaxial apparatus is capable of producing independent variations of the three principal stresses and strains. Hence, testing for effects of the intermediate principal stress and cross-anisotropic behavior is possible with this equipment.

Many studies have outlined the benefits of the true triaxial (cubical) apparatus over the cylindrical triaxial cell for testing stress-strain-strength behavior of soils, and have contributed to the mechanical characterization of dry and saturated soils for multiaxial stress states under drained or undrained conditions. However, experimental evidence on the true triaxial behavior of unsaturated soils under suction-controlled conditions is rather limited. The following section describes some previous work and check-out verification testing of the new cubical apparatus developed in this present research work.

3.2 Previous Work by Hoyos and Macari (2001)

Hoyos and Macari (2001) implemented a mixed-boundary type of true triaxial apparatus, with a 10-cm side specimen seated on top of a HAE disk and between five flexible latex/porexTM membranes on the remaining sides of the cube, as shown in figure 3.1a. The setup consists basically of a frame (1) that accommodates five (one top and four lateral) flexible latex/porexTM (2), and a cubical base piece (3) housing a 5-bar HAE disk (4). Once the specimen (5) is compacted, the remaining five walls (6) are assembled to the frame. Three LVDTs per face (7) monitor soil deformations. Hydraulic fluid is used to pressurize the specimen. External pressure is transmitted to hydraulic fluid through pressure inlet/outlet connections (8) on the walls. Pore-air pressure, u_a ,is applied to the top and four lateral faces of the specimen via a small cooper block (9) attached to the flexible membranes with a threaded stem. External air pressure is applied via flexible nylon tubing (10). A 5-outlet manifold distributes the air pressure to the top and lateral faces simultaneously. Pore-water pressure, $u_{w,}$ is applied at the bottom of the specimen via the HAE disk (4). Water pressure is also applied via nylon tubing (11). A flushing mechanism (12) is added to the bottom wall assembly. Tests are entirely computer-driven.

The flexible membranes were prepared using a GIT-603TE type of latex rubber possessing medium-to-high tear strength and low stiffness, as shown in figure 3.1b. The edges of the latex were doubled in thickness to reinforce its tear resistance at these critical boundaries. A 3.2-mm thick, 9.65-cm side, coarse flexible polyethylene (porex^{TM}) sheet, is placed between the latex and the specimen to uniformly distribute the air pressure, supplied from the exterior, to the pores of the soil (Hoyos, 1998).

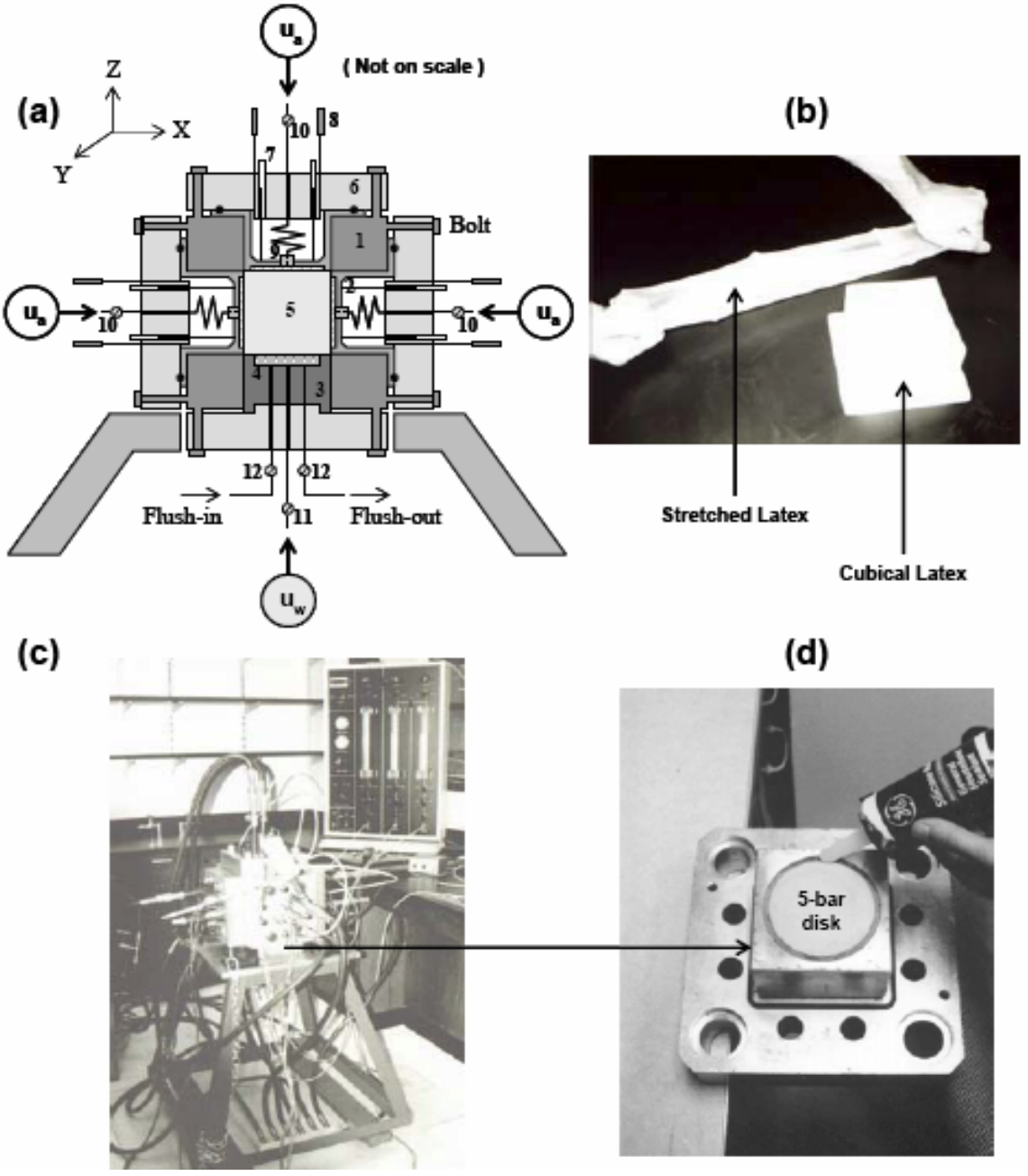

Figure 3.1 True triaxial cell with flexible loading membranes: (a) layout; (b) latex; (c) general view; (d) bottom wall with HAE disk (Hoyos and Macari 2001)

A procedure similar to that suggested by Bishop and Henkel (1962) to ensure in place saturation of a HAE disk, was adapted to the working conditions of the HAE disk in the modified test cell. After saturation of the disk, the disk remains covered with a thin film of water until the first layer of soil is to be compacted. All cubical specimens are gently compacted in 10 layers of approximately 1-cm thickness via in-place tamping compaction. Once the specimen has been fully compacted, the temporary rigid membranes are removed and the latex/porex^{TM}, along with the assemblies containing the pore-air-pressurizing units, is set into place.

Compressibility of the latex/porex^{TM} was found to be 0.065 cm under a 1 MPa pressure, which was deducted from total deformations of the specimen. The interface friction angle between porex and silty sand was found to be 6.2o from direct shear test. This results in a relatively low coefficient of friction (μ) of 0.11. Maximum pore size of the porexTM is about 130μ, considerably smaller than soil's d_{10}. Testing in the cell is stress-controlled, hence the adequate loading rate was empirically assessed. A 10 kPa/hour loading rate (for isotropic loading and shearing), was found to be appropriate for adequate equalization. Response of silty sand in the net principal stress plane for 50, 100 and 200 kPa suctions is shown in Figure 3.2.

3.3 Previous Work by Matsuoka et al. (2002)

Matsuoka et al. (2002) reported a true triaxial apparatus with three pairs of rigid loading plates in three orthogonal directions, as shown in figure 3.3. A silty soil specimen of 10-cm side seats between upper and lower loading plates with remaining four lateral surfaces

covered by latex. Each plate houses a 70-mm HAE disk (300-kPa entry value) and two 5-mm coarse stones covered with polyfluorotetraethylene filters.

Suction in the specimen is attained by inducing negative pore-water pressures via an external vacuum based system, as shown in figure 3.4. Cubical specimens are compacted in five layers in a separate cubical frame, with each layer statically compacted 226 times using a 1.2-cm diameter plunger up to a vertical stress of 300 kPa. Ceramic disks in the upper and lower plates are carefully saturated before testing in a custom-made cylindrical cell that allows saturation of the disk while mounted in the loading plate.

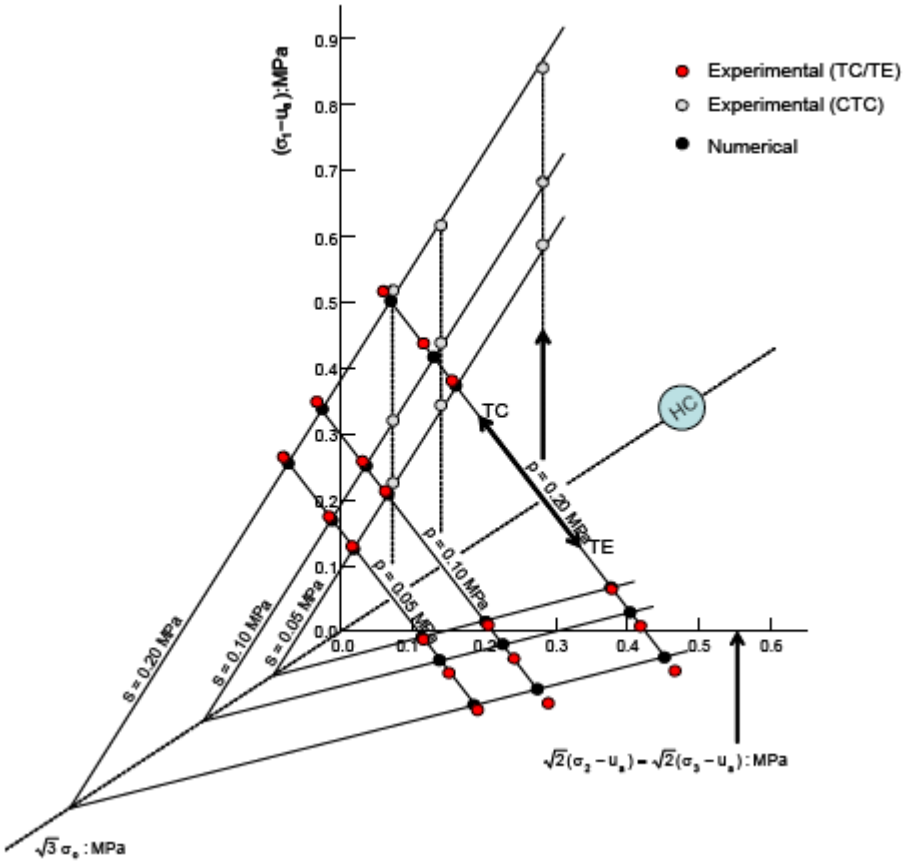

Figure 3.2 True triaxial results in net principal stress plane (Hoyos and Arduino, 2005)

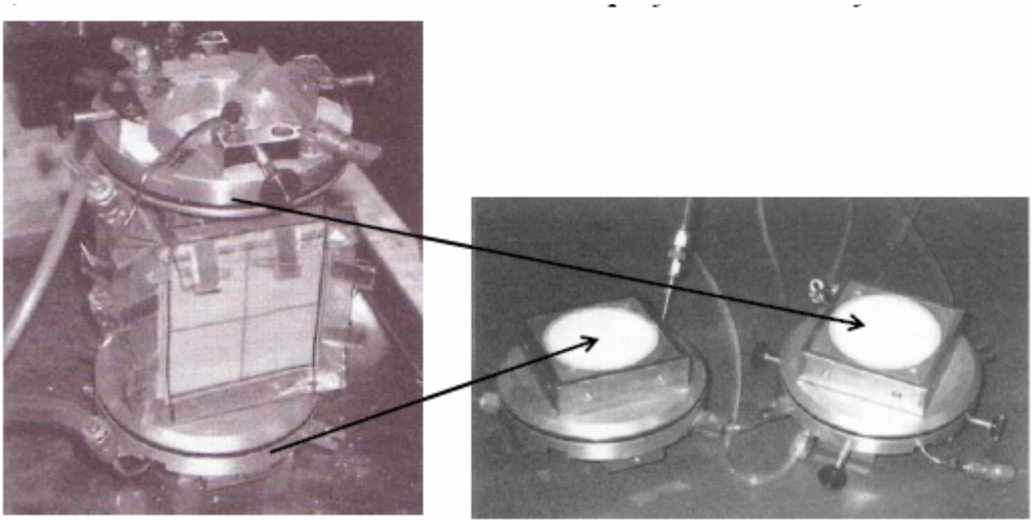

Figure 3.3 True triaxial cell with rigid loading plates (Matsuoka et al., 2002)

After setting the specimen between loading plates, a 98-kPa isotropic pressure was applied under a constant negative u_w (suction) of 59 kPa. Principal stresses are applied by stress-controlled loading method, with the full shearing process divided into about ten steps until peak failure. A new stress increment was applied when all of the axial strain rates reached less than 10^{-5}/min, and the drained volumetric strain rate reached less than 10^{-3}/h. All plain-strain shear tests were conducted under drained conditions (constant u_w) adjusting the intermediate σ_2 and minor σ_3 principal stresses to meet the requirement of absolute intermediate strain less than 0.01 % at a given σ_1. In this study, true triaxial tests were conducted along radial stress paths in the π-plane (constant Lode-angle θ). Since normal stresses on the specimen are applied by three pairs of rigid steel plates, interference between the loading plates in the σ_1 and σ_2 directions becomes notable when θ is large. Hence, only stress paths with θ = 0-30^o was accomplished, as shown in figure 3.5a.

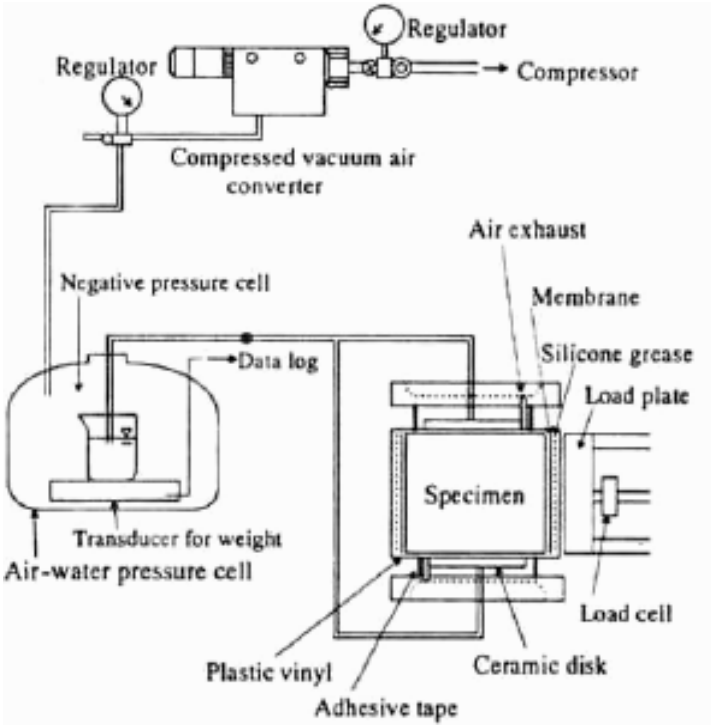

Figure 3.4. System for applying negative pore-water pressure (Matsuoka et al., 2002)

In order to calibrate the true triaxial tests, Matsuoka et al. (2002) also performed a comparison of test results for conventional triaxial and true triaxial tests using same soil and stress conditions, i.e. triaxial compression (TC) tests, $\theta = 0^o$, p = 98 kPa, and s = 59 kPa. However, the method for controlling suction in each device as different: negative uw method ($s = -u_w$, $u_a = 0$) was used during true triaxial testing while positive u_a method ($s = u_a$, $u_w = 0$) was used during conventional triaxial testing. Stress-strain relationships measured by the two methods showed reasonably good agreement, as shown in figure 3.5b.

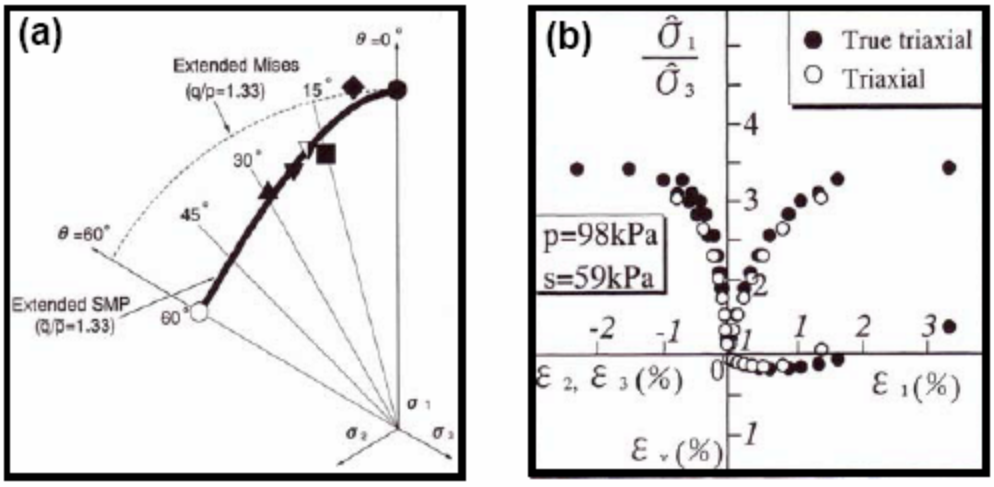

Figure 3.5 True triaxial results: (a) stress paths in octahedral plane; (b) stress-strainrelationships (Matsuoka et al., 2002)

3.4 Performance Testing of a New True Triaxial Cell

In late 2004, the core of a novel true triaxial setup was developed and implemented at the University of Texas at Arlington. The core system of the device was manufactured at the University of Colorado at Boulder, under direct supervision of Professor Stein Sture of the UC-Boulder Geotechnical Group.

Park (2005) performed a series of tests with the newly developed cell along a variety of stress paths on pluviated silty sand with naturally occurring suction. The experimental program was designed to calibrate and check-out verify the correct functioning of each basic component of the new true triaxial apparatus. Results are summarized in the following.

3.4.1 Calibration of Liner Variable Displacement Transducers

A data acquisition system controls and records the excitation and output of the LVDTs (3 LVDTs per face of cubical cell). As the core of LVDT move up and down within the housing, it causes change in the magnitude of voltage corresponding to the magnitude of

deformation (i.e., measured in inches). Based on the above concept, calibration of each of LVDTs was performed by stacking up 0.1-inch aluminum stacks or taking out stacks one by one as shown in figure 3.6.

Approximately 0.1-inch deformation corresponds to 0.1-voltage reading; however, each of LVDTs has slightly different corresponding magnitude between voltage and deformation. In order to obtain precise corresponding magnitudes (i.e., slopes of calibration curve) from each LVDT, voltage versus inch responses were plotted. Figure 3.7 shows an example of the calibration curve and slope from X1(+) face of the cell. Table 3.1 summarizes the calibration data from all faces.

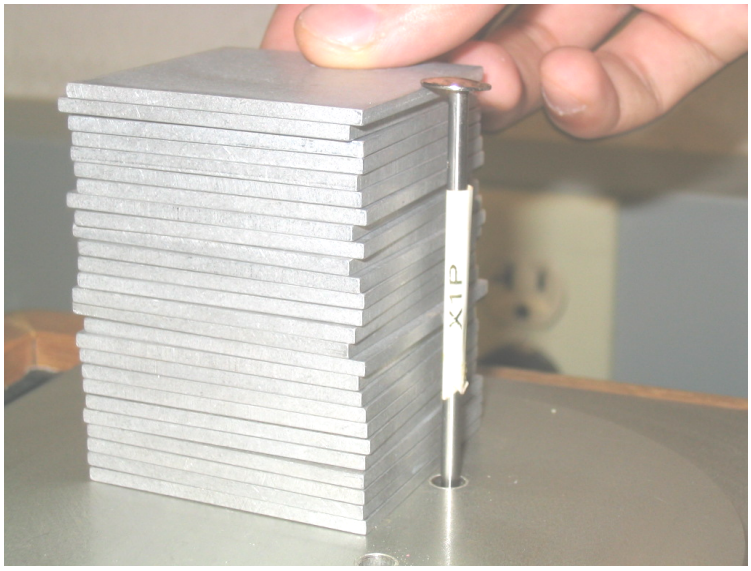

Figure 3.6 LVDT calibration process

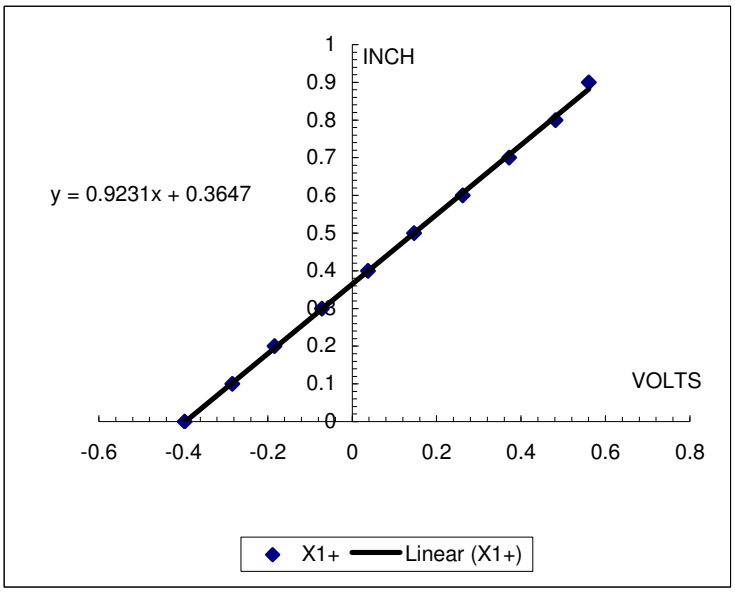

Figure 3.7 Example of calibration curve (X1(+) face) (Park 2005)

Table 3.1 LVDT calibration data (Park 2005)

SLOPE	X1+	X2+	X3+	X1-	X2-	X3-
slope (up)	0.9231	1.0395	1.0242	1.0366	1.0295	1.0479
slope (down)	0.9092	1.0136	1.0104	1.0261	1.0013	1.0483
average slope of X	0.9162	1.0266	1.0173	1.0314	1.0154	1.0481
SLOPE	Y1+	Y2+	Y3+	Y1-	Y2-	Y3-
slope (up)	1.0205	1.0287	0.9945	1.0706	1.0292	1.3391
slope (down)	1.0193	1.0238	1.0137	1.0509	1.0200	1.3604
average slope of Y	1.0199	1.0263	1.0041	1.0608	1.0246	1.3498
SLOPE	Z1+	Z2+	Z3+	Z1-	Z2-	Z3-
slope (up)	1.0286	0.9985	1.0216	0.9845	0.9905	0.9787
slope (down)	1.0178	0.9947	1.0138	0.9767	1.0041	0.9972
average slope of Z	1.0232	0.9966	1.0177	0.9806	0.9973	0.9880

3.4.2 Experimental Variables

The experimental program under taken by Park (2005) was designed to study the stress-strain-strength behavior of partially saturated silty sand subjected to three-dimensional stress states along a variety of multiaxial stress paths. The soil tested was artificially prepared by mixing 30% silt (from North Arlington, Texas) and 70% clean sand (commercially supplied locally). The air-dried water content is 2.0% and the maximum dry unit weight attained via pluviation technique is 14.9 kN/m^3, which corresponds to a moisture content of 5.3%.

The pluviation-based specimen preparation process was aimed at reproducing specimens with extremely low preconsolidation pressure. Initially induced conditions are summarized in table 3.2. All three-inch soil specimens were pluviated in five layers using pluviation technique. Water was added to each layer to achieve target moisture content by spraying.

Table 3.2 Initial pluviation-induced soil conditions (Park 2005)

Soil Condition	Water Content (%)	Total Water Added (ml)	Dry Unit Weight (kN/m^3)	Void Ratio	Degree of Saturation (%)	Suction (kPa) from SWCC
Air-dried	2	Not Added	14.79	0.804	6.77	5516
85% (dry)	4.5	68.25	14.88	0.793	15.44	2514
Optimum	5.3	80.60	14.92	0.788	18.28	1632
85% (wet)	6.1	92.75	14.91	0.789	21.02	1035

Partially saturated silty sand samples were artificially prepared at four different moisture contents corresponding to four different values of initial suction prior to testing: air-dried water content corresponding to soil suction of 800 psi (5516 kPa); w = 4.5% corresponding to soil suction of 365 psi (2514 kPa); w = 5.3% corresponding to soil suction of 237 psi (1632 kPa); and w = 6.1% corresponding to soil suction of 150 psi (1035 kPa). The corresponding value of suction for a given moisture content was obtained from the soil water characteristic curve (SWCC) shown in figure 3.8.

3.4.3 Hydrostatic Compression (HC) Test Results

A series of 4 HC tests were successfully conducted in the new cubical setup on 4 specimens of artificially prepared silty sand at different moisture contents referring to initial values of suction of Ψ = 5516 kPa (800 psi), 2514 kPa (365 psi), 1632 kPa (237 psi), and 1035 kPa (150 psi). In each test, stress increment (Δσ) was 1 psi/hr, and the maximum hydrostatic pressure was 20 psi. HC test results are presented in figure 3.9. The three principal strains measured are plotted against mean pressure in figure 3.9, as well.

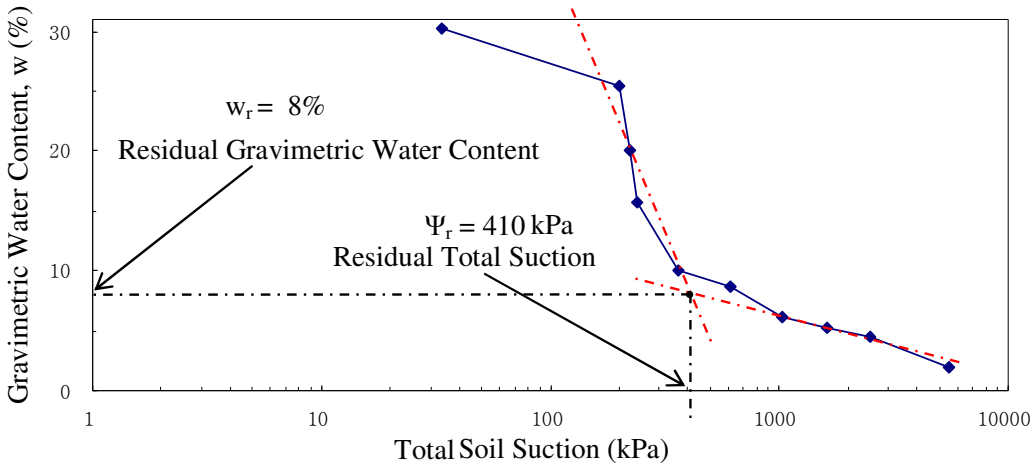

Figure 3.8 Soil water characteristic curve (SWCC) of silty sand (Park 2005)

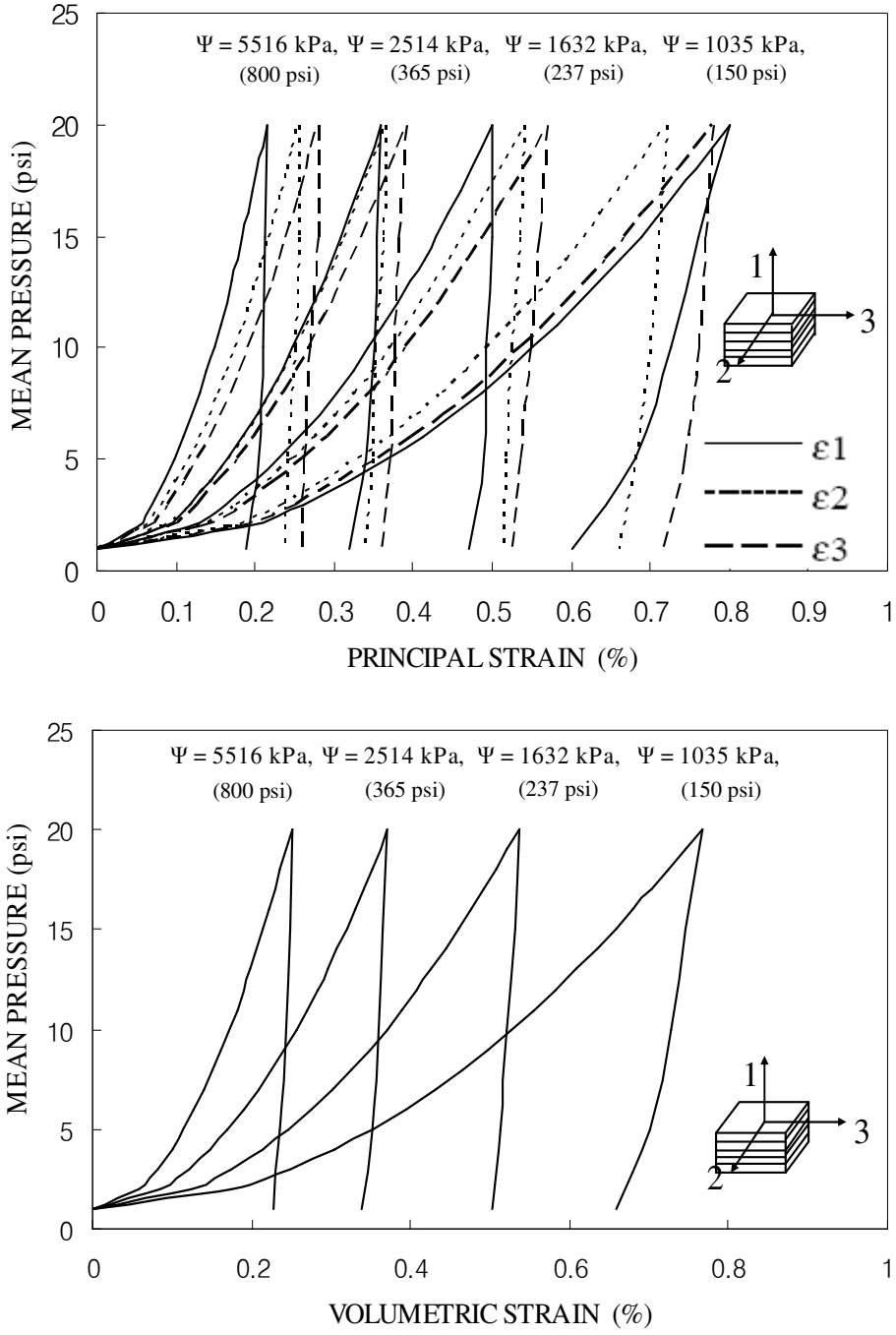

Figure 3.9 Hydrostatic compression (HC) test results (Park 2005)

.

3.4.4 Triaxial Compression (TC) Test Results

A series of 12 TC tests were successfully performed in the new cubical setup on 12 specimens of artificially prepared silty sand at different moisture contents referring to initial values of suction of Ψ = 5516 kPa (800 psi), 2514 kPa (365 psi), 1632 kPa (237 psi), and 1035 kPa (150 psi) under effective confining pressures of 20, 30, and 40 psi.

Figure 3.10 shows the stress-strain response for silty sand under optimum moisture. In these tests, values of two principal stresses was equally decreased (i.e., $\Delta\sigma_2 = \Delta\sigma_3 = -\Delta\sigma_1/2$) while the other stress was increased, such that σ_{oct} remained constant. As the minor (σ_3) and intermediate (σ_2) stresses were decreased equally, the corresponding strains (ϵ_3, ϵ_2) were found expansive, indicating isotropic behavior in the lateral direction.

The major (σ_1) principal stress was increased during testing; consequently, its corresponding major principal strain was compressive (+).

3.4.5 Triaxial Extension (TE) Test Results

A series of 12 TE tests were successfully conducted in the new cubical setup on 12 specimens of artificially prepared silty sand at different moisture contents referring to initial values of suction of Ψ = 5516 kPa (800 psi), 2514 kPa (365 psi), 1632 kPa (237 psi), and 1035 kPa (150 psi). The TE tests were performed under effective confining pressures of 20, 30, and 40 psi. Figure 3.11 presents the stress-strain response for silty sand under air-dried moisture. In these tests, the intermediate (σ_2) and major (σ_1) principal stresses were equally increased (i.e., $\Delta\sigma_2 = \Delta\ \sigma_3$), whereas the minor ($\sigma_3$) principal stress was decreased (i.e., $\Delta\sigma_3 = -2\Delta\sigma_2 = -2\Delta\sigma_1$). Thus, the intermediate (ϵ_2) and major (ϵ_1)

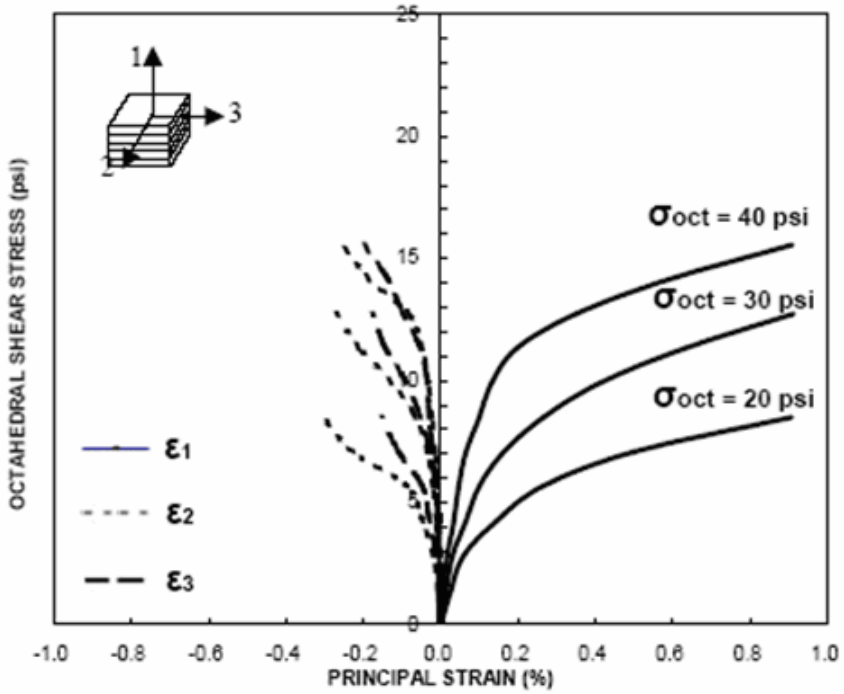

Figure 3.10 TC test results for silty sand under optimum moisture (Park 2005)

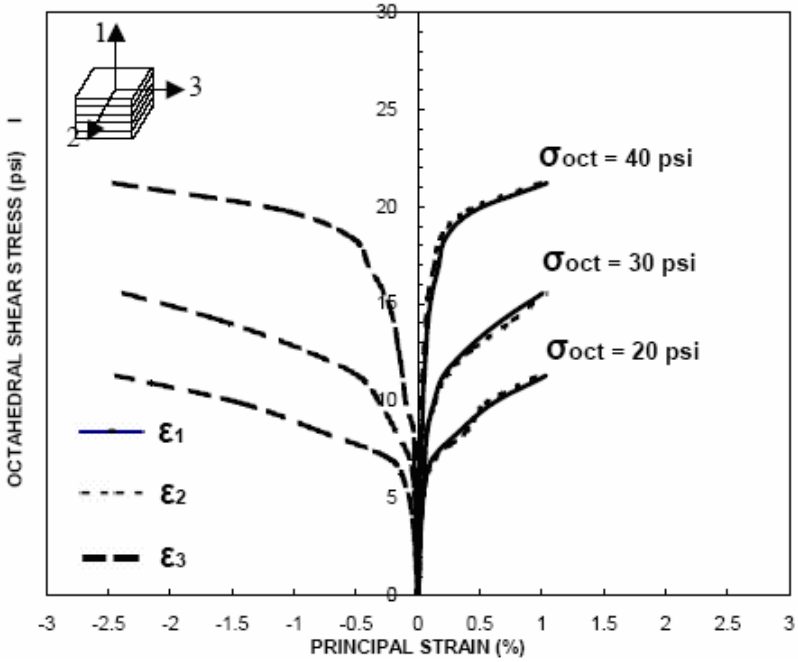

Figure 3.11 TE test results for silty sand under air-dried moisture (Park 2005)

principal strains were found to be compressive (+), and the minor (ϵ_3) principal strain was expansive (-).

3.4.6 Simple Shear (SS) Tests

A series of 12 SS tests were successfully conducted in the new cubical set up on 12 specimens of artificially prepared silty sand at different moisture contents corresponding to inital values of suction of Ψ = 5516 kPa (800 psi), 2514 kPa (365 psi), and 1632 kPa (237 psi), and 1035 kPa (150 psi). The SS tests were performed at σ_{oct} = 20, 30, and 40 psi, and results obtained are shown in figure 3.12. During SS testing, the major principal stress (σ_1) was increased and at the same time the minor principal stress (σ_3) was decreased in the same magnitude (i.e., $\Delta\sigma_3 = -\Delta\sigma_1$), while the intermediate (σ_2) principal stress was maintained constant (i.e., $\Delta\sigma_2 = 0$). Accordingly, the major (ϵ_1) principal strain was compressive (+), and the minor (ϵ_3) principal strain was expansive (-). As the intermediate (ϵ_2) principal strain was very small, this type of test condition closely corresponds to a plane strain condition.

3.4.7 Incipient Failure Envelopes on Octahedral Plane

Figure 3.13 shows the projection of incipient failure envelopes from all true triaxial tests onto the octahedral plane (π-plane) on the basis of initial total suction (ψ) and octahedral stress (σ_{oct}) level**.** Overall, figure 3.13 shows a significant influence of total suction on the size, and position of the incipient failure envelopes.

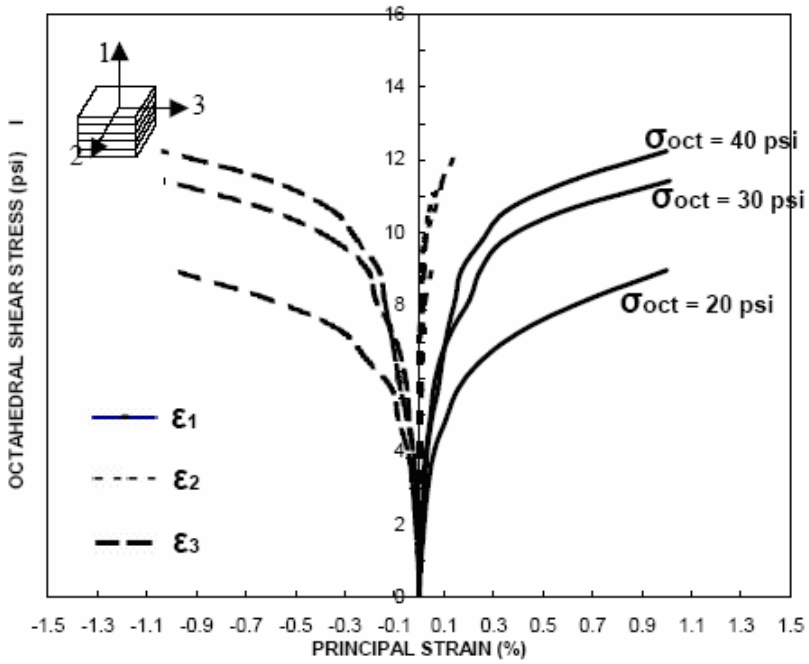

Figure 3.12 SS test results for silty sand under 85% wet of optimum (Park 2005)

3.4.8 Conclusions from Park (2005)

The main objective of the experimental program undertaken by Park (2005) was to perform a thorough check-out verification of the new true triaxial device by investigating the multiaxial stress-strain behavior of partially saturated silty sand specimens artificially prepared in the laboratory.

The new cell was successfully used to study multiaxial stress-strain behavior of silty sand at high values of pluviation-induced suction assessed from SWCC. It was observed that the initial total suction has a significant influence on stress-strain-strength behavior of artificially prepared silty sand along a wide range of stress paths.

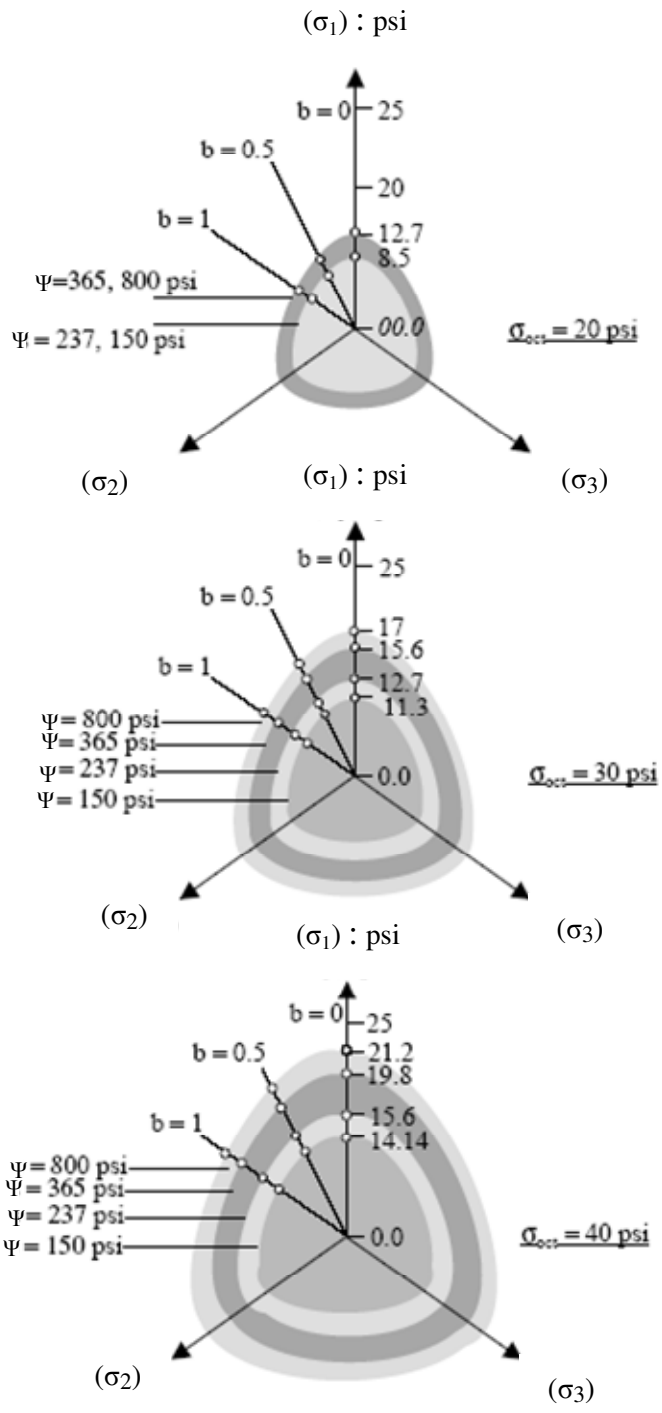

Figure 3.13 Projection of incipient failure envelopes onto the octahedral plane (Park 2005)

The next chapter describes the main features of the suction-controlled cubical testing device developed in this study, including the step-by-step assembly process. Description of the pore-air and pore-water pressure control/monitoring systems is also presented in detail. The fundamentals of true triaxial testing schemes, the saturation process of high-air-entry ceramic disks, and the specimen preparation method are also described in the following chapter.

CHAPTER 4

A NOVEL SUCTION-CONTROLLED TRUE TRIAXIAL TEST CELL

4.1 Introduction

Geotechnical laboratory testing of unsaturated soils requires special modifications of the conventional oedometer, triaxial, and direct shear apparatuses commonly used to analyze the stress-strain-strength characteristics of saturated soil specimens. These modifications must accommodate the independent measurement or control of the pore-air, u_a, and pore-water, u_w, pressures in the unsaturated soil sample. In classical soil mechanics, the important link between volume change and shear stress has been considered for many years, and generalized constitutive models based on critical state theory are now well established. Most of the volume change constitutive relations, the shear stress characteristics, and the elasto-plastic critical state constitutive models proposed for unsaturated soils involve oedoemeter, triaxial, and direct shear testing using the axis translation technique originally proposed by Hilf (1948, 1956). However, only recently have concrete efforts been made to develop corresponding generalized constitutive models for unsaturated soils.

The first part of this chapter presents a brief review on the fundamentals of suction-controlled true triaxial testing schemes. The second part is devoted to describing the main features of the computer-based, suction-controlled cubical test cell implement in this work, including the description of the pore-air and pore-water pressure control monitoring systems

and some special design considerations. The third part describes the HAE ceramic saturation process. The forth part of this chapter describes the specimen preparation process. Feasibility of axis-translation technique is described in part fifth. The step-by-step assembly process is presented in detail in sixth part. The last part of this chapter presents some repeatability results of suction-controlled tests using the newly developed device.

4.2 Suction-Controlled True Triaxial Testing Schemes

A conventional triaxial cell for testing saturated soils (Bishop and Henkel 1962) can be modified to accommodate the suction-controlled testing of unsaturated soil. The test procedure can be conducted either on one specimen (i.e., multistage), or on several specimens at similar initial (i.e., pre-testing) stress and volume-weight conditions. The major modification to a conventional triaxial cell involves the sealing of a HAE disk on the base pedestal of the triaxial cell.

4.2.1 Fundamentals of Cubical Cell Testing

Cylindrical triaxial devices are able to generate only axisymmetric $\left(\sigma_2 = \sigma_3\right)$ and hydrostatic $\left(\sigma_1 = \sigma_2 = \sigma_3\right)$ stress states, as depicted in figure 4.1(a). However, cubical cell devices are capable of generating complete stress paths under a variety of stress states: (1) Axisymmetric $\left(\sigma_2 = \sigma_3\right)$ stress states, (2) Hydrostatic $\left(\sigma_1 = \sigma_2 = \sigma_3\right)$ stress states, and (3) Cubical cell $\left(\sigma_1 \neq \sigma_2 \neq \sigma_3\right)$ stress states, as shown in figure 4.1(b). In nature, soils, rocks, and other materials are subjected to three-dimensional stress gradients; therefore, tests based on cubical cell stress states are required to investigate the three dimensional behavior of soils, rocks, and other nature materials for accurate prediction purposes.

The three-dimensional state of stress can be expressed in terms of the normal and tangential components of stresses acting on the octahedral plane defined by $\sigma_1 + \sigma_2 + \sigma_3 = const$, as shown in figure 4.2. The normal component, σ_{oct}, and the tangential component, τ_{oct}, are generally called "*mean principal stress*" and "*octahedral shear stress*", respectively, and are calculated as (Yamada and Ishihara 1982):

$$\sigma_{oct} = \frac{\sigma_1 + \sigma_2 + \sigma_3}{3} \tag{3.1}$$

$$\tau_{oct} = \frac{1}{3}\sqrt{(\sigma_1 - \sigma_2)^2 + (\sigma_2 - \sigma_3)^2 + (\sigma_3 - \sigma_1)^2} \tag{3.2}$$

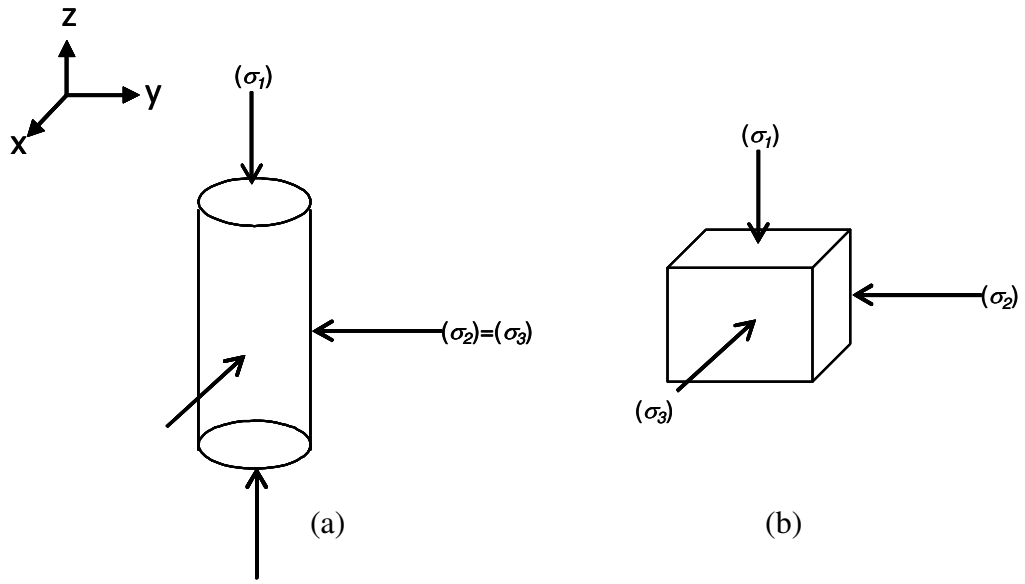

Figure 4.1 Stress state variables (a) axisymmetric $(\sigma_2 = \sigma_3)$ and hydrostatic ($\sigma_1 = \sigma_2 = \sigma_3$) stress states; (b) cubical cell $(\sigma_1 \neq \sigma_2 \neq \sigma_3)$ stress states

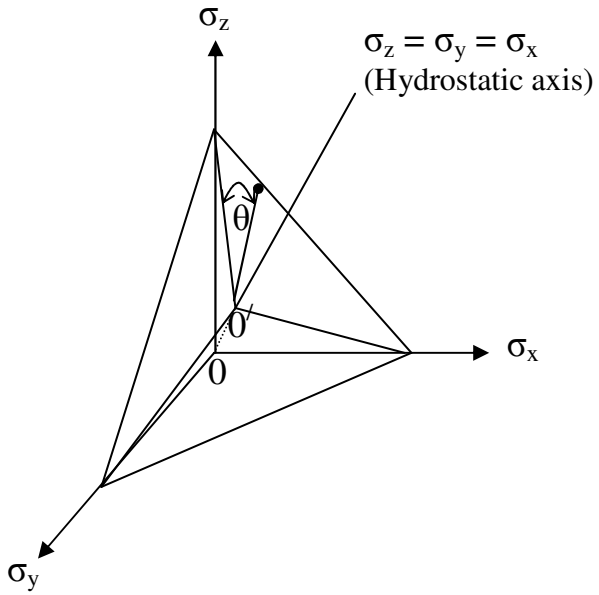

Figure 4.2 Representation of stress conditions in the octahedral plane (Yamada and Ishihara, 1982)

In order to specify three-dimensional stress conditions, it is necessary to adopt another independent variable, θ, which determines the direction of the shear stress on the octahedral plane, as shown in figure 4.2. This variable may be given by (Yamada and Ishihara 1982):

$$\tan\theta = \frac{\sqrt{3}(\sigma_y - \sigma_x)}{2\sigma_z - \sigma_x - \sigma_y} \tag{3.3}$$

The volumetric strain, ε_v, is then defined as follows:

$$\varepsilon_v = \frac{1}{3}\left(\varepsilon_x + \varepsilon_y + \varepsilon_z\right) \tag{3.4}$$

where, ε_x is normal strain in the x-direction, ε_y is normal strain in the y-direction, and ε_z is normal strain in the z-direction.

4.2.2 Stress Paths

A change in the stress state of an unsaturated soil can be described using a stress path, i.e., a curve drawn through the stress points for successive stress states (Lambe 1967, Fredlund and Rahardjo 1993). Consider an unsaturated soil element under axisymmetric conditions $\left(\sigma_2 = \sigma_3\right)$, the stress paths shown in Figure 4.3 illustrates a loading condition where the matric suction, $s = \left(u_a - u_w\right)$, is maintained constant. Similar loading conditions can also be preformed at other matric suction values. The stress paths can then be plotted on different planes, parallel to each other, depending upon the matric suction value or the *s*-coordinate, as demonstrated in Figure 4.4. Figure 4.5 present the stress paths in $(p:q:s)$ stress space for various loading patterns while maintaining a constant matric suction, $s = \left(u_a - u_w\right)$. Suction-controlled tests where the matric suction is maintained constant by using the axis translation technique are know as constant-suction, *drained* tests (Hilf 1956 and Hoyos 1998).

The stress paths descried above apply exclusively to unsaturated soils under axisymmetric conditions $\left(\sigma_2 = \sigma_3\right)$. In nature, soils located above the ground water table are subjected to three dimensional stress states, $\left(\sigma_{ij} - u_a\delta_{ij}\right)$ and $\left(u_a - u_w\right)\delta_{ij}$, as a result of external stress gradients and varying matric suction conditions. It is in this context where a cubical cell testing device, capable of controlling the value of matric suction, $s = \left(u_a - u_w\right)$, experienced by unsaturated soil specimens, plays a fundamental role in the stress-strain-strength characterization of an unsaturated soil (Fredlund and Rahardjo 1993).

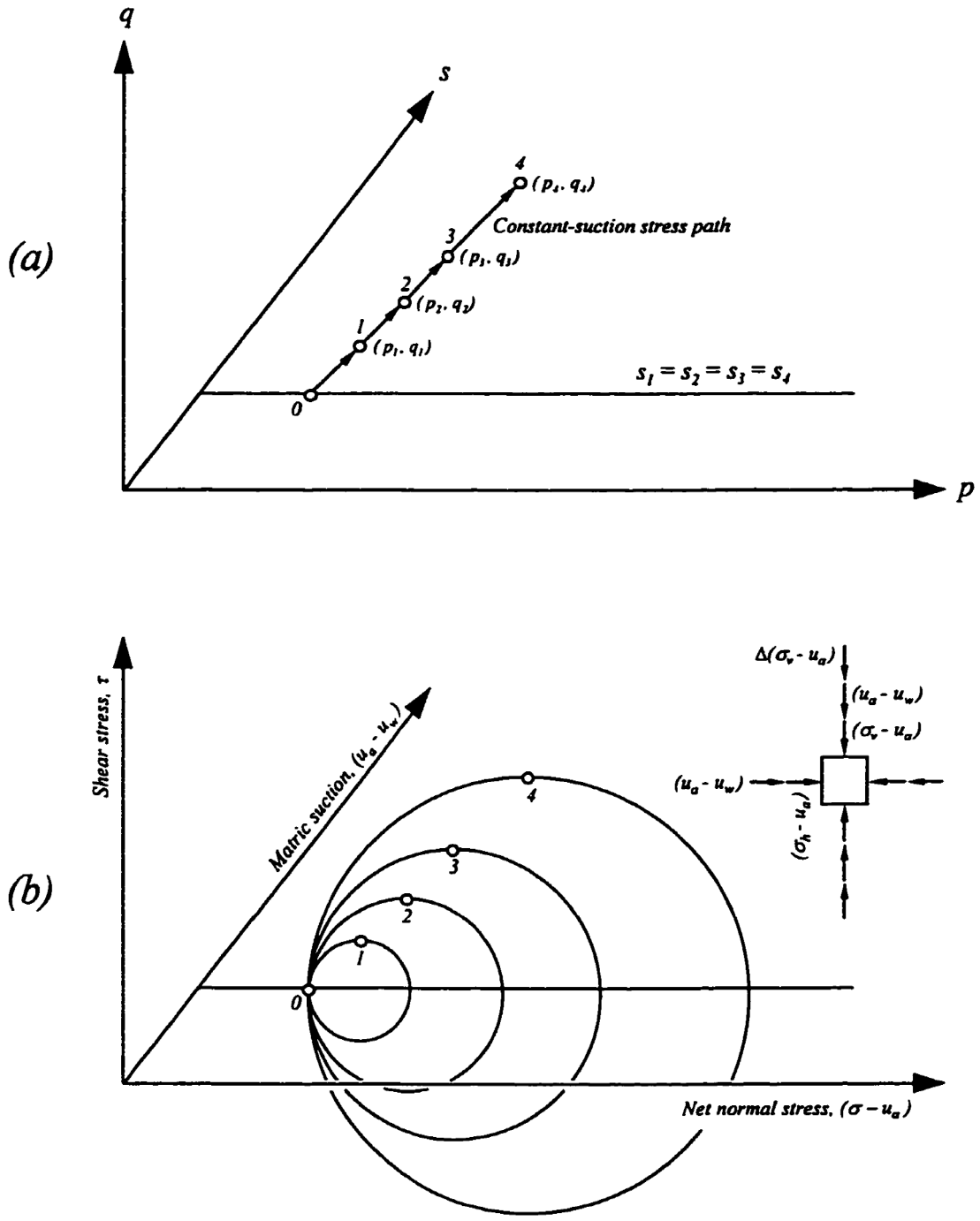

Figure 4.3 Stress path experienced by an unsaturated soil element for a series of stress states at a particular value of matric suction, $s = \left(u_a - u_w\right)$: (a) stress path in $(p:q:s)$ stress space; (b) mohr circles in $(\tau : \sigma - u_a : u_a - u_w)$ stress space (Hoyos 1998)

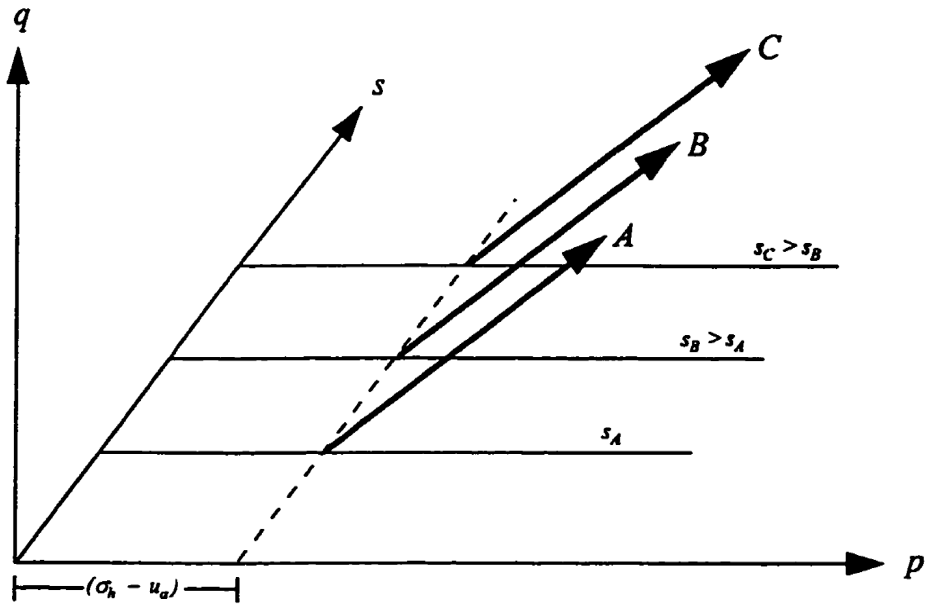

Figure 4.4 Stress paths for different matric suction values in $(p:q:s)$ stress space (Fredlund and Rahardjo 1993)

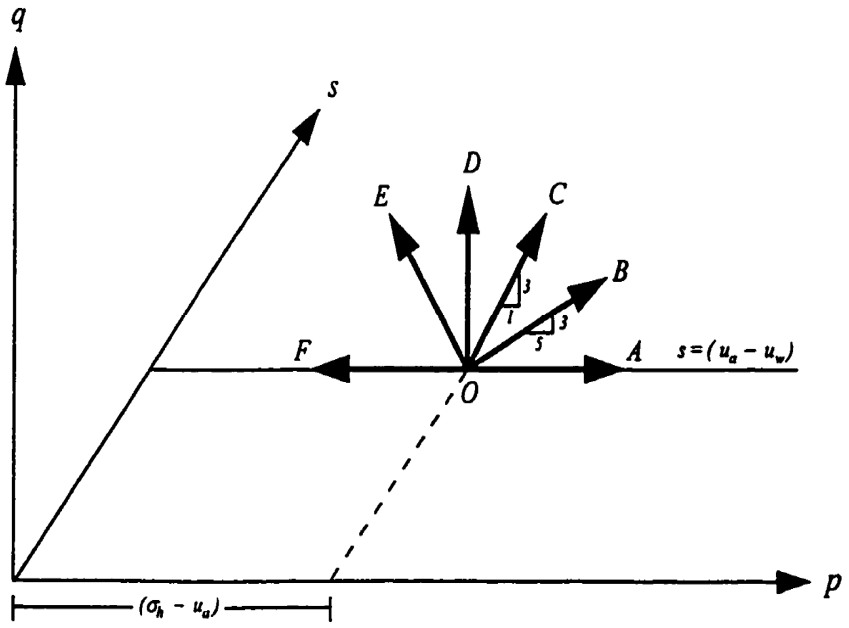

Figure 4.5 Stress paths corresponding to various p and q loading combinations at a constant value of matric suction in $(p:q:s)$ stress space (Lambe and Whitman 1979, Fredlund and Rahardjo 1993)

A schematic various stress paths in Figure 4.5 are represented in terms of the net major principal stress, $(\sigma_1 - u_a)$, the net intermediate principal stress, $(\sigma_2 - u_a)$, and the net minor principal stress, $(\sigma_3 - u_a)$ at a particular value of matric suction using a suction-controlled cubical cell testing device. For the case of constant-suction cubical cell test, the matric suction acts equally on all three principal planes (Hoyos 1998).

4.2.3 Stress Ratio

Stress ratio, b, is defined as:

$$b = \frac{(\sigma_2 - \sigma_3)}{(\sigma_1 - \sigma_3)} \tag{3.5}$$

where σ_1, σ_2 and σ_3 are the major, intermediate, and minor principal stresses, respectively (figure 4.7).

Shear tests on octahedral planes can be performed with a variety of b values. In the previous chapters, TC, SS, and TE stress paths were mentioned, and the corresponding b values of these stress paths are b = 0, b = 0.5, and b = 1, respectively. In the present work, suction-controlled TC and TE paths, which correspond to b = 0 and b = 1, respectively, were accomplished during the experimental portion of this work. Simple shear (SS) testing was out of the scope of this work due to time constraints and limitations.

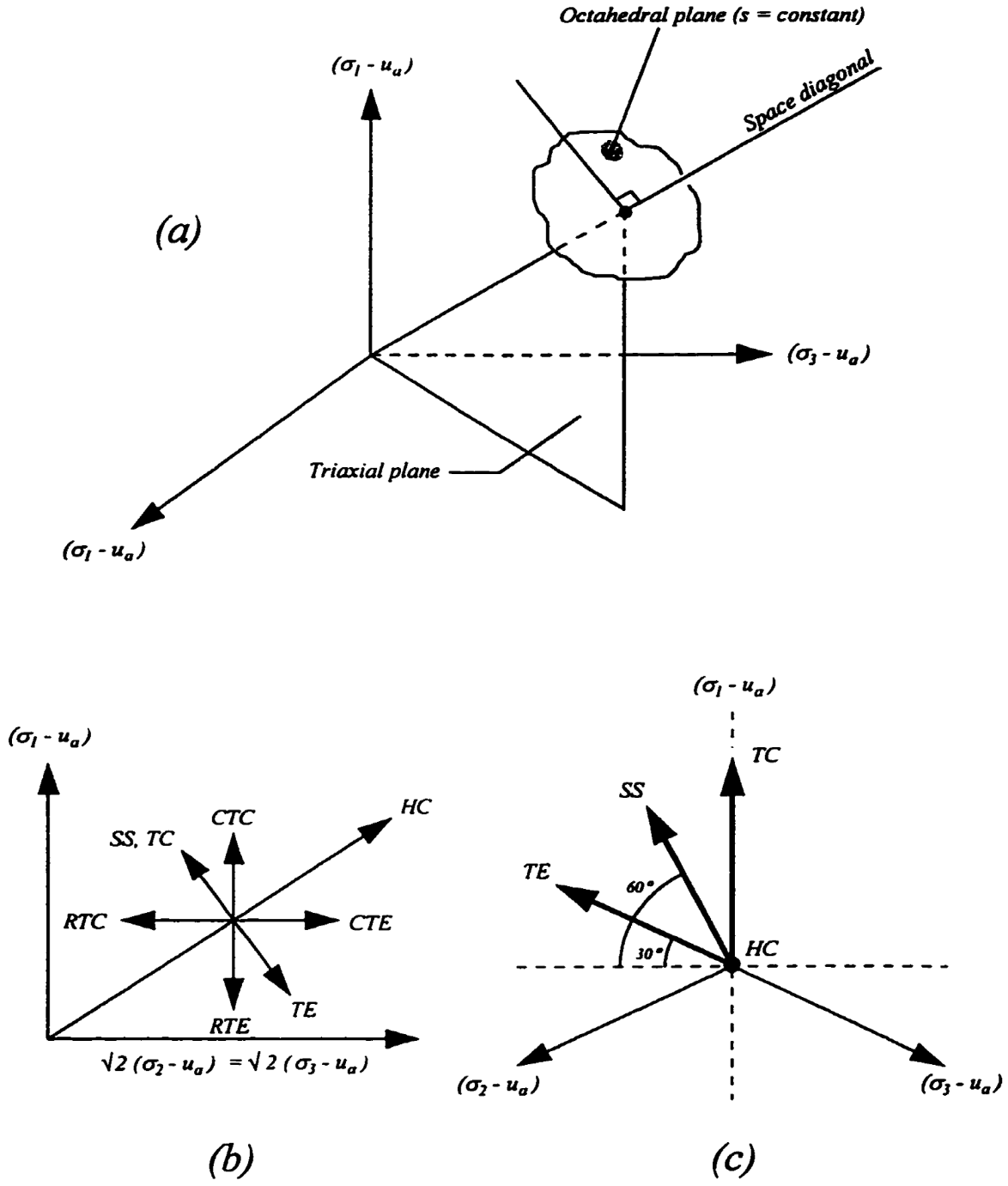

Figure 4.6 Representation of stress paths for an unsaturated soil for a constant value of matric suction: (a) net principal stress space; (b) projection on triaxial plane; (c) octahedral plane, (Hoyos 1998)

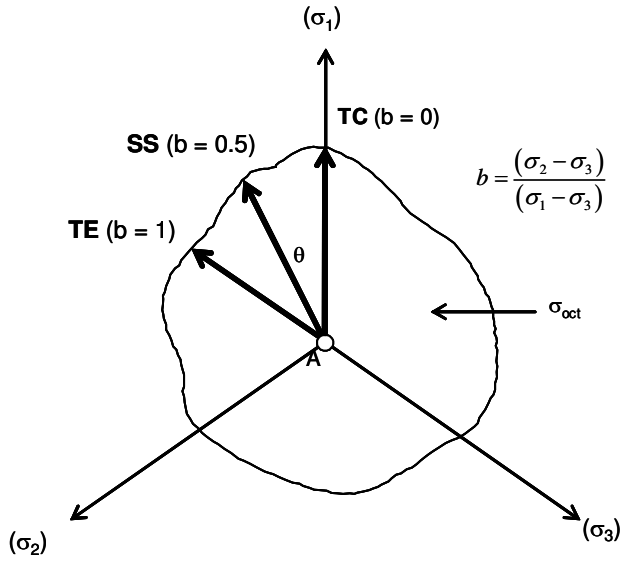

Figure 4.7 Representation of shear stress paths on octahedral plane

4.3 A Novel Suction-controlled Cubical Test Cell

The suction-controlled cubical test cell developed in this work is made up of the following nine principal components or modules: (1) core frame, (2) five wall assemblies, (3) bottom wall assembly, (4) deformation measuring system, (5) stress-control system, (6) cubical latex membranes, (6) pore-air pressure control/monitoring system, (7) data acquisition and process control system, and (8) suction-controlled control/monitoring system. A detail, illustrated description of these components follows.

4.3.1 Cubical Core Frame

The cubical core frame was machined from solid aluminum. The outside of the frame was machined to dimensions of 9.09 in, and the six inner square cavities to accommodate the membranes and to form the pressures cavities have each a dimension of 3.07 in, as show in figure 4.8. The frame supports the top and lateral wall assemblies, the soil specimen, and the

bottom assembly modified for suction-controlled testing. Each face features six connection bolts to fix the wall assemblies onto the core frame. Figure 4.9 shows the core frame along with the supporting base.

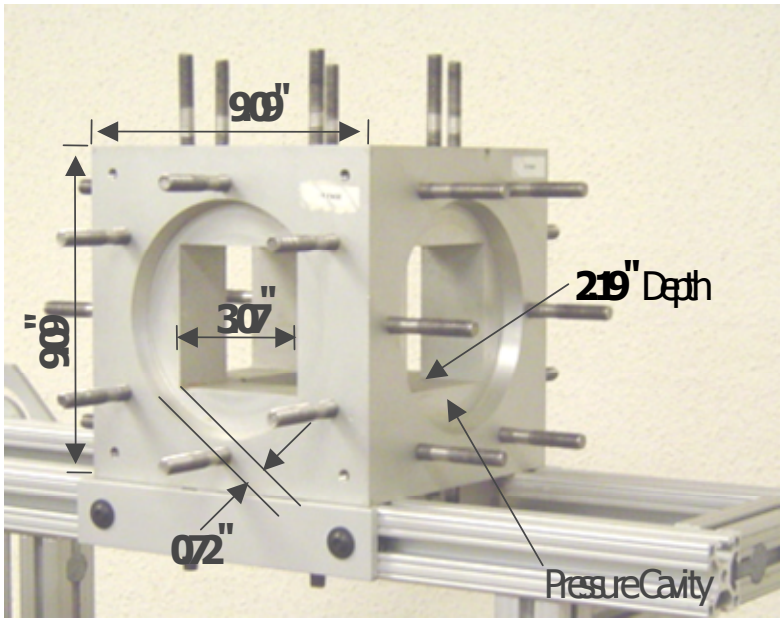

Figure 4.8 Close photograph of cubical core frame

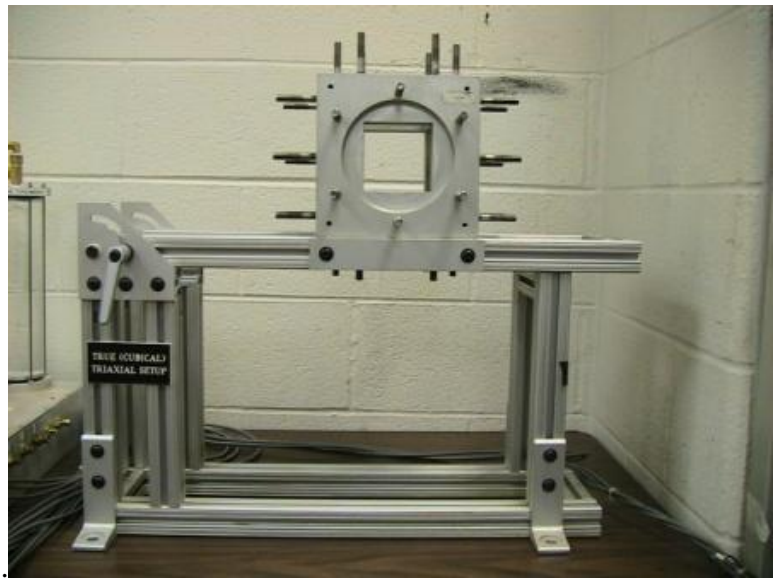

Figure 4.9 Photograph of cubical core frame

4.3.2 Top and Later Wall Assemblies

The top and later wall assemblies also were machined from solid aluminum. Each wall assembly consist of the following three components: (1) a main cover plate, (2) a pressure inlet/outlet connection, and (3) three threaded holes machined into each cover plate to receive the stainless steel housing of three linear variable differential transformers (LVDT).

When the membranes are mounted onto the frame, each assembly provides an effective seal against the leaking of the pressurized fluid (water) to the atmosphere. A gasket forms the pressure seal between the wall assembly and the reaction frame. Figures 4.10 and 4.11 show the cross sectional view and photograph of a typical wall assembly.

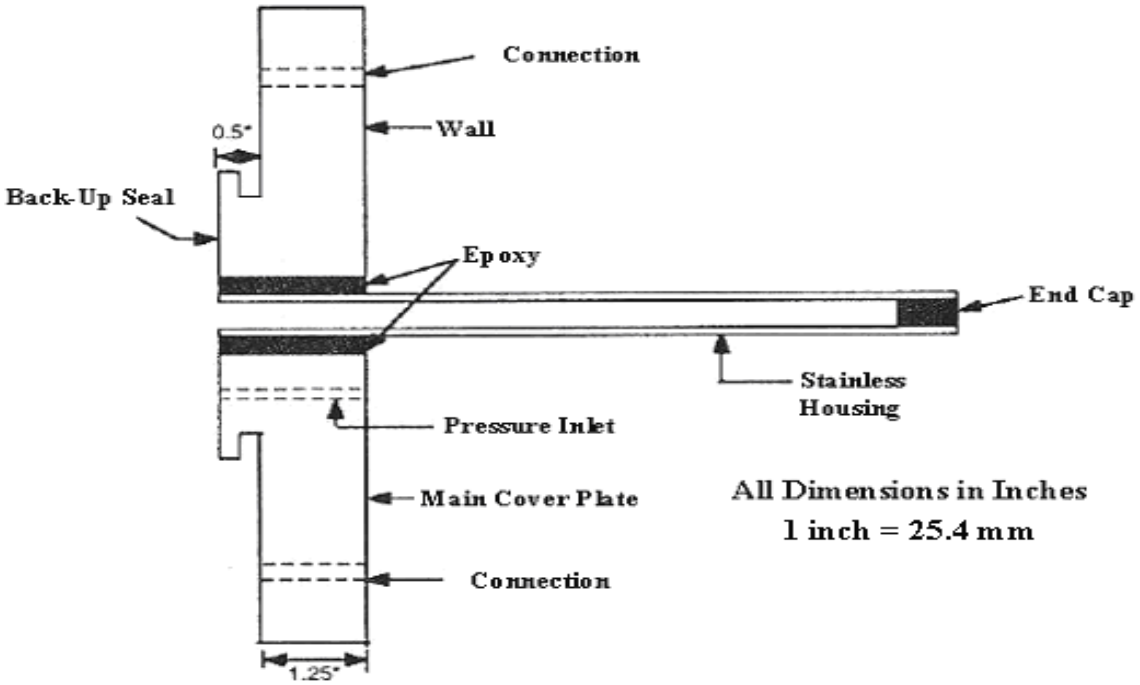

Figure 4.10 Cross-sectional view of wall assembly

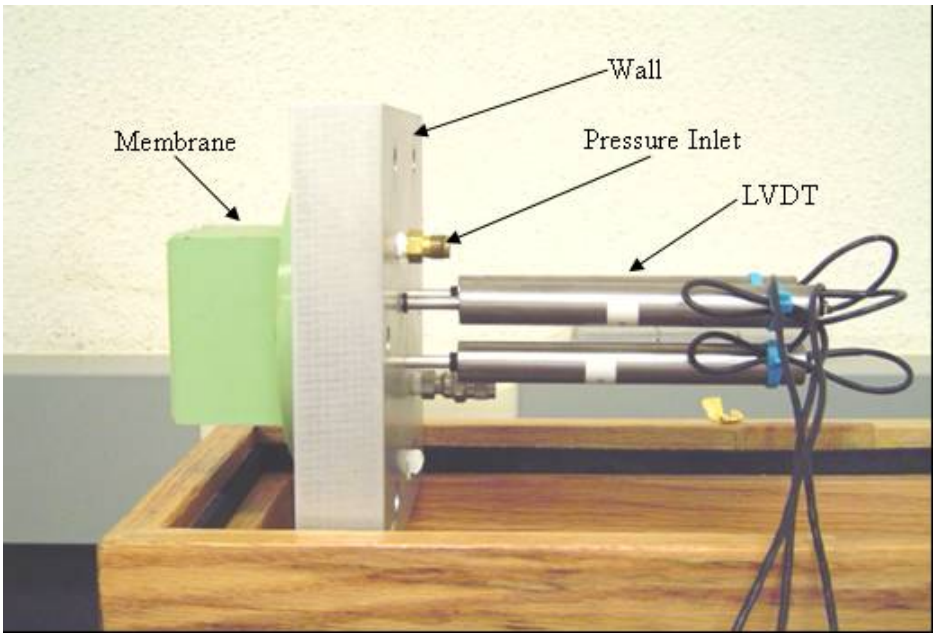

Figure 4.11 Photograph of wall assembly

4.3.3 Bottom Wall Assembly

In order to use the axis-translation technique in cubical specimens, the bottom wall assembly must be modified to control pore-air and pore-water pressures independently. The bottom wall assembly was machined from solid aluminum by Geotechnical Consulting and Testing Systems (GCTS), Tempe, Arizona.

A cubical base aluminum piece, as shown in figure 4.12, was designed to conform to the bottom square cavity of the core frame. A 0.25-in height, 2.7-in diameter cavity was machined at the center of the top surface of the cubical base aluminum piece for housing a 5-bar ceramic disk. This cavity has a grooved water compartment underneath the ceramic disk that serves as water channels for flushing air bubbles that may be trapped or have accumulated as a result of diffusion, and for a uniform distribution of the pressure applied to the pore-water via the HAE disk. The fittings for the supply of pore-water pressure consist

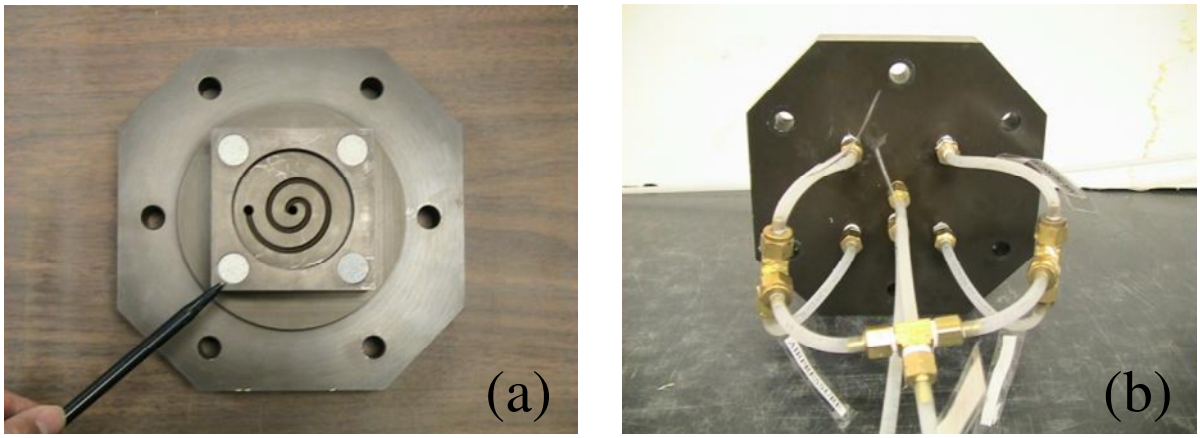

Figure 4.12 Photograph of bottom wall assembly: (a) top view; (b) suction-controlling connections

basically of two, 0.5-in diameter, nylon tubes quick-connected into the outside face of the bottom wall assembly.

In addition, four 0.75-in diameter cavities were machined on each corner of the top surface of the cubical base which pore-air pressure is supplying to the specimen to receive four symmetrically spaced coarse porous stones, through the fittings for the supply of pore-air pressure are also shown in figure 4.12(b).

4.3.4 Soil Deformation Measuring System

The axial deformation of each side of the cubical soil specimen, along a particular direction, is measured by averaging the output from three DC-type LVDTs, corresponding to the soil's face, X(+), X(-), Y(+), Y(-), or Z(+), perpendicular to that particular direction. The unsaturated soil sample is not pressurized at the bottom side, Z(-), since this side is directly in contact with the 5-bars disk, resulting in a fixed boundary. The LVDTs are located at a 120^{o} spacing on a 1.25-in radius on each of the top and four lateral wall assemblies. The core of

each LVDT and its extension rod are thrust into contact with the flexible membranes by a low-stiffness spring, as shown in figure 4.13. A data acquisition system controls and records the excitation and output of the LVDTs. Details on the data acquisition and process control system are presented later in this section.

4.3.5 Stress Application and Control System

In this study, distilled water is used as soil pressurizing fluid, which is applied via the cubical latex membranes to the top and four lateral sides of the cubical soil specimen. The water is pressurized by a 50-gallon standard air pump manufactured by Husky, which can deliver a variable output pressure up to 125 psi on each side of the soil specimen. Three independent compressed-air pressure regulators control the pressure supplied to the pressurizing fluid against the latex membranes, as shown in figure 4.14. Three DPG 500 OM model pressure transducers, manufactured by Omega Engineering, are used to measure/control the supply of air pressures up to 200 psi, which allows for the application of three independent principal stresses to the specimen. A schematic of the compressed-air pressure control system is shown in figure 4.15. Pressure regulators can be operated independently and simultaneously, which allows for any stress path application in the first octant. A Lab-View based data acquisition system can automatically record and store all transducer output.

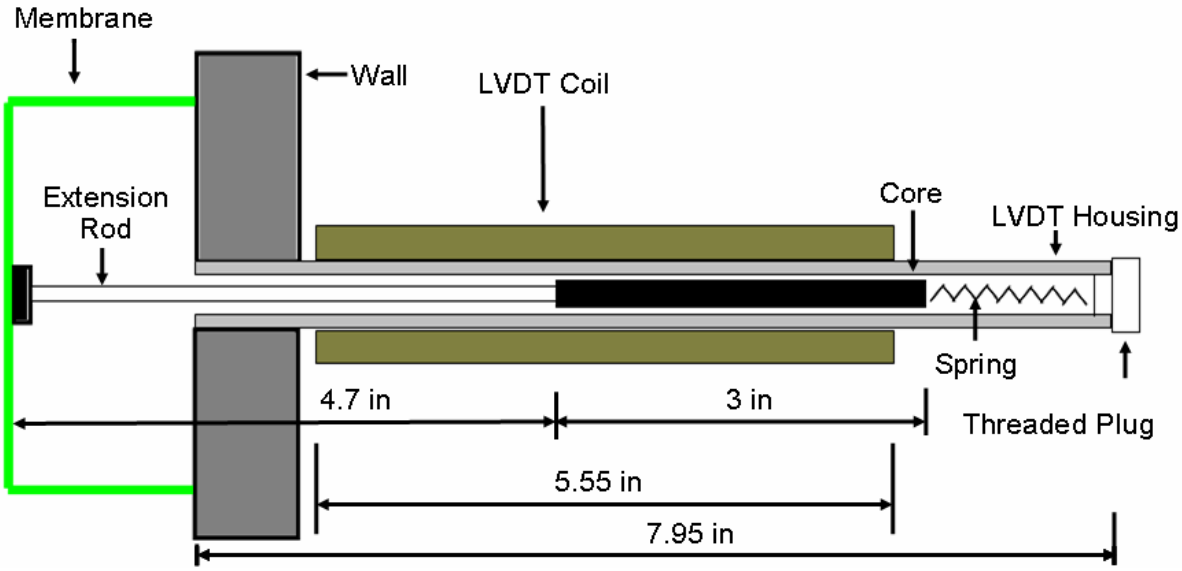

Figure 4.13 Deformation measuring system

Figure 4.14 External pressure application panel

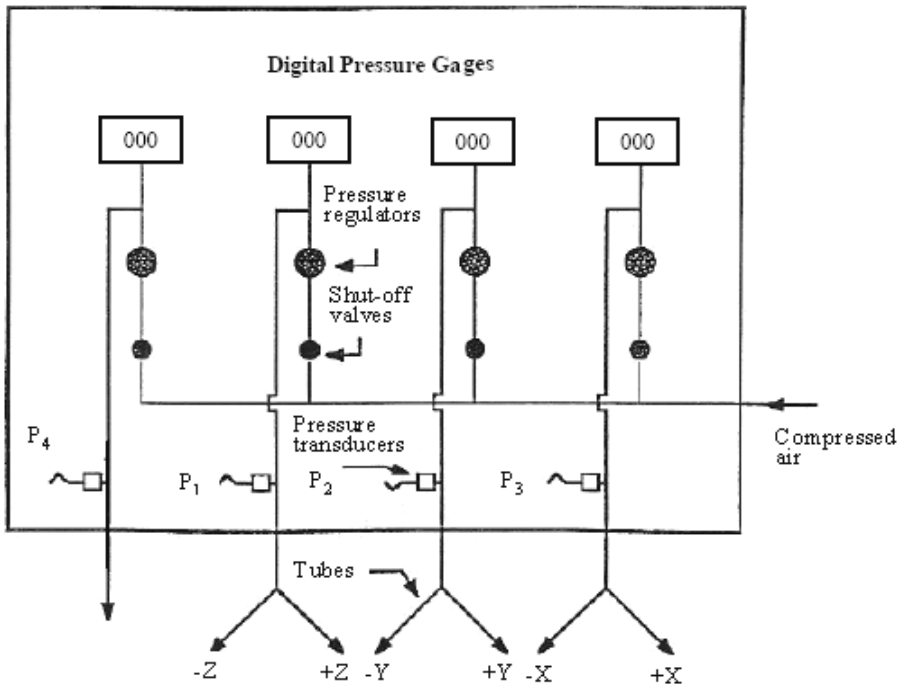

Figure 4.15 Schematic of compressed-air pressure control system layout

4.3.6 Cubical Latex Membranes

The latex membranes transmit the applied pressure uniformly to the top and four lateral faces of the cubical soil specimen. The membranes were prepared using a Dow Corning silicone rubber (i.e., Silastic J-RTV type). A silicone rubber possessing high tear strength and low stiffness were used to prepare the membranes in the laboratory. A custom-made assembly, consisting of top and bottom molds machined from aluminum to conform to the design dimensions of the membranes, was used. The silicone rubber and curing agent were mixed to a uniform consistency and transferred in the bottom mold for curing and de-air processing in a custom-made vacuum chamber for approximate 2 hours, as shown in figure 4.16. After curing and de-air process, the top mold was carefully bolted, and the mixture was

allowed to cure for 24 hours in the mold. The fabricated membrane was then gently removed from the mold and stored in a 100% humidity room.

4.3.7 Data Acquisition System

An automated data acquisition system was assembled to control the external pressures applied to the specimen and to monitor and store its resulting deformation captured by the LVDT's. Figure 4.17 shows the schematic of the data acquisition system layout. A PCI-6603E direct interface card (from National Instruments) is plugged in the CPU of the based computer, as shown in figure 4.18. The analog input signals (Voltage) delivered by the LVDT are converted into digital signals by an analog-to-digital converter (SCB-100 from National Instruments) connected to the direct interface card (PCI-6603E from National Instruments). For signal conditioning, DC Power Supply (6303D from Topward) was used. The data acquisition can handle the 18 LVDTs for deformation and 3 pressure transducers for

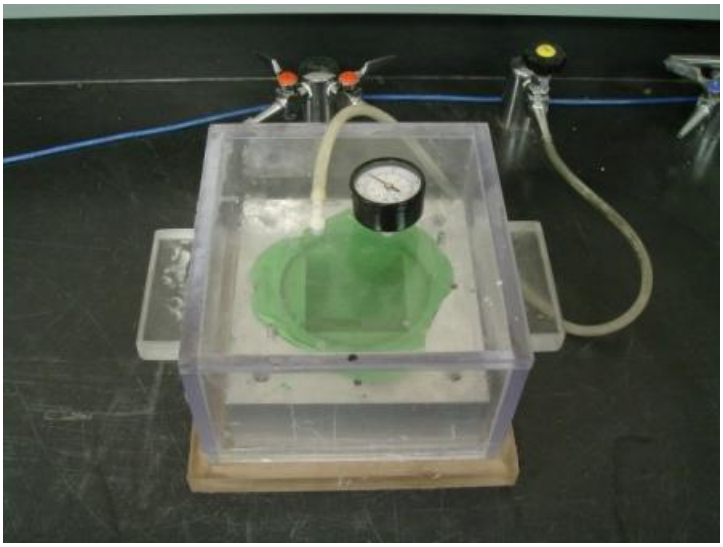

Figure 4.16 Photograph of vacuum chamber and bottom mold

principal stresses. The raw data (output voltages) was calibrated by using Lab-view 7.0 computer software (from National Instruments).

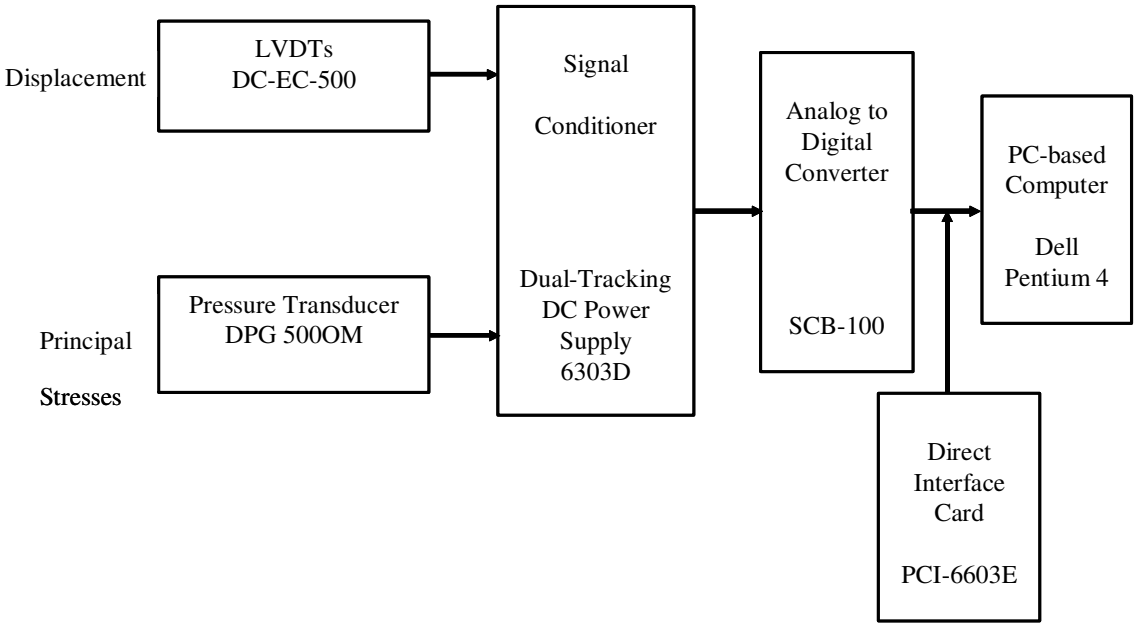

Figure 4.17 Schematic of data acquisition system layout

Figure 4.18 Photograph of soil pressure/deformation data acquisition system

4.3.8 Suction Control/Monitoring System

A PCP-5000-UNSAT pressure control panel, manufactured by Geotechnical Consulting and Testing Systems (GCTS), Tempe, Arizona, was used for control and monitoring of suction states in the soil during true triaxial testing, as show in figure 4.19. The PCP-5000-UNSAT pressure control panel is able to control both air and water pressure/volume simultaneously. The pore-air pressure is supplied at the bottom of the specimen via a full set of air-pressurized manifolds with nylon tubing connected to the PCP-5000-UNSAT pressure control panel, as shown in figure 4.19a. Pore-water pressure can also be applied and controlled at the bottom of the specimen through the 5-bar ceramic disk. Water pressure is also supplied via nylon tubing from the PCP-5000-UNSAT pressure panel, as shown in figure4.20. Figure 4.21 shows a schematic of the PCP-5000-UNSAT pressure control system layout.

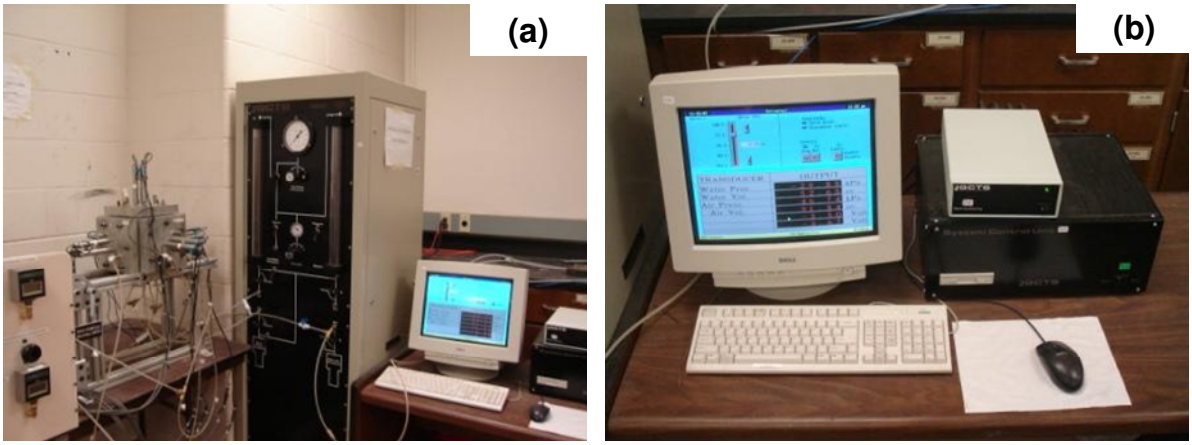

Figure 4.19 PCP-5000-UNSAT pressure control panel: (a) panel interacting with cubical cell; (b) computer, servo amplifier, and signal conditioning hardware

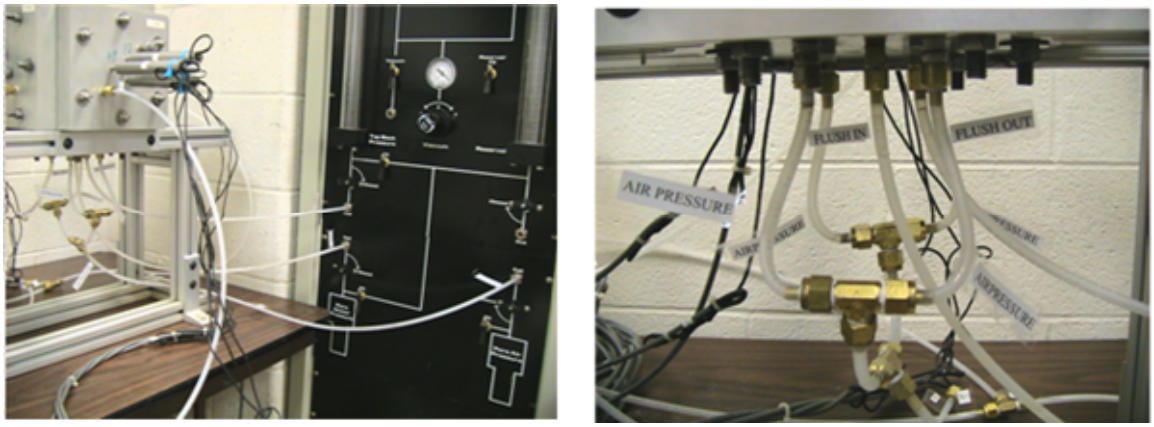

(a) (b)

Figure 4.20 Suction-controlled mechanism: (a) cubical cell interacting with PCP-5000-UNSAT panel; and (b) pore-air pressure, pore-water pressure, and flushing systems

In this research work, the input pore-air pressure value ($s=u_a$) is converted into a digital signal. The digital signal is then converted into analog (volts) by a digital-to-analog board (figure 4.21). The analog pore-air pressure signal is then delivered to a servo amplifier. This novel system has been successfully utilized in cylindrical cells, and it features pressure/volume control cell pressure, pore/back pressure, pore-air pressure (u_a) with 2 MPa (300 psi) pressure range, and 300 cc (18 in^3) volume capacity. It also includes hydraulic servo valves, electro-hydraulic pump, pressure transducers with 0.1 kPa (0.02 psi) resolution, and specific water volume ($v_w = 1+eS_r$) change transducer with 0.01 cc resolution.

4.4 Saturation of HAE Ceramic Disk

A procedure similar to that suggested by Bishop and Henkel (1962) and Fredlund (1973), to ensure proper saturation of a HAEV disk, was adapted to the working conditions of the 5-bar disks in the modified test cell. The same approach was successfully used by Hoyos (1998).

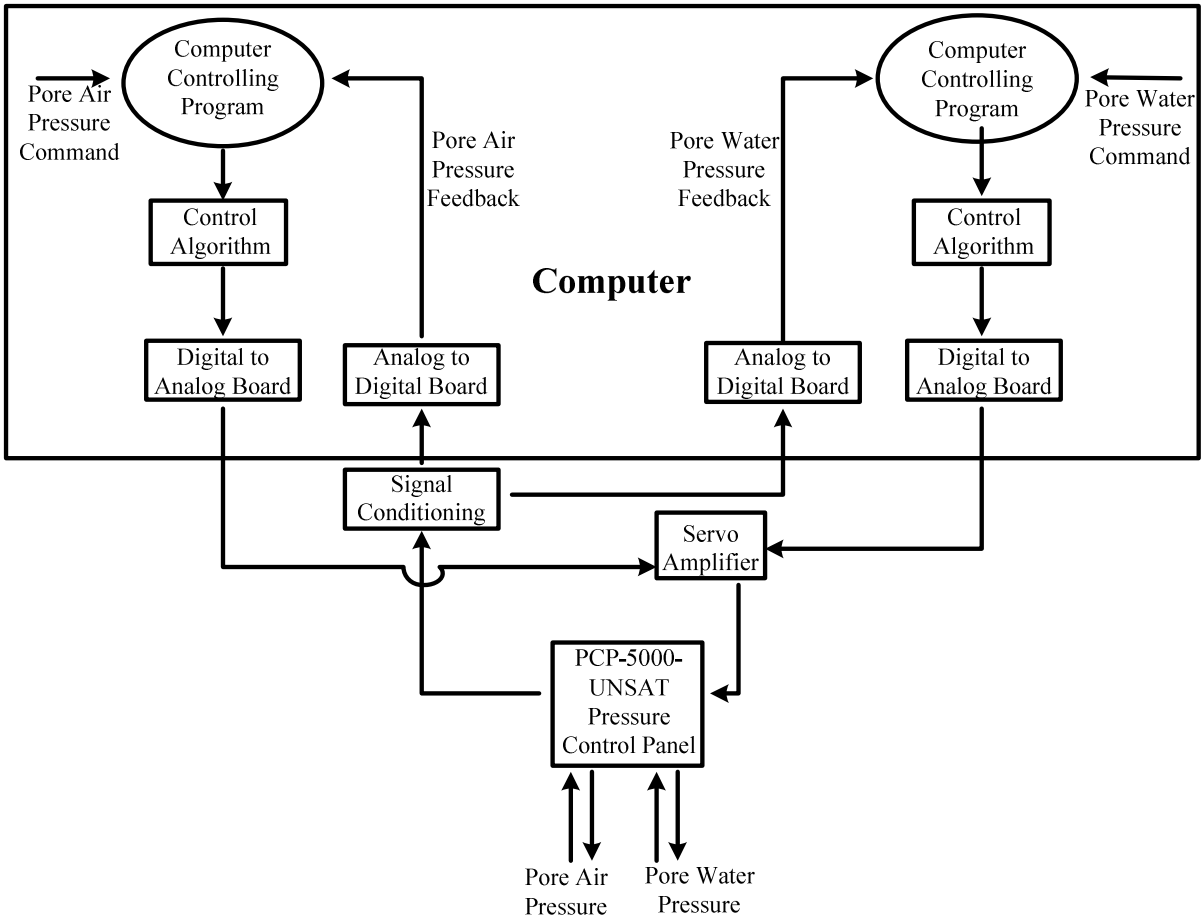

Figure 4.21 Schematic of suction control system layout

A custom-made saturation chamber, made of high burst-resistance acrylic and capable of housing up to three HAE ceramics at the same time, was designed and utilized for saturation of the 5-bar ceramics used in this work, as shown in figure 4.22.

After the 5-bar ceramics are fully sealed and set into place, the inner cavity of the assembled saturation chamber is filled with distilled, de-aired water to a height of about 25 mm (1 in) above the disks. The water is poured into the cavity using a pipette to minimize the generation of air bubbles.

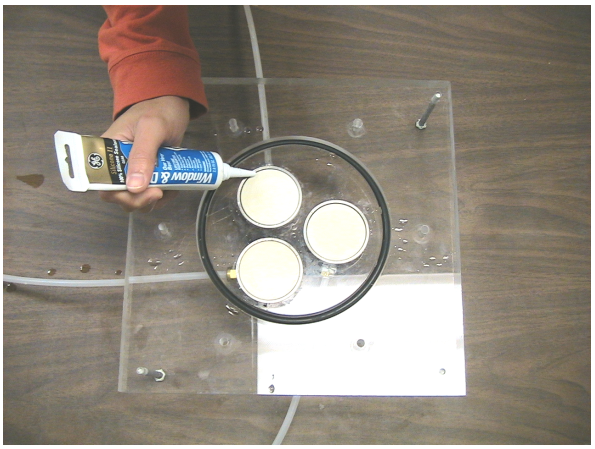

Figure 4.22 Bottom plate of custom-made chamber housing three 5-bar disks

.

Once the cavity is partially filled with water and the top plate of the chamber is set into place, the water film is subjected to an air pressure of 600 kPa (87psi), as shown in Figure 4.23. The water is then allowed to flow through the disks under this constant pressure until air in the disks dissolves in the grooved, saturated compartments underneath them.

4.5 Specimen Preparation Technique

Poorly graded silty sand was used for suction-controlled testing in this research work. After saturation of the 5-bar disk, the bottom and the four lateral wall assemblies are then set into place. A typical 3-in (7.5-cm) side, cubical specimen is then prepared in-place using a combined pluviation-tamping compaction process, as shown in figure 4.24.

The specimen is prepared in approximately eight pluviated layers, with each layer compacted at a target moisture content 4% greater than standard Proctor optimum. Tamping corresponds to a compactive effort considerably less than that of standard Proctor compaction. The intention is to reproduce specimens with low preconsolidation stress values, so that, subsequently, it is relatively feasible to reconsolidate the soil to a virgin state. A

custom-made, 0.01-in thick, stainless steel shaft introduced into the cubical cavity of the frame facilitates the pluviation-tamping compaction process for each layer (figure 4.24).

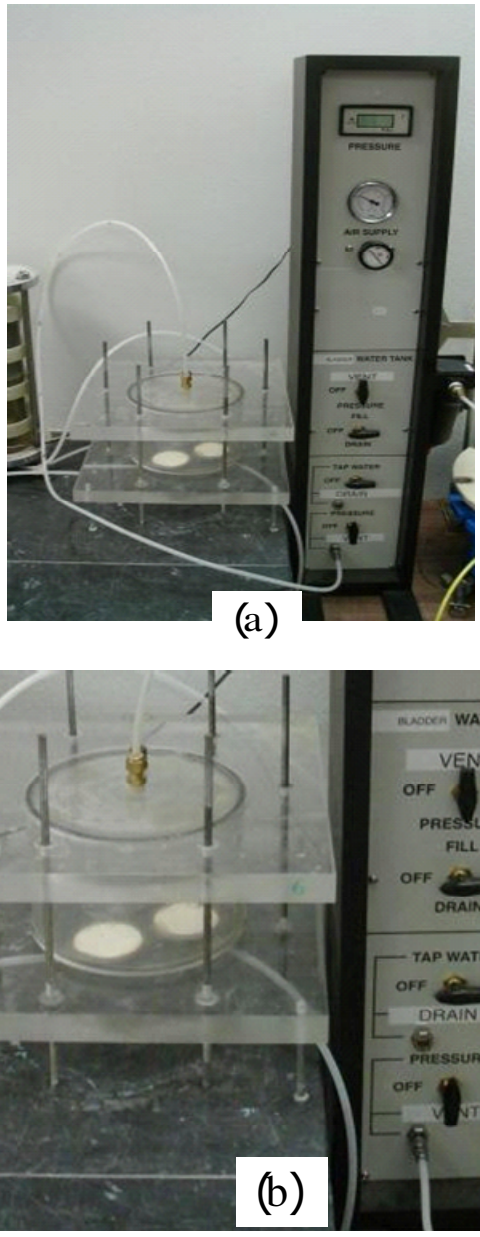

Figure 4.23 Saturation process of 5-bar ceramic disks: (a) HEAV saturation setup; (b) close up photograph of custom-made saturation chamber

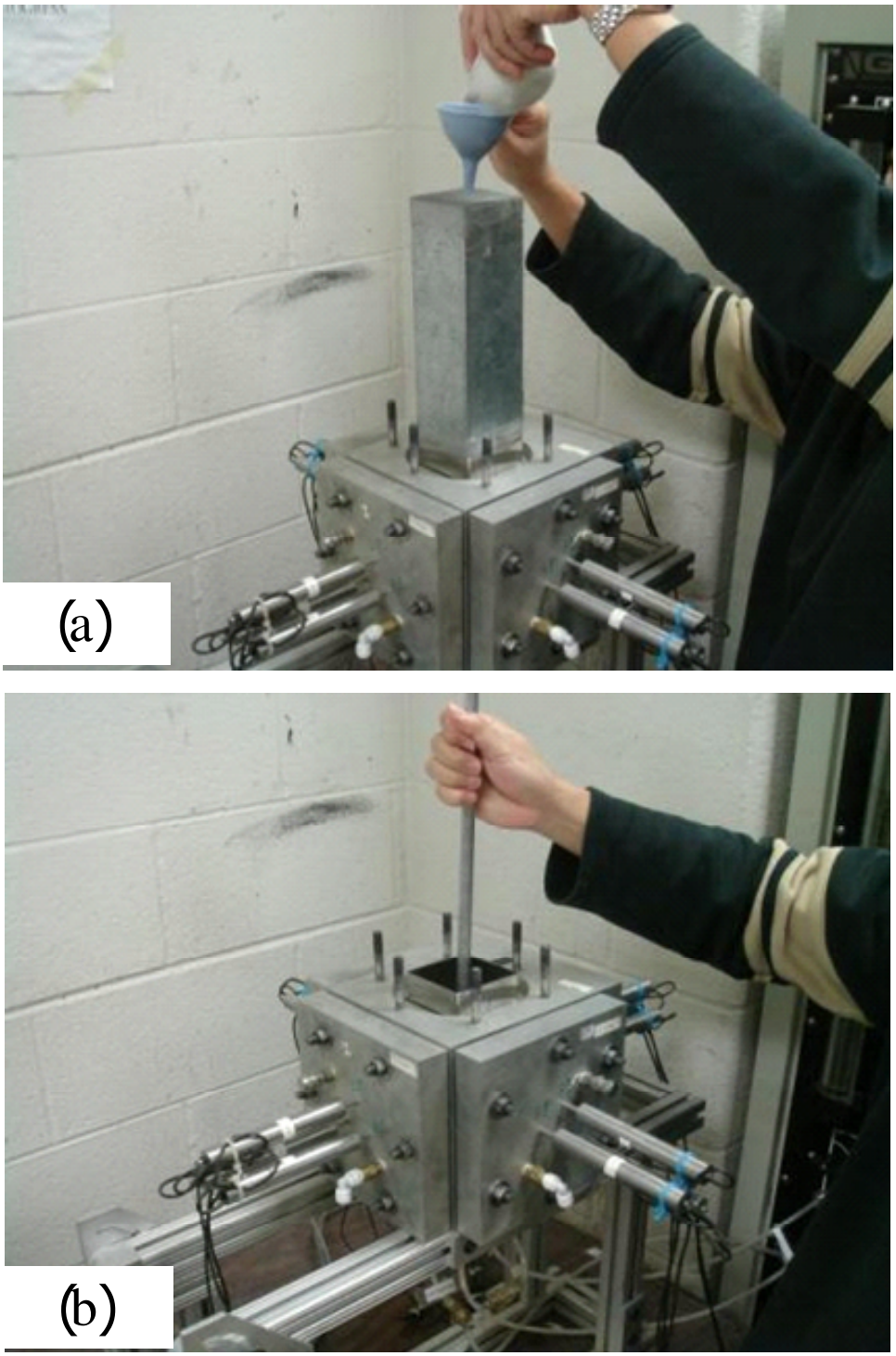

Figure 4.24 In-place combined pluviation and tamping compaction process: (a) pluviation process; (b) tamping compaction process

Upon completion of the soil compaction process, the pluviation mold is gently removed and the top assembly of the cell, as well as the remaining components and connections for external stress and suction state applications, are set into place.

4.6 Assessing Feasibility of Axis-Translation Technique

To verify consistency in the application of the axis-translation technique using the new cubical cell, a series of suction-controlled test trials were first conducted to ensure reproducibility of suction states via the soil water characteristic curve of silty sand used in this work. Specimens were brought, via axis-translation, from an initial matric suction state corresponding to a 11.5% moisture content to different target values of applied matric suctions ($s=u_a$). Once no further water-volume change was detected from the sample, the final moisture content of the specimen was measured and the corresponding value of matric suction assessed from the soil water characteristic curve, which was obtained via pressure plate testing, as shown in figure 4.25. Result from 8 trial tests are summarized in table 4.1, which show the feasibility of the axis-translation technique in the cubical apparatus.

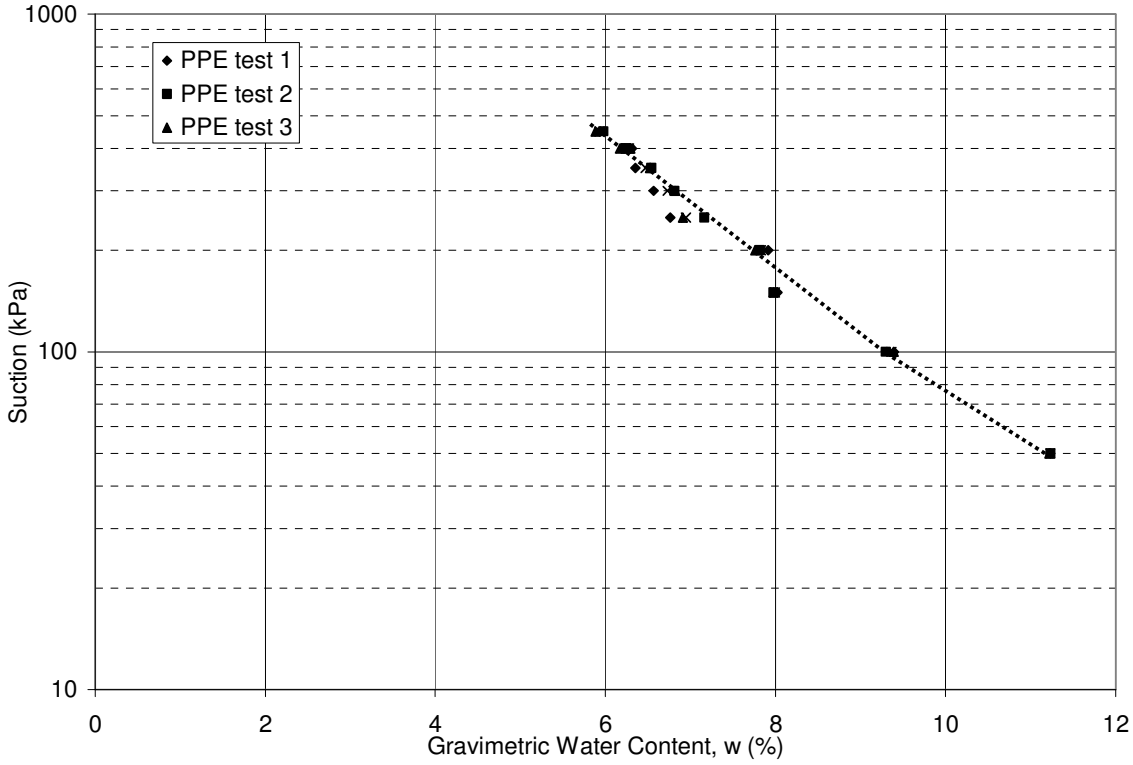

Figure 4.25 Soil water characteristic curve (SWCC) of silty sand from three trail pressure plate tests

Table 4.1 Feasibility of axis-translation technique

Test	Initial Water Content (%)	Applied Matric Suction, $s = u_a$ (psi)	Final Water Content (%)	SWCC Assessed Matric Suction (psi)	Percent Difference in Matric Suction (%)
1	11.5	7	11.25	7	0.0
2	11.5	7	11.21	7	0.0
3	11.5	14	9.4	14.2	1.5
4	11.5	14	9.36	14	0.0
5	11.5	29	7.9	29.2	0.7
6	11.5	29	7.85	29	0.0
7	11.5	44	6.81	44.3	0.7
8	11.5	44	6.63	43.8	-0.7

4.7 Summary of Assembling Process

The step-by-step procedure for the complete assemblage of the testing setup is summarized and illustrated in the following.

(1) The fully saturated HAE disk is installed into the bottom wall assembly using a custom-made disk inserter, as shown in figure 4.26. GE silicone is used for sealing of ceramic disk. A sintered stainless steel ring facilitates the sealing of the ceramic, as shown in figure 4.27. The silicon is allowed to cure for 24 hours.

(2) The bottom wall assembly, contained the HAE disk, is then assembled onto the core frame, as shown in figure 4.28. An impact socket wrench is used to fully tighten the wall assembly onto the frame.

(3) The thin-walled pluviation shaft is then installed for specimen preparing process, as shown in figure 4.29, and all the lateral wall assemblies are fully assembled afterwards, as shown in figure 4.30. The soil specimen is then prepared as explain in section 4.5.

(4) After the combined pluviation-tamping process is completed, the thin-walled shaft is gently is removed and the top wall assembly is set into place, as illustrated in figures 4.31 and 4.32, respectively. At this point, the soil is ready for testing.

(5) The inlet/outlet hoses of the external pressure system are then connected to the top and four lateral wall assemblies, as shown in figure 4.33.

(6) The pore-air and pore-water pressure lines of the suction-controlled system are then connected to the PCP-5000-UNSAT pressure control panel from the bottom wall assembly, as shown in figure 4.34.

(7) The complete test layout is shown schematically in figures 4.35 and 4.36. A panoramic photograph of the complete setup is shown in figure 4.37.

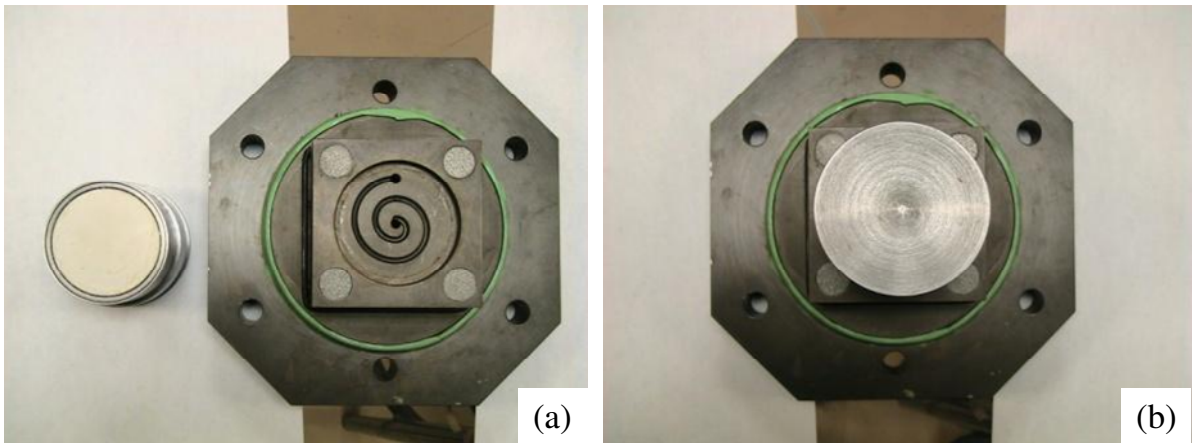

Figure 4.26 Installation of ceramic disk: (a) bottom wall assembly and custom made HAE disk inserter; (b) insertion of previously saturated 5-bar ceramic into bottom wall assembly via custom-made disk inserter

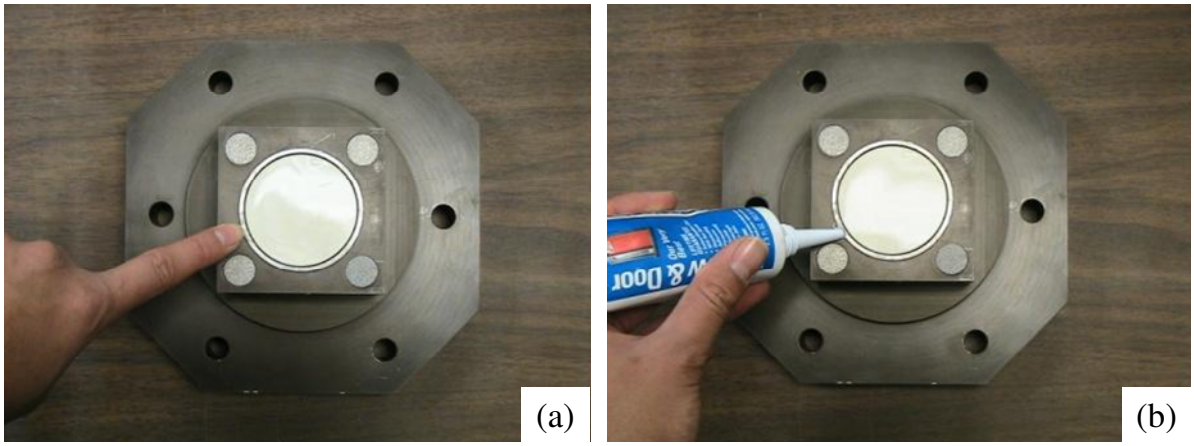

Figure 4.27 Ceramic sealing process (a) bottom wall assembly with 5-bar ceramic; (b) sealing of 5-bar ceramic

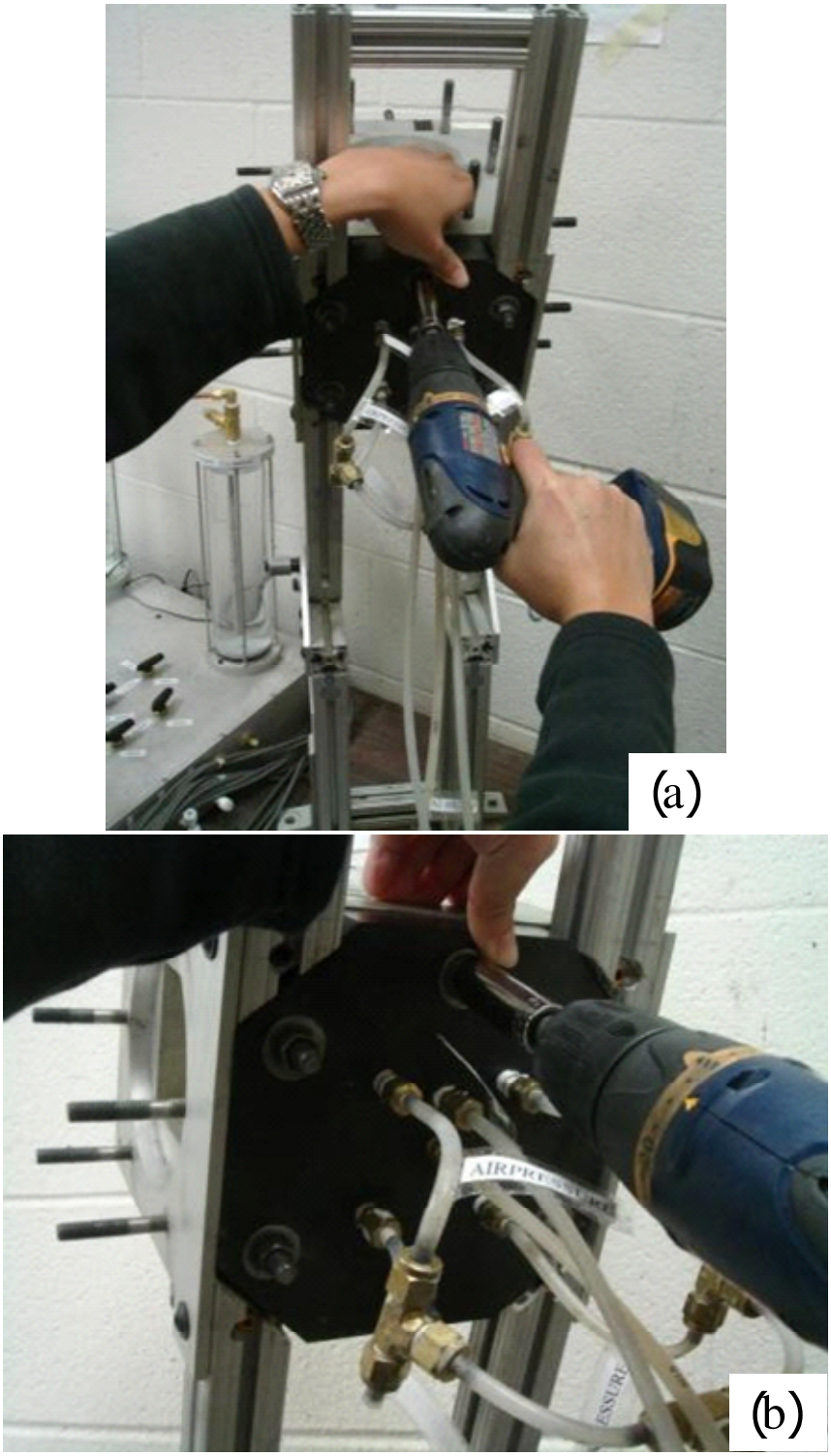

Figure 4.28 Bottom wall assembly installation: (a) assembling process; (b) close up photograph

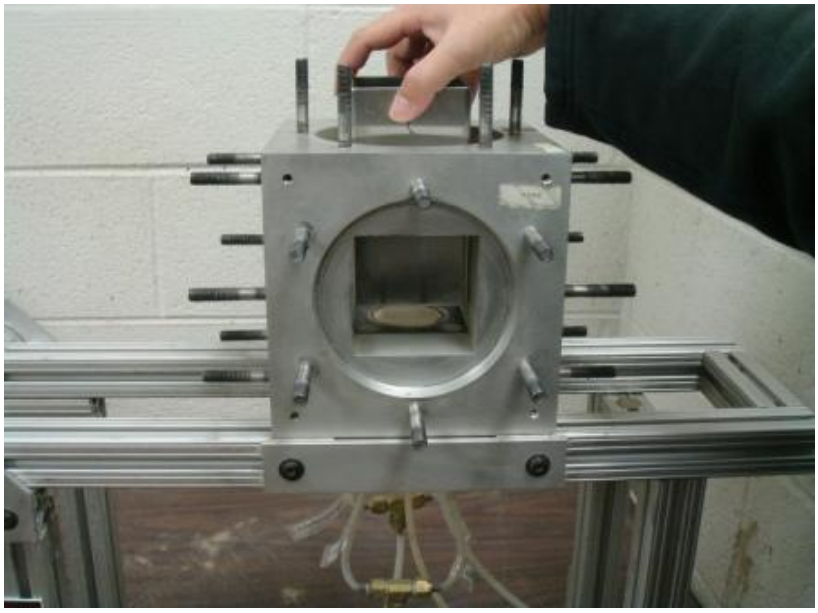

Figure 4.29 Installation of thin-walled pluviation shaft

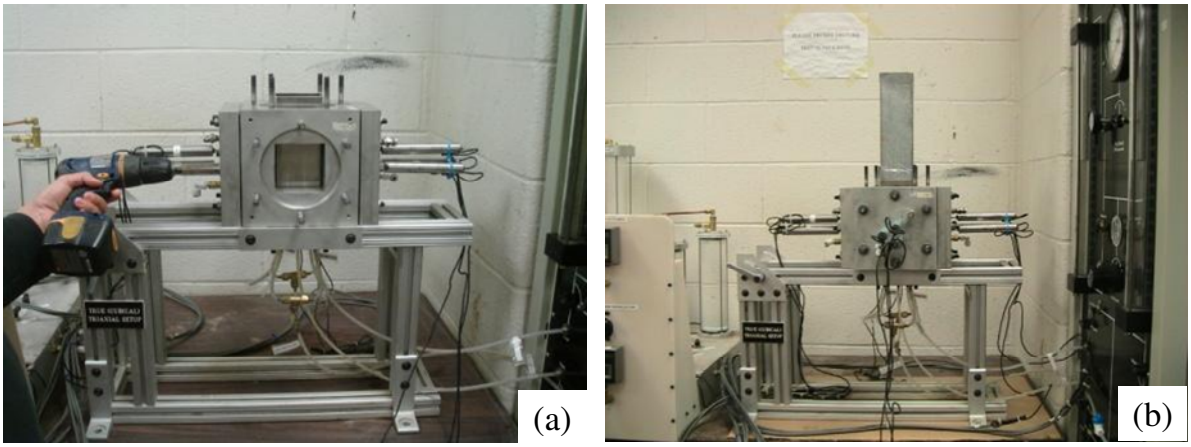

Figure 4.30 Lateral wall assemblies installation: (a) assembling process; (b) partially assembled cell with pluviation shaft

Figure 4.31 Removal of thin-walled pluviation shaft

Figure 4.32 Top wall assembly installation

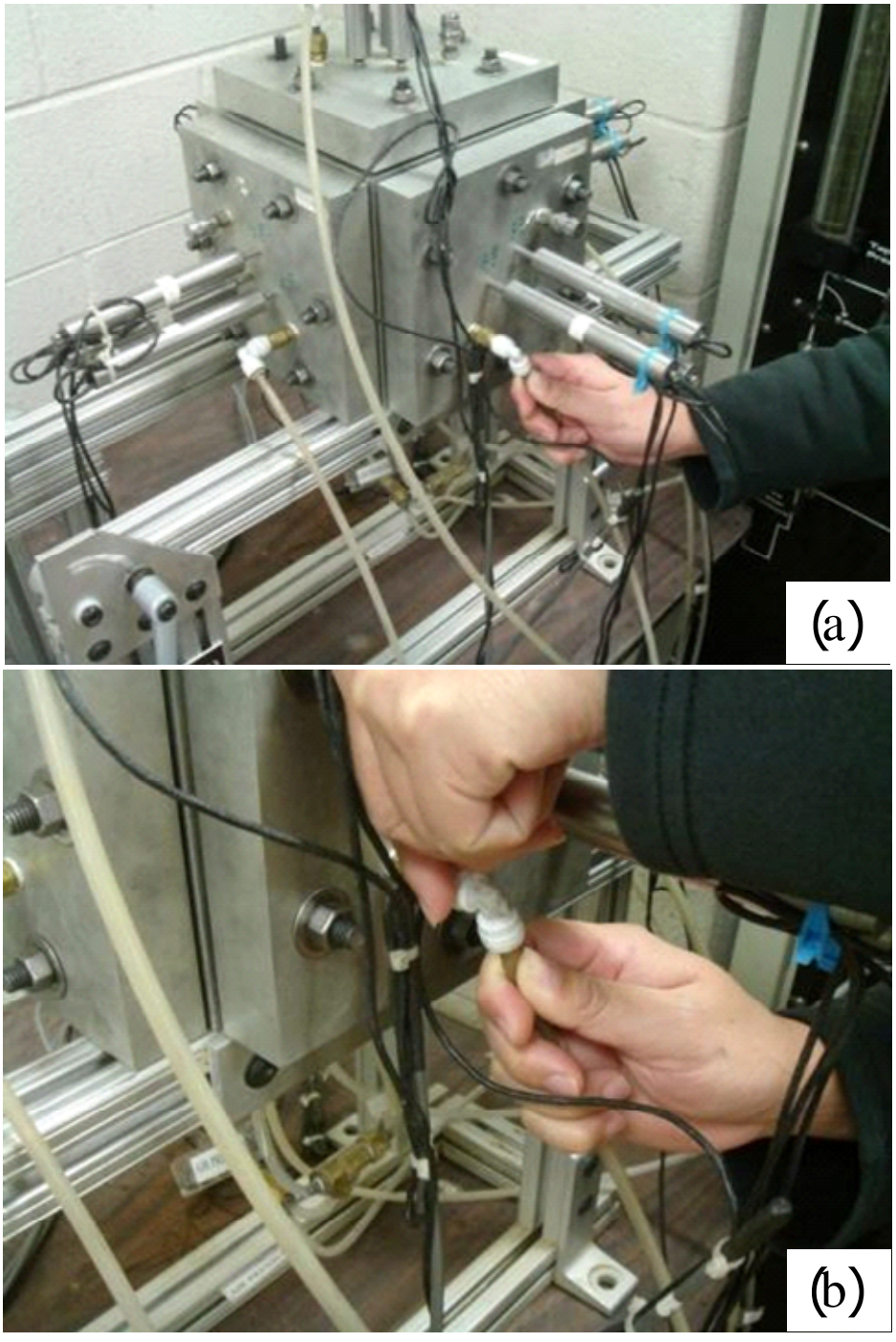

Figure 4.33 Assembling of pressure inlets/outlets: (a) installation process; (b) close-up photograph

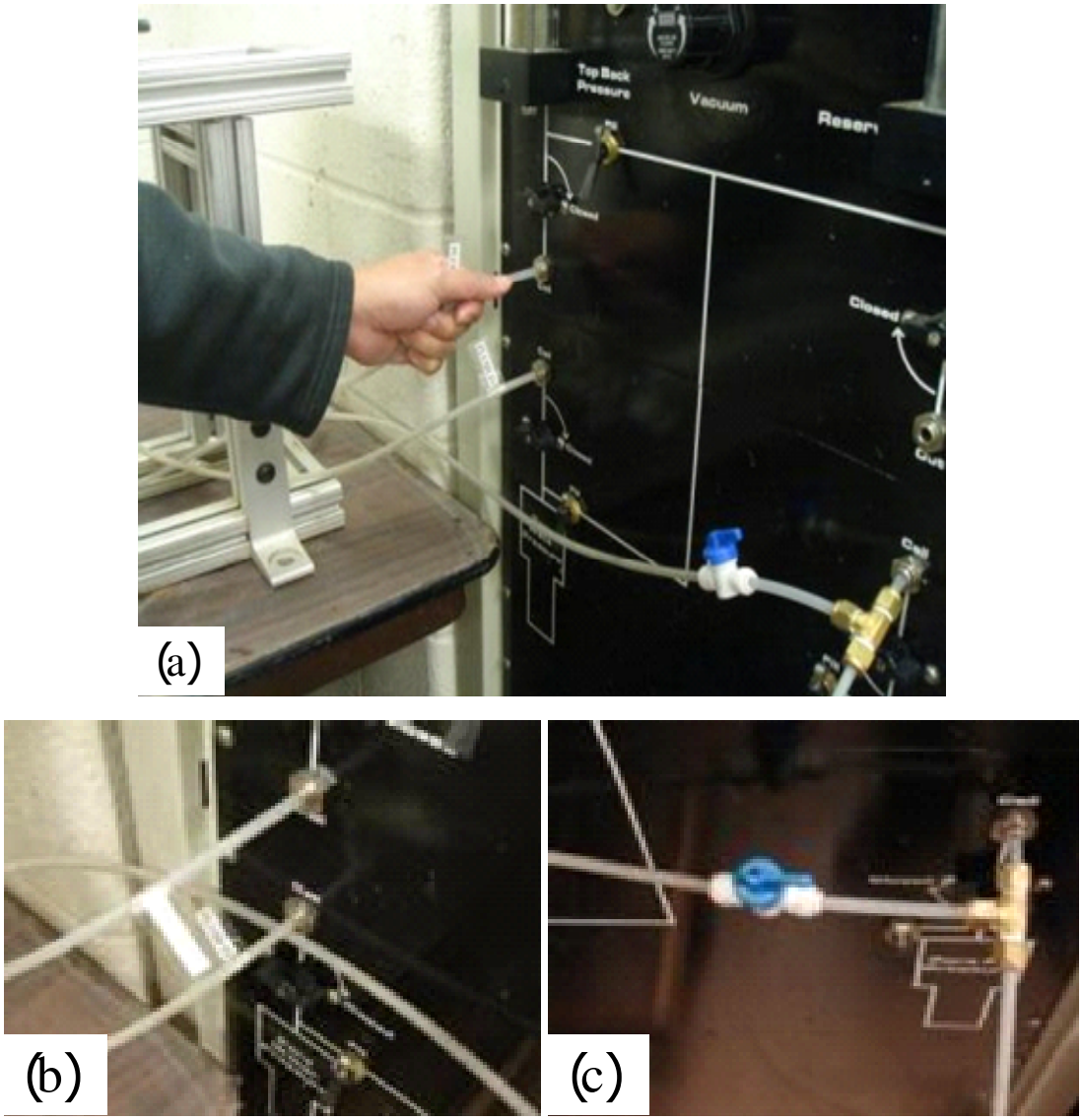

Figure 4.34 Assembling of suction-controlled system: (a) connection of water lines; (b) water and flushing line connections; (c) air line connection

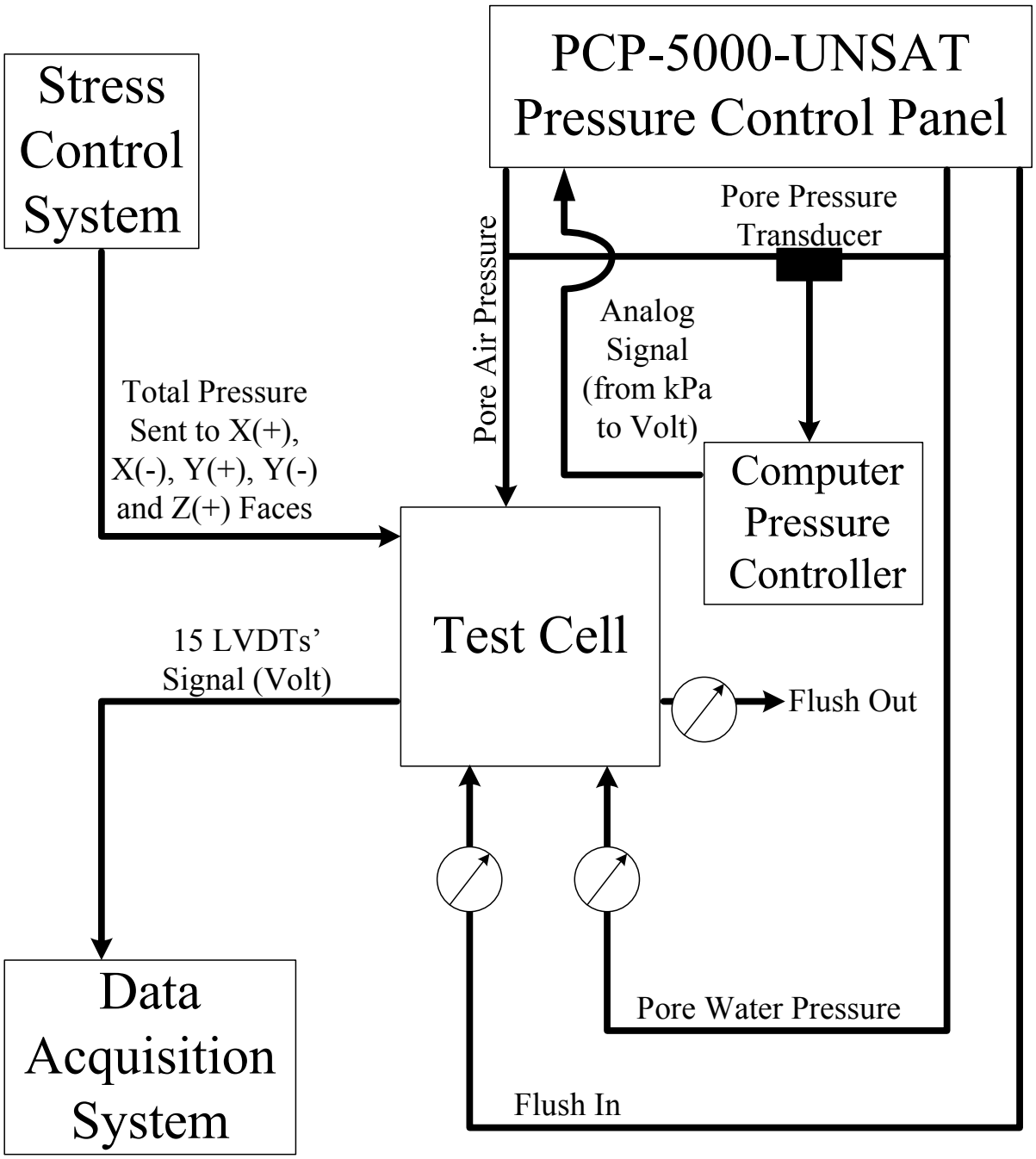

Figure 4.35 Schematic of complete test layout

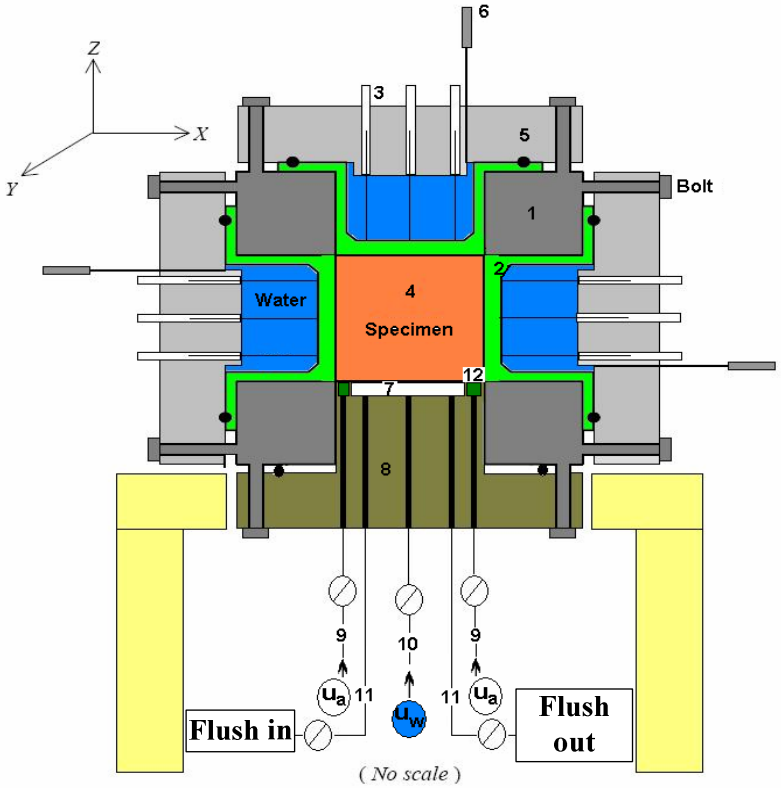

1. Frame **5. Top/Lateral Walls** **9. Air-Pressurized Nylon Tubing**

2. Latex Membrane **6. External Pressure Inlet/Outlet** **10. Water-Pressurized Nylon Tubing**

3. LVDTs (3/Face) **7. 5-Bar HAE Ceramic** **11. Flushing System**

4. Soil Specimen **8. Cubical Base Piece** **12. Coarse Porous Stones**

Figure 4.36 Schematic of fully assembled cubical test cell (cross-sectional view)

4.8 Repeatability of Suction-Controlled Testing

The suitability of the axis-translation technique, for testing cubical unsaturated soil specimens in the cubical device implemented in this research work, was also experimentally validated through a series of repeatability tests.

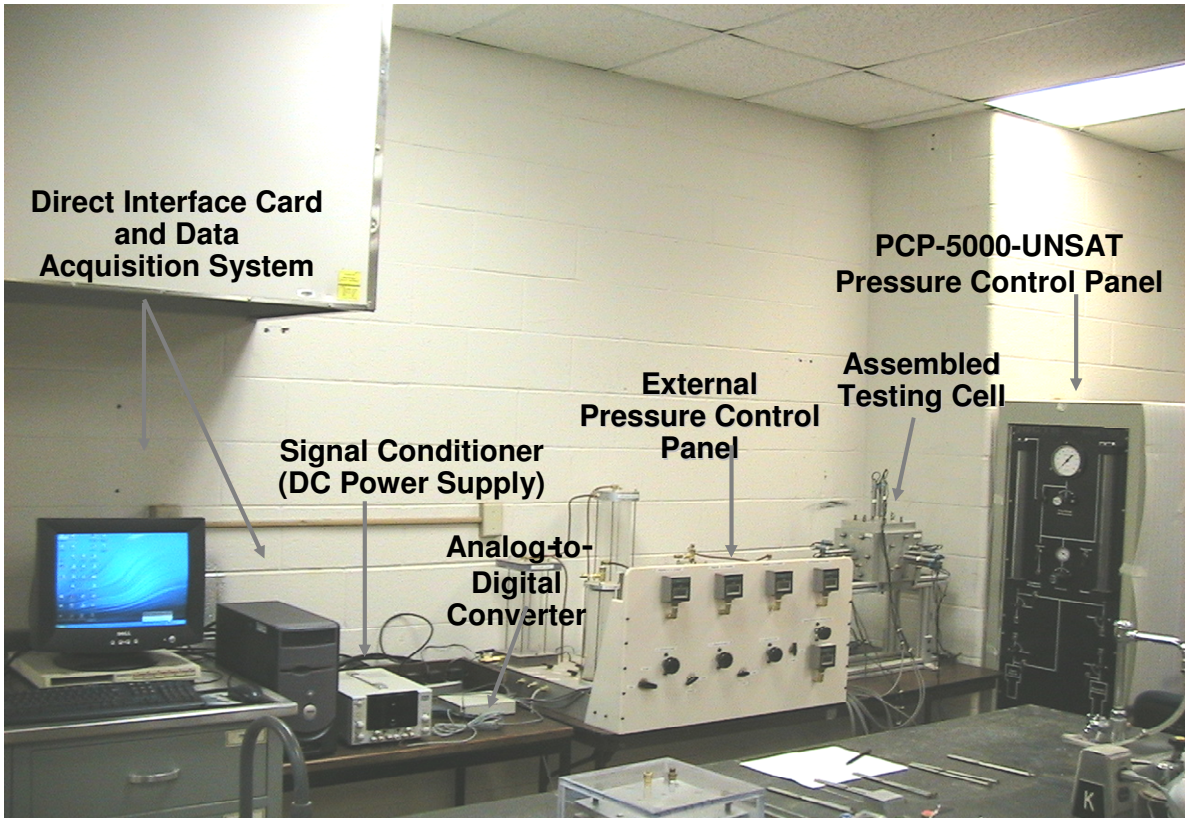

Figure 4.37 Panoramic view of complete test setup

A series of 2 suction-controlled hydrostatic compressions (HC) tests on clean sand were conducted in the cubical cell from a net mean pressure, p_{net}, of 7 kPa (1 psi) to 250 kPa (25 psi) under constant matric suction of 50 kPa (7 psi). Results from HC tests are shown in figure 4.38.

Also, a series of 2 suction-controlled conventional triaxial compression (CTC) tests, 4 triaxial compression (TC) tests, and 2 triaxial extension (TE) tests were conducted. Results are shown in figures 4.39 to 4.42.

Overall, test results confirm the following: (1) proper functionality of system at high and low values of controlled matric suction, (2) feasibility of the axis-translation technique in

the newly developed apparatus, and (3) reasonable repeatability of suction-controlled multiaxial testing.

Next chapter describes the experimental program and procedure followed in this research work, including a comprehensive analysis of all suction-controlled true triaxial test results on unsaturated silty sand.

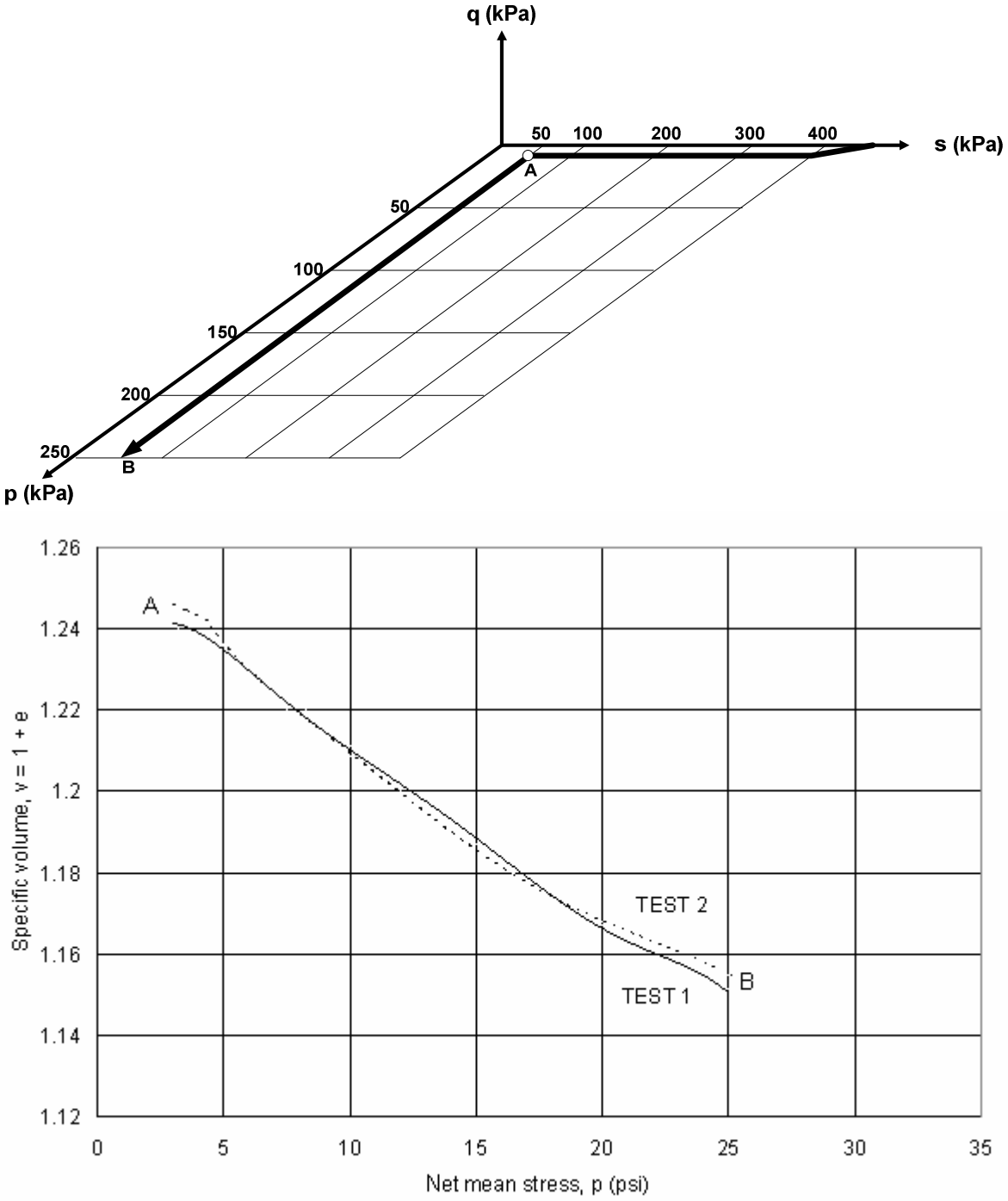

Figure 4.38 Repeatability of HC tests: (u_a-u_w) = 50 kPa

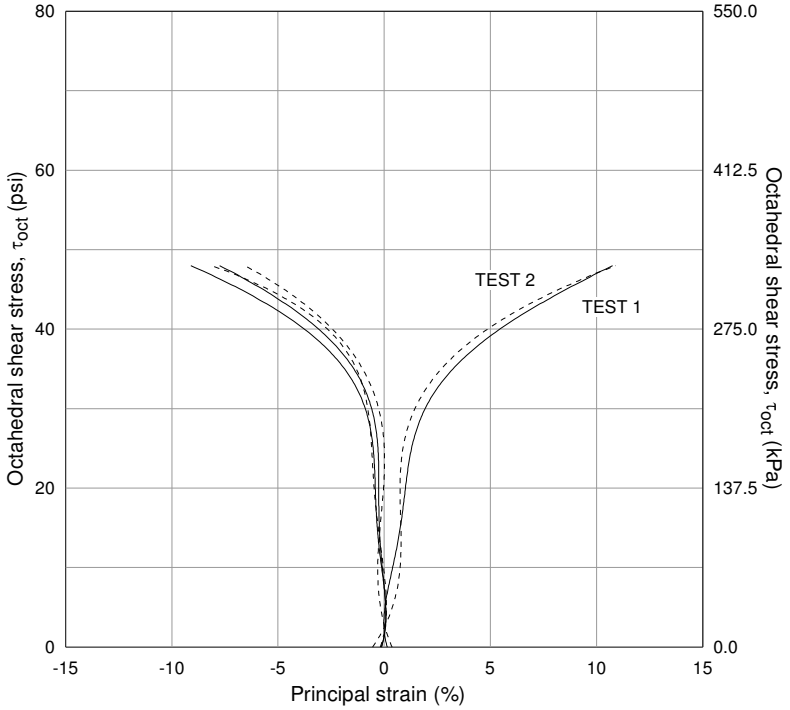

Figure 4.39 Repeatability of CTC tests: p_{net} = 100 kPa, (u_a-u_w) = 100 kPa

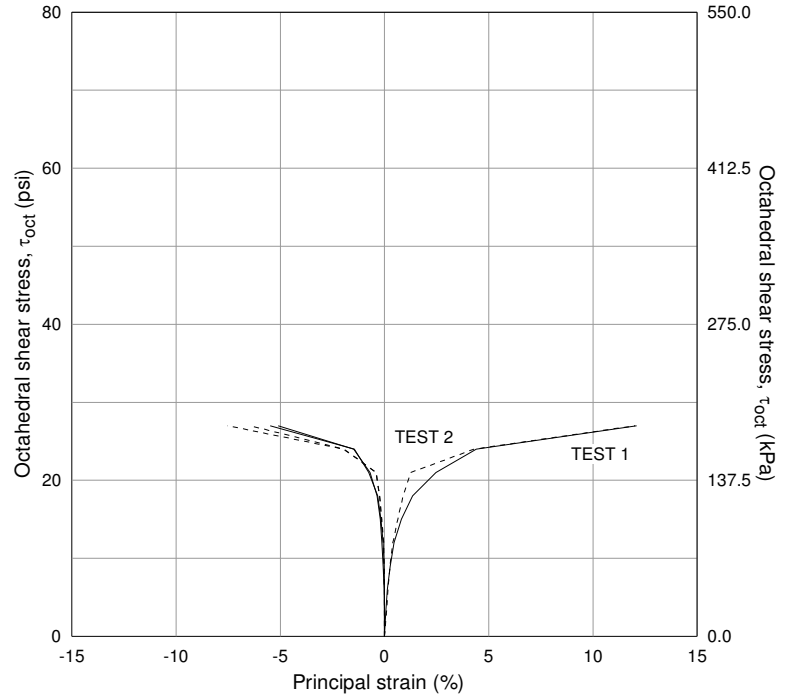

Figure 4.40 Repeatability of TC tests: p_{net} = 100 kPa, (u_a-u_w) = 50 kPa

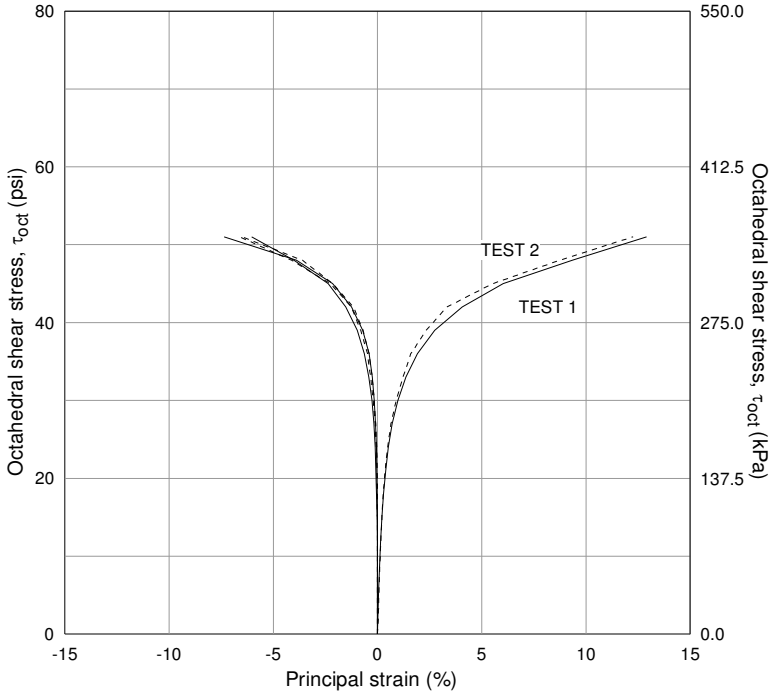

Figure 4.41 Repeatability of TC tests: p_{net} = 200 kPa, (u_a-u_w) = 200 kPa

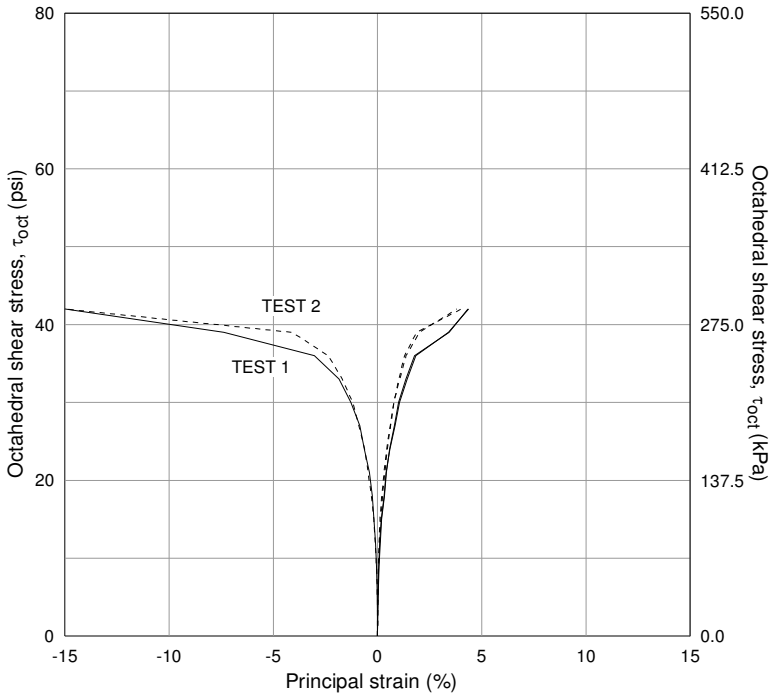

Figure 4.42 Repeatability of TE tests: p_{net} = 200 kPa, (u_a-u_w) = 100 kPa

CHAPTER 5

SUCTION-CONTROLLED TEST PROGRAM AND RESULTS

5.1 Introduction

The computer-based, mixed-boundary type, suction-controlled cubical test cell developed as part of this research work was used to study the mechanical response of unsaturated soil under multiaxial stress states. To this purpose, a comprehensive series of drained (constant suction), suction-controlled HC, CTC, TC, and TE tests were conducted on identically prepared, 3-in (7.6-cm) cubical specimens of silty sand at different matric suction states.

This chapter presents a comprehensive analysis of all test results, focusing on the effect of matric suction and net confinement on the general stress-strain response of silty sand in q-p plane, principal stress plane and octahedral plane.

5.2 Test Soil Properties

The soil used in this work was artificially prepared by mixing 20% silt (from North Arlington, Texas) and 80% clean sand (commercially supplied locally). The air-dried water content is 2.0% and the maximum dry unit weight attained via pluviation-tamping technique is 14.9 kN/m^3, which corresponds to a moisture content of 11.3%. Sieve analysis (figure 5.1) shows an effective grain size (D_{10}) of 0.15-mm. The soils classifies as SP-SM according to the USCS. The basic engineering properties of the test soil are summarized in table 5.1.

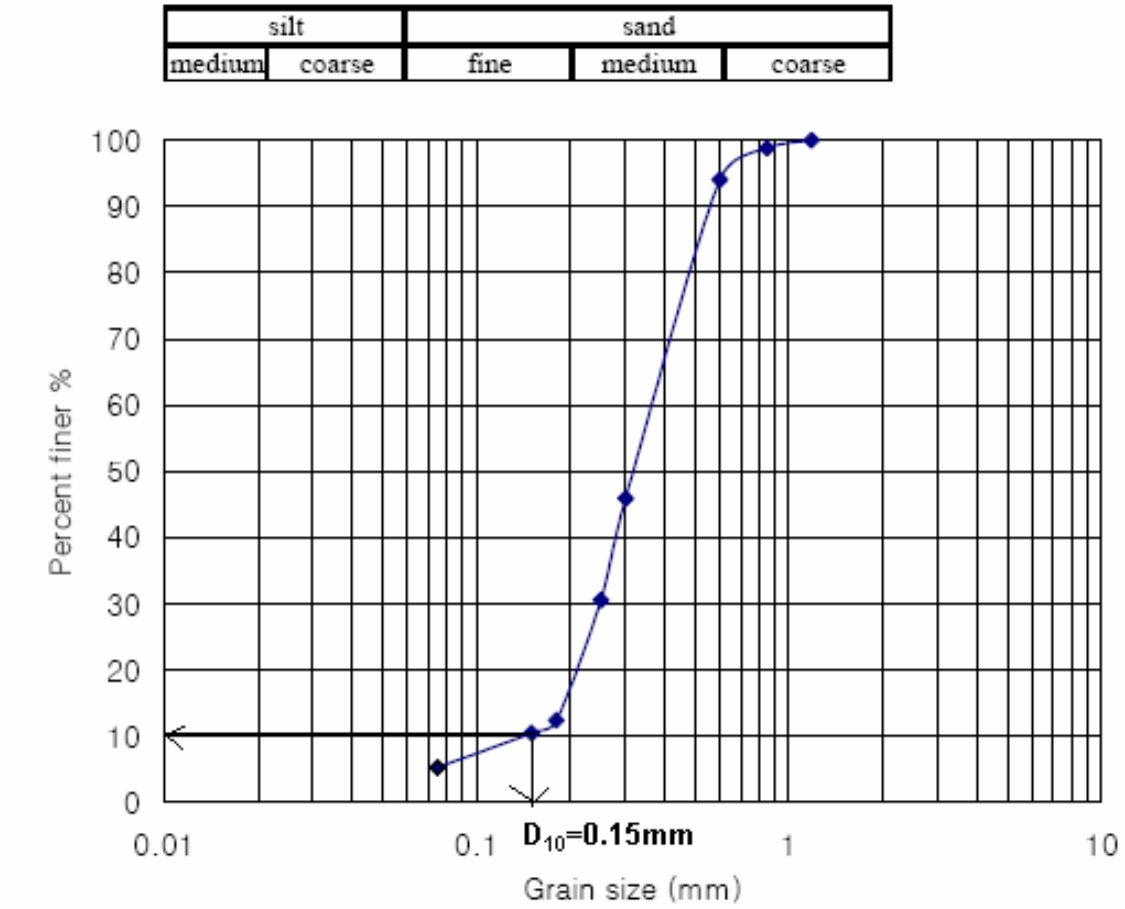

Figure 5.1 Particle size distribution of artificially prepared silty sand

Table 5.1 Basic engineering properties of test soil

Property	**Magnitude**
Optimum moisture content*, $w_{opt}(\%)$	11.3
Maximum dry unit weight*, $\gamma_{d\text{-}max}$ (kN/m^3)	14.9
USCS Classification	SP-SM
D_{10} (mm)	0.15

* via pluviation-tamping technique

5.3 Experimental Program and Procedure

After the specimen has been prepared via pluviation-tamping and the suction-controlled cubical test cell is fully assembled, as presented in Chapter 4, the specimen is subject to an initial isotropic stress state $(\sigma - u_a)$ and s = u_a. Equalization is then allowed in the pore-water under the desired confinement and pore-air pressure, u_a. Once no further pore-water volume change is detected from within the specimen, the soil is considered to be at equilibrium (equalization of pore fluids) under the applied stresses. The change in pore-water volume is recorded by the PCP-5000 UNSAT panel. Changes in the overall volume of the specimen during application of suction (s = u_a), which usually involves a drying process, were also record via LVDTs.

For further isotropic loading and/or shear loading, the specimen is loaded at a constant stress rate. Any excess in the pore-air pressure, Δu_a, and pore-water pressure, Δu_w, caused by the applied load, are then dissipated by allowing the pore fluids (air and water) to flow in or out of the soil specimen. The suitable stress rate in this research work was found to be 1 psi per hour (approximate 10 kPa/h), similar to the one reported by Hoyos (1998).

Table 5.2 summarizes all the experimental variables used in this work for suction-controlled cubical cell testing. All specimens were prepared at an initial water content of 11.5%, which corresponds to a matric suction of 50 kPa (7 psi), according to SWCC shown in figure 4.25. A wide range of suction states of 50, 100, 200, 300, and 400 kPa (7, 15, 29, 44, and 58 psi) were induced on the test specimens. Tests were conducted at initial values of net mean stress of 50, 100, 150, and 200 kPa (7, 15, 22, and 29 psi), according to the stress path intended to be followed. Tests were performed along four different suction-controlled

stress paths, which include hydrostatic compression (HC), conventional triaxial compression (CTC), triaxial compression (TC), and triaxial extension (TE).

5.4 Response Under Hydrostatic Compression (HC)

A series of 5 drained (suction-controlled) HC tests were successfully conducted in the cubical setup on 5 identically prepared cubical silty sand specimens. In each case, a ramped consolidation stage, from $p = 6.89$ kPa (1 psi) to $p = 400$ kPa (58 psi), followed the equalization stage for the pre-established matric suction, $s = 50$ kPa (7 psi), 100 kPa (15 psi), 200 kPa (29 psi), 300 kPa (44 psi), or 400 kPa (58 psi) as show in figure 5.2.

Table 5.2 Experimental variables for suction-controlled testing

Variable	**Number**	**Description**
Soil type	1	• Silty Sand (80% Sand and 20% Silt) • Optimum moisture content*, w_{opt} = 11.3% • Maximum dry unit weight*, $\gamma_{d\text{-}max}$ = 14.9 kN/m^3 • USCS Classification : SP-SM
Initial moisture content	1	• 11.5 %
Controlled-suction states ($s = u_a$)	5	• 50 kPa (7 psi) • 100 kPa (15 psi) • 200 kPa (29 psi) • 300 kPa (44 psi) • 400 kPa (58 psi)
Net mean stress	4	• 50 kPa (7 psi) • 100 kPa (15 psi) • 150 kPa (22 psi) • 200 kPa (29 psi)
Suction-controlled stress path	5	• Hydrostatic compression (HC) • Conventional triaxial compression (CTC) • Triaxial compression (TC) • Triaxial extension (TE)

* via pluviation-tamping technique

Figure 5.3 shows the specific volume, $v = 1 + e$, versus net mean stress, p_{net}, response of silty sand from the series of 5 HC tests. Test results show that rate of the change in specific volume (stiffness) at higher matric suction is less than that at lower matric suction. It can be noticed, hence, the paramount influence of matric suction on the volumetric stiffness of silty sand.

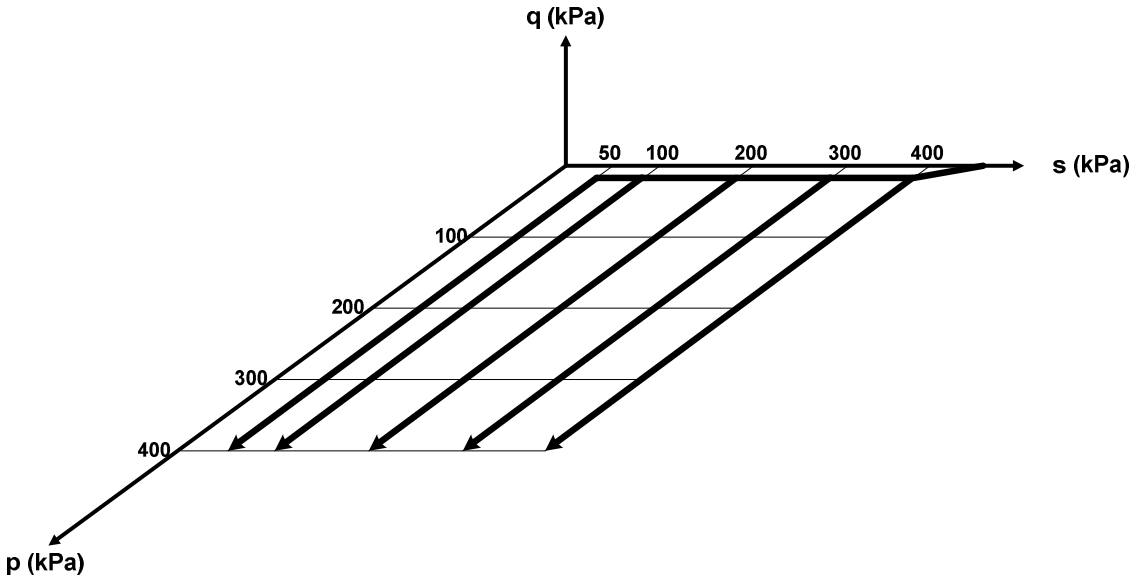

Figure 5.2 Suction-controlled Hydrostatic Compression (HC) stress paths

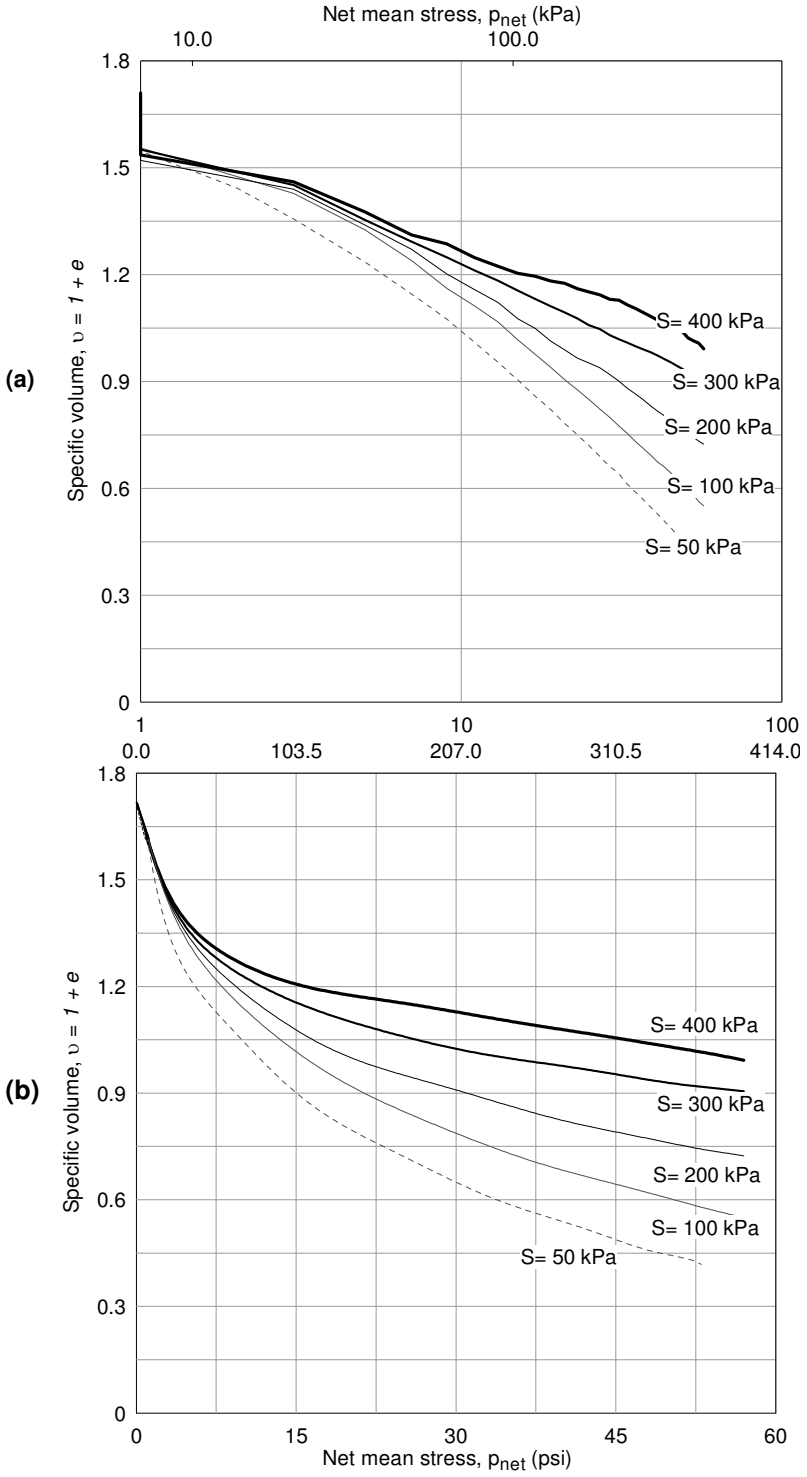

Figure 5.3 Variation of specific volume, $v = 1 + e$, during suction-controlled HC tests

5.5 Response Under Conventional Triaxial Compression (CTC)

A series of 7 drained (constant-suction) CTC tests were successfully conducted on 7 identically prepared cubical silty sand specimens to study the mechanical behavior of unsaturated soil under axisymmetric $(\sigma_2 = \sigma_3)$ shearing.

Four CTC tests were carried out under a net mean stress, p_{net}, of 50 kPa at four controlled matric suction states of 50 kPa, 100 kPa, 200 kPa. and 300 kPa, Three more CTC tests were conducted under net mean stress, p_{net}, of 100 kPa at three controlled matric suction states of 50 kPa, 100 kPa, and 200 kPa. During each test, the intermediate and minor principal stresses were maintained constant $(\sigma_2 = \sigma_3)$ while the major principal stress, σ_1, was increased.

5.5.1 Effect of Matric Suction State

Results from suction-controlled CTC testing are shown in figures 5.4 and 5.5, where the deviatoric stress is plotted against the total shear strain, $\varepsilon_q = \frac{2}{3}(\varepsilon_1 - \varepsilon_3)$. The incipient critical state condition was identified when the specimen reached approximately 12% of total shear strain.

In all cases, matric suction exerts a considerable influence on the stress-strain response of silty sand.

As expected, an increase in net mean stress, p_{net}, yields a noticeable increase in silty sand strength, as will be further substantiated in the following section.

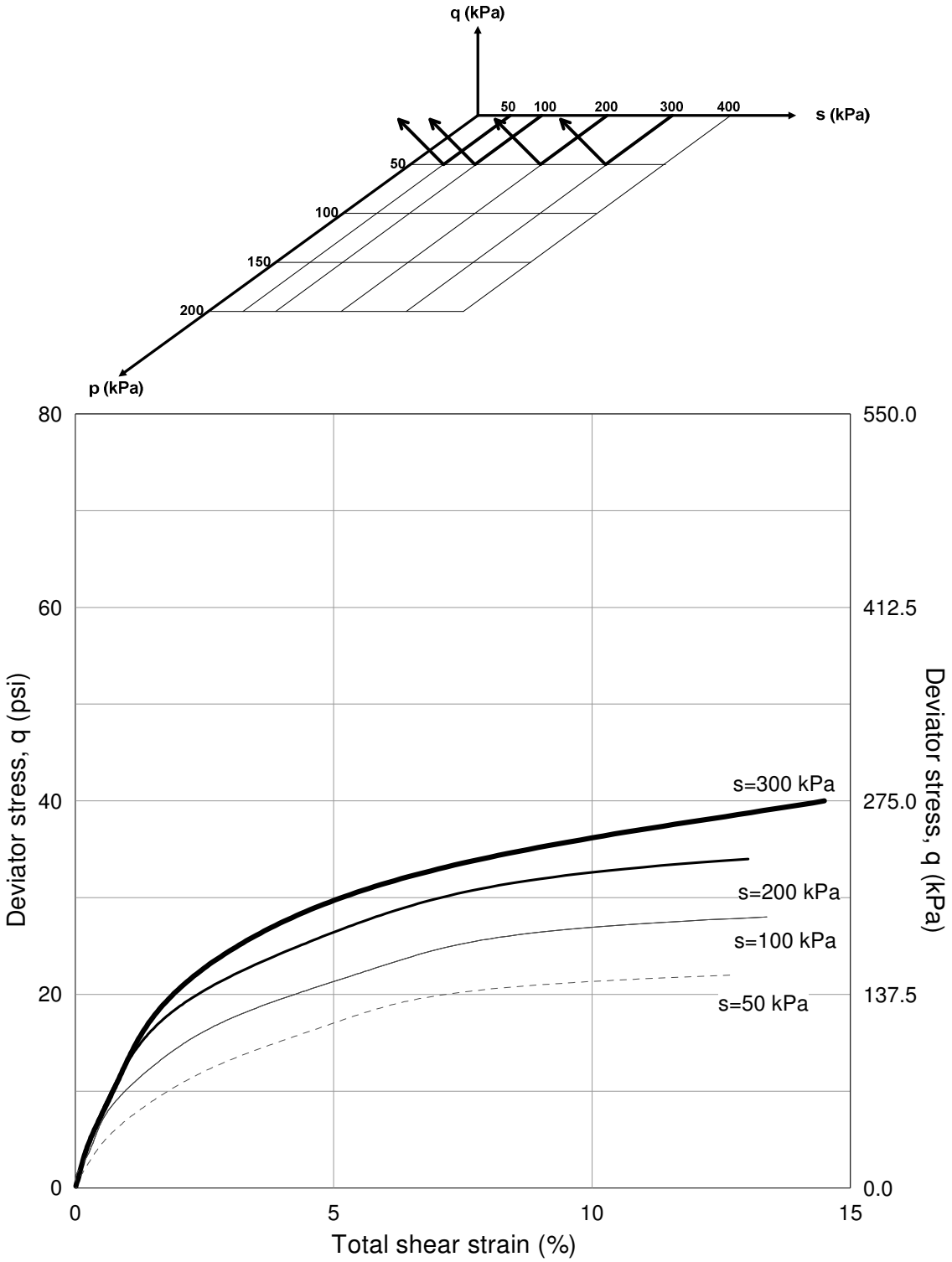

Figure 5.4 Silty sand response from suction-controlled CTC tests at p_{net} = 50 kPa

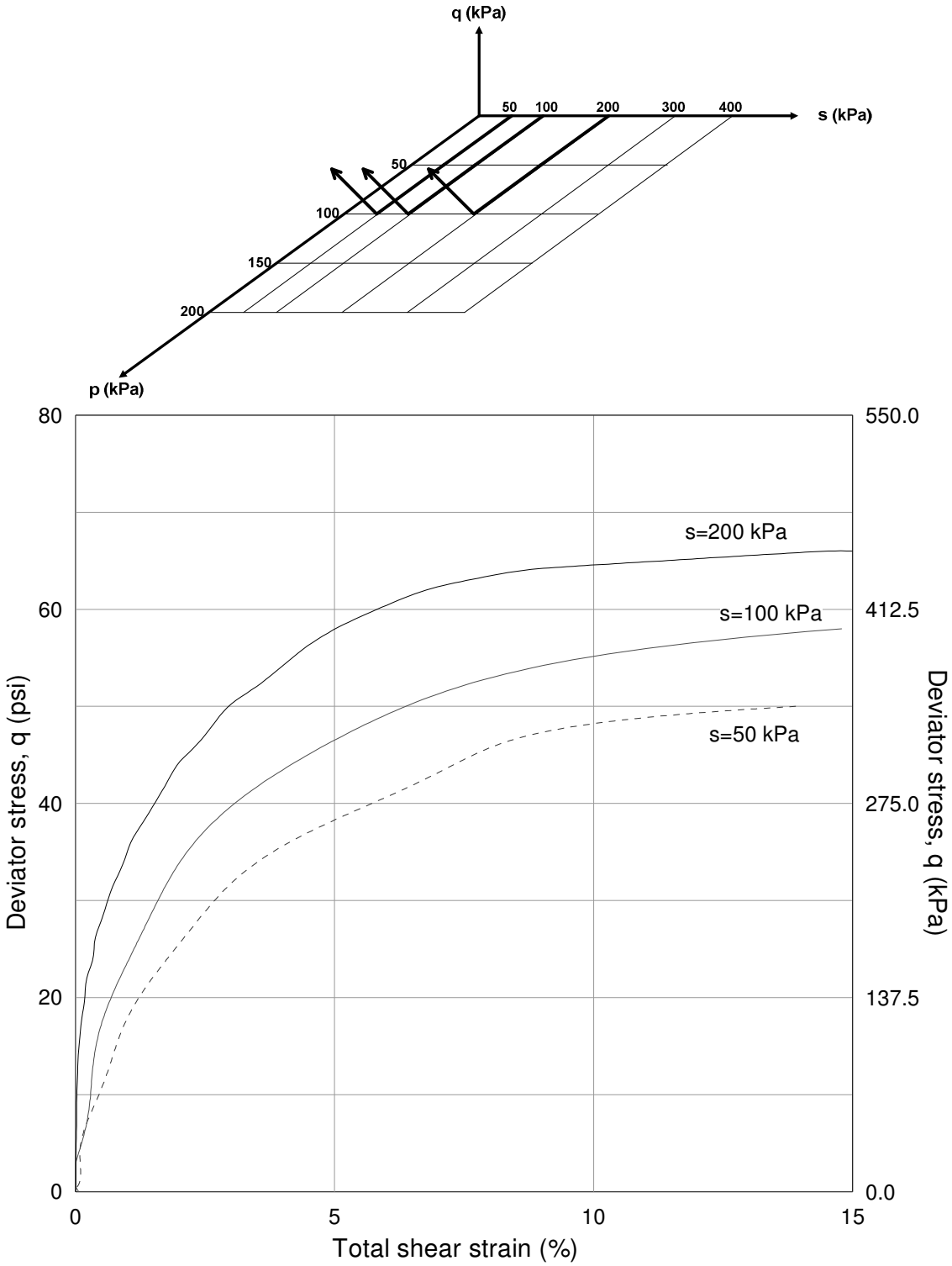

Figure 5.5 Silty sand response from suction-controlled CTC tests at p_{net} = 100 kPa

5.5.2 Effect of Net Confinement

Results from CTC tests have been replotted in figures 5.6 to 5.9 to highlight the influence of net confinement, p_{net}, on soil's stress-strain behavior. It appears that the effect of net confinement on peak strength is the same regardless of the level of matric suction applied to the soil. This could be attributed to the predominantly granular nature of the test soil (80% sand).

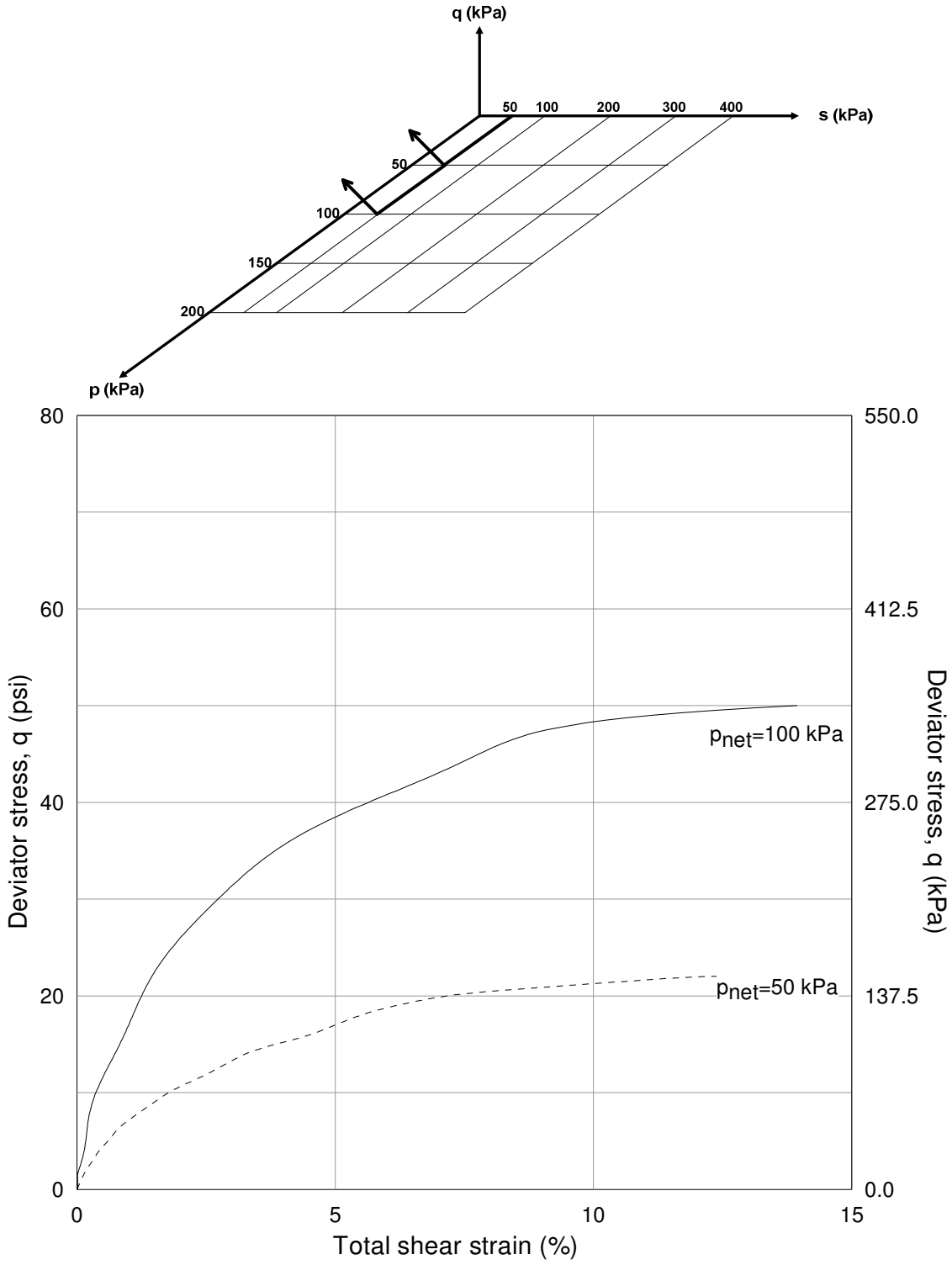

Figure 5.6 Silty sand response from suction-controlled CTC tests at (u_a-u_w) = 50 kPa

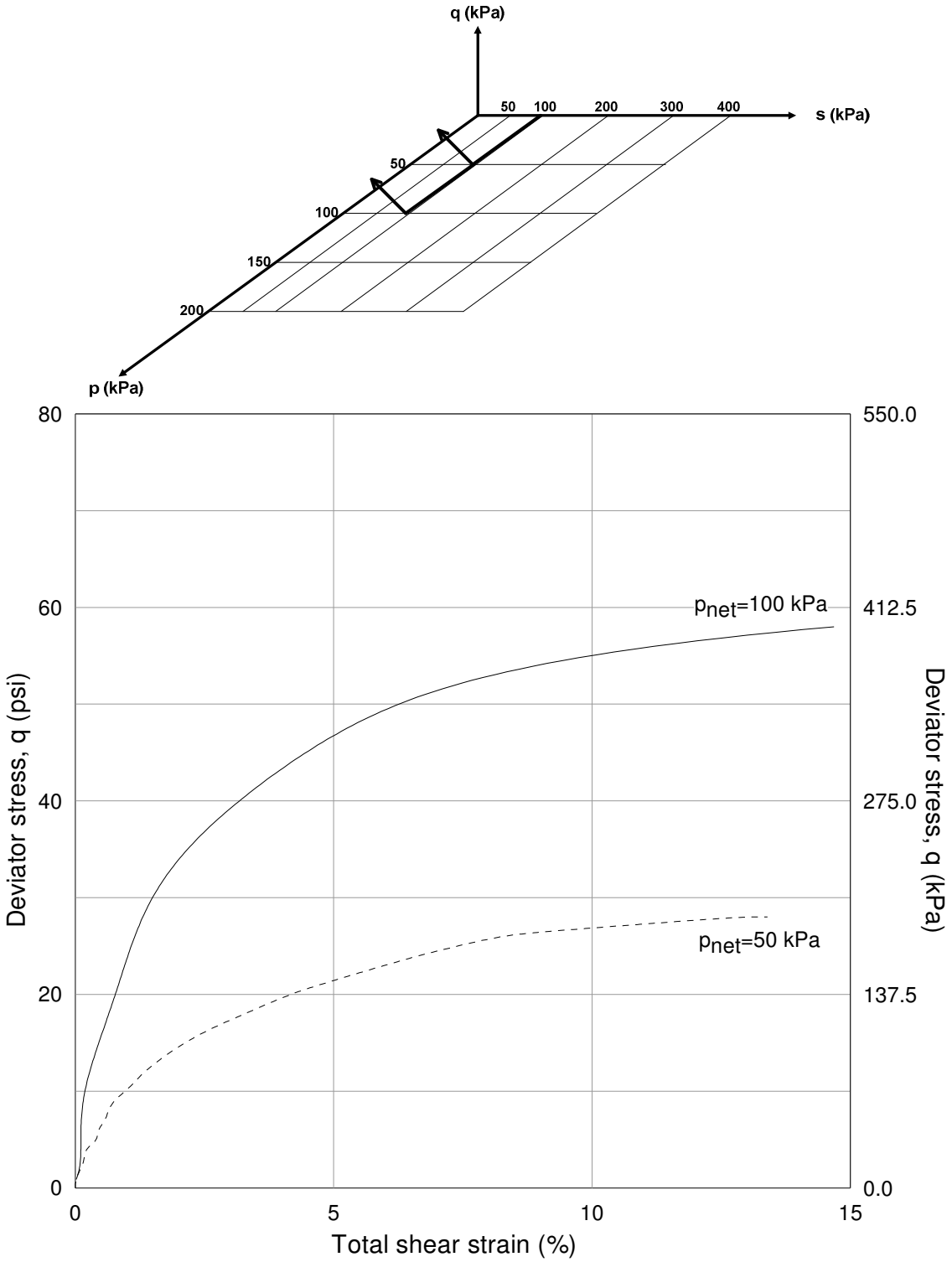

Figure 5.7 Silty sand response from suction-controlled CTC tests at (u_a-u_w) = 100 kPa

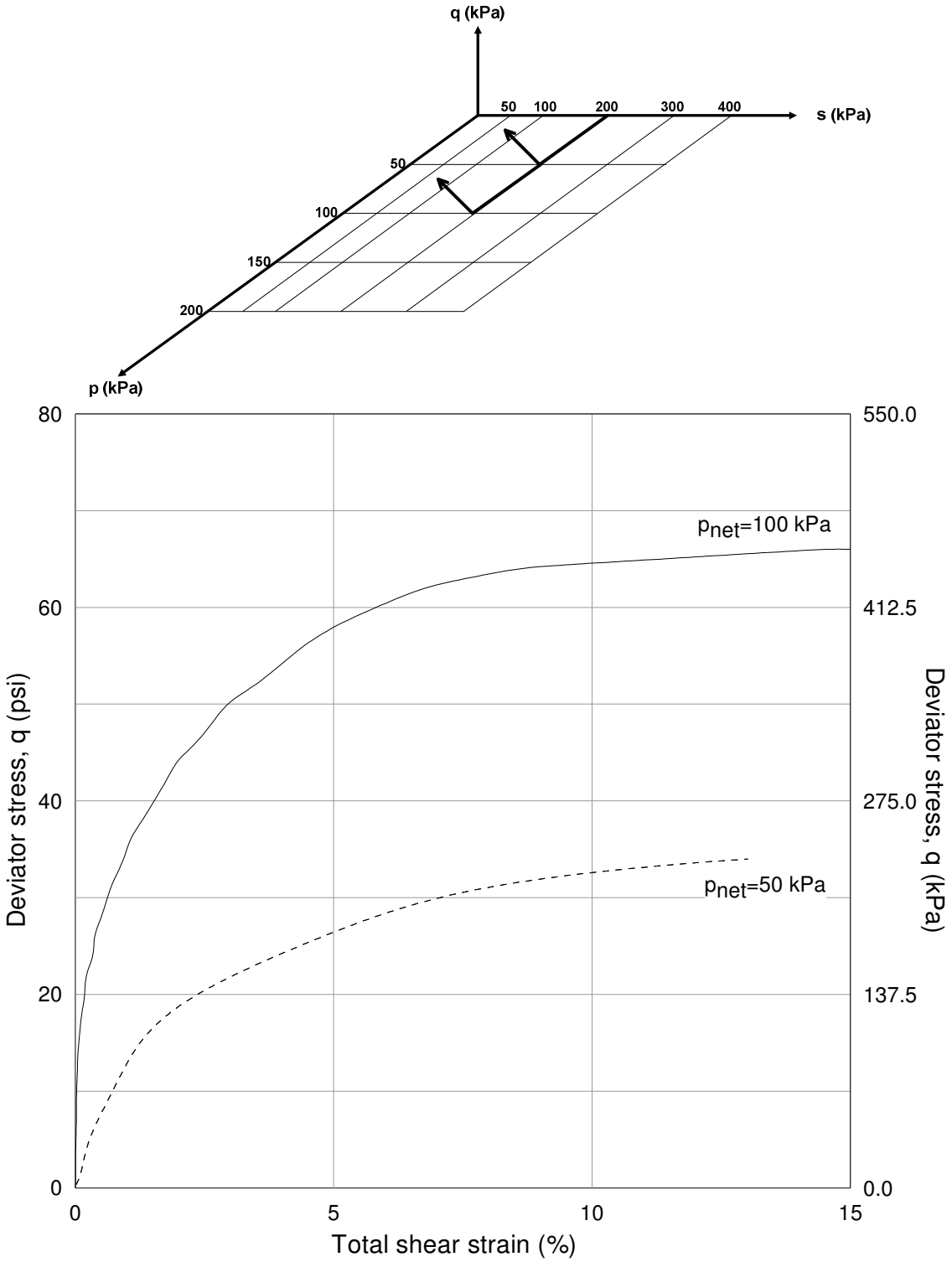

Figure 5.8 Silty sand response from suction-controlled CTC tests at (u_a-u_w) = 200 kPa

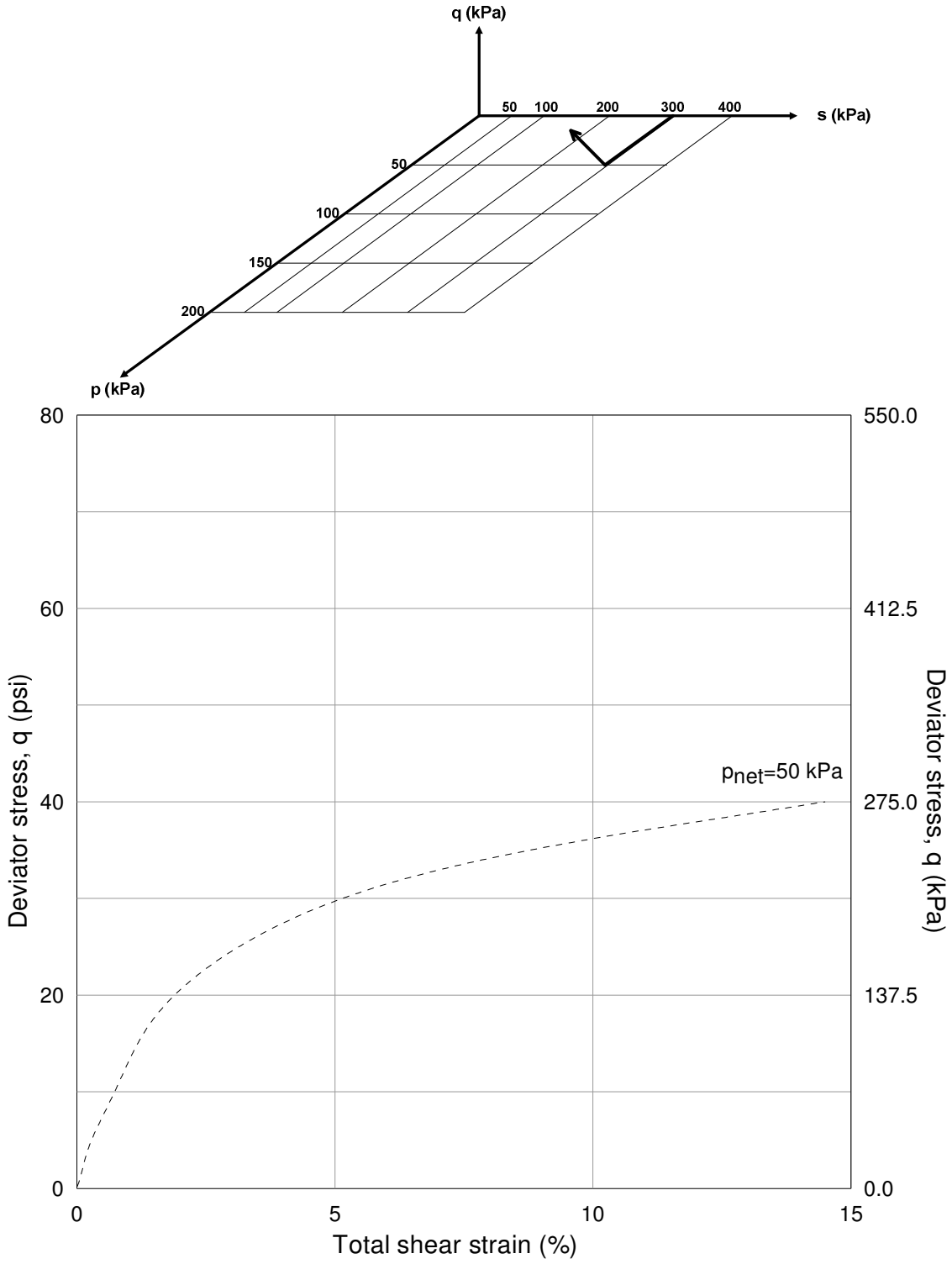

Figure 5.9 Silty sand response from suction-controlled CTC test at (u_a-u_w) = 300 kPa

5.6 Response Under Triaxial Compression (TC)

A series of 20 TC tests were successfully performed in the suction-controlled cubical cell testing device on 20 specimens of artificially prepared silty sand at different controlled matric suction of 50 kPa (7 psi), 100 kPa (15 psi), 200 kPa (29 psi), 300 kPa (44 psi) and 400 kPa (58 psi) under net mean stress, p_{net}, of 50 kPa (7 psi), 100 kPa (15 psi), 150 kPa (22 psi) and 200 kPa (29 psi).

A series of 20 drained (constant-suction), suction-controlled triaxial compression (TC) tests were conducted on several silty sand specimens, to experimentally study the mechanical characteristics of the behavior of unsaturated soil under varying matric suction conditions.

During the test the intermediate and minor principal stresses equally decreased (i.e., $\Delta\sigma_2 = \Delta\sigma_3 = \frac{-\Delta\sigma_1}{2}$) while the major principal stress, σ_1 was increased, so that the net mean stress, p_{net}, remained constant.

5.6.1 Effect of Matric Suction State

Results from suction-controlled TC testing are shown in figures 5.10 and 5.13, where the deviatoric stress is plotted against the total shear strain, $\varepsilon_q = \frac{2}{3}(\varepsilon_1 - \varepsilon_3)$. The incipient critical state condition was identified when the specimen reached approximately 12% of total shear strain.

In all cases, matric suction exerts a considerable influence on the stress-strain response of silty sand.

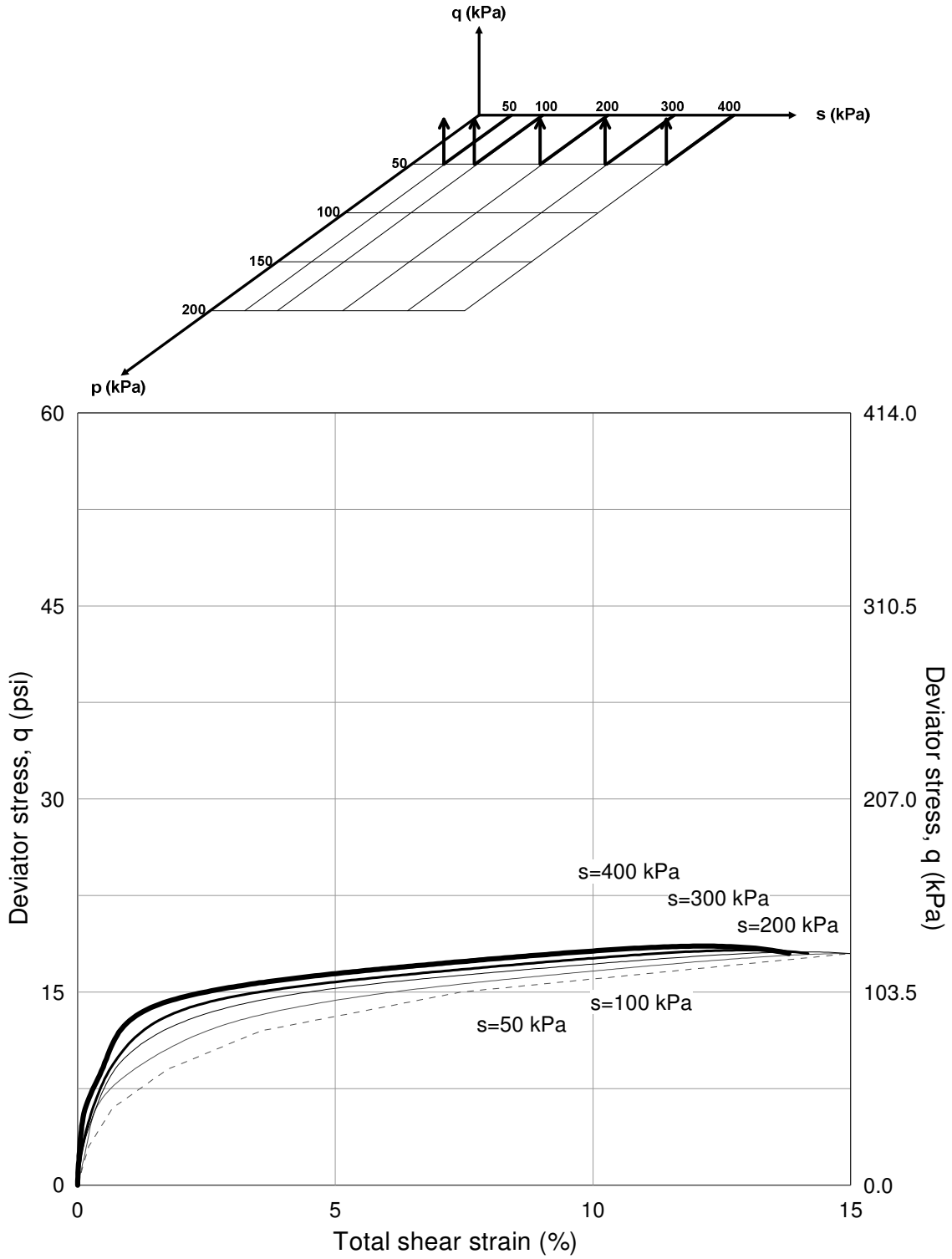

Figure 5.10 Silty sand response from suction-controlled TC tests at p_{net} = 50 kPa

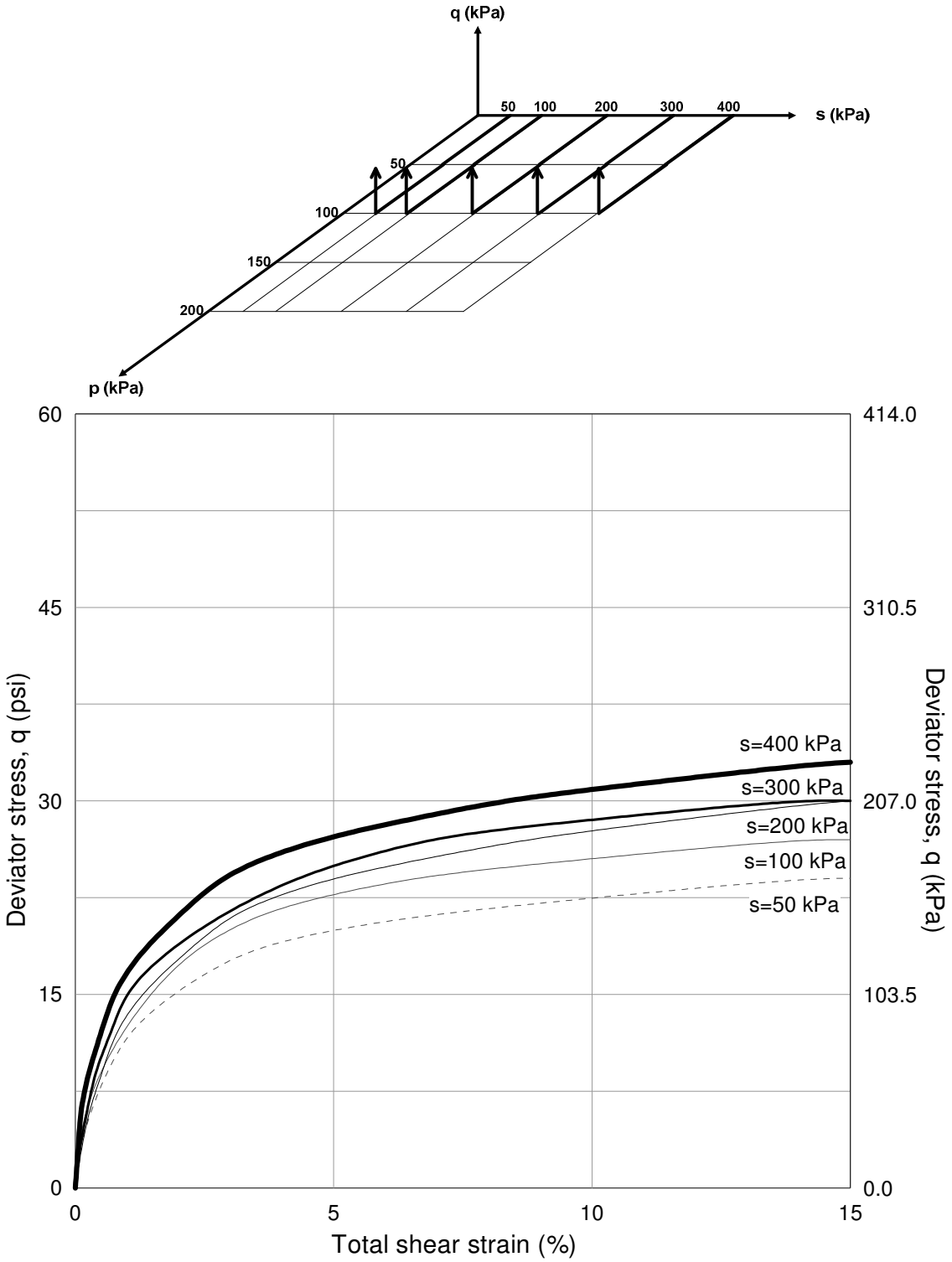

Figure 5.11 Silty sand response from suction-controlled TC tests p_{net} = 100 kPa

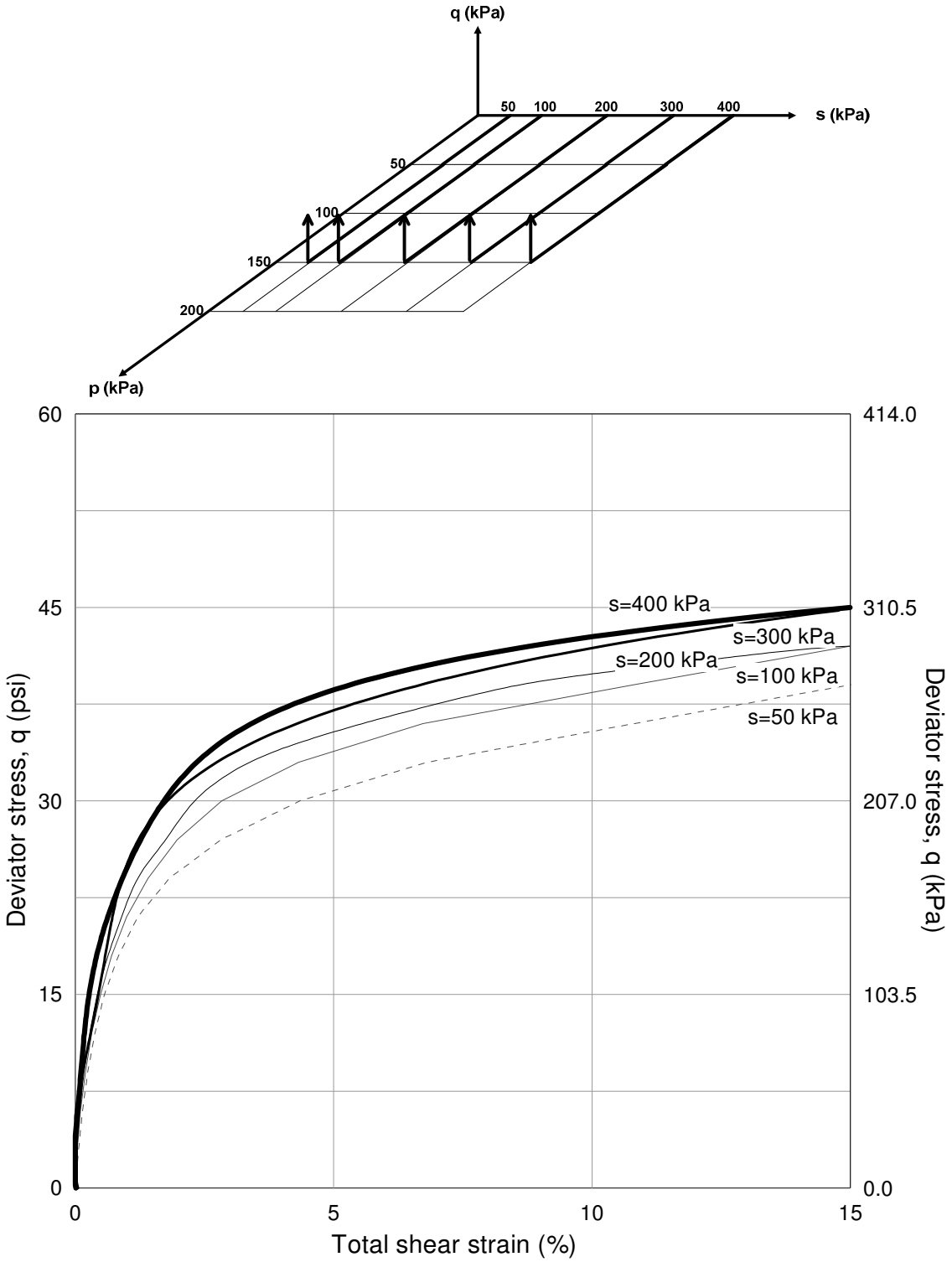

Figure 5.12 Silty sand response from suction-controlled TC tests at p_{net} = 150 kPa

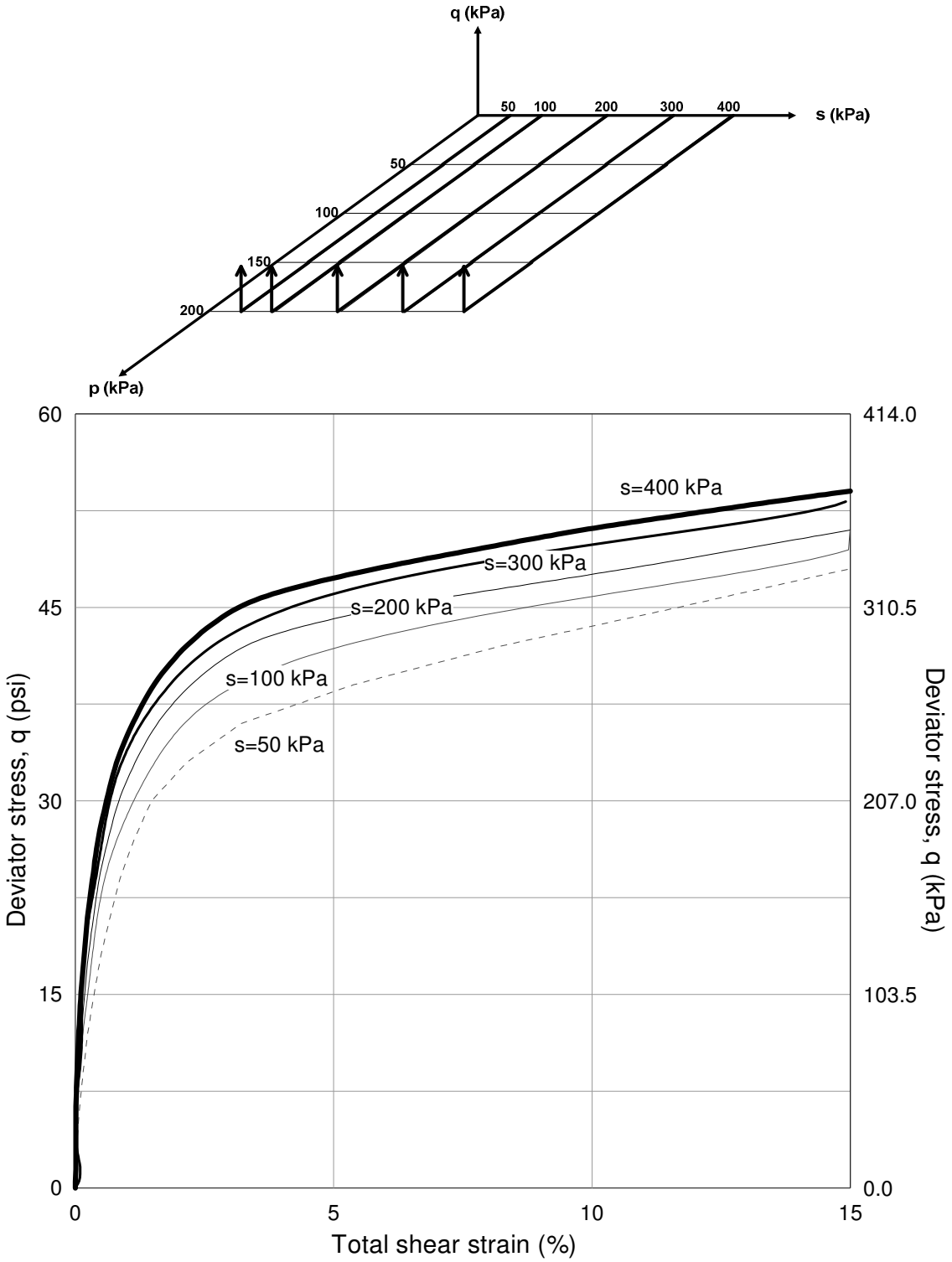

Figure 5.13 Silty sand response from suction-controlled TC tests at p_{net} = 200 kPa

As expected, an increase in net mean stress, p_{net}, yields a noticeable increase in silty sand strength, as will be further substantiated in the following section.

5.6.2 Effect of Net Confinement

Results from TC tests have been replotted in figures 5.14 to 5.18 to highlight the influence of net confinement, p_{net}, on soil's stress-strain behavior. It appears that the effect of net confinement on peak strength is the same regardless of the level of matric suction applied to the soil. This could be attributed to the predominantly granular nature of the test soil (80% sand).

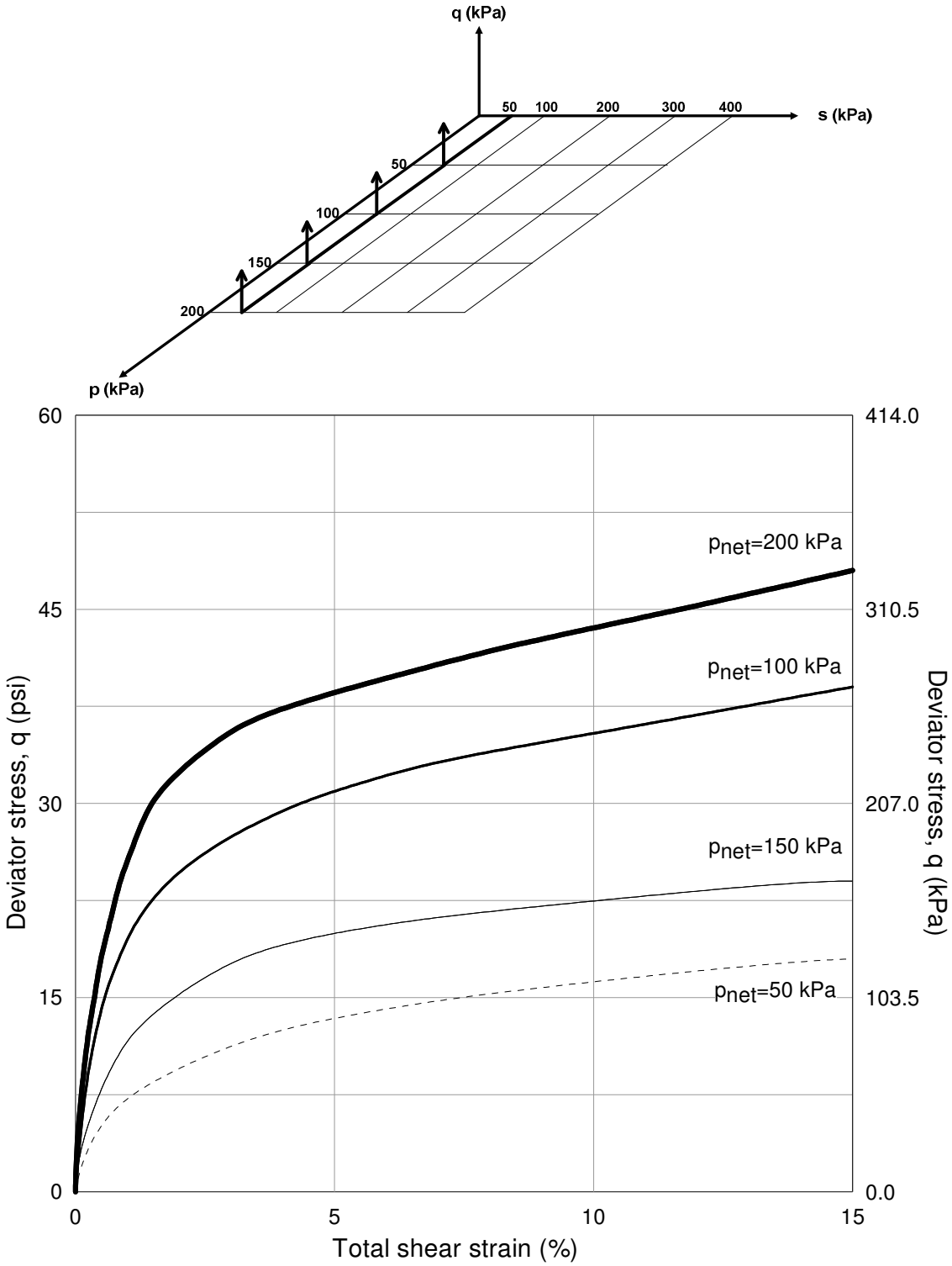

Figure 5.14 Silty sand response from suction-controlled TC tests at (u_a-u_w) = 50 kPa

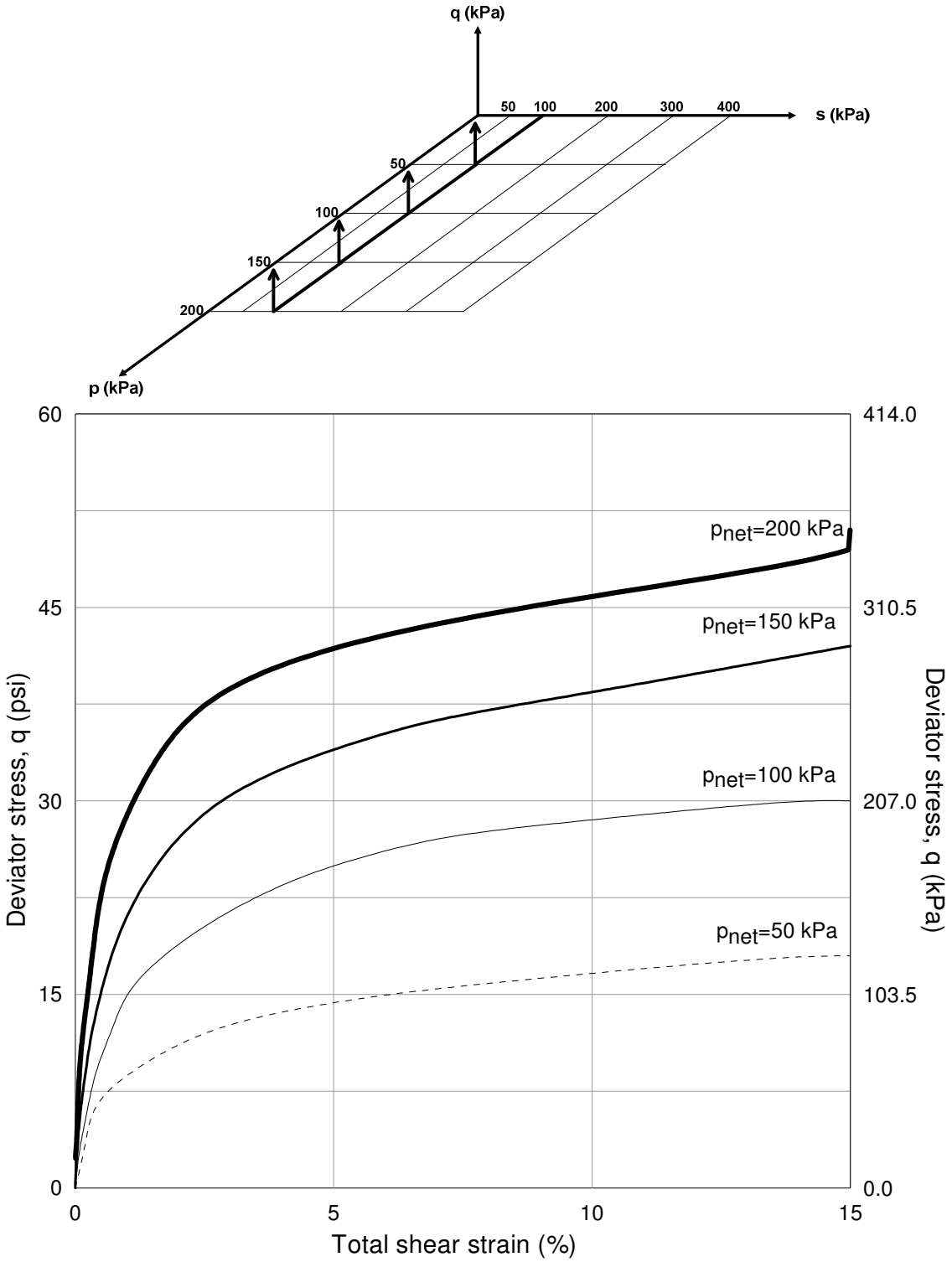

Figure 5.15 Silty sand response from suction-controlled TC tests at (u_a-u_w) = 100 kPa

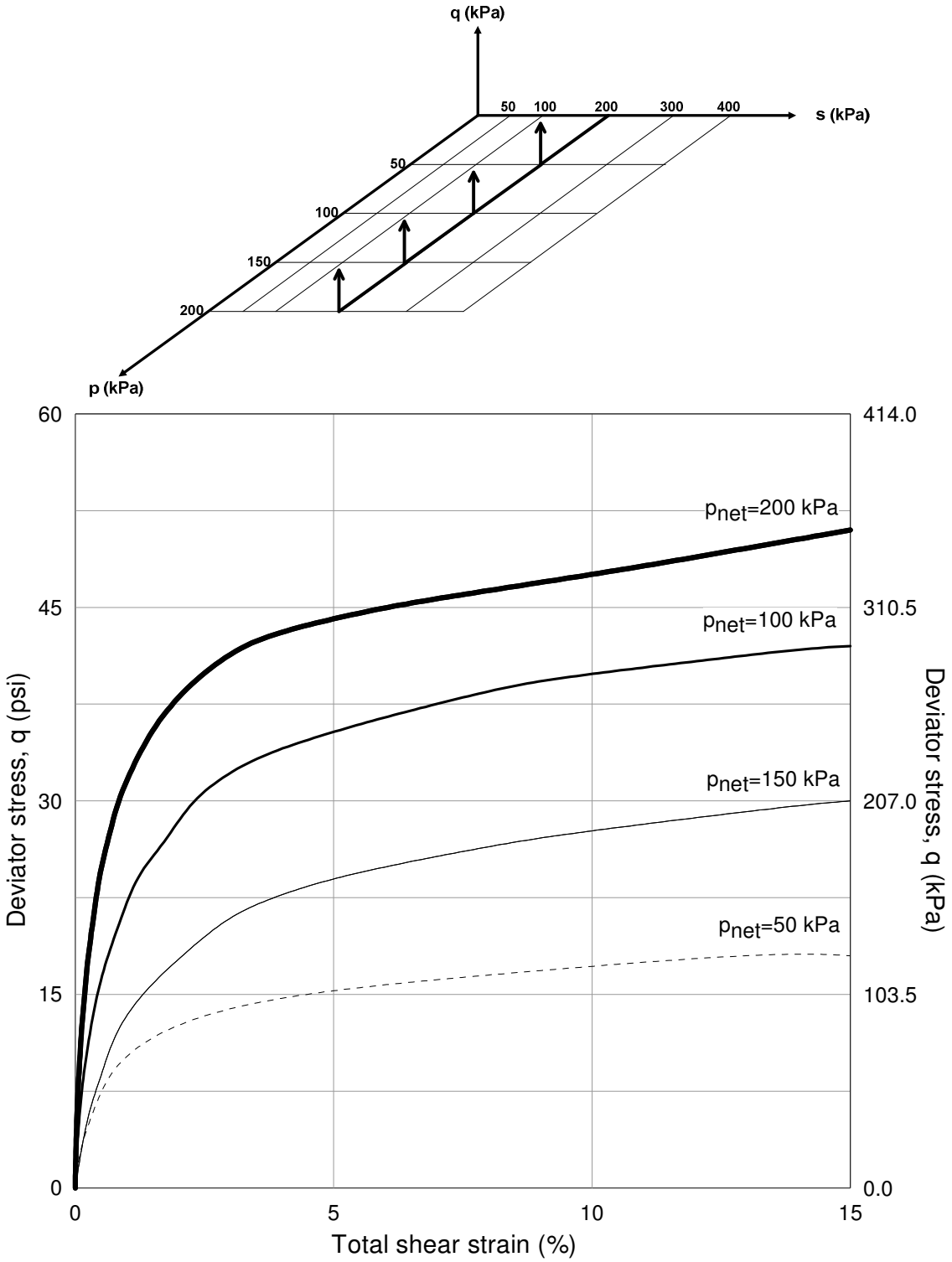

Figure 5.16 Silty sand response from suction-controlled TC tests at (u_a-u_w) = 200 kPa

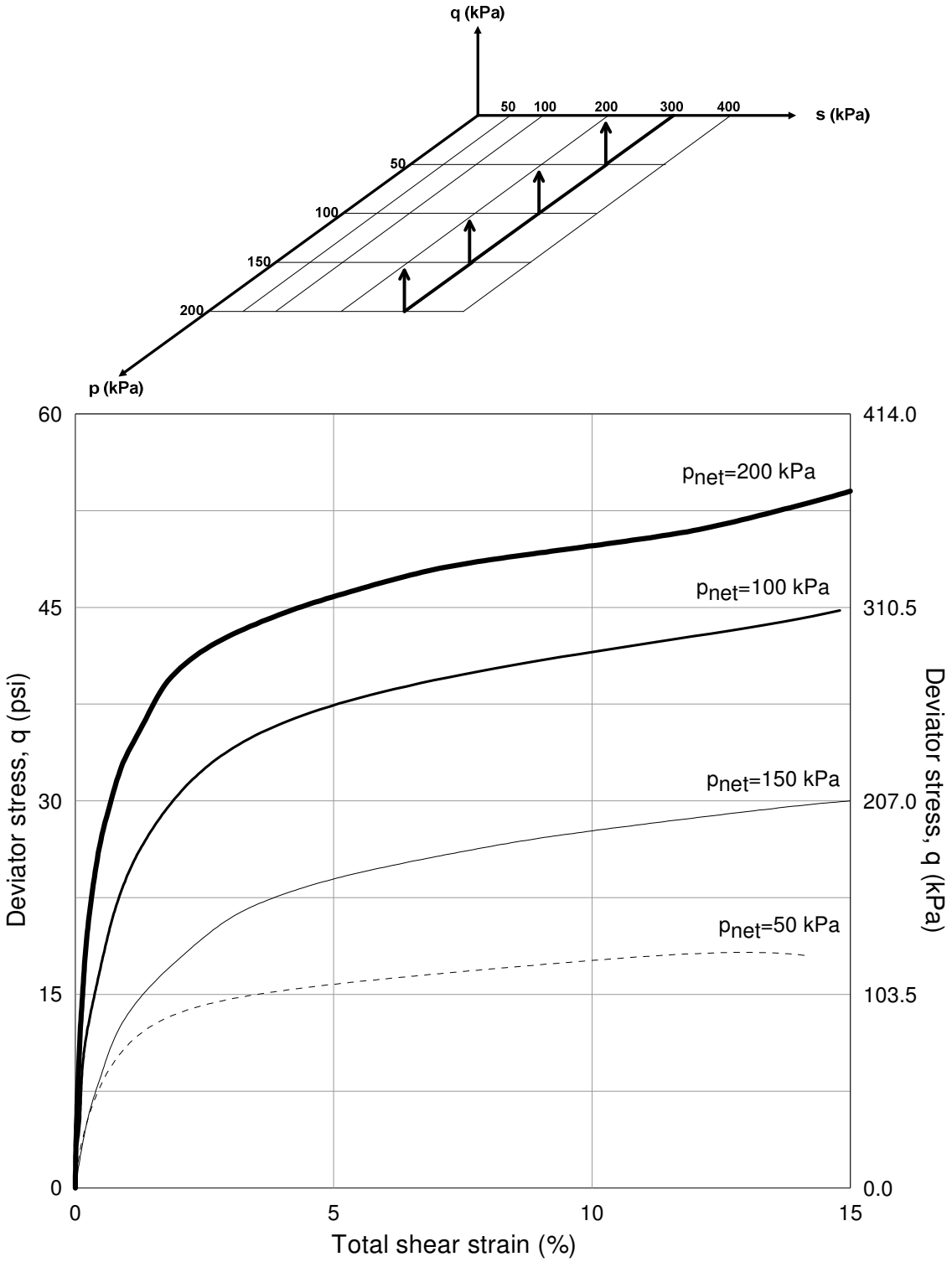

Figure 5.17 Silty sand response from suction-controlled TC tests at (u_a-u_w) = 300 kPa

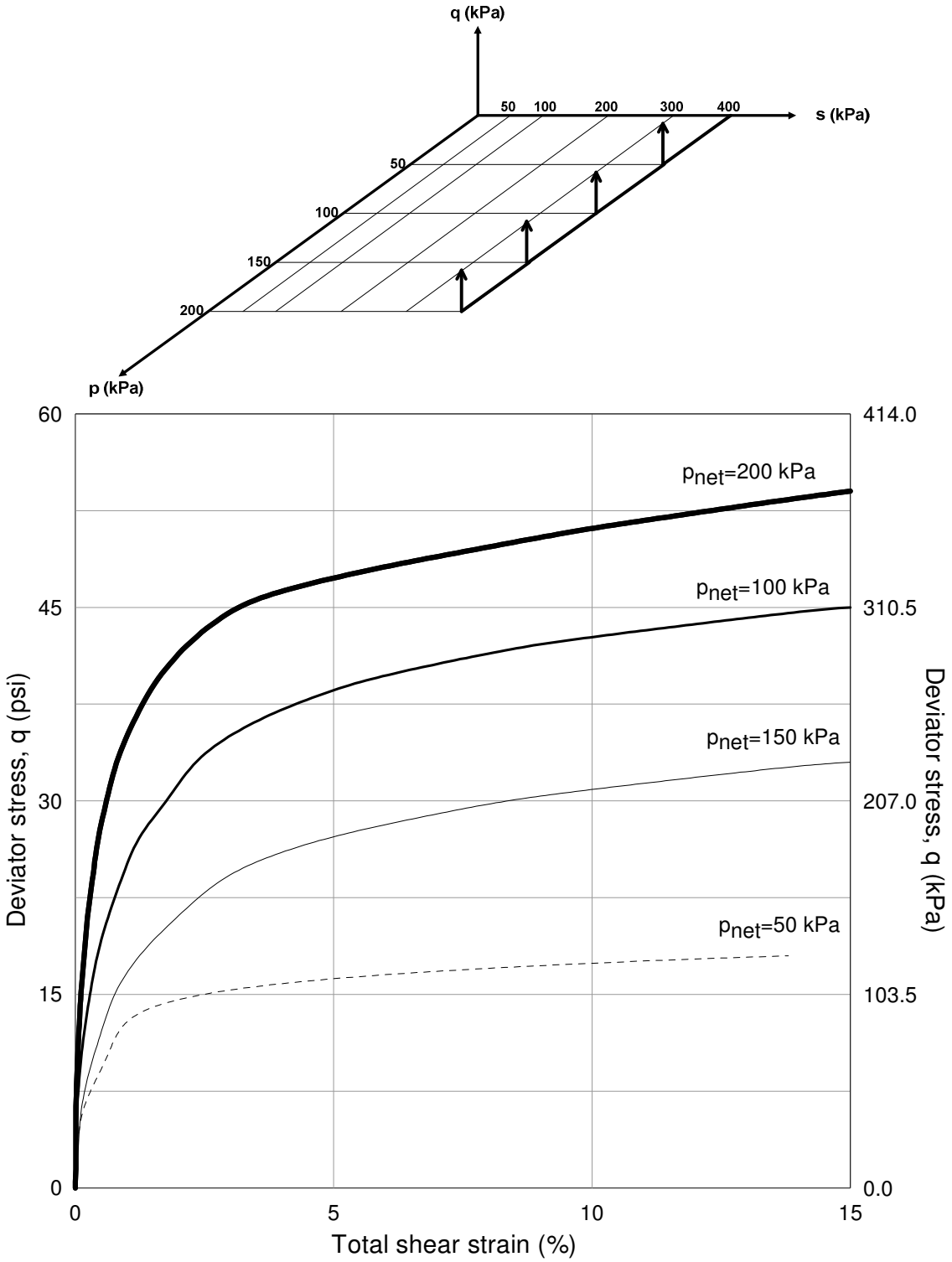

Figure 5.18 Silty sand response from suction-controlled TC tests at (u_a-u_w) = 400 kPa

5.7 Assessment of Suction-Dependent Critical State Lines

Peak results from the series of 27 suction-controlled CTC and TC tests, defined at ε_q = 10-12 %, are plotted on q-p plane in figure 5.19. Best-fitting critical state lines (CSL) for different matric suction states are shown. The corresponding best-fitting CSL for each suction level are also shown in the embedded table of figure 5.19, as well as the corresponding value of the coefficient of determination, R^2.

Although, there is a fairly significant scatter in the CSL fitting, some general trends can be observed. Matric suction has a significant influence on the position of the CSL, with the uppermost CSL corresponding to the highest matric suction state of s = ua = 400 kPa (58 psi). However, the orientation of the best-fitting CSL' can be reasonably assumed to be parallel, with an average slope for all CSL's of M = 1.5.

The unusually high value of M (usually between 0.85 and 1.30 for most soils) can be attributed to the artificial nature of the soil and the extremely low compactive effort used in the preparation of the specimen. This makes the soil unusually susceptible to increase in net confinement, yielding overestimated peak values at higher net confinements.

5.8 General Response Under True Triaxial Stress States

5.8.1 Conventional Triaxial Compression (CTC) Tests

Figures 5.20 and 5.21 show the octahedral shear stress τ_{oct} versus principal strain response of cubical silty sand specimens under constant octahedral normal stress σ_{oct} at different matric suction conditions, $s = u_a$. As mentioned before, during CTC tests, the intermediate and minor principal stresses were maintained constant $(\sigma_2 = \sigma_3)$ while the

major principal stress σ_1 was increased. It can be observed from figures 5.20 and 5.21 that the principal strain responses in X and Y directions are slightly expansive (-) while the principal strain in Z direction is compressive (+). Results from the seven tests show no significant difference between intermediate and minor principal strains ($\varepsilon_2, \varepsilon_3$), an indication of lateral isotropy achieved during pluviation-tamping compaction.

Figures 5.20 and 5.21 again show the influence exerted by matric suction on the shear resistance of the cubical silty sand specimens, with a considerable increase in the ultimate τ_{oct} for s = 300 kPa (44 psi) under σ_{oct} of 50 kPa (7 psi) and τ_{oct} for s = 200 kPa (29 psi) under σ_{oct} of 100 kPa (15 psi).

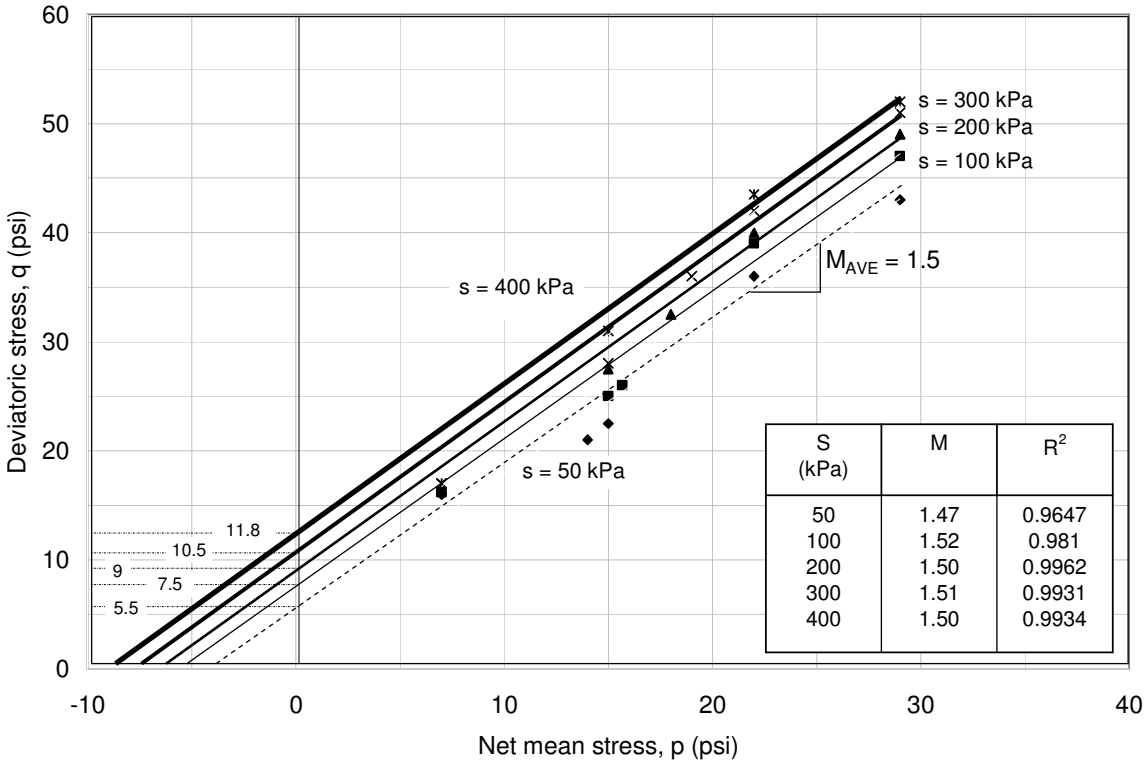

Figure 5.19 Silty sand peak response on q-p plane

As previously shown in figures 5.6 to 5.9, the net octahedral stress σ_{oct}, which is directly related to the net mean stress pnet, has a paramount influence on the soil strengths. This effect is show in figures 5.22 to 5.25.

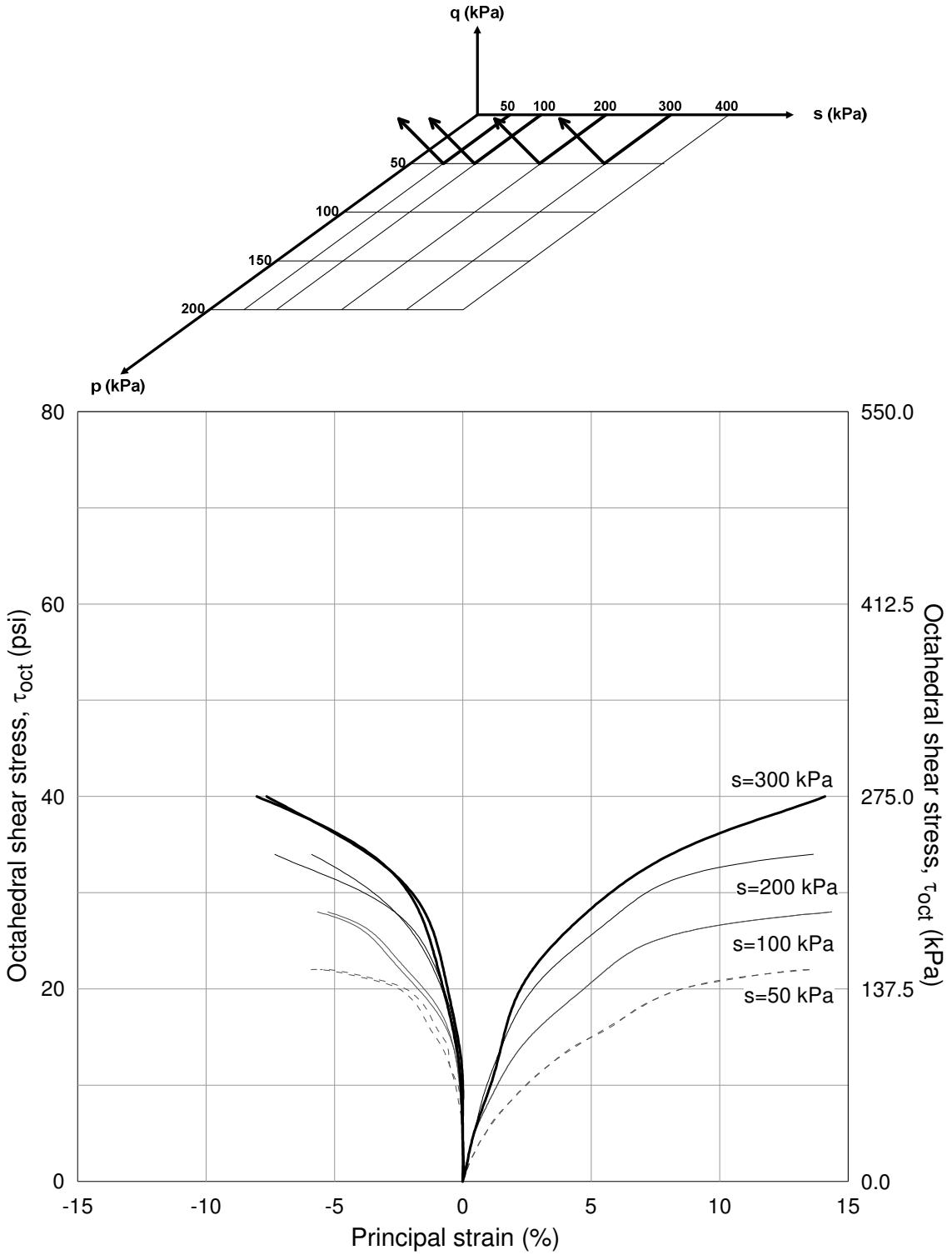

Figure 5.20 Silty sand response from suction-controlled CTC tests at σ_{oct} = 50 kPa

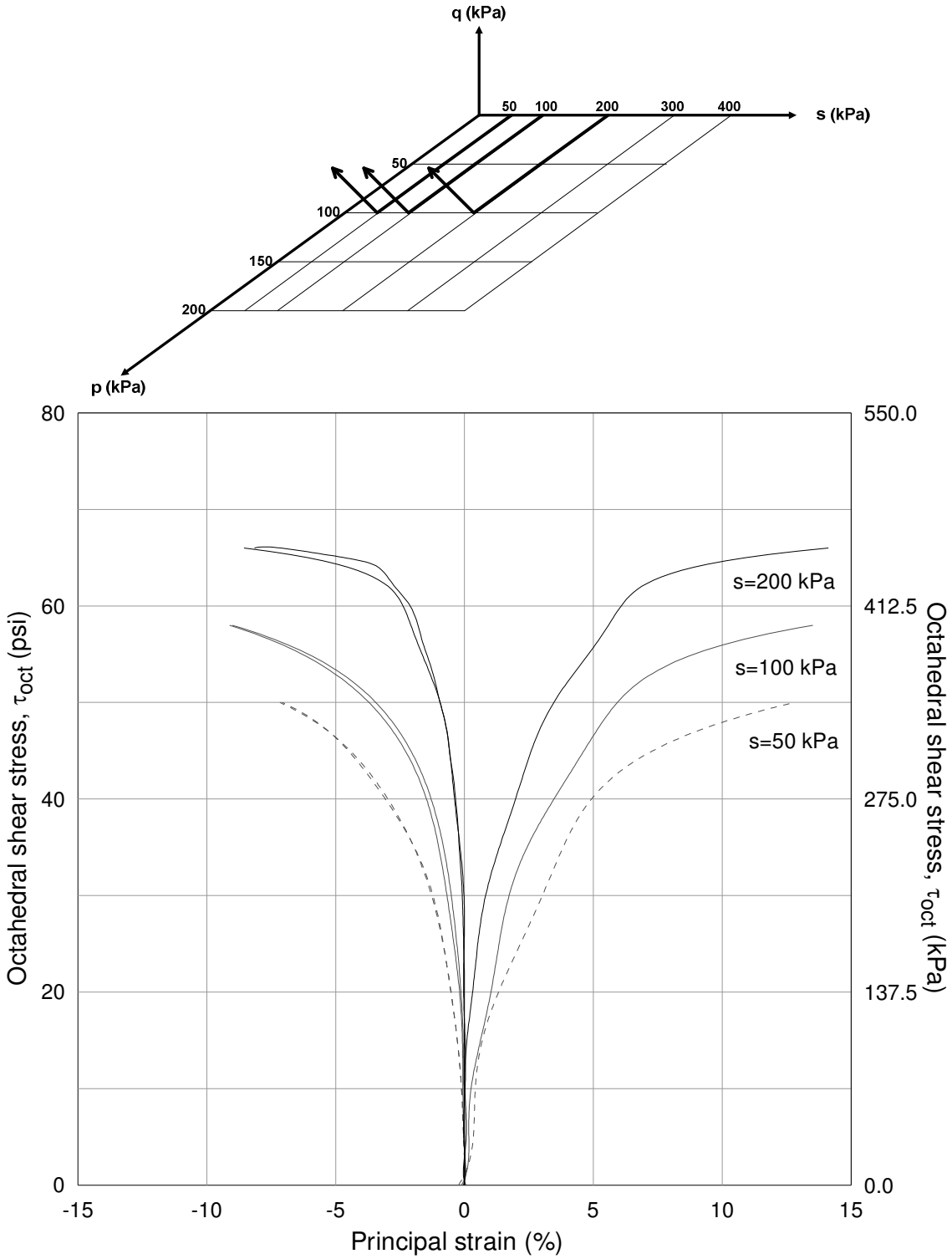

Figure 5.21 Silty sand response from suction-controlled CTC tests at σ_{oct} = 100 kPa

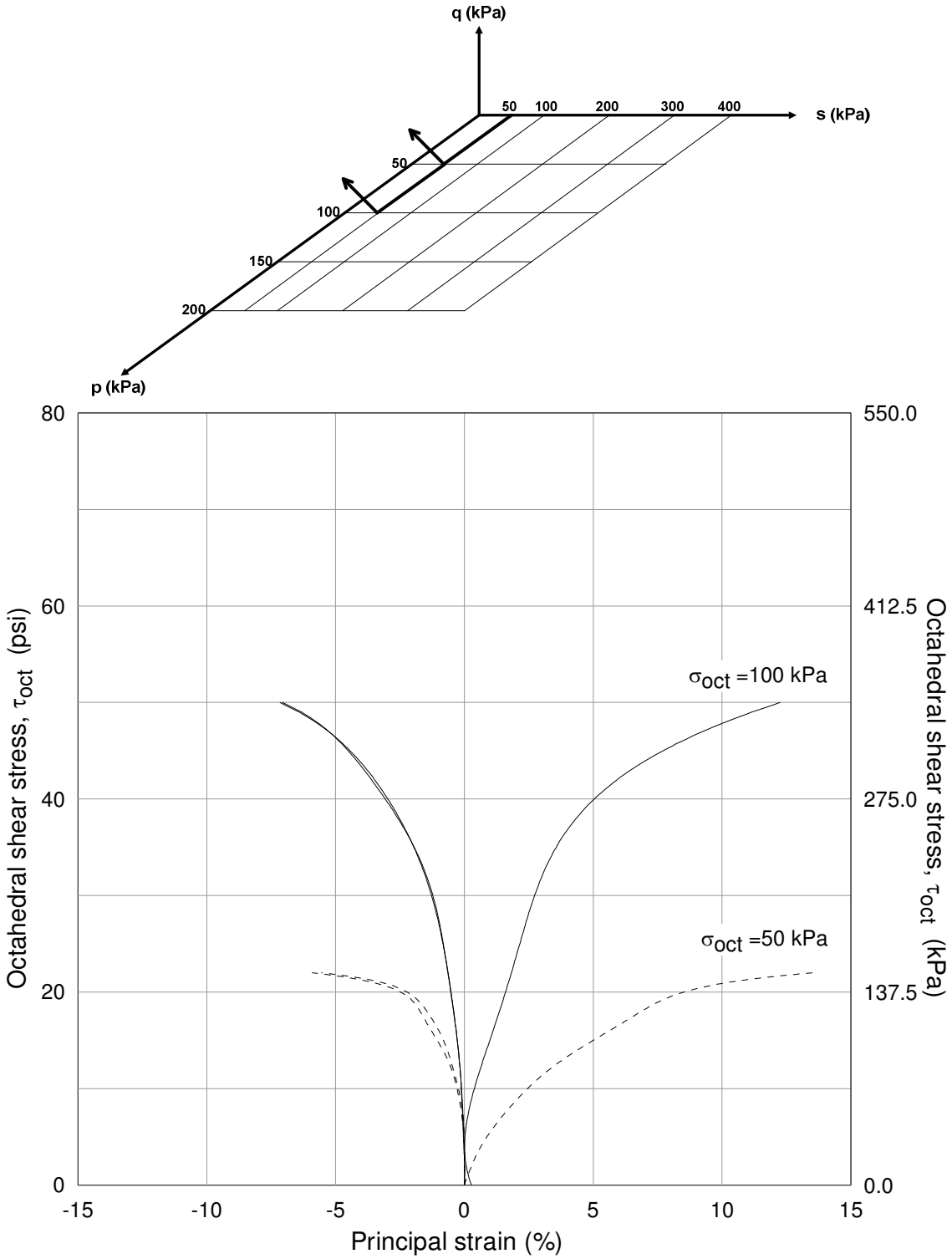

Figure 5.22 Silty sand response from suction-controlled CTC tests at (u_a-u_w) = 50 kPa

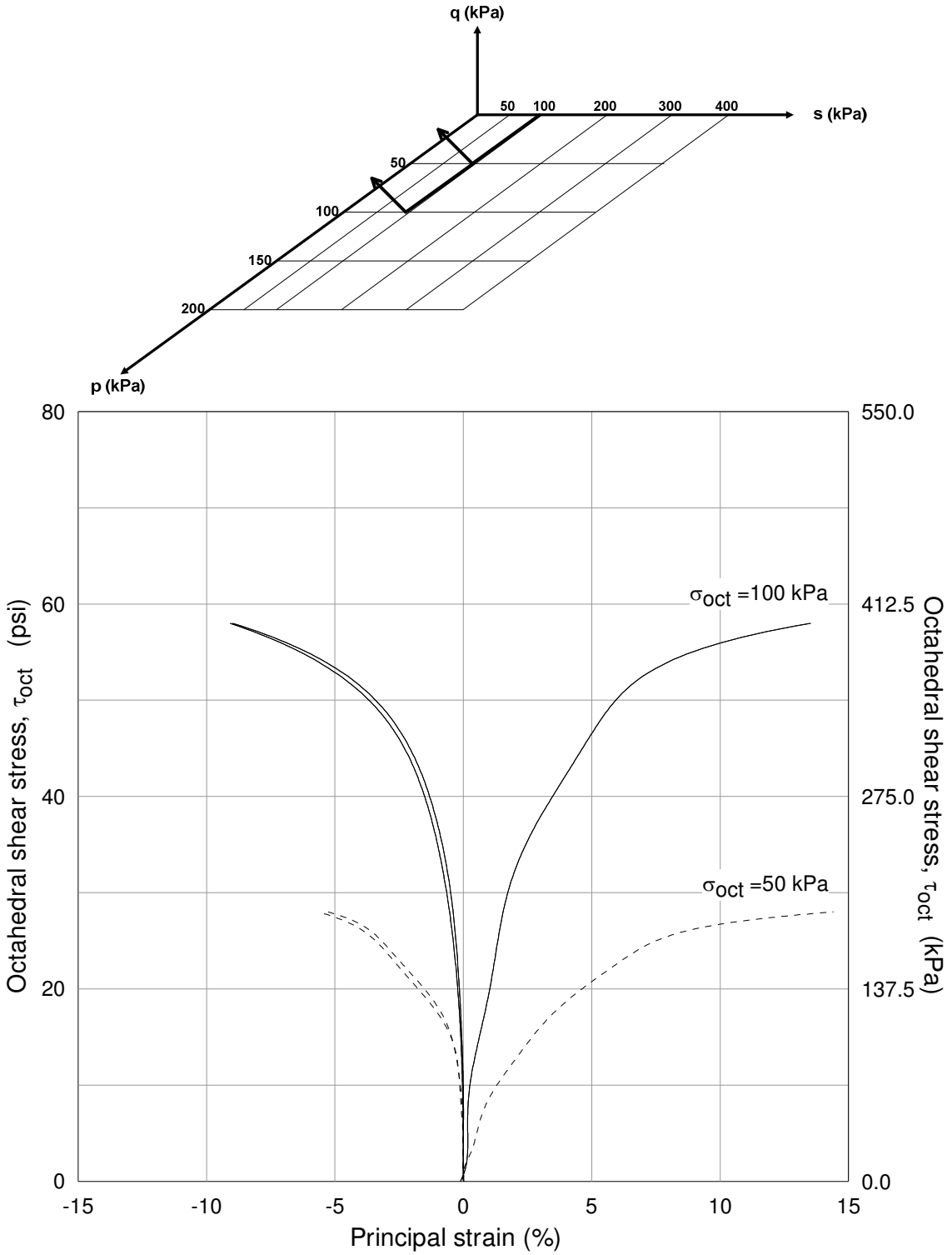

Figure 5.23 Silty sand response from suction-controlled CTC tests at (u_a-u_w) = 100 kPa

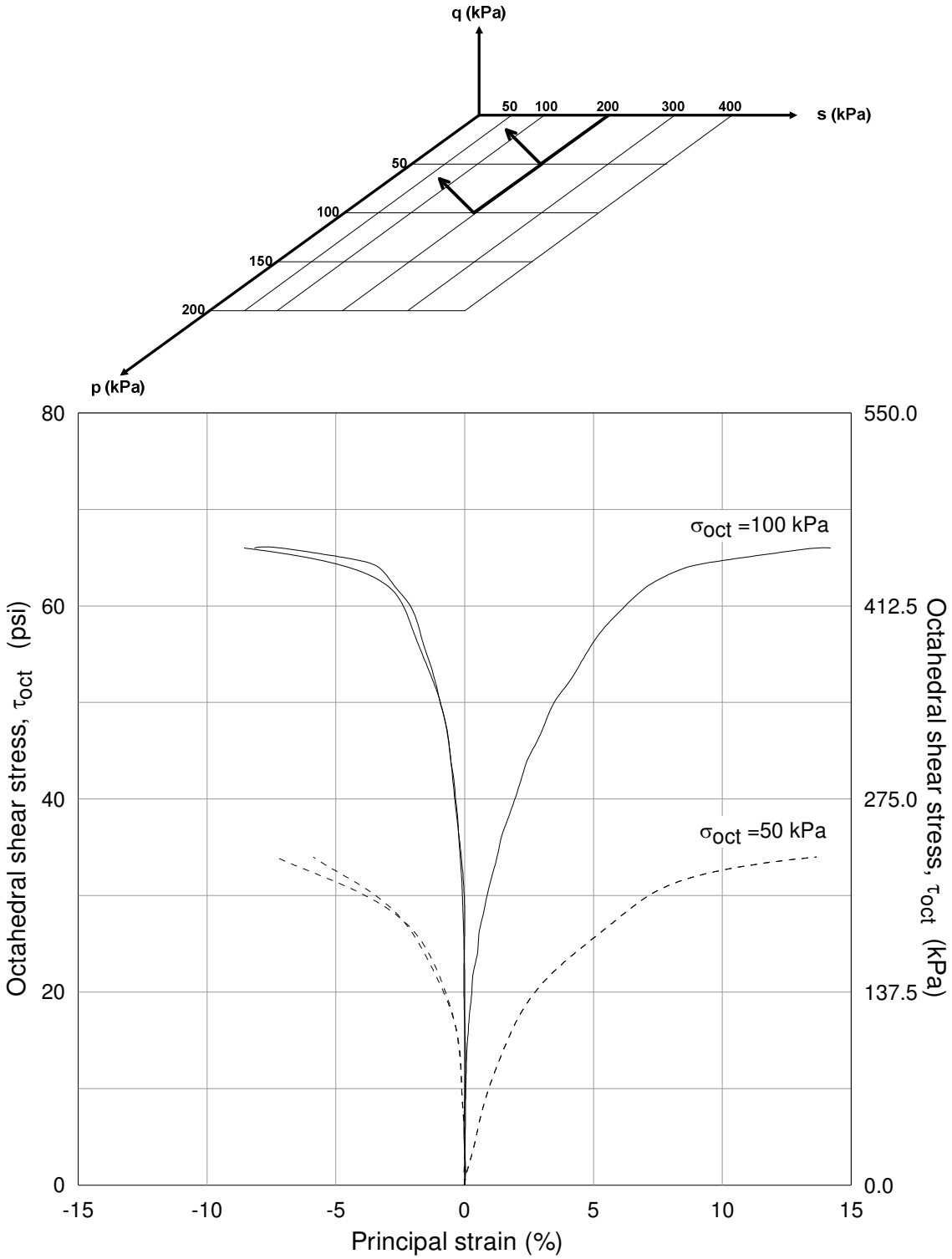

Figure 5.24 Silty sand response from suction-controlled CTC tests at (u_a-u_w) = 200 kPa

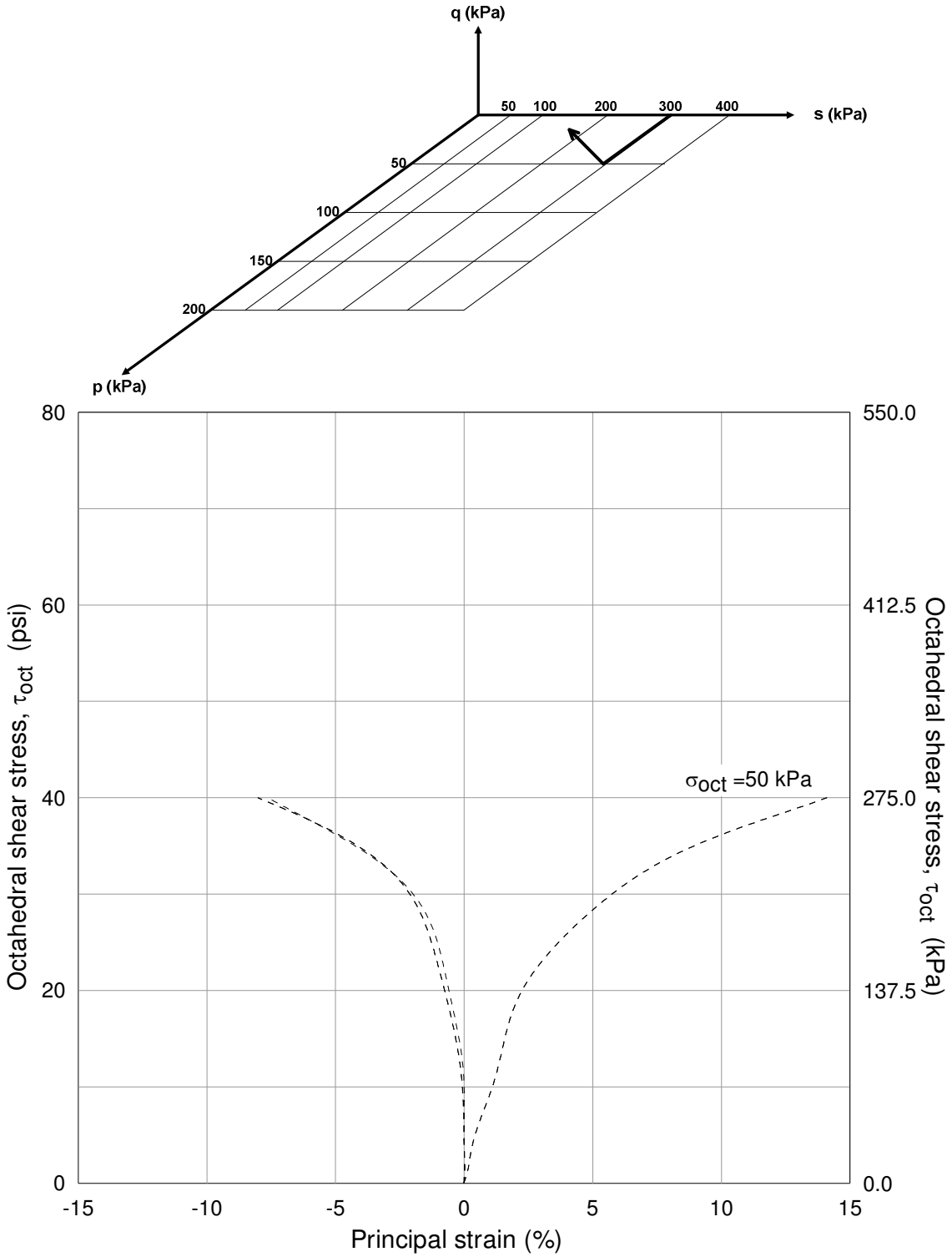

Figure 5.25 Silty sand response from suction-controlled CTC tests at (u_a-u_w) = 300 kPa

5.8.2 Triaxial Compression (TC) Tests

Figures 5.26 and 5.29 show the octahedral shear stress τ_{oct} versus principal strain response of cubical silty sand specimens under constant octahedral normal stress σ_{oct} at different matric suction conditions, $s = u_a$. As mentioned before**,** During TC testing, the major principal stress σ_1 was increased, whereas the intermediate σ_2 and minor σ_3 principal stresses were reduced, such that the net octahedral normal stress σ_{oct}, remained constant. As the minor σ_3 and the intermediate σ_2 principal stresses were equally decreased (i.e., $\Delta\sigma_2 = \Delta\sigma_3 = -\Delta\sigma_1/2$), the corresponding minor ε_3 and intermediate ε_2 principal strains were found to be expansive (–). The major principal stress σ_1 was increased during testing, and consequently, its corresponding major principal strain ε_1 was compressive (+). Matric suction was also found to exert an important influence on the degree of anisotropy of the specimens, with similar response (i.e., less anisotropy) in the minor ε_3 and intermediate ε_2 principal strains as matric suction increased.

Figures 5.26 to 5.29 again show influence exerted by matric suction on the shear resistance of the cubical silty sand specimens, with a considerable increase in the ultimate τ_{oct} for s = 400 kPa (58 psi) under σ_{oct} of 200 kPa (29 psi).

As previously shown in figures 5.14 to 5.18, the net octahedral stress σ_{oct}, which is directly related to the net mean stress p_{net}, has a paramount influence on the soil strengths. This effect is show in figures 5.30 to 5.35.

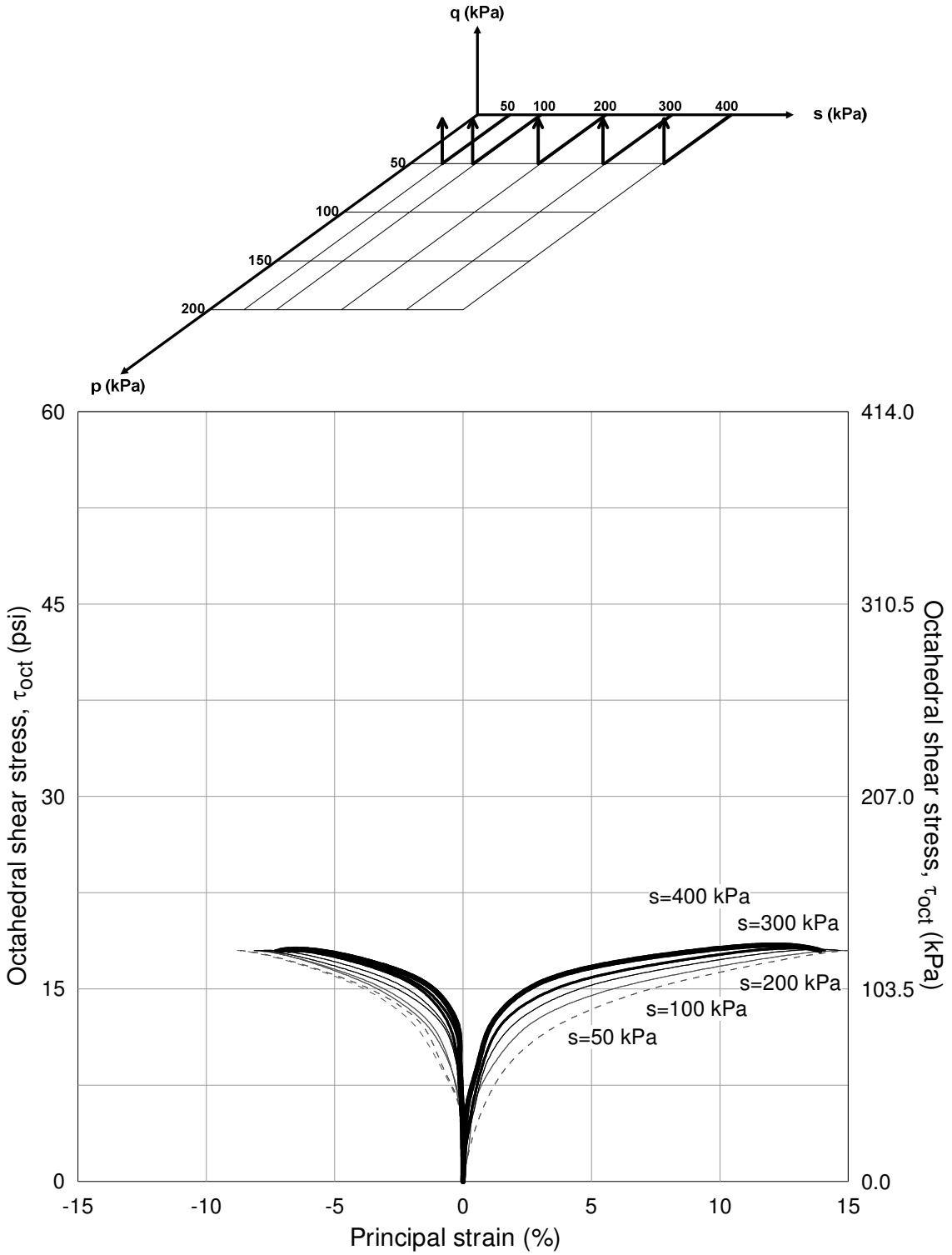

Figure 5.26 Silty sand response from suction-controlled TC tests at σ_{oct} = 50 kPa

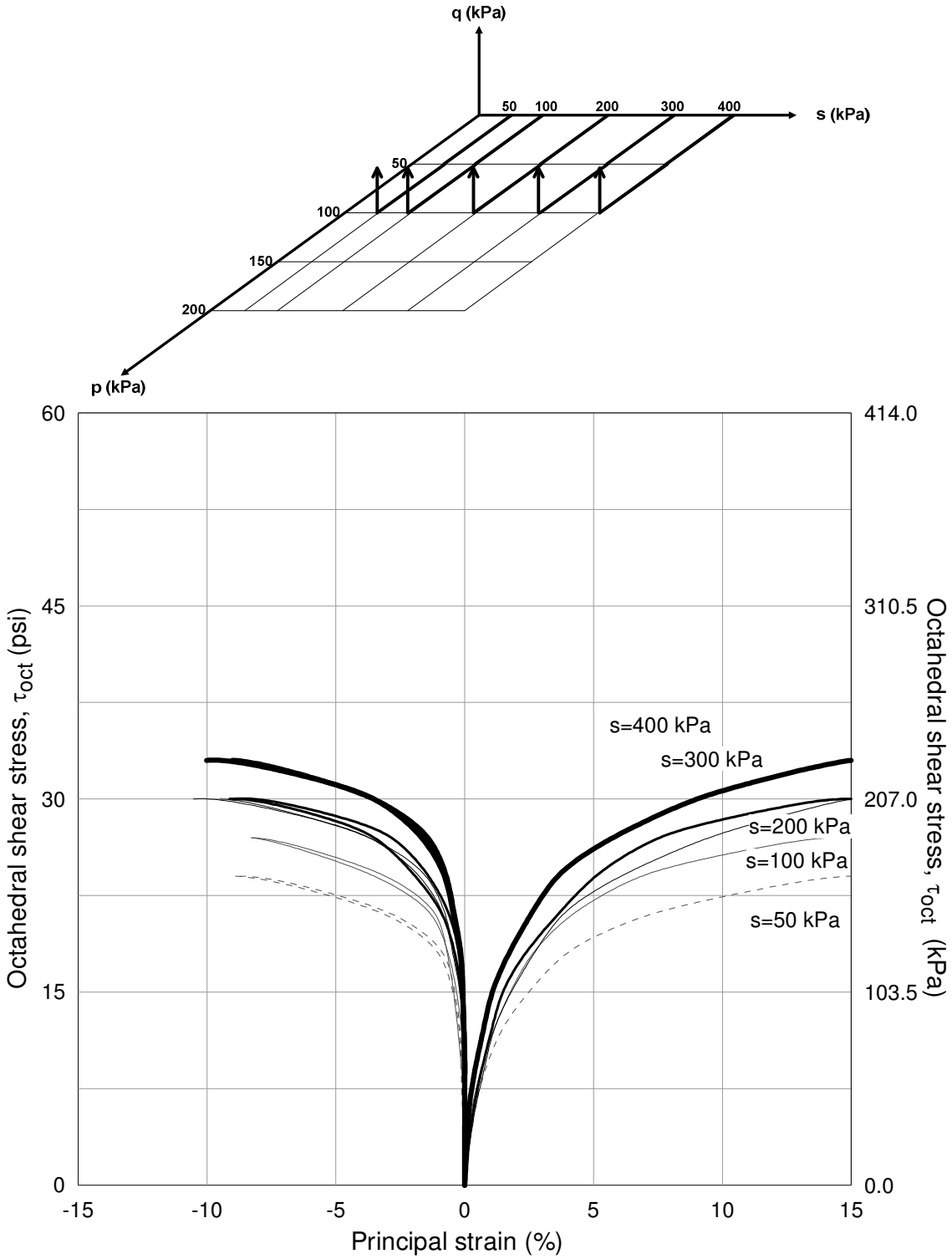

Figure 5.27 Silty sand response from suction-controlled TC tests at σ_{oct} = 100 kPa

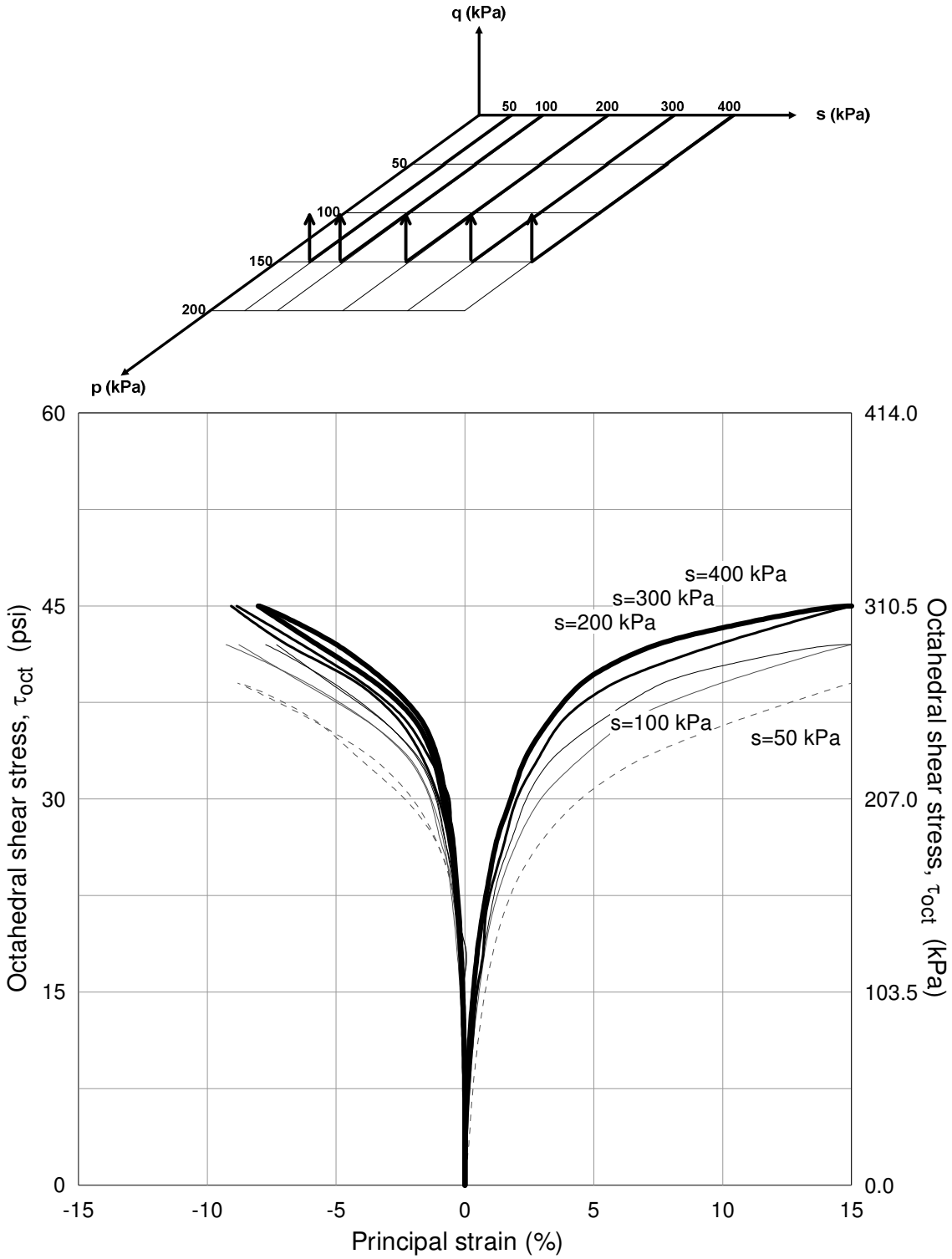

Figure 5.28 Silty sand response from suction-controlled TC tests at σ_{oct} = 150 kPa

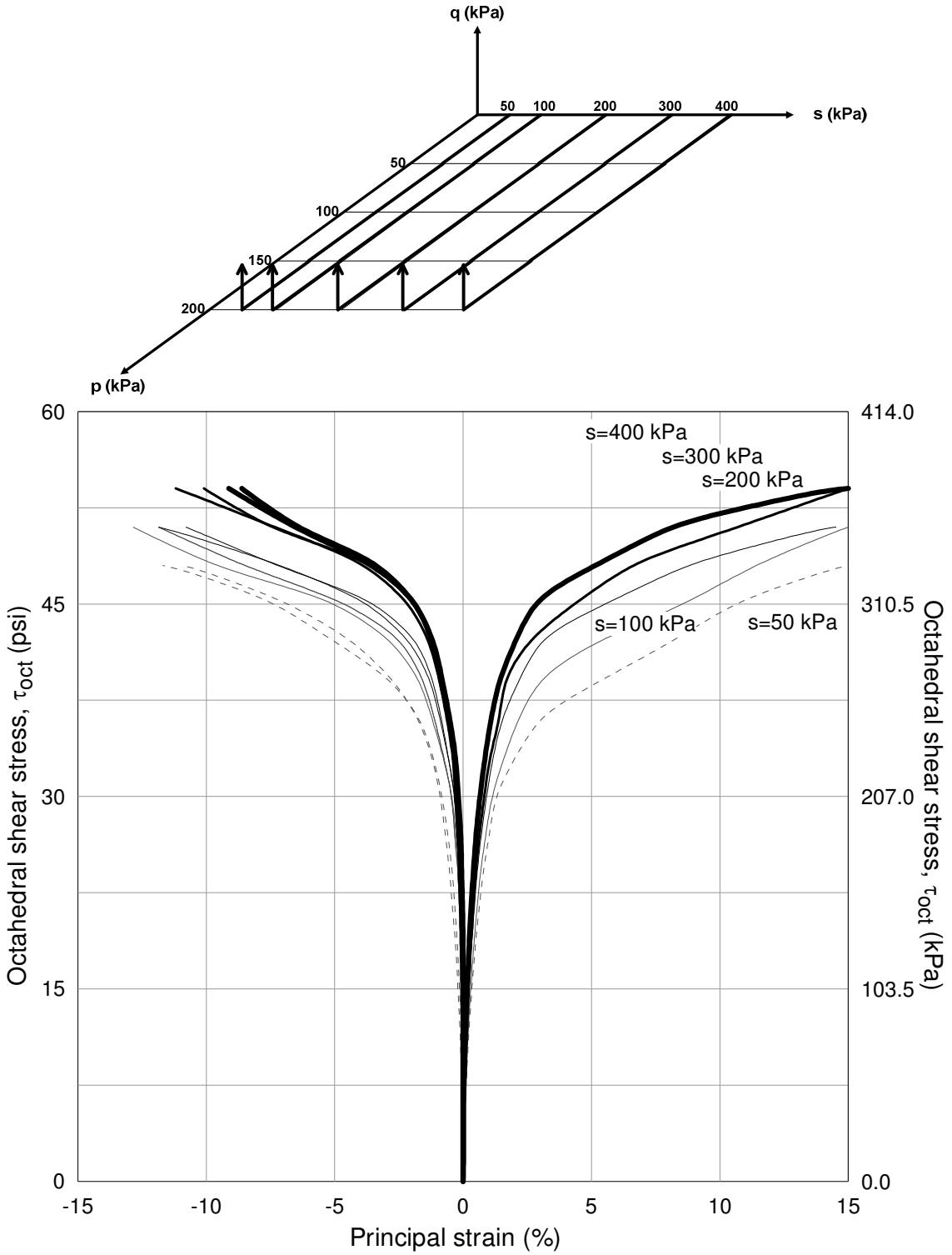

Figure 5.29 Silty sand response from suction-controlled TC tests at σ_{oct} = 200 kPa

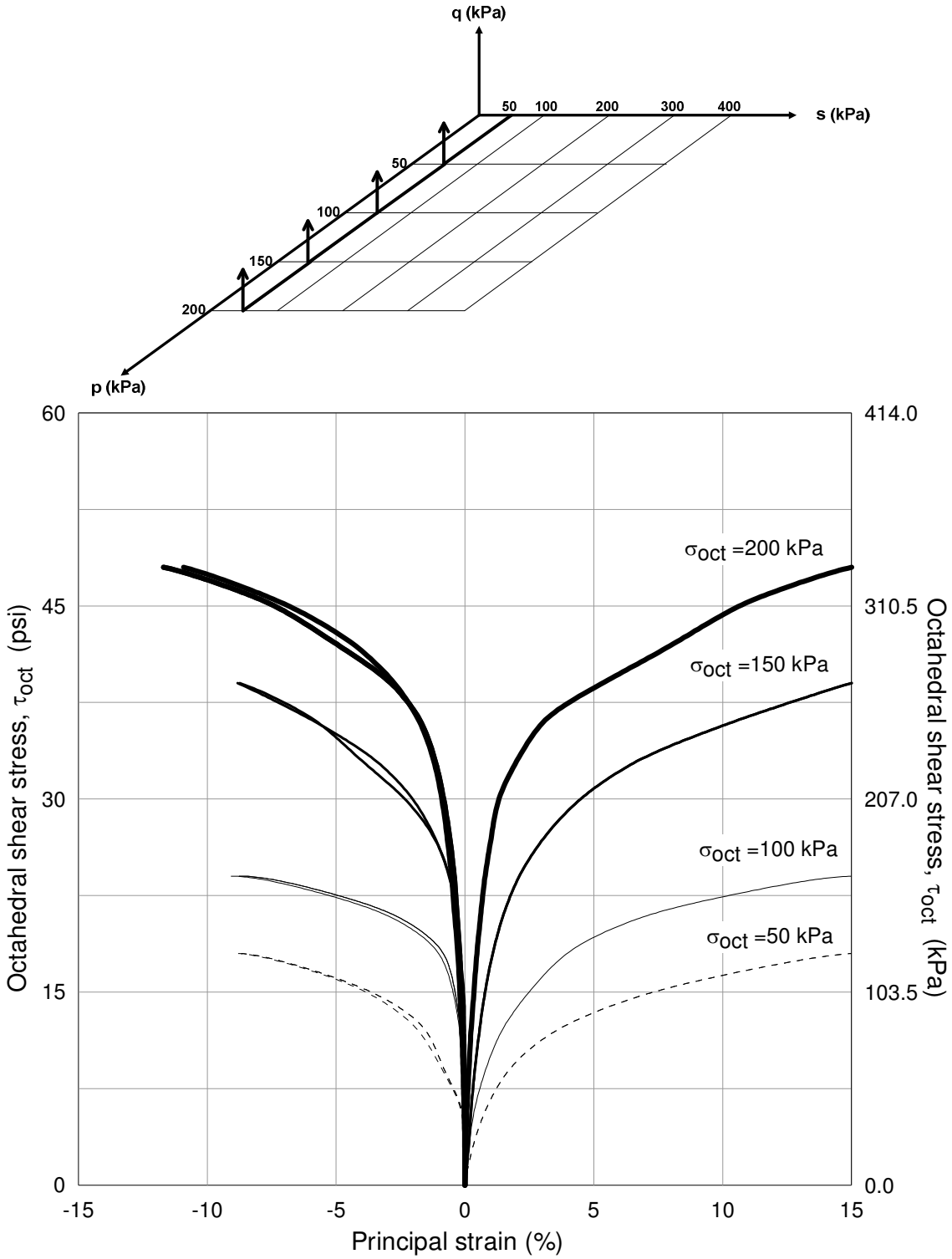

Figure 5.30 Silty sand response from suction-controlled TC tests at (u_a-u_w) = 50 kPa

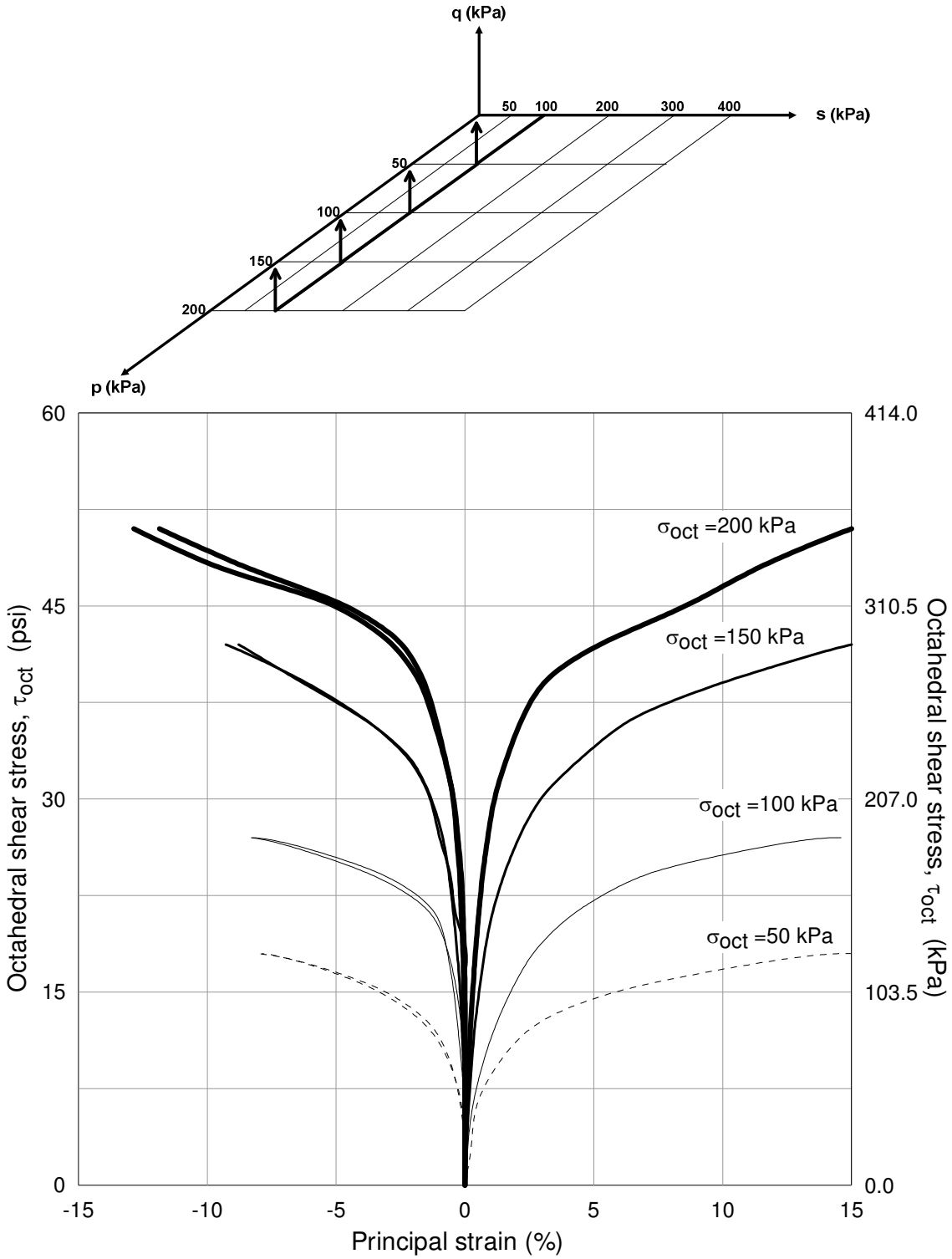

Figure 5.31 Silty sand response from suction-controlled TC tests at (u_a-u_w) = 100 kPa

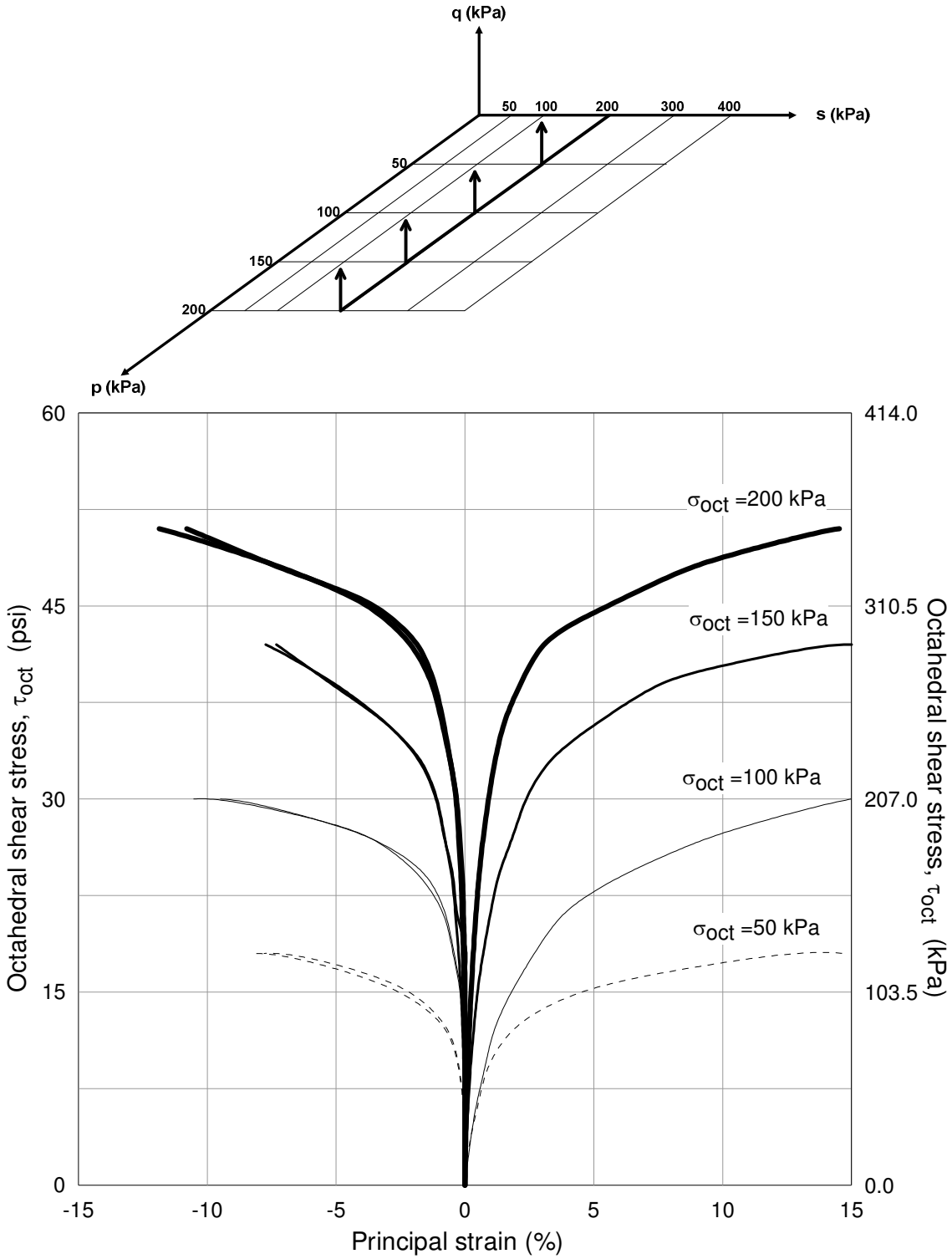

Figure 5.32 Silty sand response from suction-controlled TC tests at (u_a-u_w) = 200 kPa

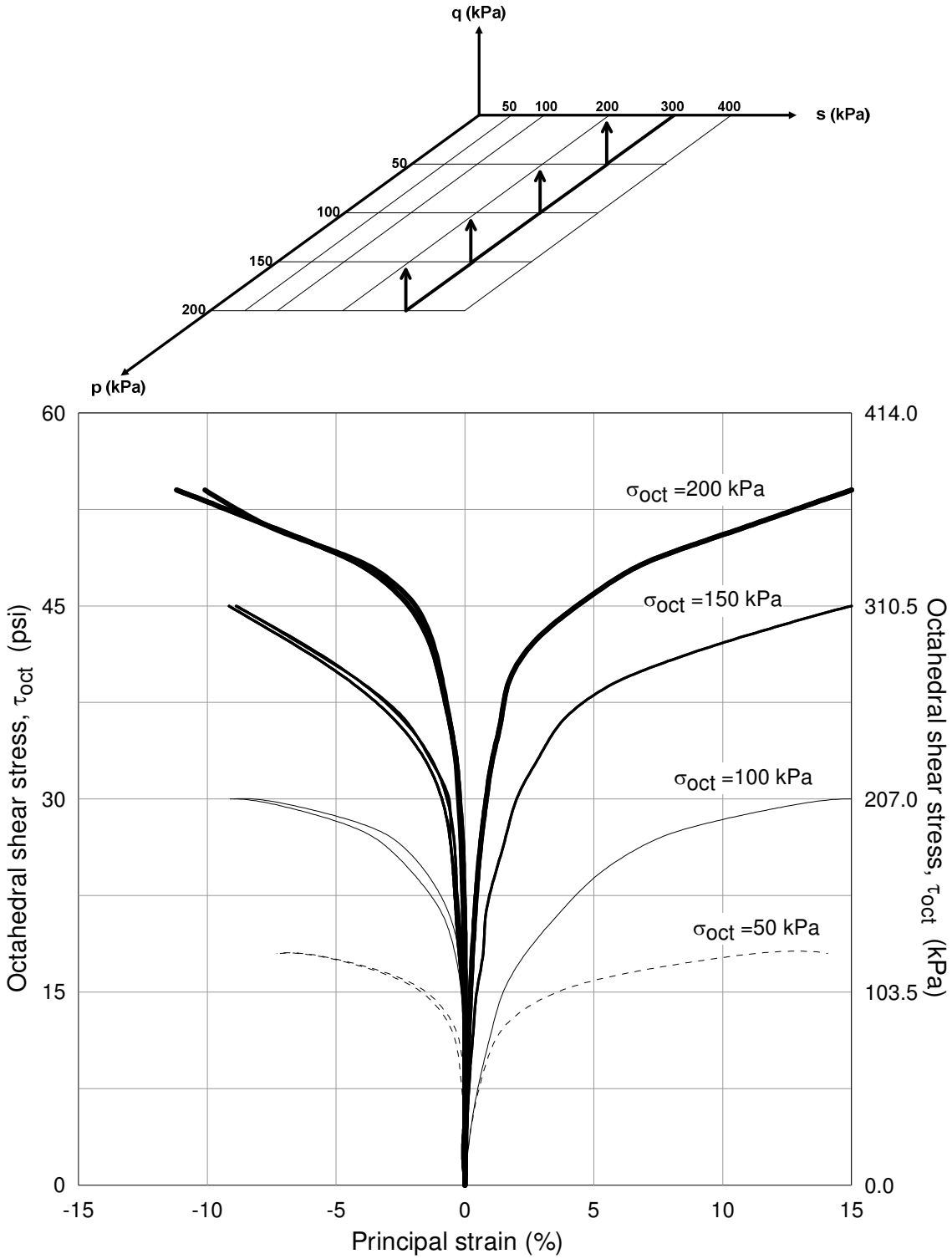

Figure 5.33 Silty sand response from suction-controlled TC tests at (u_a-u_w) = 300 kPa

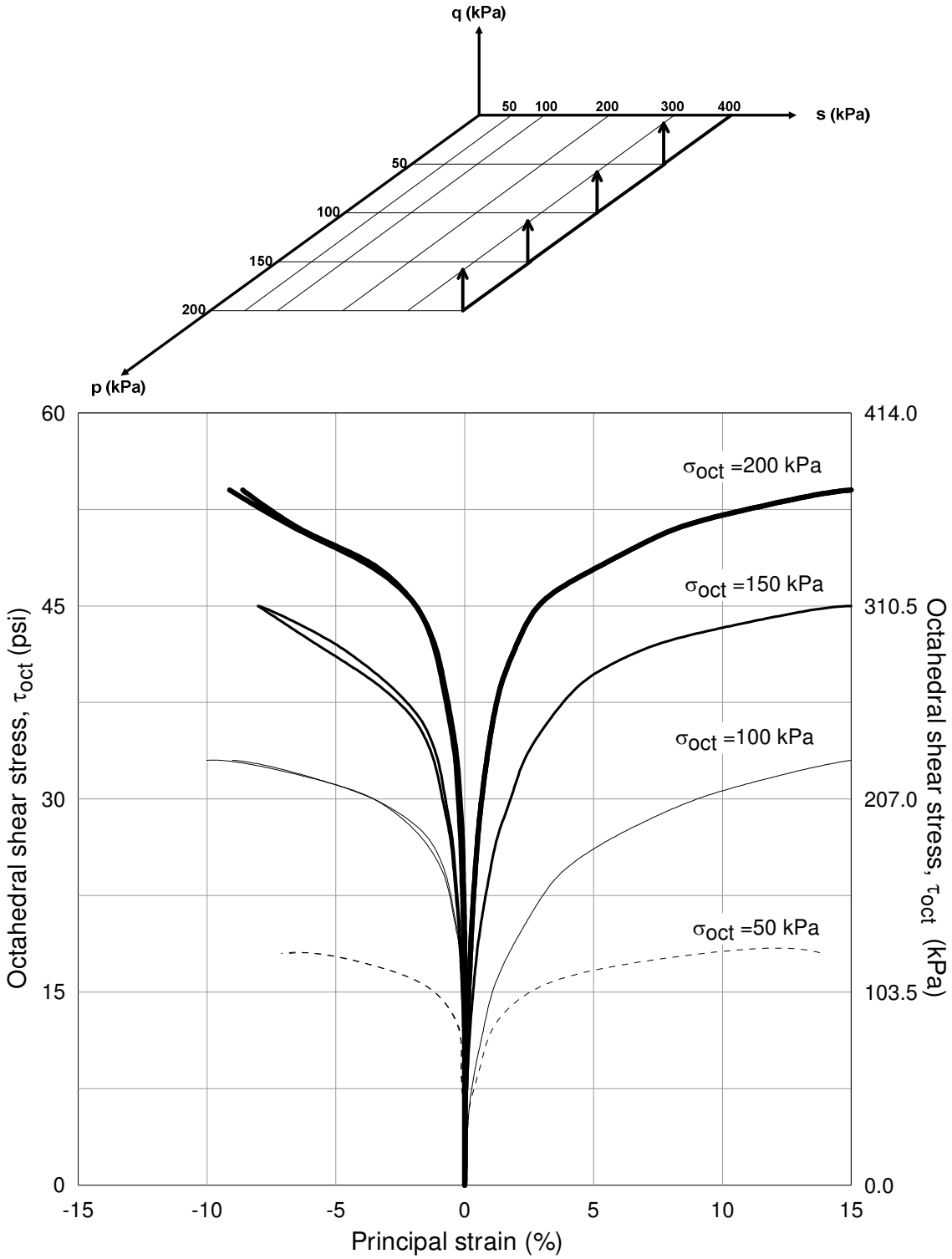

Figure 5.34 Silty sand response from suction-controlled TC tests at (u_a-u_w) = 400 kPa

5.8.3 Triaxial Extension (TE) Tests

A series of 20 TE tests were successfully performed in the suction-controlled cubical cell testing device on 20 specimens of artificially prepared silty sand at different controlled matric suction of 50 kPa (7 psi), 100 kPa (15 psi), 200 kPa (29 psi), 300 kPa (44 psi) and 400 kPa (58 psi) under octahedral normal stress, σ_{oct}, of 50 kPa (7 psi), 100 kPa (15 psi), 150 kPa (22 psi) and 200 kPa (29 psi).

A series of 20 drained (constant-suction), suction-controlled triaxial compression (TE) tests were conducted on several silty sand specimens, to experimentally study the mechanical characteristics of the behavior of unsaturated soil under varying matric suction conditions.

Figures 5.35 to 5.38 present the octahedral shear stress (τ_{oct}) versus principal strain (ε_i) response from the series of 20 tests. In general, Figure 5.35 to 5.38 show an important influence of matric suction on the shear resistance of the silty sand specimens. During TE testing, the intermediate σ_2 and minor σ_3 principal stresses were equal and equally increased (i.e., $\Delta\sigma_2 = \Delta\sigma_3$), while the major principal stress σ_1 was decreased (i.e., $\Delta\sigma_1 = -2\Delta\sigma_2 = -2\Delta\sigma_3$). Consequently, the intermediate ε_2 and minor ε_3 principal strains were found to be compressive (+), and the major ε_1 principal strain was expansive (-).

Figures 5.35 to 5.38 again show influence exerted by matric suction on the shear resistance of the cubical silty sand specimens, with a considerable increase in the ultimate τ_{oct} for s = 400 kPa (58 psi) under σ_{oct} of 200 kPa (29 psi).

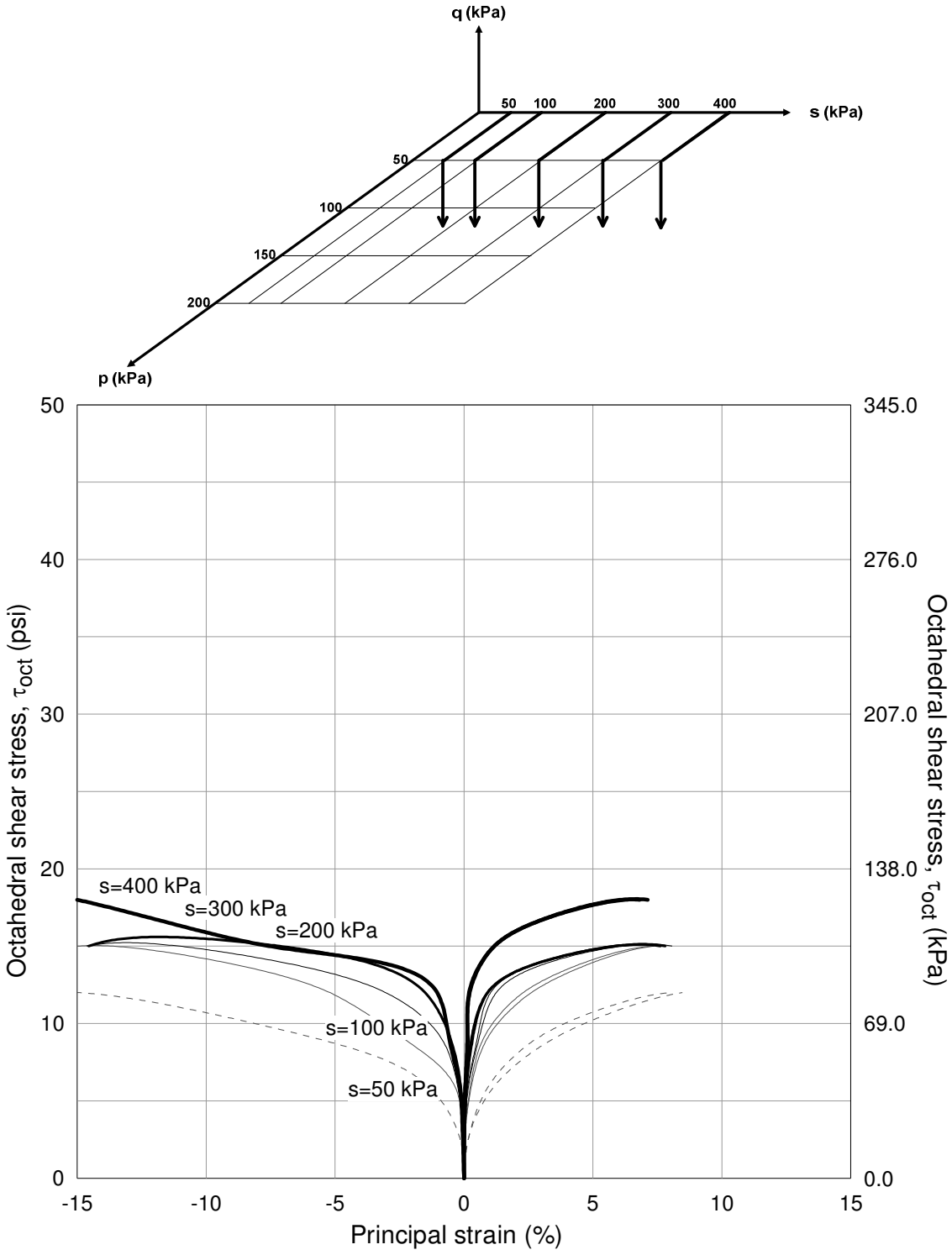

Figure 5.35 Silty sand response from suction-controlled TE tests at σ_{oct} = 50 kPa

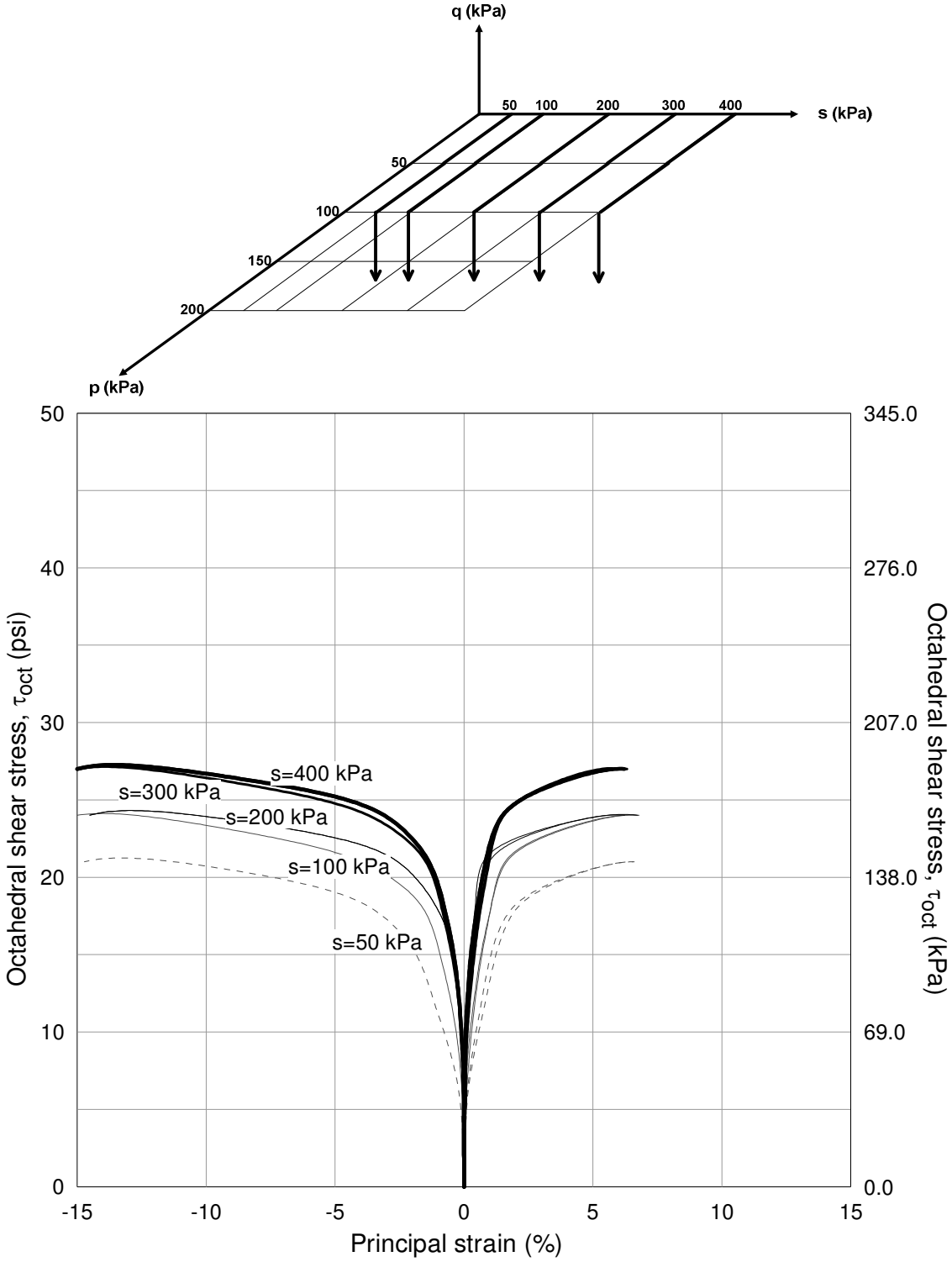

Figure 5.36 Silty sand response from suction-controlled TE tests at σ_{oct} = 100 kPa

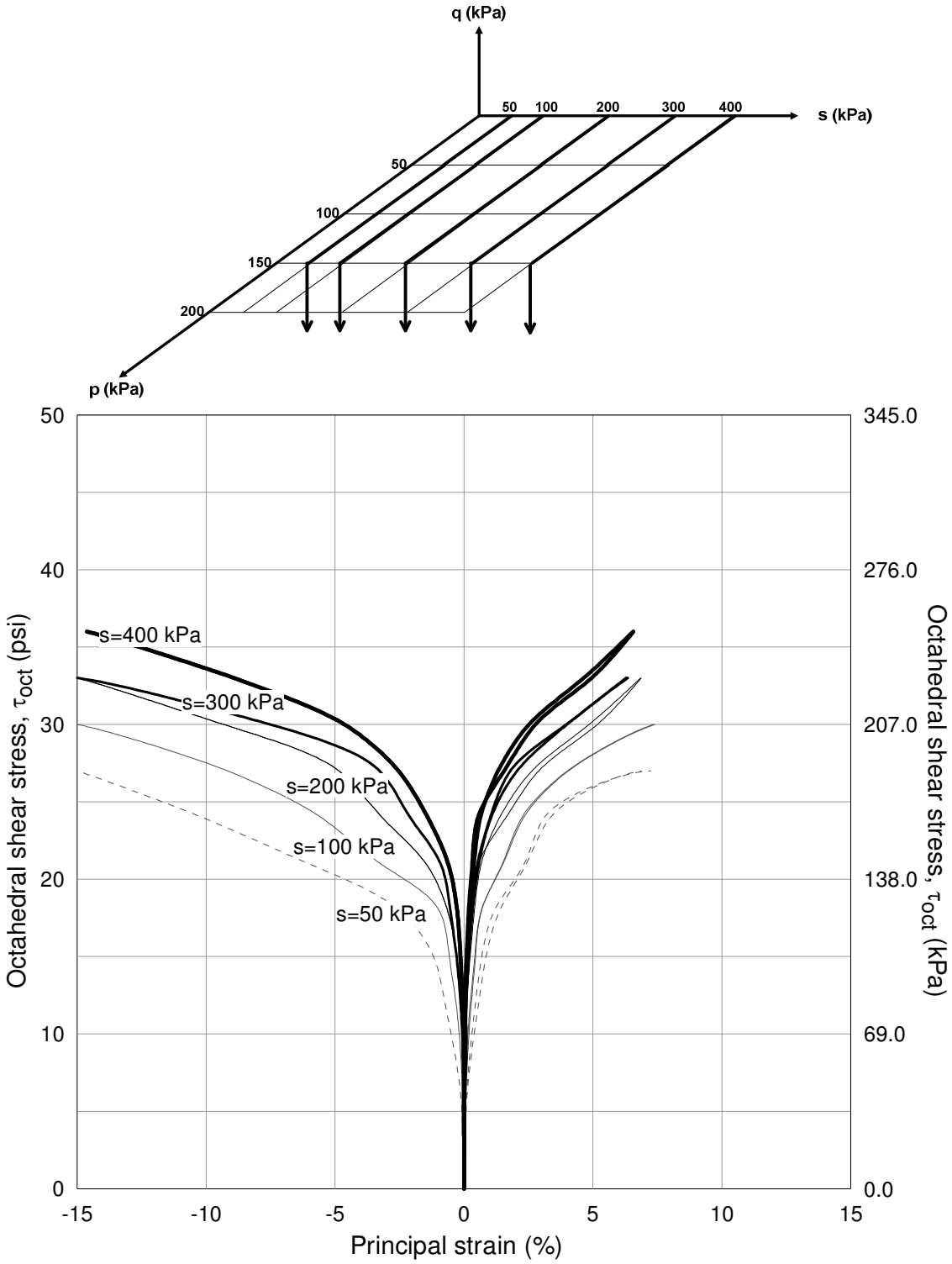

Figure 5.37 Silty sand response from suction-controlled TE tests at σ_{oct} = 150 kPa

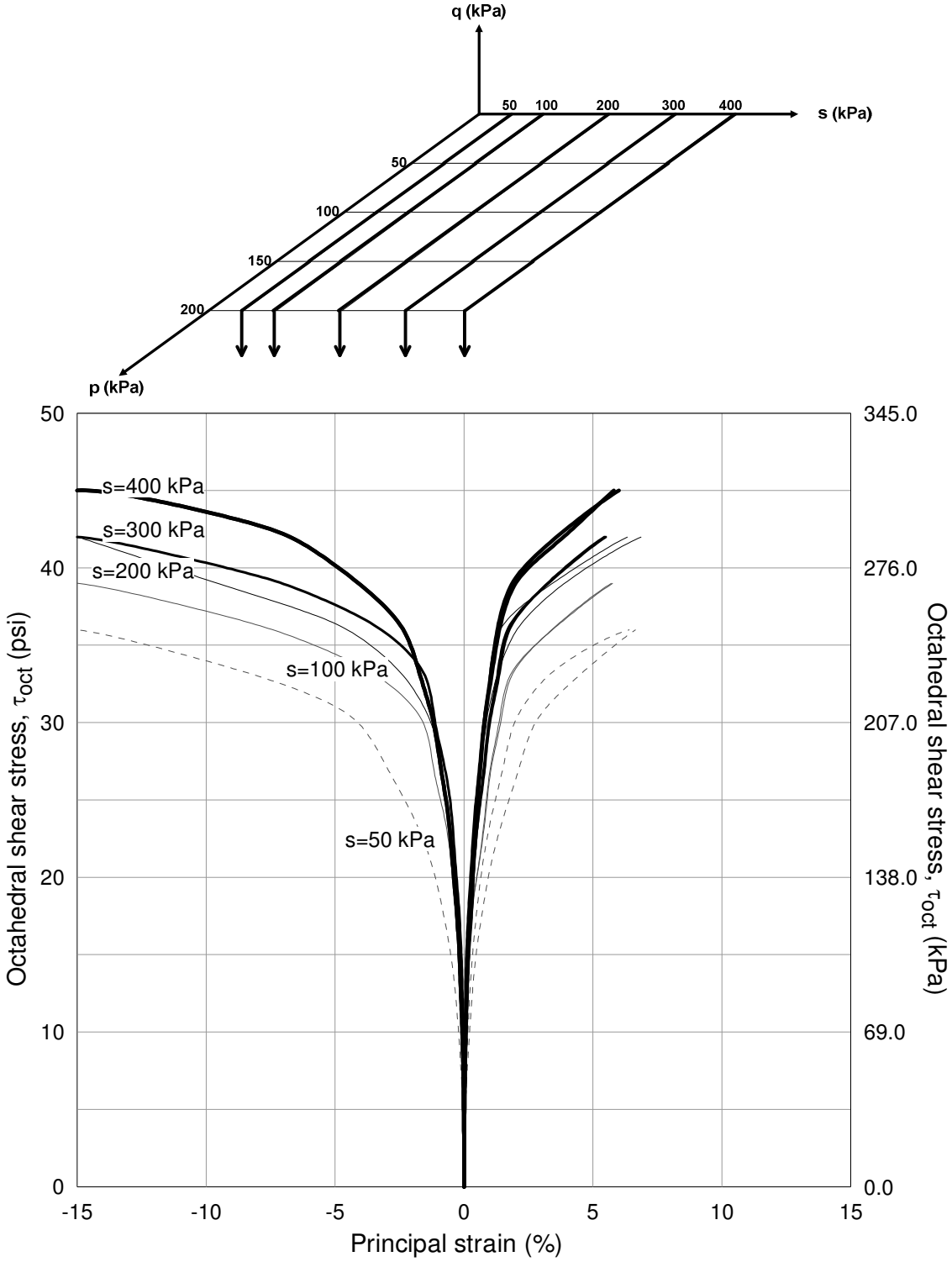

Figure 5.38 Silty sand response from suction-controlled TE tests at σ_{oct} = 200 kPa

Results from TE tests have been replotted in figures 5.39 to 5.43 to highlight the influence of octahedral normal stress, σ_{oct}, which is directly related to the net mean stress p_{net} ,on soil's stress-strain behavior. It appears that the effect of net confinement on peak strength is the same regardless of the level of matric suction applied to the soil. This could be attributed to the predominantly granular nature of the test soil (80% sand).

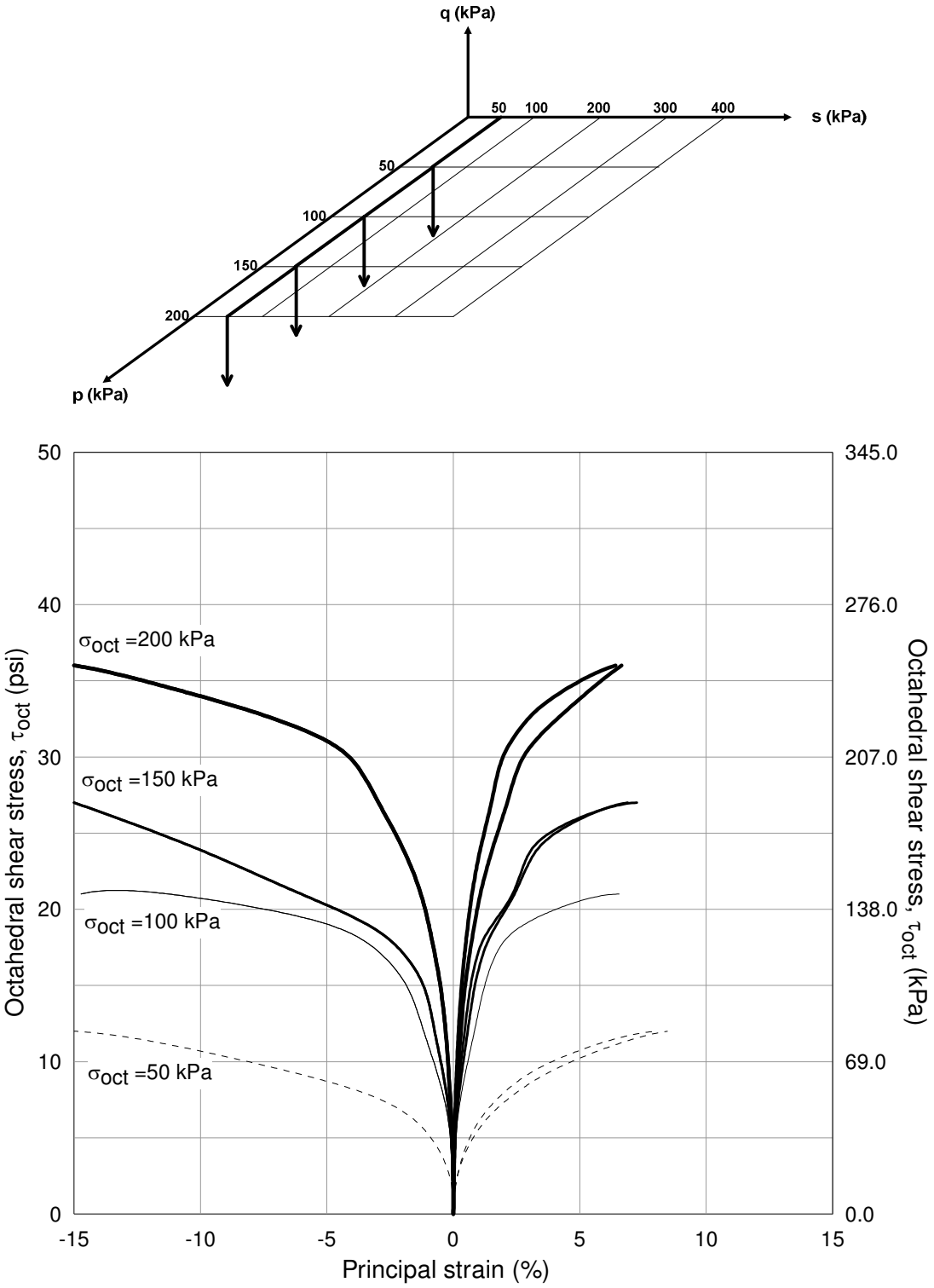

Figure 5.39 Silty sand response from suction-controlled TE tests at (u_a-u_w) = 50 kPa

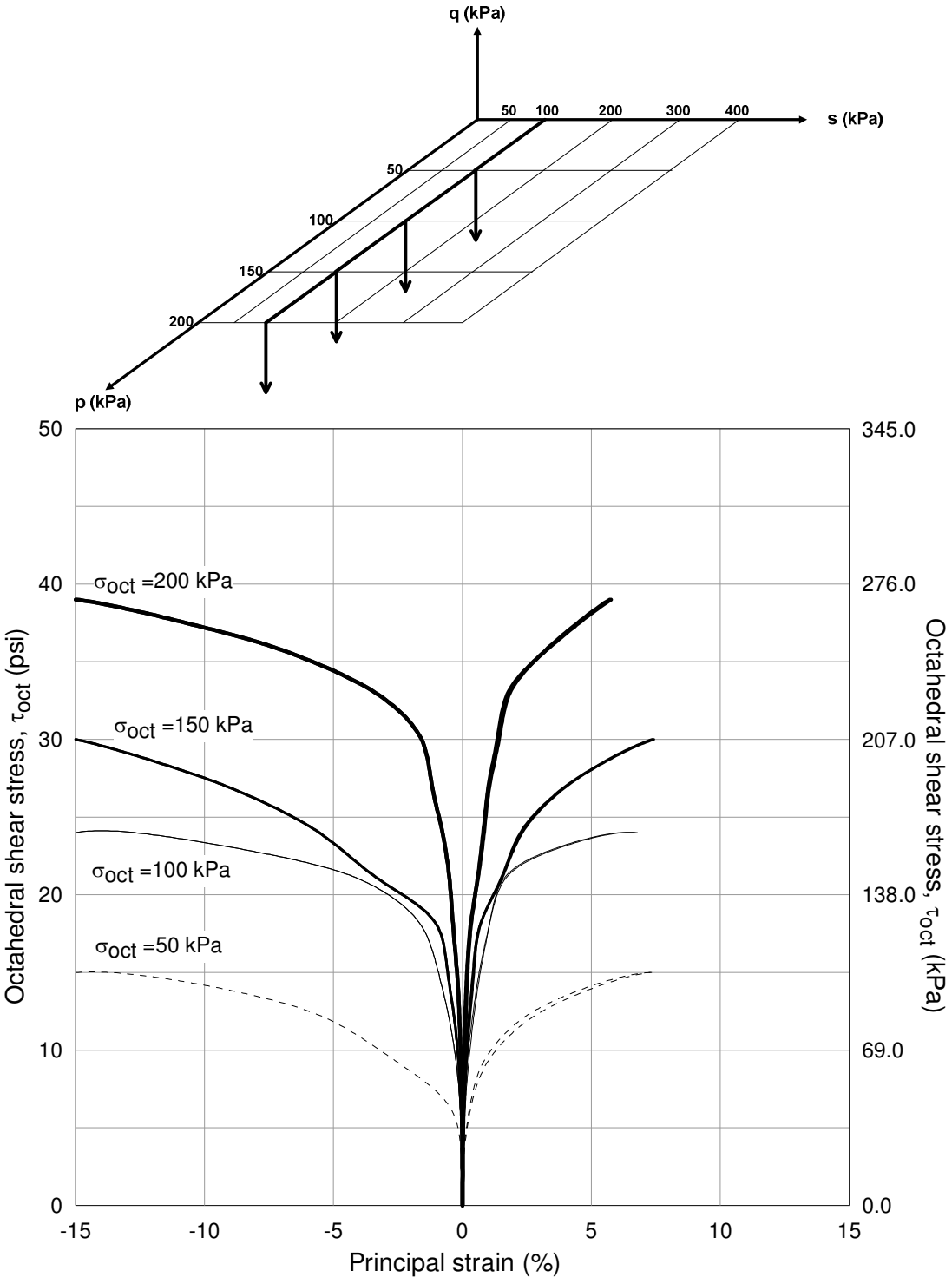

Figure 5.40 Silty sand response from suction-controlled TE tests at (u_a-u_w) = 100 kPa

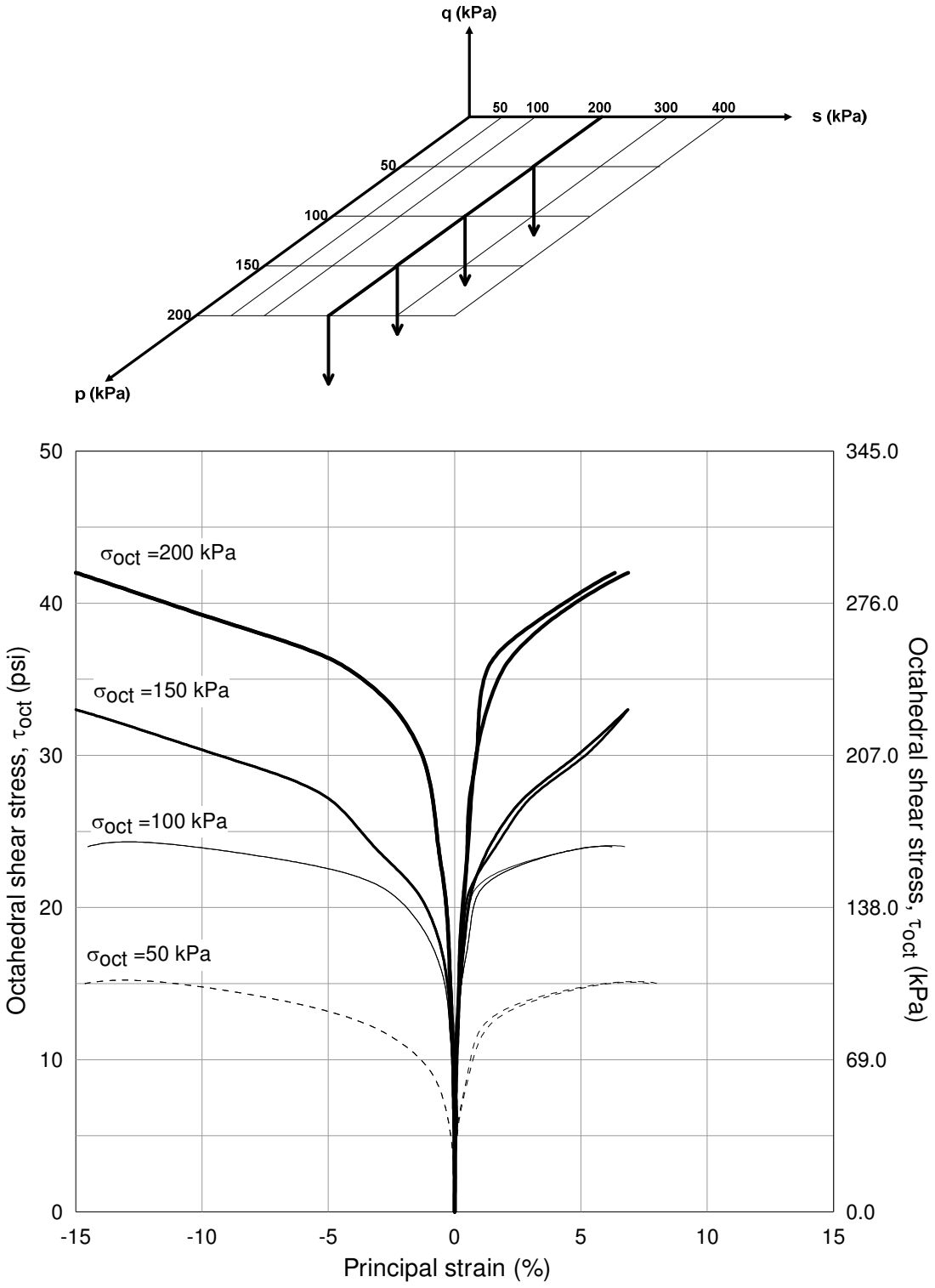

Figure 5.41 Silty sand response from suction-controlled TE tests at (u_a-u_w) = 200 kPa

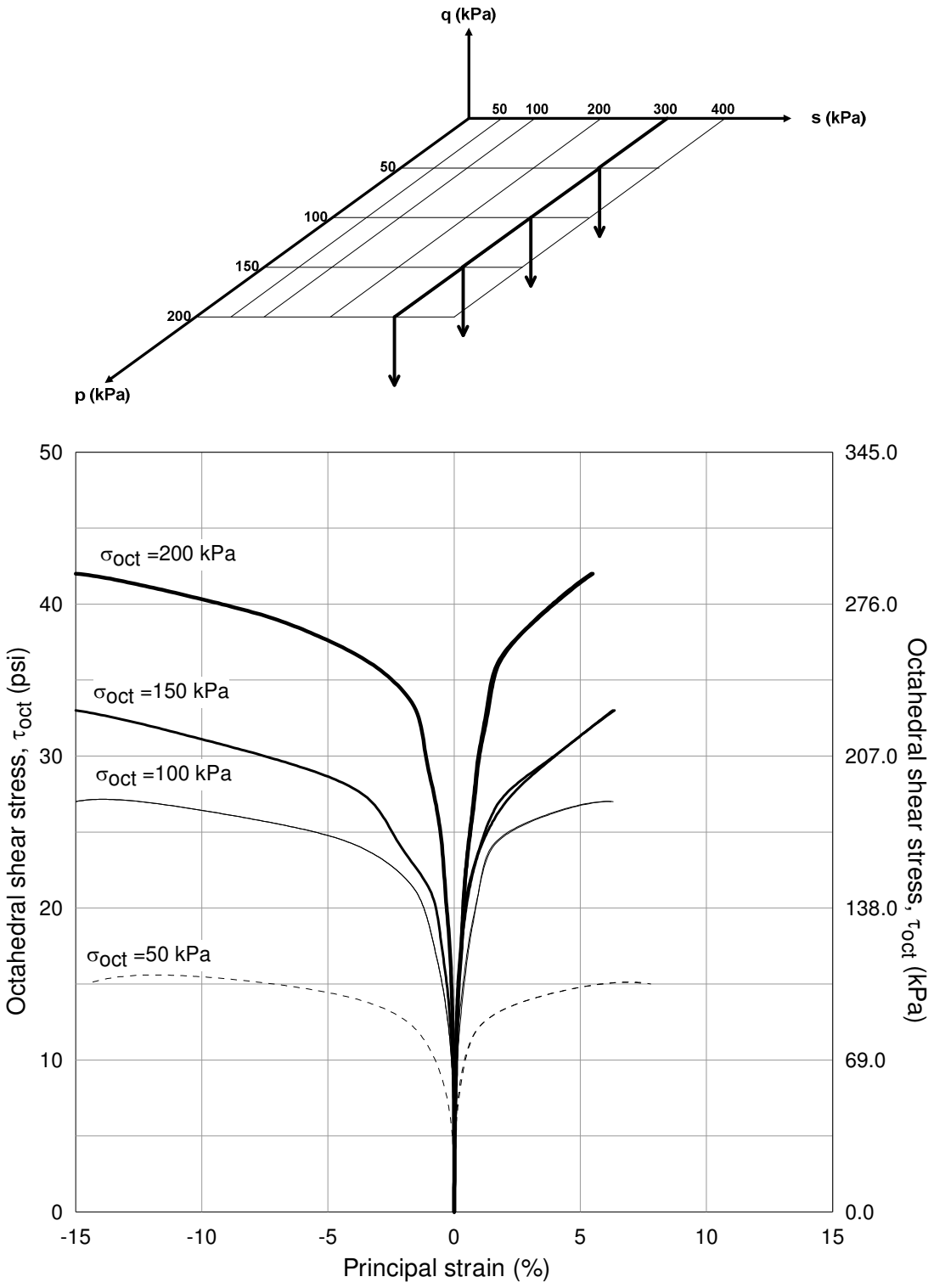

Figure 5.42 Silty sand response from suction-controlled TE tests at (u_a-u_w) = 300 kPa

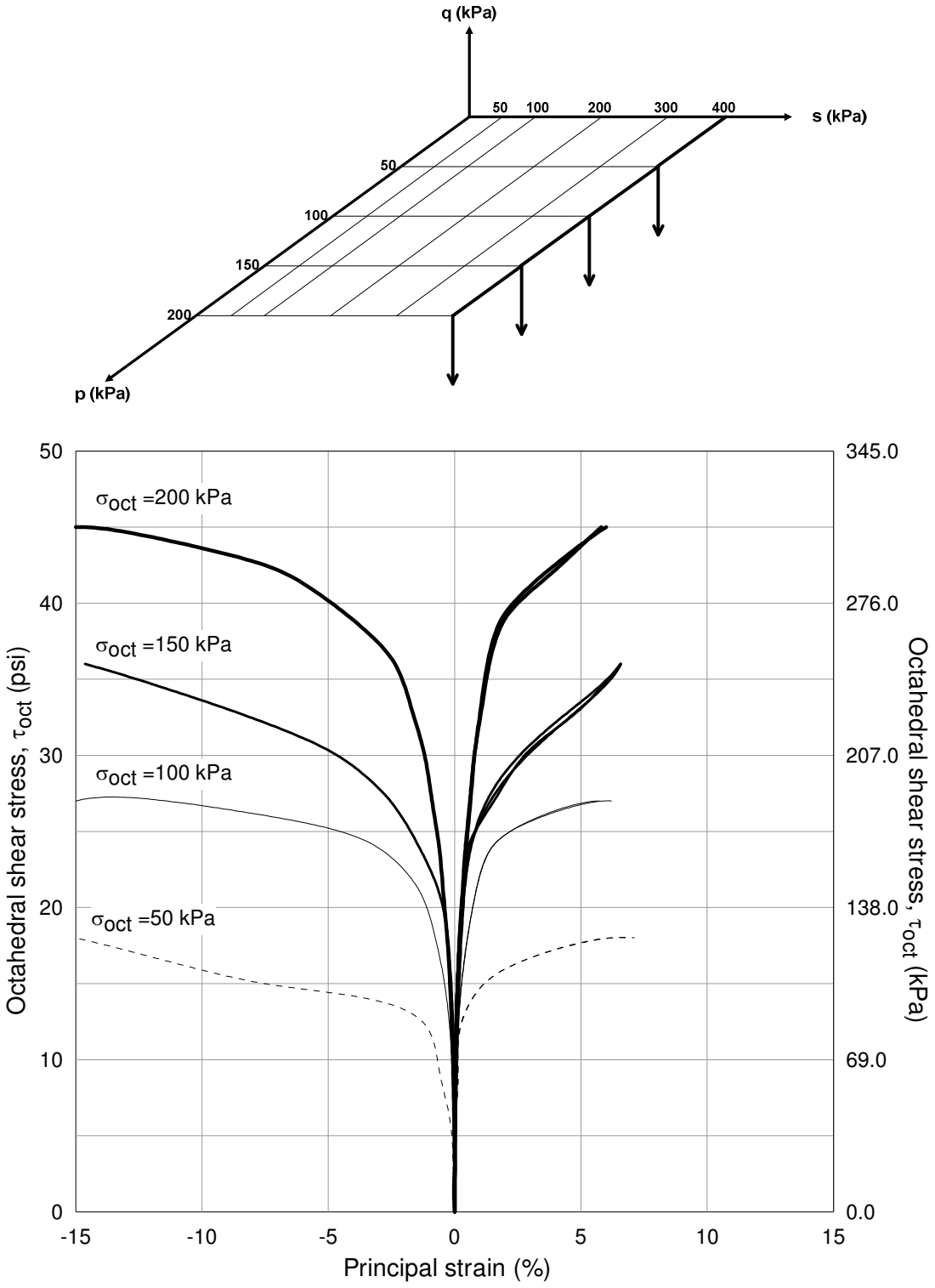

Figure 5.43 Silty sand response from suction-controlled TE tests at (u_a-u_w) = 400 kPa

5.8.4 Failure Envelops in Net Octahedral Stress Plane

Figures 5.44 and 5.45 show the projection of the failure surface (incipient critical state condition at ε_q^{tot} = 10%), identified during TC and TE tests, on the octahedral ($\sigma_1 - u_a : \sigma_2 - u_a : \sigma_3 - u_a$) stress plane (or π-plane) for different values of matric suction, s = 50 kPa (7 psi), 100 kPa (14 psi), 200 kPa (29 psi), 300 kPa (44 psi), and 400 kPa (58 psi), as a function of the net octahedral normal stress, σ_{oct}.

Projections in figures 5.44 and 5.45 further highlight the significant influence of matric suction on the size and position of the failure envelopes, with a considerable expansion of the surface for s = 58 psi (400kPa). Moreover, and as expected, the net octahedral stress has a direct effect on the octahedral failure envelope.

Figure 5.46 shows the peak results from suction-controlled TC and TE test plotted on the triaxial (Rendulic) stress plane, ($\sigma_1 - u_a : \sqrt{2}(\sigma_2 - u_a) : \sqrt{2}(\sigma_3 - u_a)$), for different values of matric suction, s = 50 kPa (7 psi), 100 kPa (14 psi), 200 kPa (29 psi), 300 kPa (44 psi), and 400 kPa (58 psi). Failure envelops are found to be paralled, in accordance to findings in section 5.7. The proximity of the failure envelopes at higher suction values is also typical of granular materials.

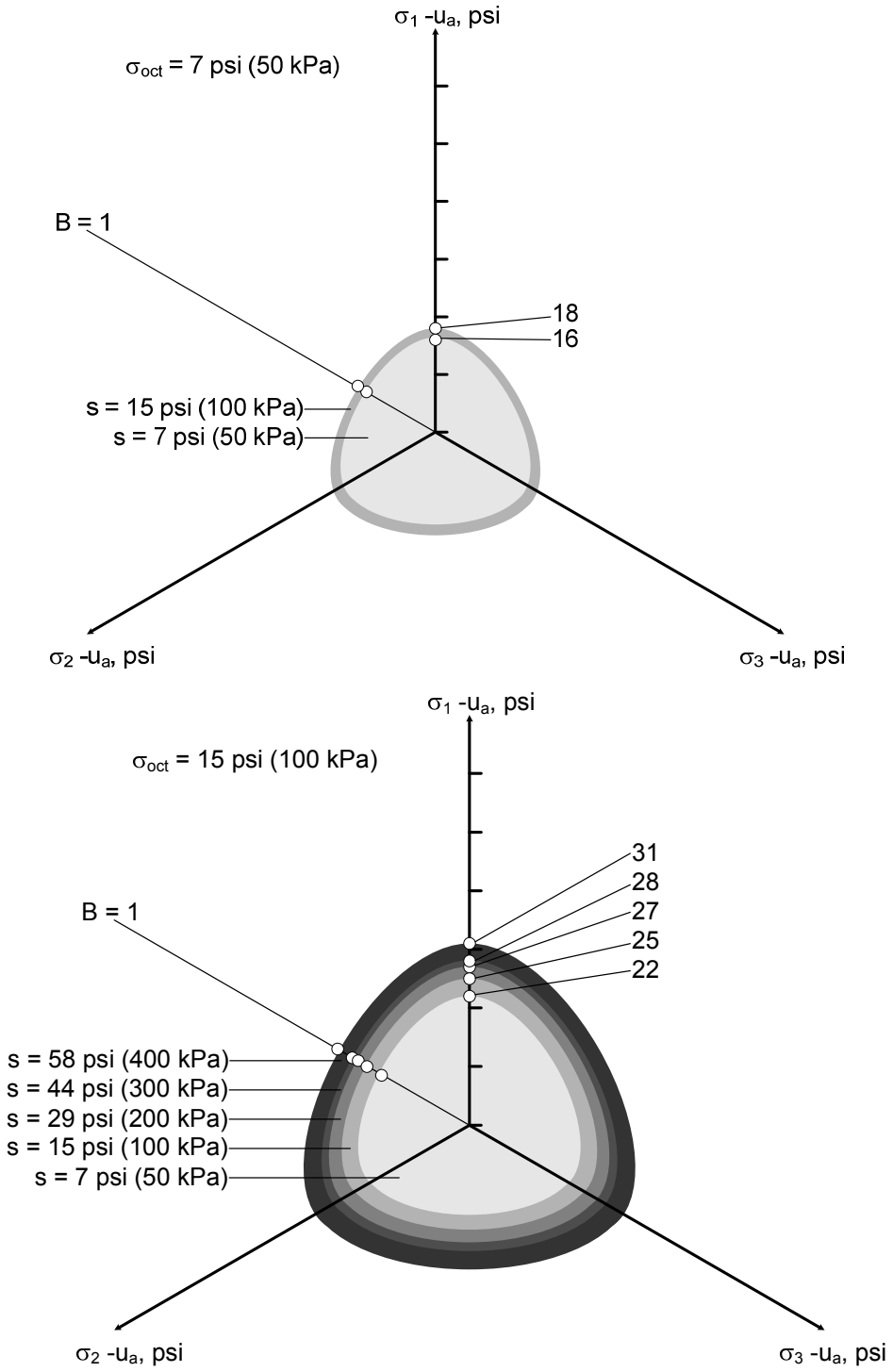

Figure 5.44 Projections of incipient failure envelopes on octahedral plane at σ_{oct} = 50 kPa and 100 kPa

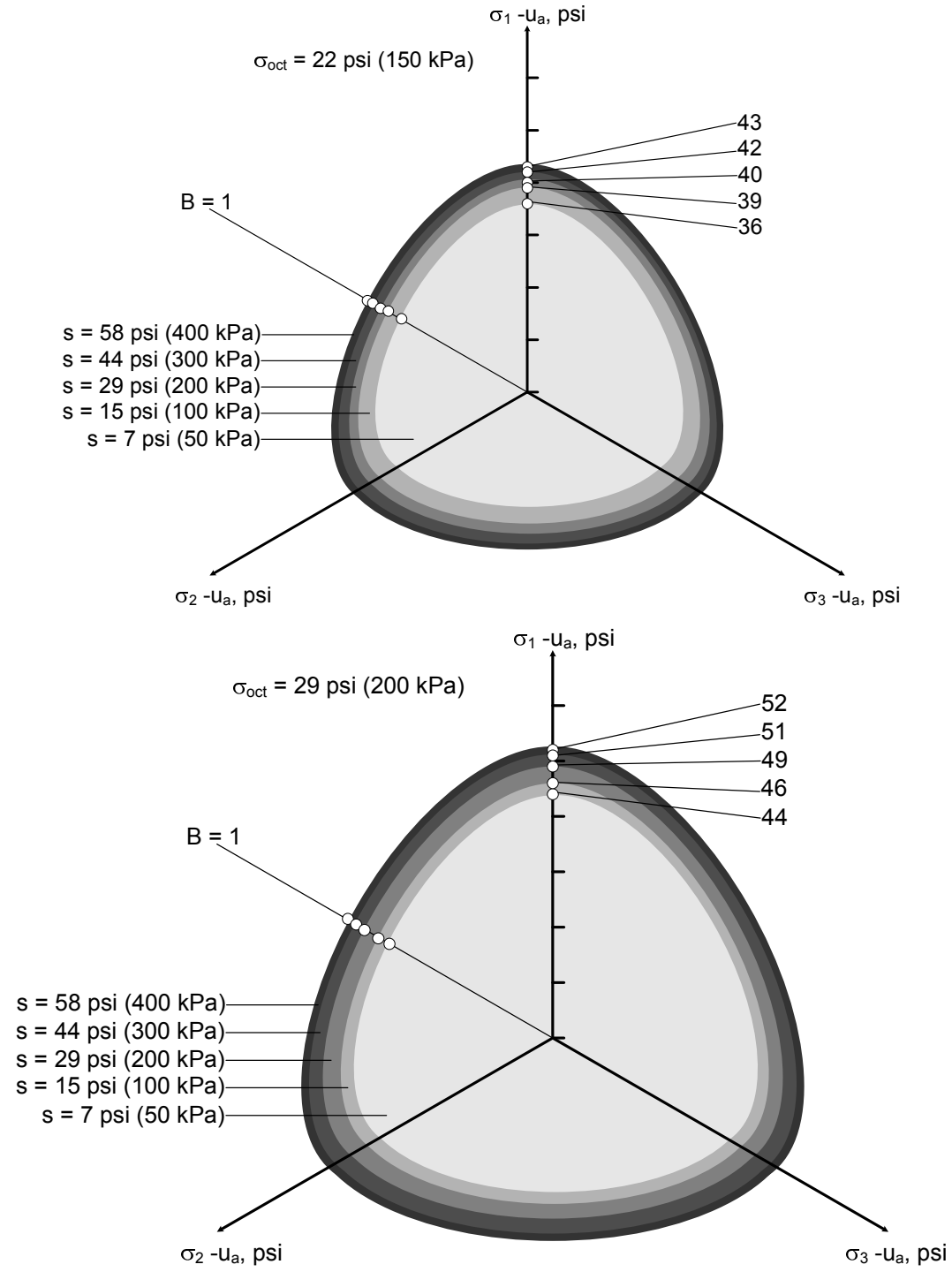

Figure 5.45 Projections of incipient failure envelopes on octahedral plane at σ_{oct} = 150 kPa and 200 kPa

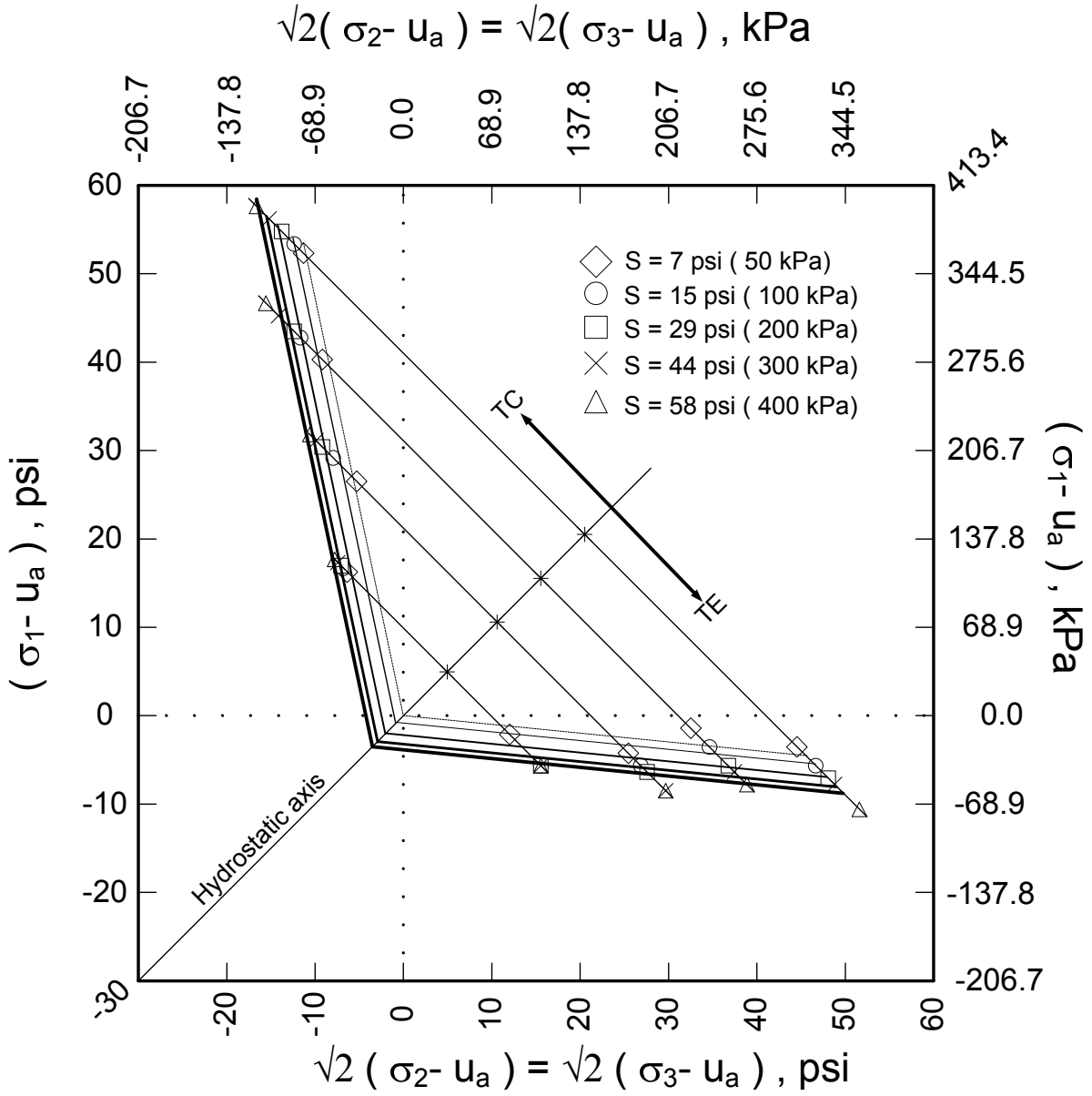

Figure 5.46 TC and TE stress paths on triaxial plane

The next chapter describes the conceptual framework of the Barcelona model. Results from suction-controlled HC, TC and CTC tests on silty sand are used for calibration and validation of the model.

CHAPTER 6

MODELING CONSTITUTIVE BEHAVIOR OF UNSATURATED SILTY SAND

6.1 Introduction

Several attempts have been made in the last few decades to describe the volume change behavior of unsaturated soils under different stress state conditions. The constitutive relations describing the volume change behavior of unsaturated soils relate the deformation state variables (e.g., volumetric strain ε_v or void ratio e) to the stress state variables, $(\sigma - u_a)$ and $(u_a - u_w)$. These constitutive relations require knowledge of soil characteristics that generally must be evaluated experimentally. Soil properties used in the volume change constitutive equations are know as volumetric deformation coefficients (Alonso et al 1987, 1990, Toll 1990, Vaunat et al. 2000, Wheeler and Sivakumar 1992,1995).

Adopting the excess of total stress, σ, over pore-air pressure, u_a (i.e., net normal stress), $(\sigma - u_a)$, and the pore-water pressure deficiency (i.e., matric suction), $(u_a - u_w)$, as the relevant stress state variable, several aspects of the mechanical behavior of an unsaturated soil have been modeled in the past through constitutive relationships (Fredlund and Rahardjo 1993). In this research work, an attempt has been made to validate the elasto-plastic framework originally postulated by Alonso et al. (1990), herein refered to as Barcelona model.

The first part of this chapter describes the conceptual framework of the Barcelona model. The second part describes the calibration of all the Barcelona model parameters for silty sand using data from suction-controlled HC, CTC, and TC tests. The last part presents the model predictions for different CTC and TC stress paths.

6.2 Barcelona Model

The critical state based model proposed by Alonso et al. (1990) is defined in terms of four state variables, i.e., the net mean stress, $p = \frac{1}{3}(\sigma_1 + \sigma_2 + \sigma_3) - u_a$, the deviatoric stress, $q = (\sigma_1 - \sigma_3)$, the matric suction, $s = (u_a - u_w)$, and the specific volume, $v = 1 + e$. The model features elastic strains when the soil state lies inside a state boundary hypersurface, and plastic strain starting when the state boundary hypersurface is reached. Plastic behavior, as the soil state traverses the state boundary hypersurface, corresponds to an expansion of a yield surface in $(p : q : s)$ space (Alonso et al. 1990).

6.2.1 Model Formulation for Isotropic Stress States

The loading-collapse (LC) yield curve postulated by Alonso et al. (1990) for an unsaturated soil under isotropic loading condition in the $(p : s)$ plane explains not only the apparent increase in the preconsolidation stress associated with an increase in matric suction, but also the collapse phenomena observed during inundation (wetting) of an unsaturated soil sample, i.e., decrease in the matric suction.

Consider an unsaturated soil sample under volumetric and stress state condition represented by point A in figure 6.1. The value of the net mean stress, p, at C, i.e., $p_o(0)$, indicates the isotropic preconsolidation stress of the soil sample under fully saturated

conditions, i.e., $s = (u_a - u_w) = 0$. This isotropic preconsolidation stress of the soil under fully saturated (s=0) conditions, i.e., $p_o(0)$, induces an initial loading-collapse (LC) yield curve in the $(p:s)$ plane. The equation relating the isotropic preconsolidation stress at full saturation (s=0), i.e., $p_o(0)$, and the corresponding isotropic preconsolidation stress (yield net mean stress) at any particular value, s, of matric suction, i.e., $p_o(0)$, is given by

$$\frac{p_o(s)}{p^c} = \left\{ \frac{p_o(0)}{p^c} \right\}^{\frac{\lambda(0)-\kappa}{\lambda(s)-\kappa}} \tag{6.1}$$

where,

$$\lambda(s) = \lambda(0)[(1-r)\exp(-\beta s) + r] \tag{6.2}$$

where s is matric suction, p^c is a reference stress state parameter, κ is the elastic volumetric stiffness for changes in p, $r = \lambda(s \to \infty) / \lambda(0)$, and β is a parameter that controls the rate of increase of soil stiffness with matric suction, s.

Equation 6.1 and 6.2 describe the spatial location of the loading-collapse, LC_C, yield curve in the $(p:s)$ plane (Alonso et al. 1990).

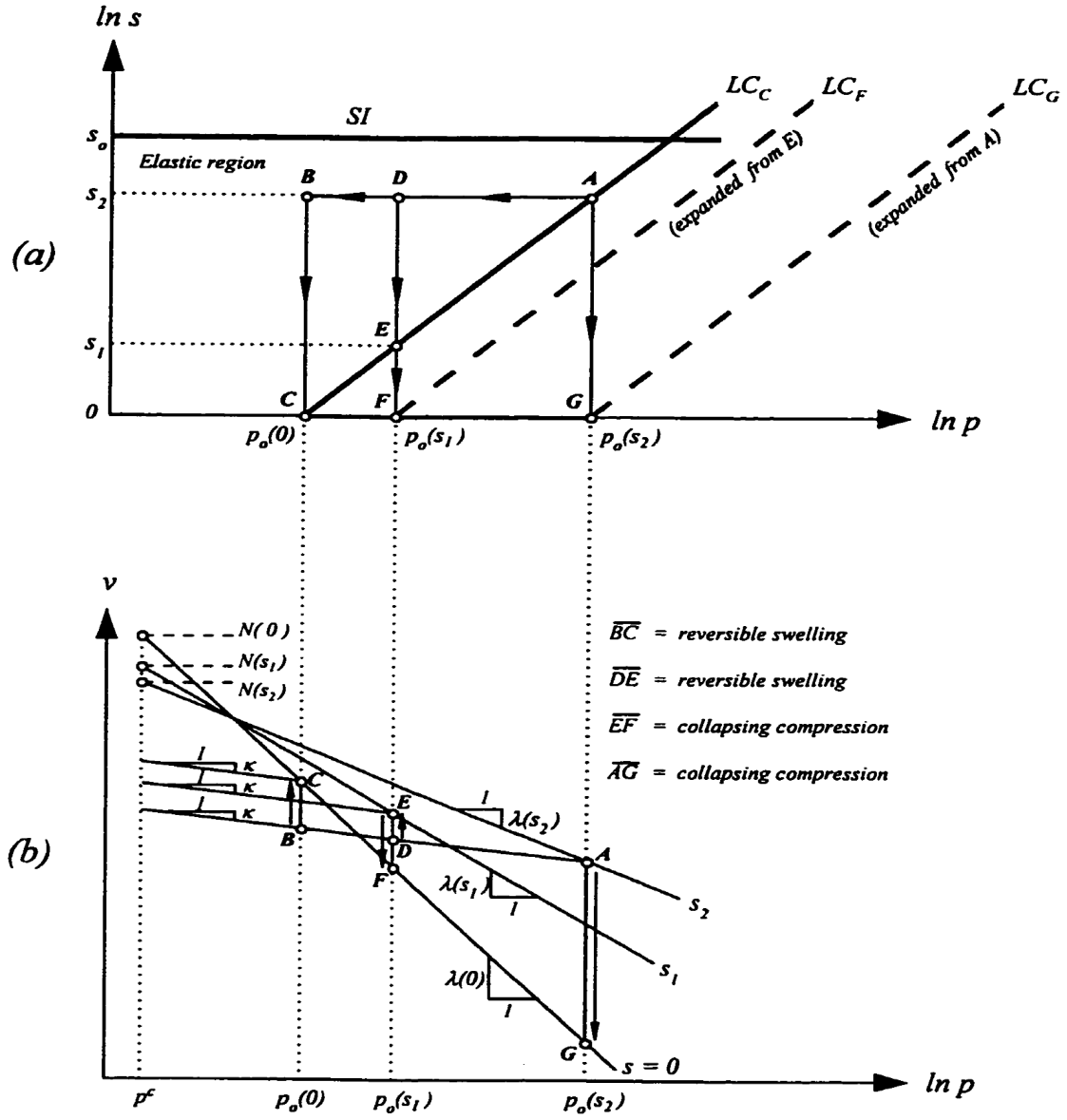

Figure 6.1 Model's framework for isotropic stress states: (a) loading-collapse (LC) yield curve; (b) swelling-collapse behavior v-p plane (Alonso et al 1990)

6.2.2 Model Formulation for Shear Stress States

The critical state lines (CSL) represent the state of the soil when sheared to ultimate or critical state conditions. The proposed critical state framework is an elasto-plastic constitutive model, with elastic behavior when the soil state lies inside the yield locus, and plastic strains staring when this yield locus is reached and surpassed. Plastic behavior, as the soil state traverses the yield locus, induces an expansion of the yield loci in $(p:q:s)$ stress space. Figure 6.2 shows the corresponding elastic region enclosed by the loading-collapse (LC) and suction-increase (SI) yield loci in the $(p:s)$ plane.

The model's formulation is extend to the $(p:s)$ plane by incorporating a third stress state parameter or deviatoric stress, $q=(\sigma_1-\sigma_3)$, to account for the effect of shearing. For fully saturated condition (s=0), the yield surface adopted is the classical ellipse of the Modified Cam-Clay (MCC) model (Roscoe and Burland 1968, Wood 1990, Gens and Alonso 1992). This may be generalized by considering different ellipses for each particular value of matric suction. The isotropic preconsolidation stress, also known as the yield net mean stress, $p_o(s)$, varies in accordance with equation 6.1. The effect of matric suction, s, is represented by an increase in apparent cohesion of the soil, i.e., intercept of the critical state line (CSL) with the q-axis, as shown schematically in figure 6.2. The slope, M, of the critical state line is considered not to depend on changes in matric suction (Alonso et al. 1990).

The assumption of a non-associative flow rule for the direction of the plastic shear strain increments $d\varepsilon_q^p$ associated with the yield locus in $(p:q:s)$ plane, as shown in figures 6.2 and 6.3, is proposed as:

$$\frac{d\varepsilon_q^p}{d\varepsilon_{vp}^p} = \frac{2\alpha q}{M^2[2p + p_s - p_o(s)]} \tag{6.3}$$

where $d\varepsilon_{vp}^p$ are the plastic volumetric strain increments. The constant α is given by

$$\alpha = \frac{M(M-9)(M-3)}{9(6-M)}\left\{\frac{1}{1-\kappa/\lambda(0)}\right\} \tag{6.4}$$

where M is the suction-independent slope of the critical state line (CSL).

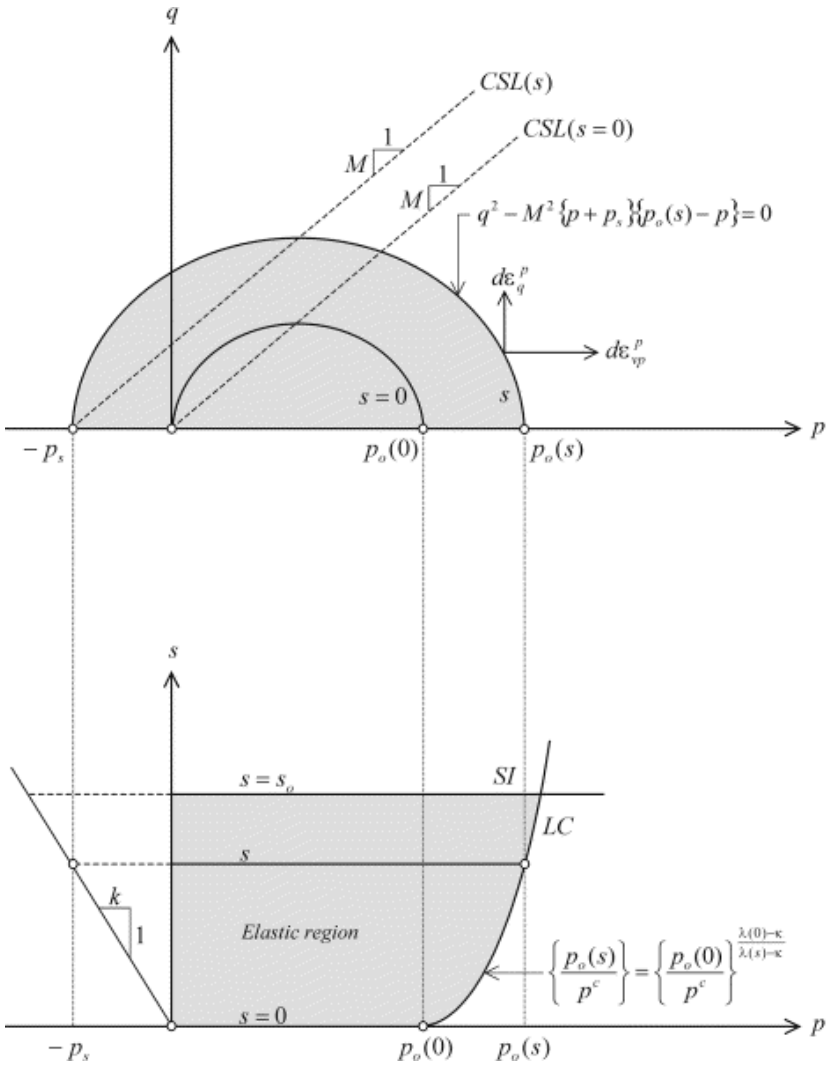

Figure 6.2 Barcelona model formulation in $(p:q:s)$ plane (Macari et al. 2003)

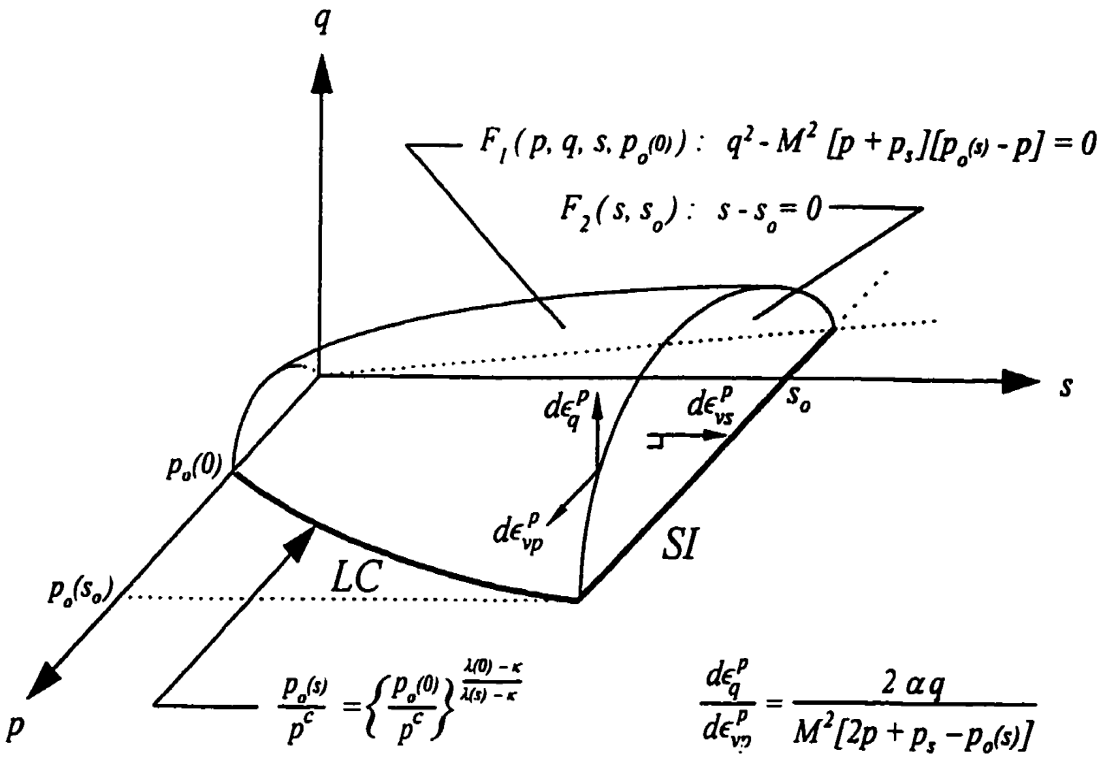

Figure 6.3 Three-dimensional view of the yield loci in $(p:q:s)$ stress space

6.2.3 Model's Parameter and Calibration

Implementation of the Barcelona model require information on model parameters, reference stresses, and initial volumetric and stress state conditions of the unsaturated test soil. This information is summarized in table 6.1.

The next section presents the computational, step-by-step sequence for explicit integration of the constitutive relations postulated by the Barcelona model, in solving the incremental stress-strain, $\sigma - \varepsilon$, behavior of an unsaturated soil, provided that all the information summarized in table 6.1 has been experimentally obtained a priori.

Table 6.1 Information required for full implementation of Barcelona model

Compressibility parameter for changes in net mean stress, p	
$\lambda(0)$	volumetric stiffness for changes in p and virgin conditions (s=0)
κ	elastic volumetric stiffness for changes in p
β	parameter controlling the rate of increase of $\lambda(s)$ with matric suction, s
r	parameter defining the maximum soil stiffness, i.e., $r = \lambda(s \to \infty) / \lambda(0)$
p^c	reference stress state parameter
Compressibility parameter for changes in matric suction, s	
λ_s	volumetric stiffness for changes in p under virgin conditions $(s > s_o)$
κ_s	elastic volumetric stiffness for changes in s
Shear strength parameters	
G	elastic shear modulus
M	slope of the critical state line (CSL)
k	parameter indicating the rate of increase in apparent cohesion with s
Initial volumetric state and stress state conditions	
p_{ini}	initial net mean stress
q_{ini}	initial deviatoric stress
s_{ini}	initial matric suction
v_{ini}	initial specific volume
Reference stress parameters	
$p_o(0)$	initial isotropic preconsolidation pressure (s=0)
s_o	initial yield suction

6.2.4 Explicit Integration of Constitutive Relations

The Barcelona model response for a drained (constant–*s*) conventional triaxial compression (CTC) test is depicted in figure 6.4. The soil is initially under lightly overconsolidated conditions, i.e., $p_{ini} \le p_o(s)$, where matric suction s is to be maintained constant throughout the entire test. Given values of $\lambda(0)$, κ, β, r, p^c, G, M, k, $p_o(0)$, and $s = (u_a - u_w)$, the explicit step-by-step integration procedure of the constitutive relations may be devised as follows (Hoyos 1998):

1. Compute $\lambda(s)$ as

$$\lambda(s) = \lambda(0)[(1-r)\exp(-\beta s) + r] \tag{6.5}$$

2. Compute $p_o^B(s)$ as

$$\frac{p_o(s)}{p^c} = \left\{ \frac{p_o(0)}{p^c} \right\}^{\frac{\lambda(0)-\kappa}{\lambda(s)-\kappa}} \tag{6.6}$$

3. Compute coordinates of point *B* on the initial yield loci (notice that p_s=–ks in figure 6.2)

$$q_B = \frac{-b + \sqrt{b^2 - 4ac}}{2a} \tag{6.7}$$

$$p_B = p_{ini} + \frac{1}{3} q_B \tag{6.8}$$

where $a = 1 + (1/9)M^2$, $b = (1/3)M^2[2p_{ini} - p_o^B(s) + p_s]$, and $c = M^2[p_{ini} + p_s][p_{ini} - p_o^B(s)]$.

4. Compute the specific volume v_B at point *B* on the ir-line corresponding to p_B:

$$v_b = v_{ini} - \kappa \ln\left\{ \frac{p_B}{p_{ini}} \right\} \tag{6.9}$$

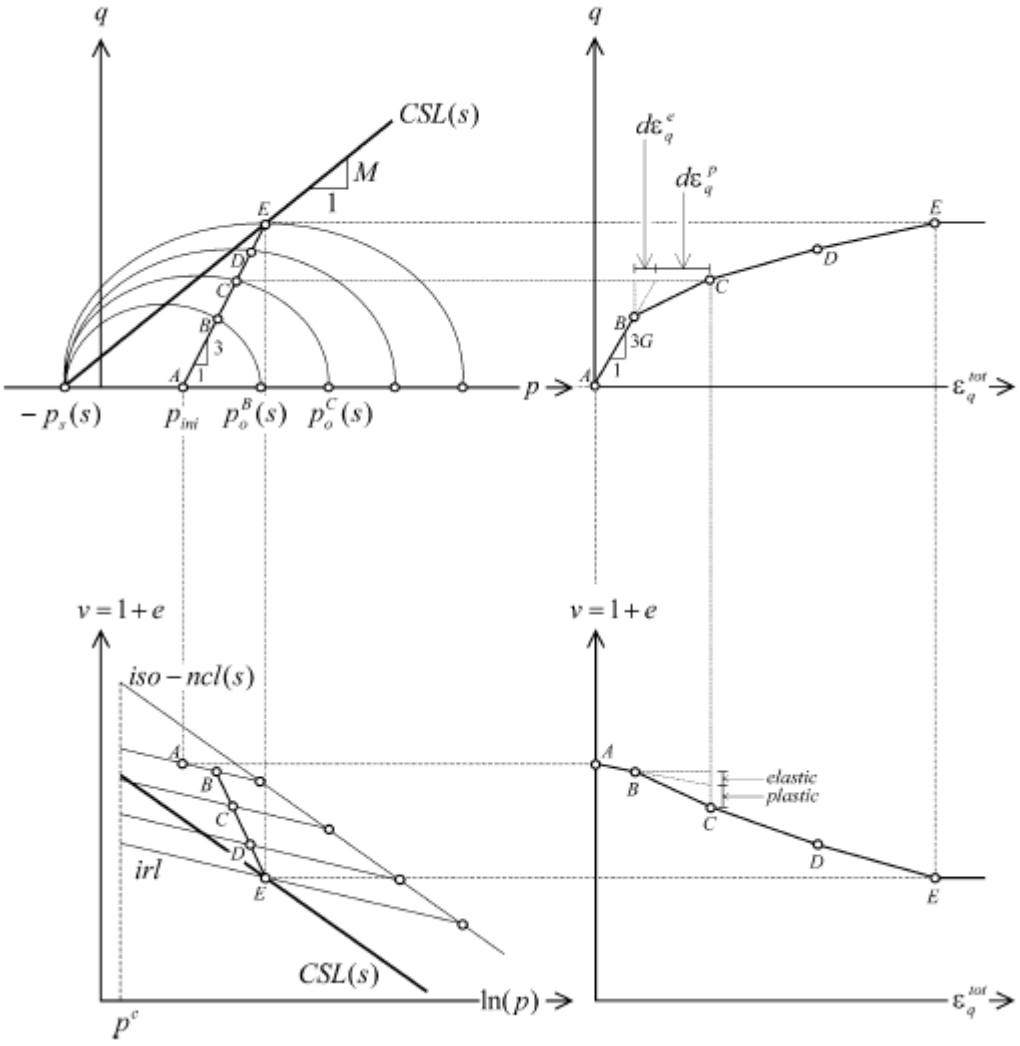

Figure 6.4 Schematic of Barcelona model response for a constant-s CTC test

5. Compute the elastic shear strain increment for path $\overrightarrow{AB}$:

$$d\varepsilon_q^e = \frac{1}{3G} q_B \tag{6.10}$$

6. Compute coordinates of the ultimate point *E* on the CSL:

$$q_E = \left\{ \frac{3M}{3-M} \right\} (p_{ini} + p_s) \tag{6.11}$$

$$p_E = p_{ini} + \frac{1}{3} q_E \tag{6.12}$$

7. Divide interval from q_B to q_E into equal deviatoric stress increments dq along $\overrightarrow{BE}$:

8. Compute the specific volume ${v_o}^B$ on the iso-nc line corresponding to $p_o^B(s)$:

$$\nu_o^B = \nu_{ini} - \kappa \ln\left\{\frac{p_o^B(s)}{p_{ini}}\right\} \tag{6.13}$$

9. Consider the first increment $\overrightarrow{BC}$ resulting from step 7. Compute coordinates of point C:

$$q_C = q_B + dq \tag{6.14}$$

$$p_C = p_B + \frac{1}{3} dq \tag{6.15}$$

10. Compute $p_o^C(s)$ for the expanded yield locus through the intermediate point C:

$$p_o^C(s) = p_C + \frac{(q_C)^2}{M^2(p_C + p_s)} \tag{6.16}$$

11. Compute the specific volume ${v_o}^C$ on the iso-nc line corresponding to $p_o^C(s)$:

$$\nu_o^C = \nu_o^B - \lambda(s) \ln\left\{\frac{p_o^C(s)}{p_o^B(s)}\right\} \tag{6.17}$$

12. Compute the specific volume v_C at point C on the ir-line corresponding to p_C:

$$\nu_C = \nu_o^C + \kappa \ln\left\{\frac{p_o^C(s)}{p_C}\right\} \tag{6.18}$$

13. Compute the elastic volumetric and shear strain increments, $d\varepsilon_{vp}^e$ and $d\varepsilon_q^e$, for path $\overrightarrow{BC}$:

$$d\varepsilon_{vp}^e = \frac{\kappa}{\nu_B}\left\{\frac{p_C - p_B}{p_B}\right\} \tag{6.19}$$

$$d\varepsilon_q^e = \frac{1}{3G}\{q_C - q_B\} = \frac{1}{3G}dq \tag{6.20}$$

14. Compute the total volumetric strain increment $d\varepsilon_{vp}^{tot}$, for path $\overrightarrow{BC}$:

$$d\varepsilon_{vp}^{tot} = \frac{v_B - v_C}{v_B} \tag{6.21}$$

15. Compute the plastic volumetric strain increment $d\varepsilon_{vp}^{p}$, for path $\overrightarrow{BC}$:

$$d\varepsilon_{vp}^{p} = d\varepsilon_{vp}^{tot} - d\varepsilon_{vp}^{e} \tag{6.22}$$

16. Compute the plastic shear strain increment $d\varepsilon_q^p$, for path $\overrightarrow{BC}$, as

$$\frac{d\varepsilon_q^p}{d\varepsilon_{vp}^p} = \frac{2\alpha q}{M^2[2p + p_s - p_o(s)]} \tag{6.23}$$

17. Compute the total shear strain increment $d\varepsilon_q^{tot} = d\varepsilon_q^e + d\varepsilon_q^p$, for path $\overrightarrow{BC}$.

18. Repeat steps 8–17 for point *D*, and for all subsequent or intermediate points along path $\overrightarrow{DE}$.

19. Finally, plot *q*–*p*, *v*–*p*, *q*– ε_q^{tot}, and *v*– ε_q^{tot}, as depicted schematically in figure 6.4.

The minimum value, $p_{\lim}$, of the initial net mean stress, p_{ini}, for the soil to be considered under lightly overconsolidated conditions is,

$$p_{\lim} = p_{mid} - \frac{q_{mid}}{3} \tag{6.24}$$

where,

$$p_{mid} = \frac{p_o^B(s) - p_s}{2} \tag{6.25}$$

$$q_{mid} = M(p_{mid} + p_s) \tag{6.26}$$

If, $p_{ini} < p_{\lim}$, the soil sample will be under heavily overconsolidated conditions. The model's framework does not support numerical analysis for this particular case due to the lack of experimental evidence on unsaturated soil behavior for this condition. Moreover, the Modified Cam-Clay (MCC) model has been shown not to represent properly the constitutive response of heavily overconsolidated soils (Macari and Arduino 1994).

The above procedure can be extended to shear stress paths involving constant net mean stress *p*, such as triaxial compression (TC) tests. A similar explicit integration procedure can also be devised for the constitutive relations proposed in the Oxford model (Sivakumar, 1993).

Test results from suction controlled HC, CTC and TC tests conducted in this research work are used to validate the model in predicting silty sand response.

6.3 Barcelona Model Parameters for Silty Sand

6.3.1 Model Parameters from Suction-Controlled Isotropic Loading

Figures 6.4 to 6.8 show the variation of the specific volume, v = 1 + e, with net mean stress, p , during the HC tests under different matric suction condition, s = 50 kPa (7 psi), 100 kPa (14 psi), 200 kPa (29 psi), 300 kPa (44 psi), and 400 kPa (58 psi), respectively. Yield stress values, $p_o(50)$ = 14 kPa (2 psi), $p_o(100)$ = 19 kPa (2.8 psi), $p_o(200)$ = 21 kPa (3.1 psi), $p_o(300)$ = 22 kPa (3.2 psi), and $p_o(400)$ = 22 kPa (3.2 psi), were identified for matric suction values, , s = 50 kPa (7 psi), 100 kPa (14 psi), 200 kPa (29 psi), 300 kPa (44 psi), and 400 kPa (58 psi) respectively.

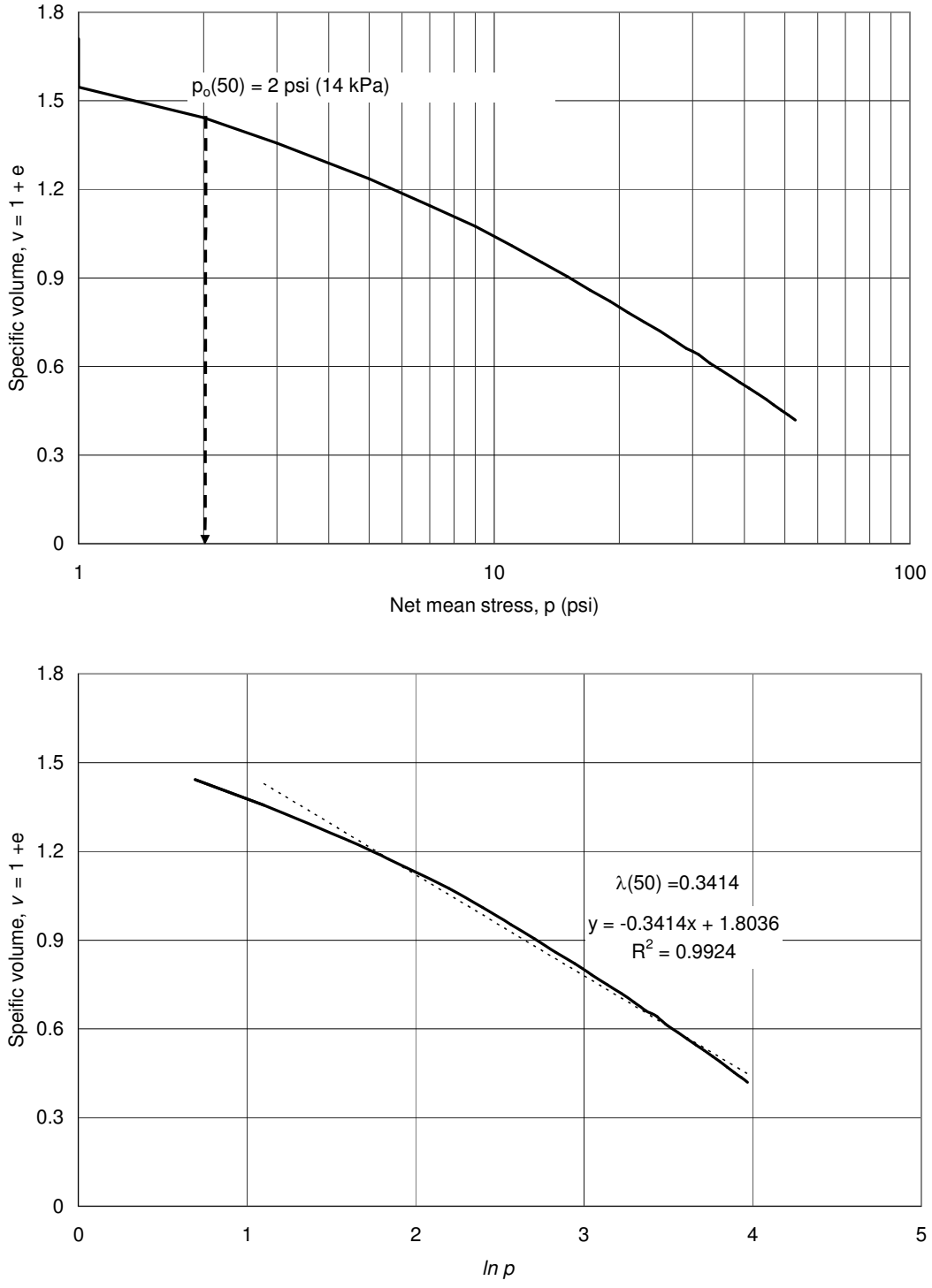

Figure 6.5 Variation of specific volume, v = 1 + e, during HC test for s = 50 kPa

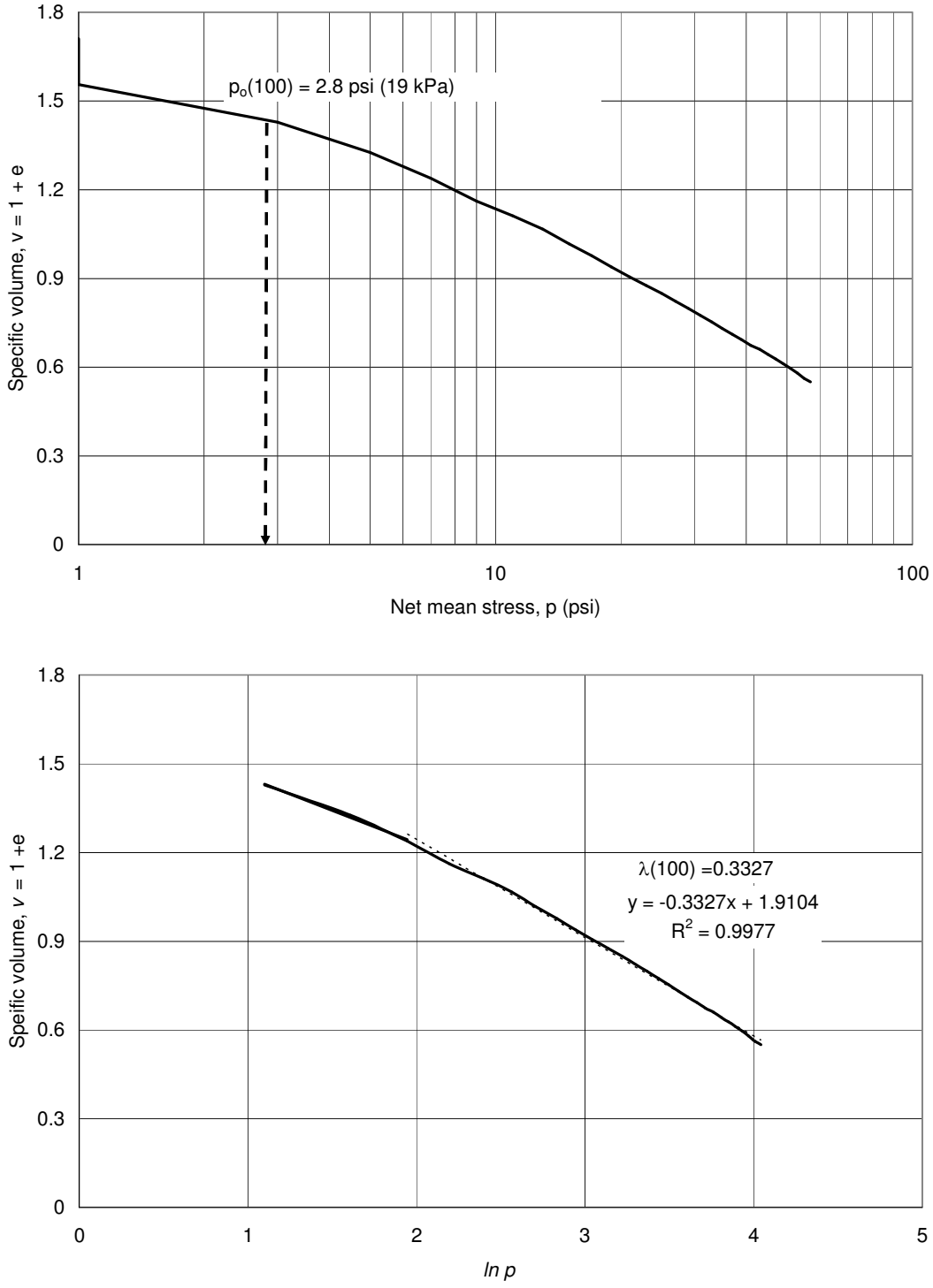

Figure 6.6 Variation of specific volume, v = 1 + e, during HC test for s = 100 kPa

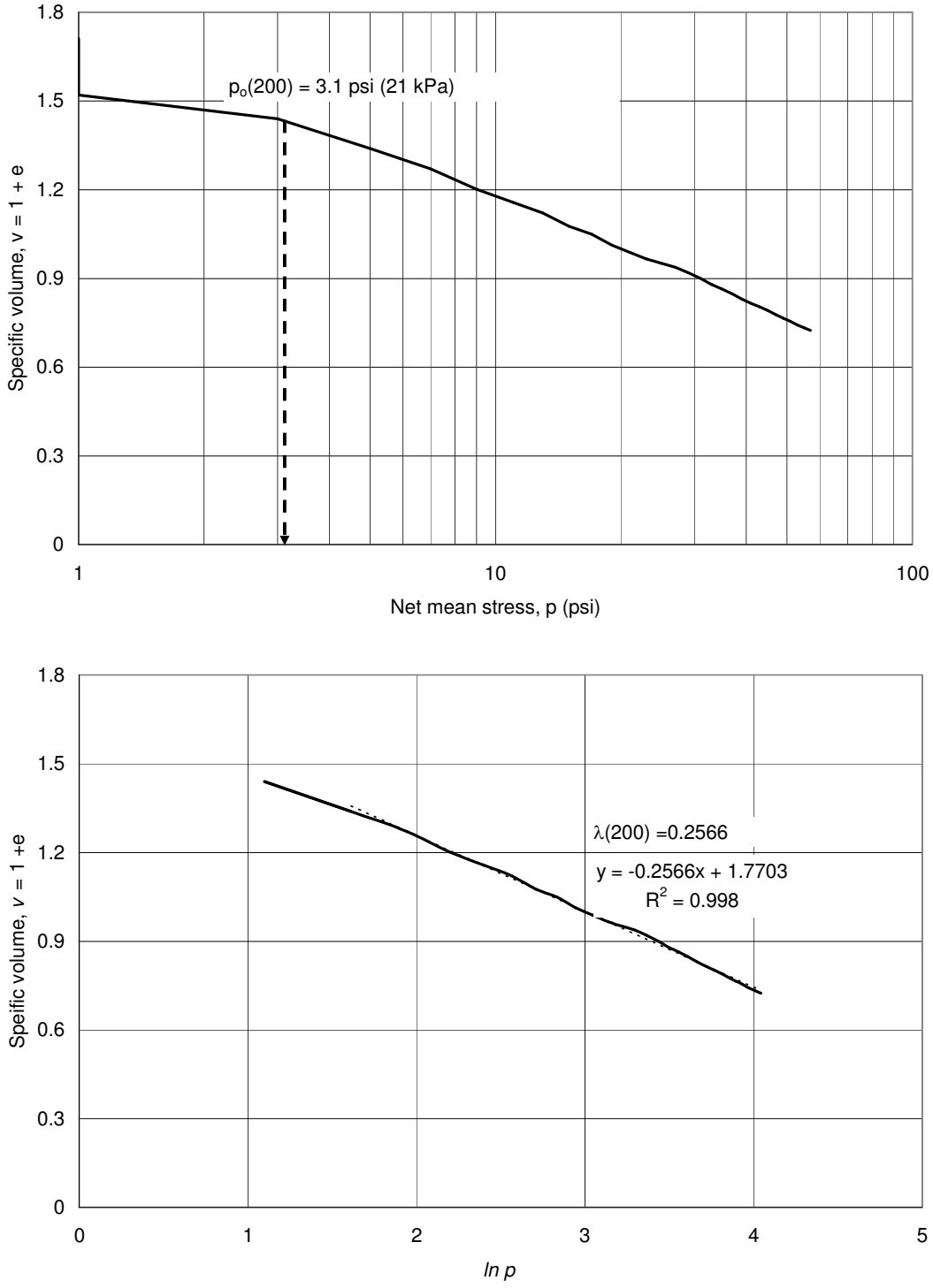

Figure 6.7 Variation of specific volume, v = 1 + e, during HC test for s = 200 kPa

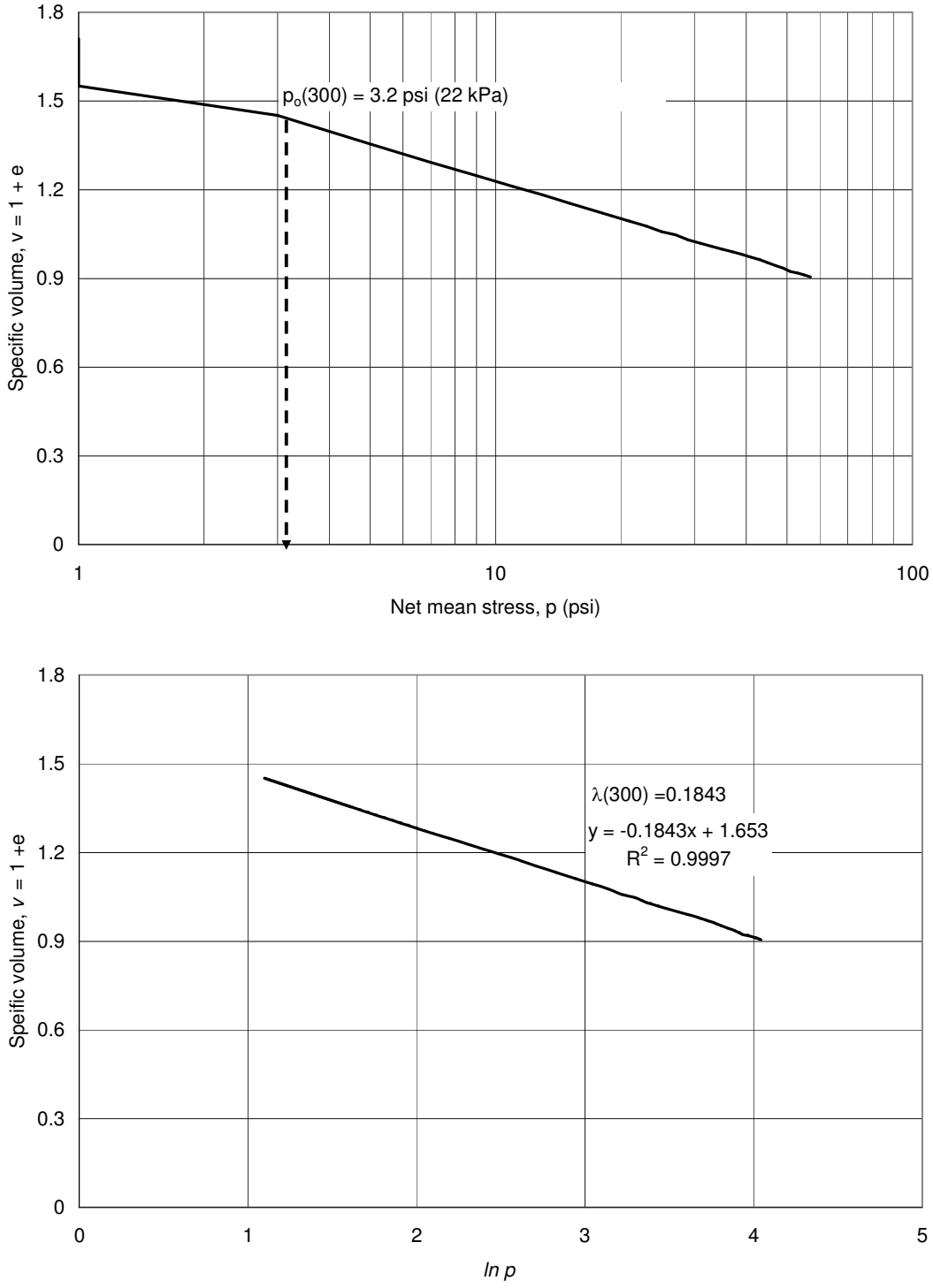

Figure 6.8 Variation of specific volume, v = 1 + e, during HC test for s = 300 kPa

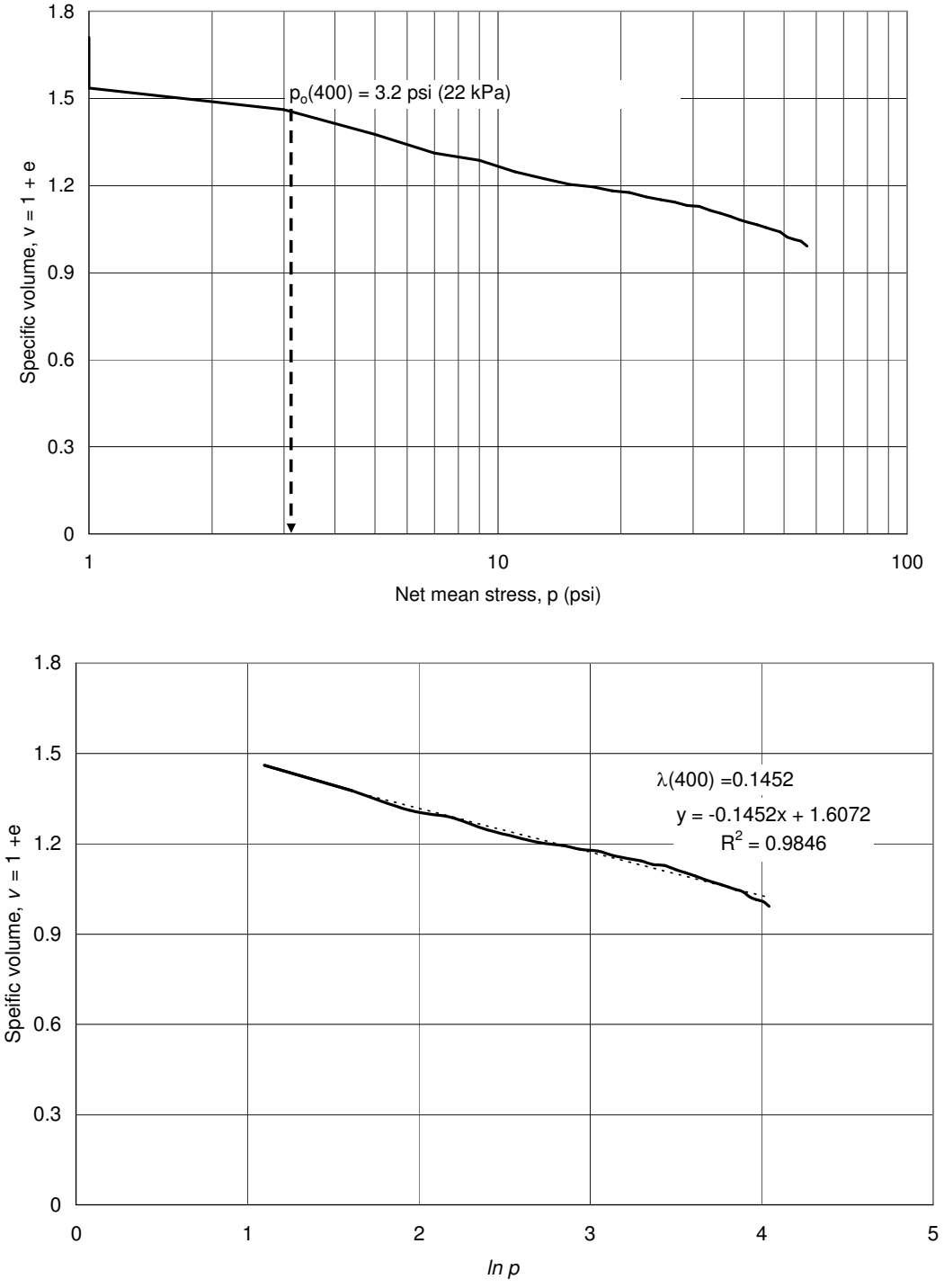

Figure 6.9 Variation of specific volume, v = 1 + e, during HC test for s = 400 kPa

The variation of the stiffness parameter, λ(s), is consistent with that propose by the Barcelona model, which suggests a monotonic decrease in λ(s) with increasing matric suction, as observed in figures 6.5 to 6.9. Best-fit values of the stiffness parameter, λ(s), were found to be, λ(50) = 0.3414, λ(100) = 0.3327, λ(200) = 0.2566, λ(300) = 0.1843, and λ(400) = 0.1452 for matric suction values, , s = 50 kPa (7 psi), 100 kPa (14 psi), 200 kPa (29 psi), 300 kPa (44 psi), and 400 kPa (58 psi), respectively.

The variation of soil stiffness, λ(s), with matric suction has been proposed as follows (Alonso et al. 1990):

$$\lambda(s) = \lambda(0)[(1-r)\exp(-\beta s) + r] \tag{6.27}$$

For the silty sand soil used in this research work, the parameters λ(0), r, and β equation 6.27 can be obtained from the experimental values, λ(s), i.e., λ(50) = 0.3414, λ(100) = 0.3327, λ(200) = 0.2566, λ(300) = 0.1843, and λ(400) = 0.1452, these values allow for the determination of the three unknown, λ(0), r, and β, in equation 6.27. It was found λ(0) = 0.5576, r = 0.45, and β = 16.087 MPa^{-1}.An average value of 0.10 was found for the elastic stiffness parameter, κ.

The loading-collapse (LC) yield curve in the Barcelona model is defined by:

$$\frac{p_o(s)}{p^c} = \left\{ \frac{p_o(0)}{p^c} \right\}^{\frac{\lambda(0)-\kappa}{\lambda(s)-\kappa}} \tag{6.28}$$

The initial position of the LC is governed by the reference stress variables, $p_o(0)$ and p^c. For the silty sand soil used in this research work, $p_o(0)$ and p^c can be obtained from test results shown in figures 6.5 to 6.9. Yield stress values, $p_o(50)$ = 14 kPa (2 psi), $p_o(100)$

= 19 kPa (2.8 psi), $p_o(200)$ = 21 kPa (3.1 psi), $p_o(300)$ = 22 kPa (3.2 psi), and $p_o(400)$ = 22 kPa (3.2 psi), allow for the determination of the two unknowns, $p_o(0)$ and p^c, through equation 6.28. A least-squares approximation procedure led to, $p_o(0)$ = 14.58 kPa (2.116 psi) and p^c = 13.23 kPa (1.92 psi). Figure 6.10 shows the approximate position of the initial LC yield curve induced by the pluviation-tamping compaction process on silty sand.

Table 6.2 summarizes the values of the model's parameters proposed by Alonso et al. (1990) for the silty sand used in this research work.

6.3.2 Model Parameters from Suction-Controlled Axisymmetric Shearing

Figures 6.11 to 6.15 illustrate the graphical assessment of the shear modulus G from CTC and TC tests. In each case, the initial linear portion of the deviatoric stress versus total shear strain response can be used to determine the elastic shear modulus, G. An average value, G = 6.3 MPa, was obtained from all tests. The rather low value of the obtained shear modulus can be attributed to the extremely loose conditions of the compacted silty sand soil.

Table 6.2 Barcelona model parameters for silty sand

Parameter	Value	Units
$\lambda(0)$	0.5576	
κ	0.1	
r	0.45	
β	16.087	MPa^{-1}
$p_o(0)$	0.015	MPa
p^c	0.013	MPa

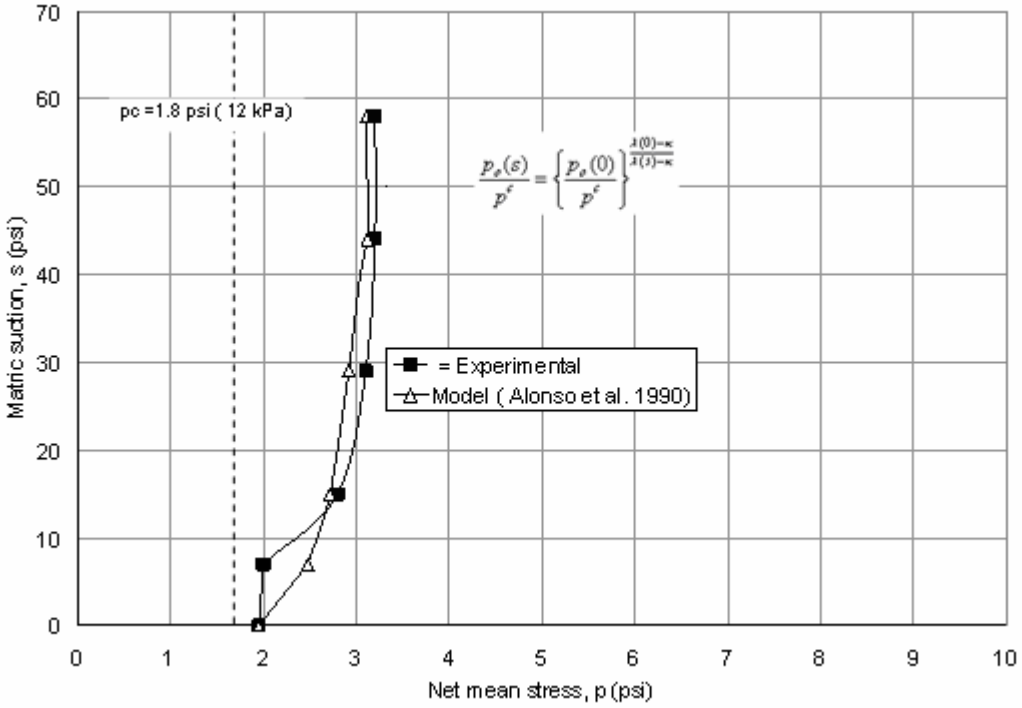
pc =1.8 psi (12 kPa)
$\frac{p_s(s)}{p^c} = \left\{\frac{p_s(0)}{p^c}\right\}^{\frac{\lambda(0)-\kappa}{\lambda(s)-\kappa}}$
= Experimental
Model (Alonso et al. 1990)
Matric suction, s (psi)
Net mean stress, p (psi)
0
10
20
30
40
50
60
70
0
1
2
3
4
5
6
7
8
9
10

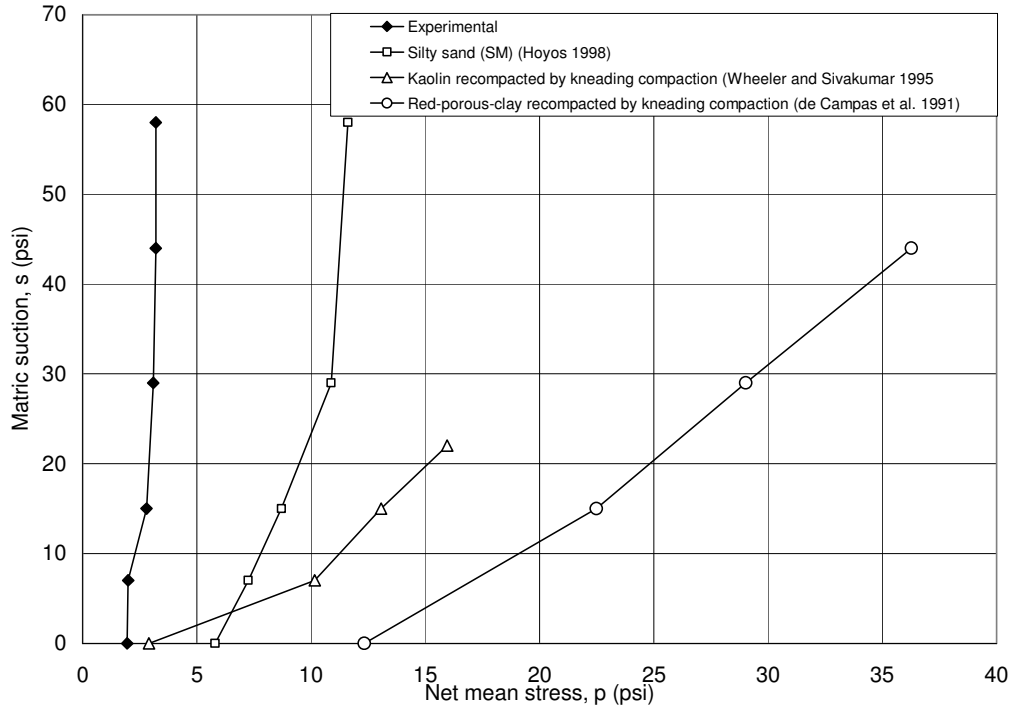
Experimental
Silty sand (SM) (Hoyos 1998)
Kaolin recompacted by kneading compaction (Wheeler and Sivakumar 1995
Red-porous-clay recompacted by kneading compaction (de Campas et al. 1991)
Matric suction, s (psi)
Net mean stress, p (psi)
0
10
20
30
40
50
60
70
0
5
10
15
20
25
30
35
40

Figure 6.10 LC yield curves for silty sand: (a) experimental and analytical LC curves; (b) initially induced and previously reported LC curves

Finally, figure 6.15 shows again the peak response on p-q plane with CSL's at different suction values, s = 50 kPa (7 psi), 100 kPa (14 psi), 200 kPa (29 psi), 300 kPa (44 psi), and 400 kPa (58 psi), along with the "apparent cohesion" (intercept with q-axis). Alinear trend is observed in the later for the range of suction values induced. Within the range of stresses applied, the plane given by:

$$Q = Mp + Mks = 1.5p + 0.33s \tag{6.29}$$

fits all the experimental values of deviatoric stress q measured at ε_{qtot} = 12%, with a standard daviation of 7.12%. Equation (6.29) provides best-fit values for M = 1.5 and k = 0.22 (figure 6.2).

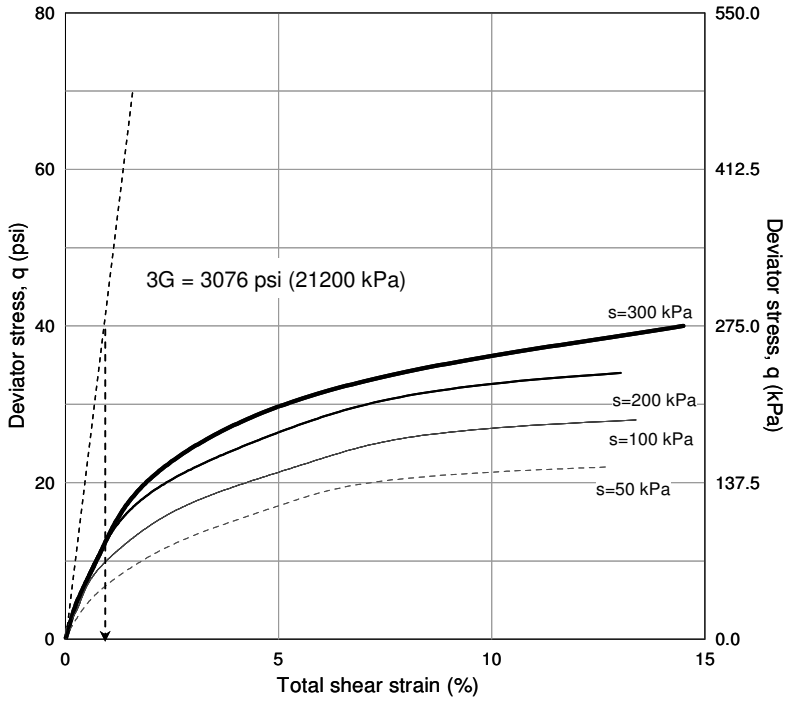

Figure 6.11 Assessment of shear modulus from CTC tests at p_{net} = 50 kPa

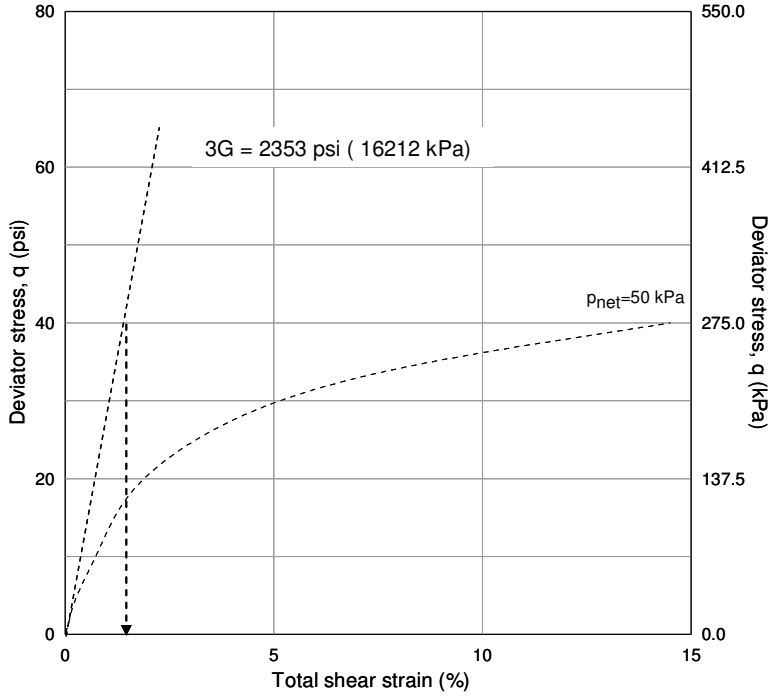

Figure 6.12 Assessment of shear modulus from CTC tests at (u_a-u_w) = 300 kPa

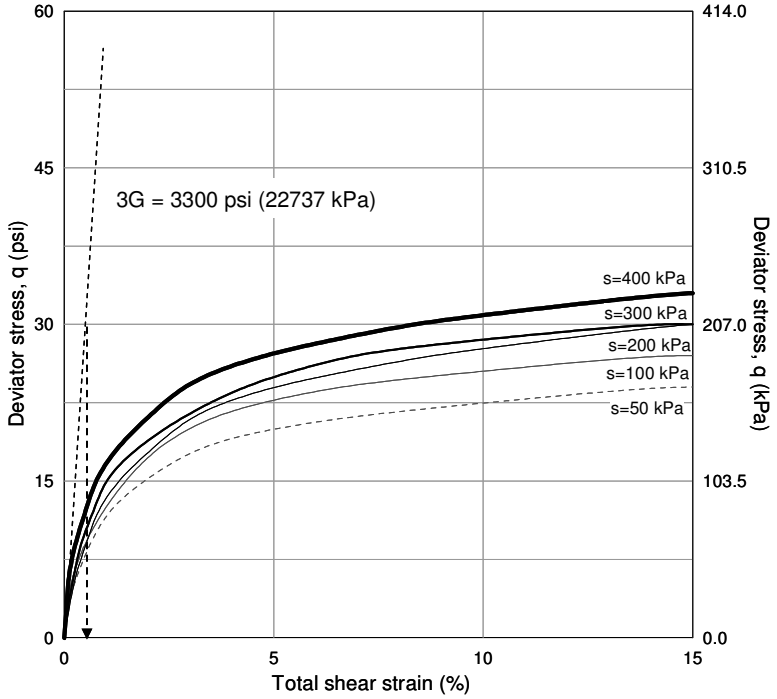

Figure 6.13 Assessment of shear modulus from TC tests at p_{net} = 100 kPa

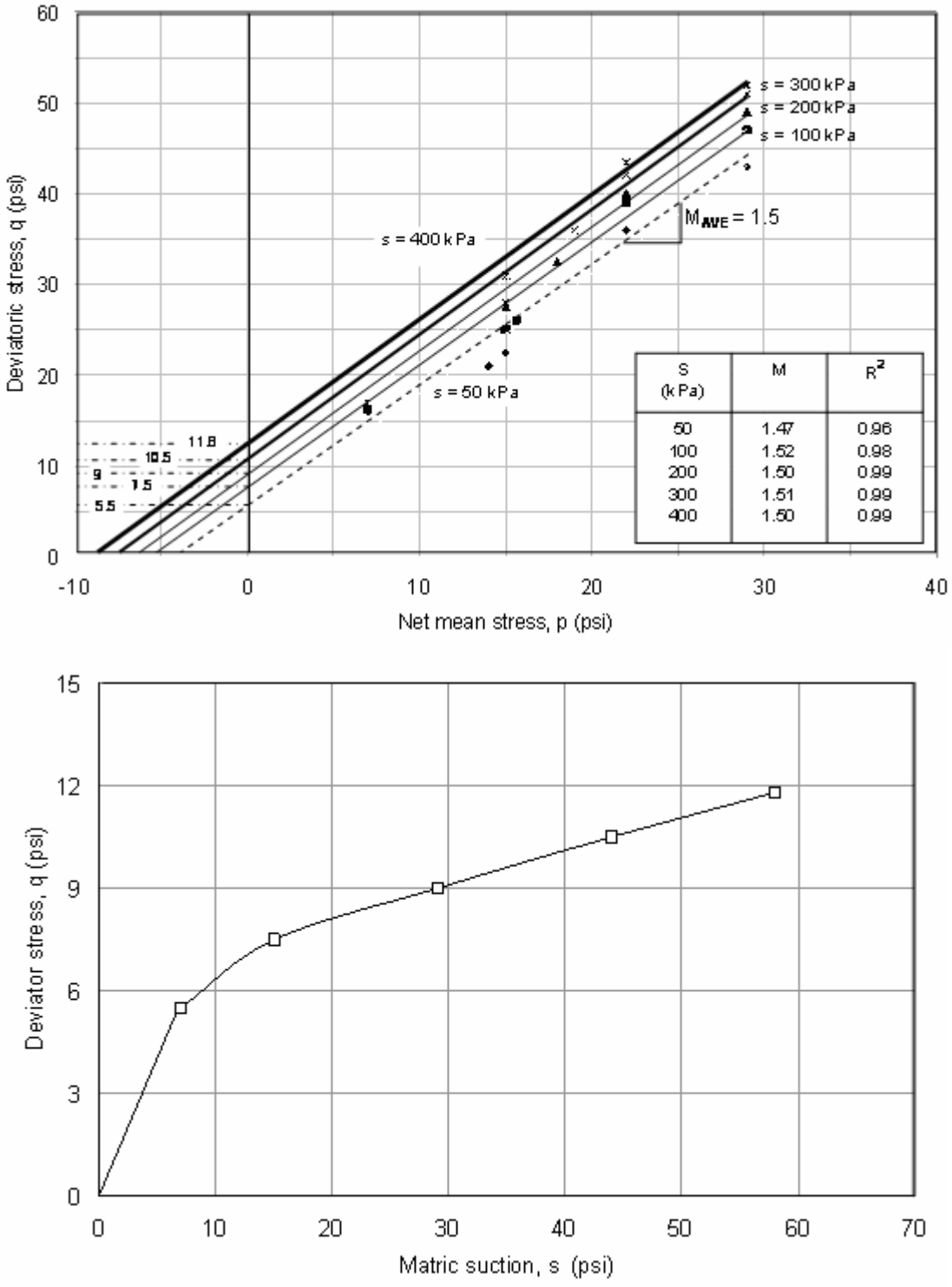

Figure 6.14 Experimental p-q and q-s responses of silty sand

6.4 Model Predictions

Table 6.3 summarizes the experimental values of all Barcelona model parameters, obtained for the silty sand soil used in this study.

Figure 6.16 to 6.22 show the comparison between experimental and predicted, deviatoric stress-total shear strain relationship from the drain (constant suction), suction-controlled CTC tests conducted on cubical silty sand specimen at different values of matric suction, s = 50 kPa (7 psi), 100 kPa (14 psi), 200 kPa (29 psi), and 300 kPa (44 psi), and initial net mean stress, p_{net}, 50 kPa (7 psi) and 100 kPa (14 psi).

Figures 6.23 to 6.42 show the comparison between experimental and predicted deviatoric stress versus total shear strain responses from all suction-controlled TC tests conducted on cubical silty sand specimen at different values of matric suction, s = 50 kPa (7 psi), 100 kPa (14 psi), 200 kPa (29 psi), 300 kPa (44 psi), and 400 kPa (58 psi), and initial net mean stress, p_{net} = 50 kPa (7 psi), 100 kPa (14 psi), 150 kPa (22 psi), and 200 kPa (29 psi).

The model shows reasonably good predictions of silty sand response under CTC stress paths. However, model predictions of silty sand stress-strain response under TC stress paths are rather underestimated.

This could be attributed to the fact that soil is tested under unusually loose conditions and low density, which may not be representative of field conditions considered by the Barcelona framework, especially the assumption of a non-associative flow rule based on expected K_o value in unsaturated soils.

Table 6.3 Summary of Barcelona model's parameters for silty sand

Parameter	Value	Units
$\lambda(0)$	0.5576	
κ	0.1	
r	0.45	
β	16.087	MPa^{-1}
p^c	0.013	MPa
G	6.3	MPa
M	1.5	
k	0.222	
$p_o(0)$	0.015	MPa
s_o	Undefined	MPa

Next chapter includes the summary and conclusions of this research work, as well as some key recommendations for future work.

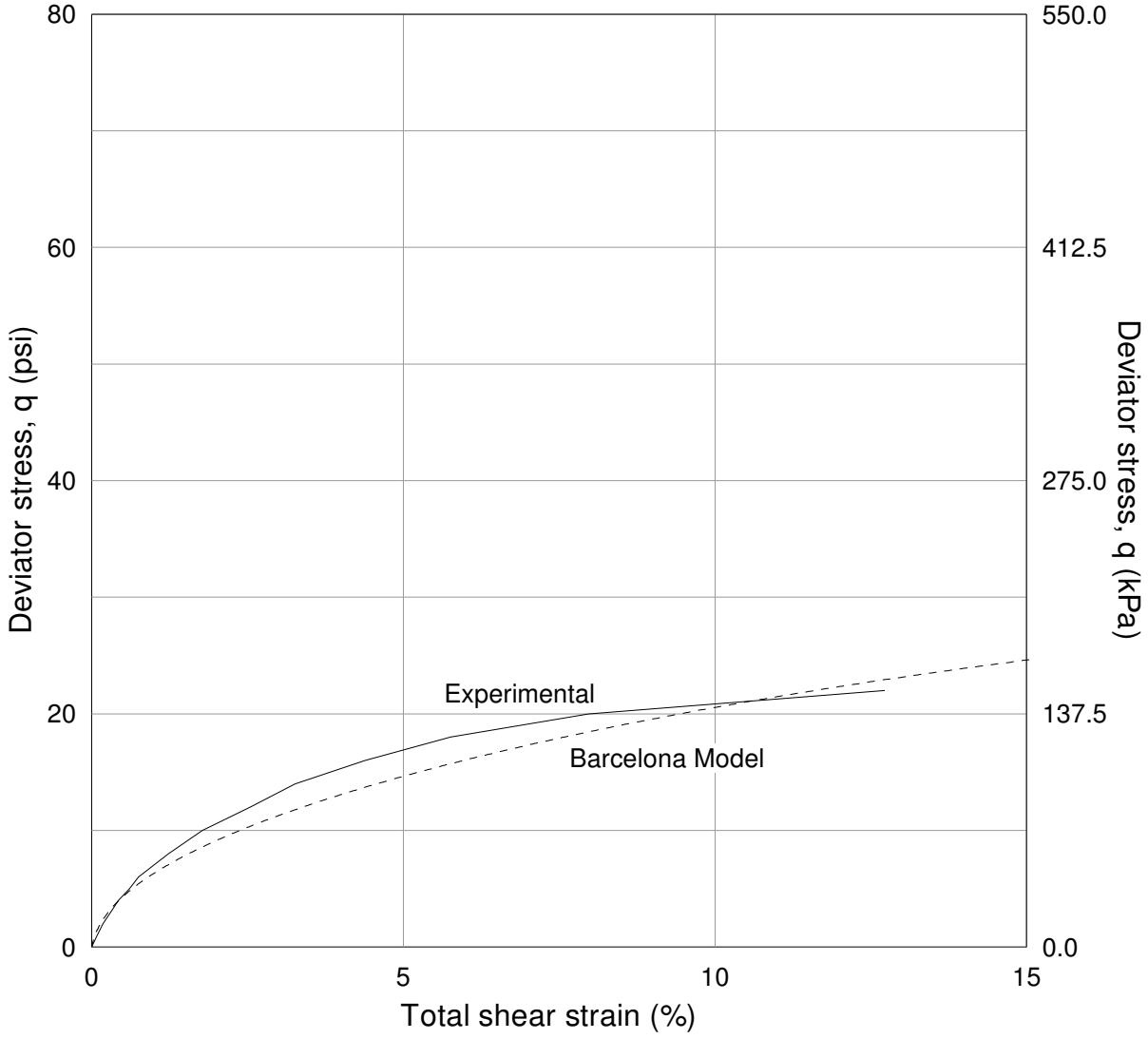

Figure 6.15 Experimental and predicted silty sand response for CTC test at s = 50 kPa initial p_{net} = 50 kPa

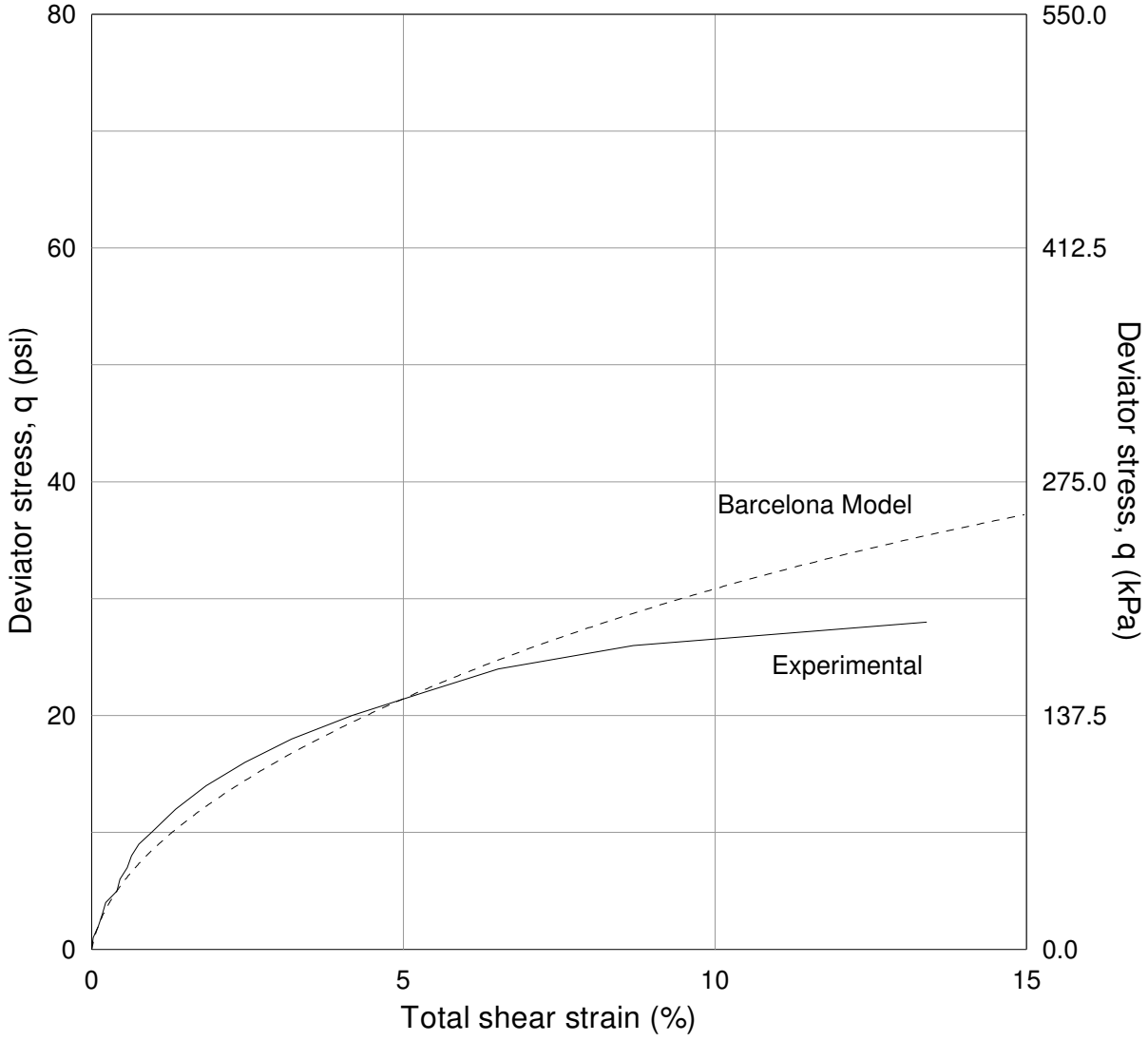

Figure 6.16 Experimental and predicted silty sand response for CTC test at s = 100 kPa initial p_{net} = 50 kPa

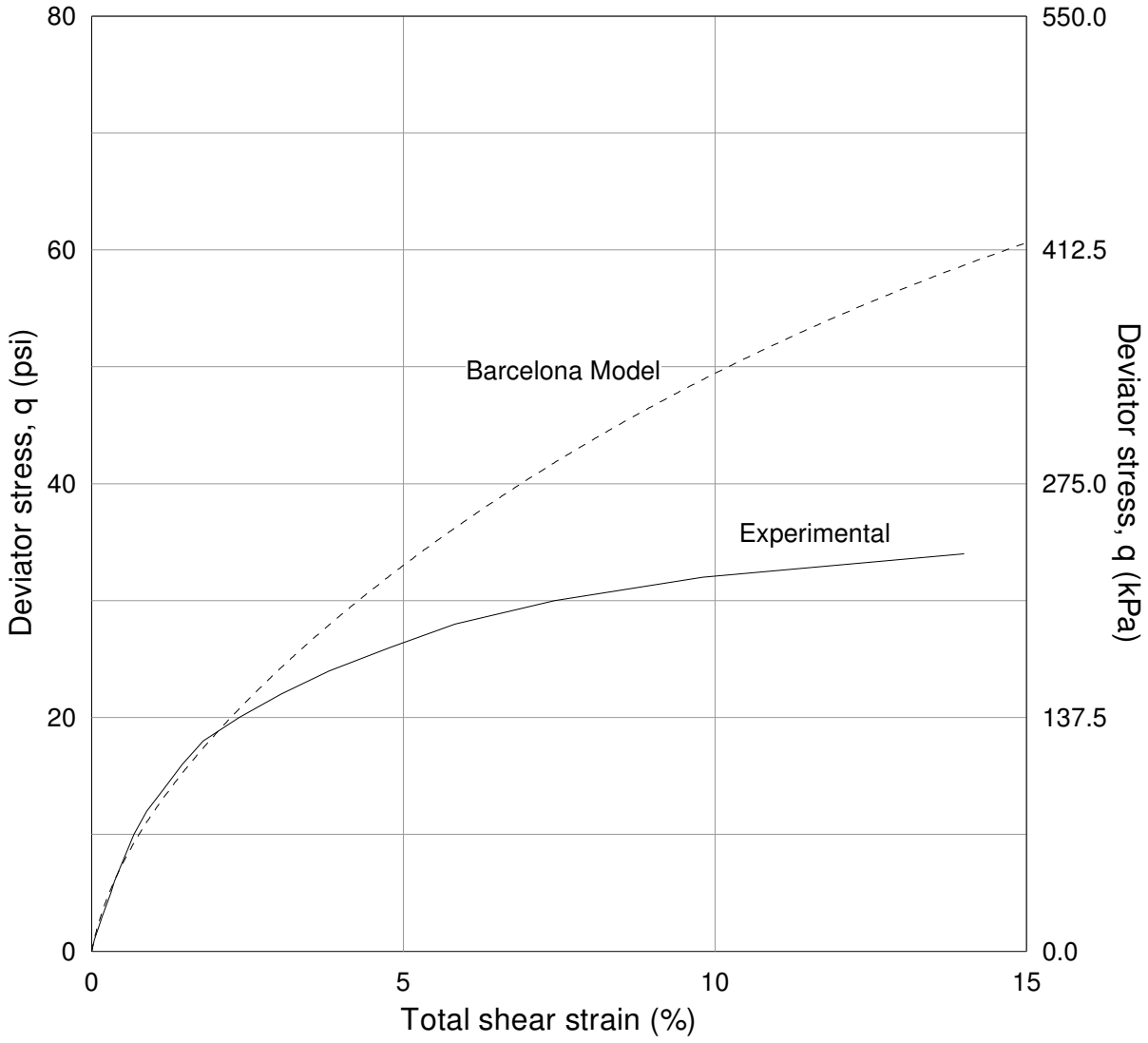

Figure 6.17 Experimental and predicted silty sand response for CTC test at s = 200 kPa initial p_{net} = 50 kPa

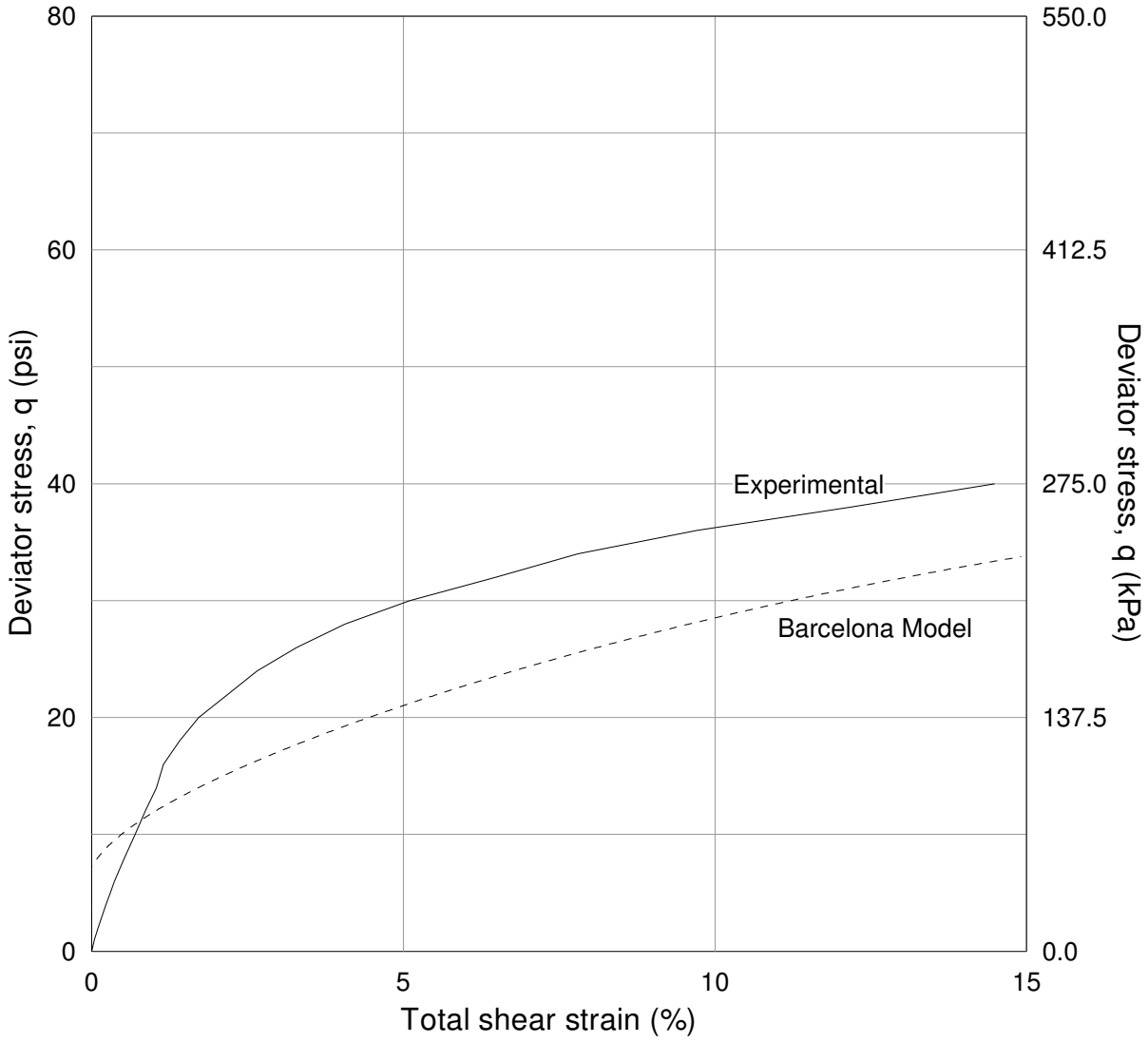

Figure 6.18 Experimental and predicted silty sand response for CTC test at s = 300 kPa initial p_{net} = 50 kPa

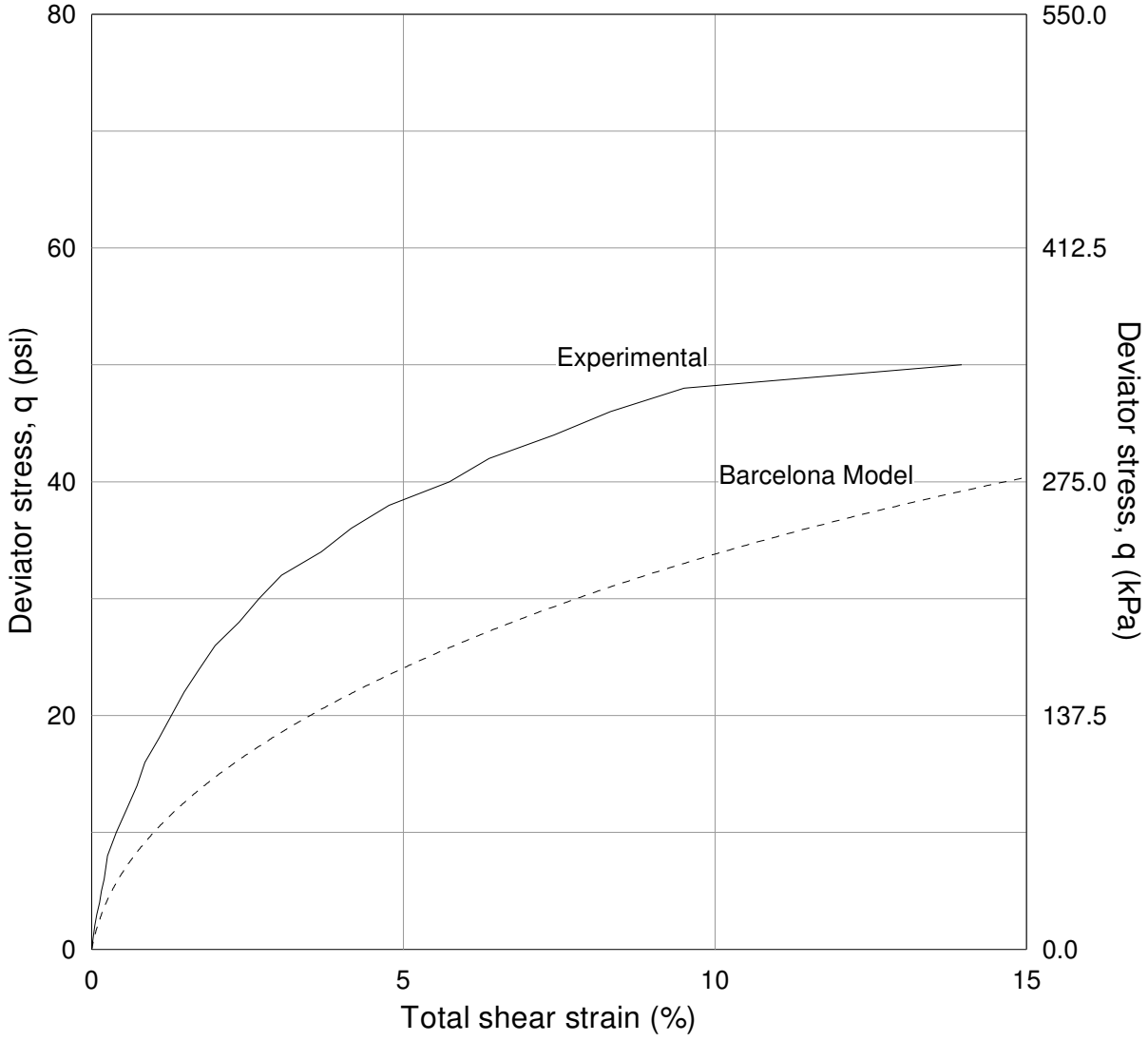

Figure 6.19 Experimental and predicted silty sand response for CTC test at s = 50 kPa initial p_{net} = 100 kPa

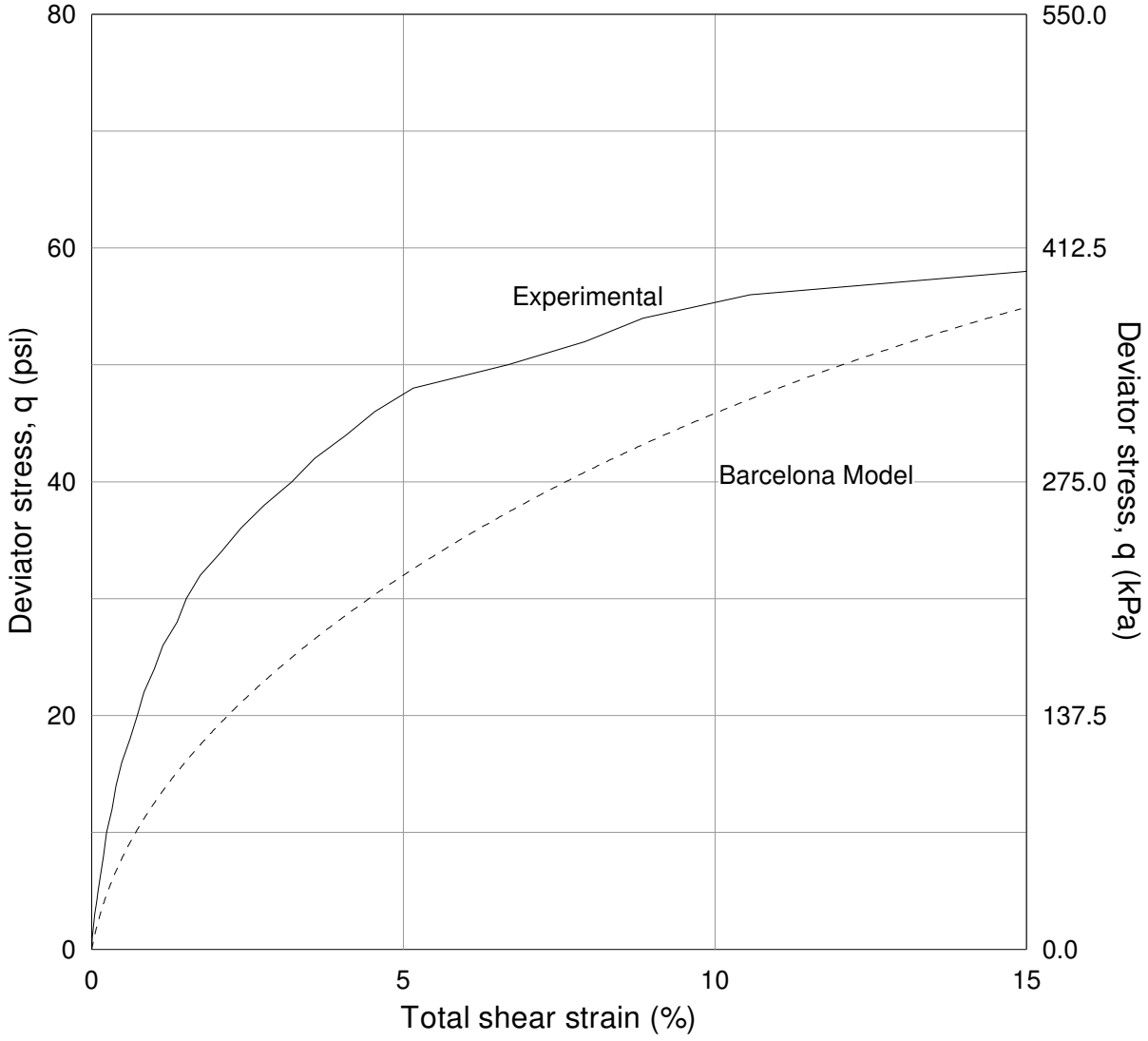

Figure 6.20 Experimental and predicted silty sand response for CTC test at s = 100 kPa initial p_{net} = 100 kPa

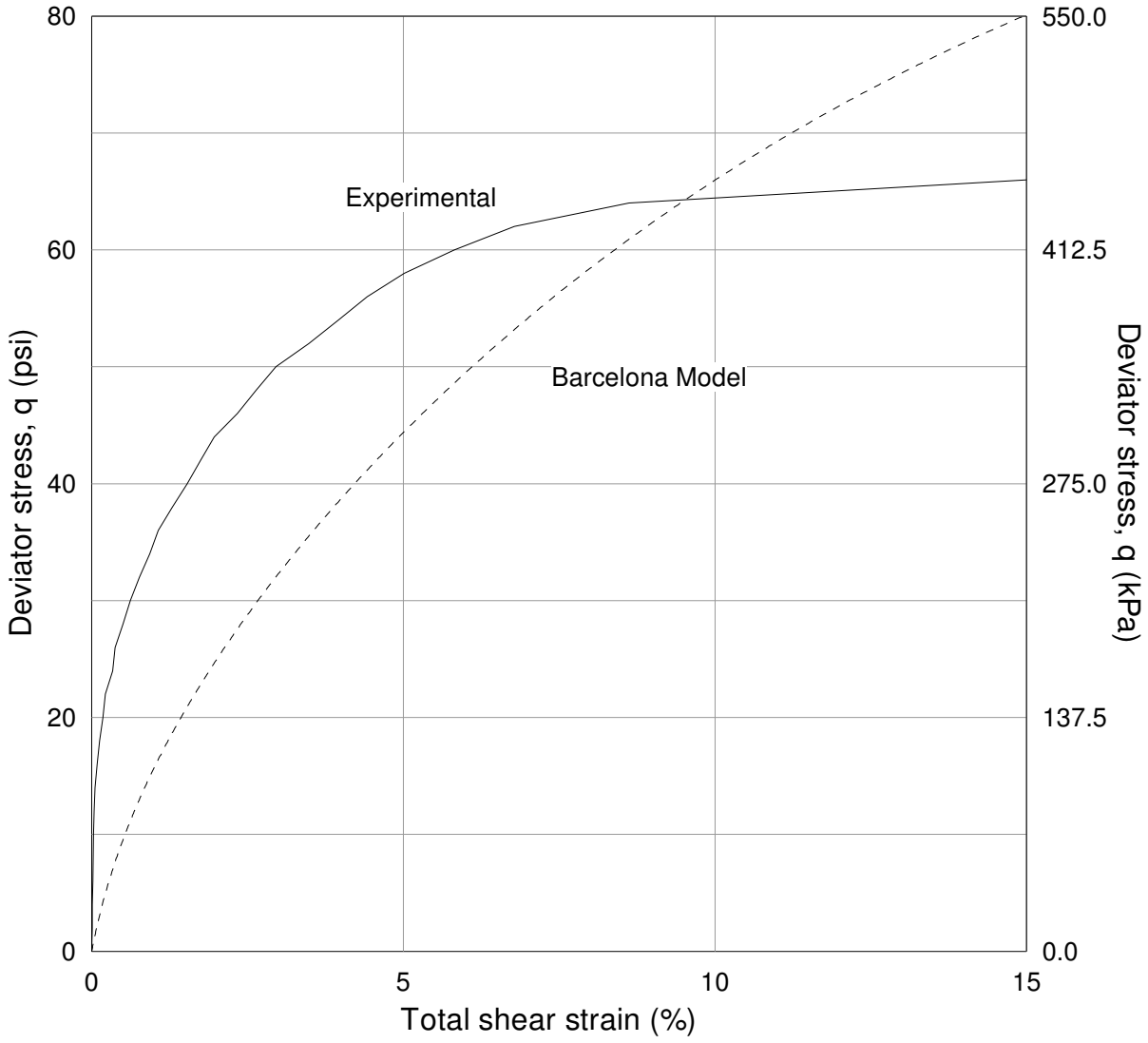

Figure 6.21 Experimental and predicted silty sand response for CTC test at s = 200 kPa initial p_{net} = 100 kPa

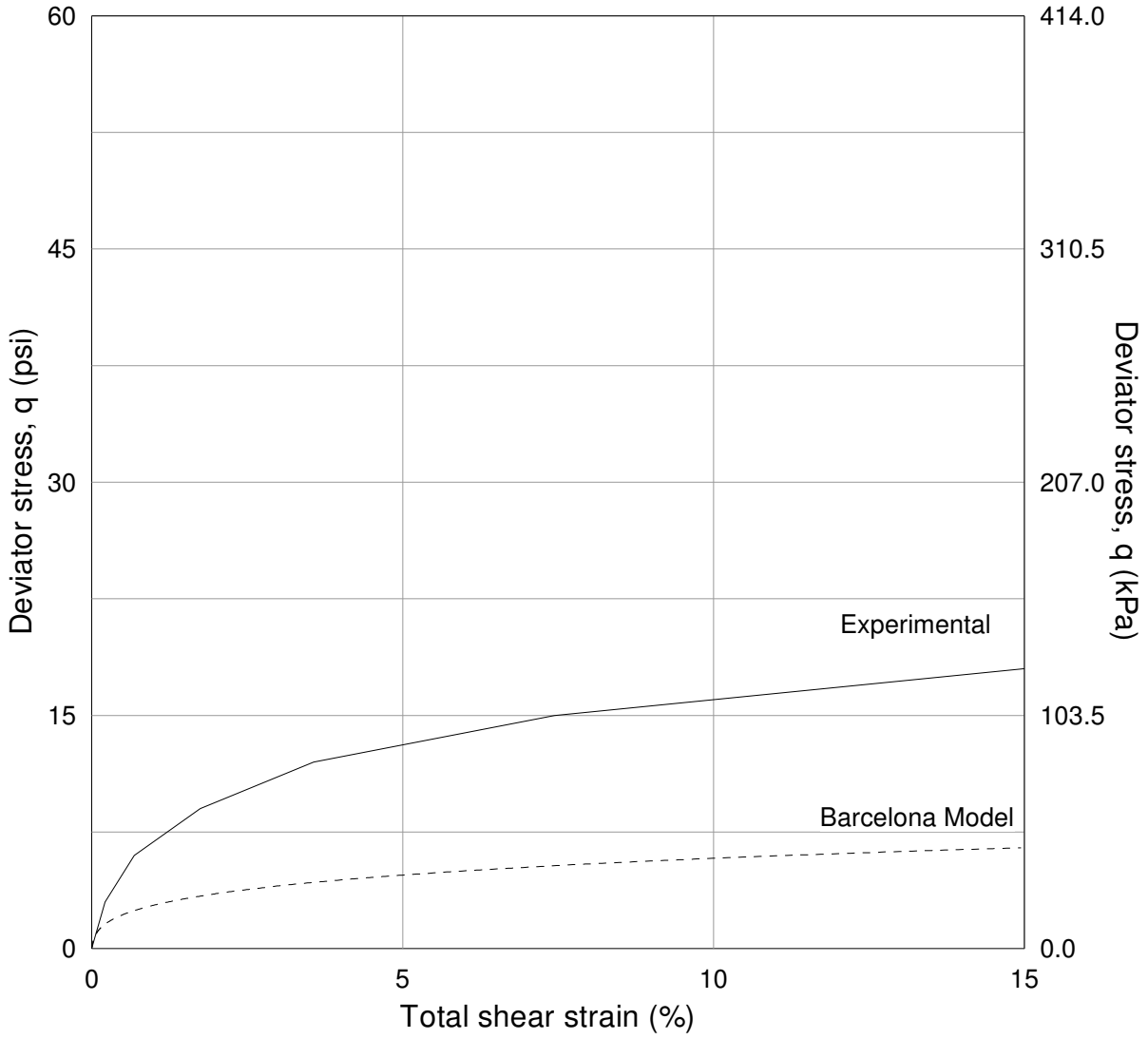

Figure 6.22 Experimental and predicted silty sand response for TC test at s = 50 kPa initial p_{net} = 50 kPa

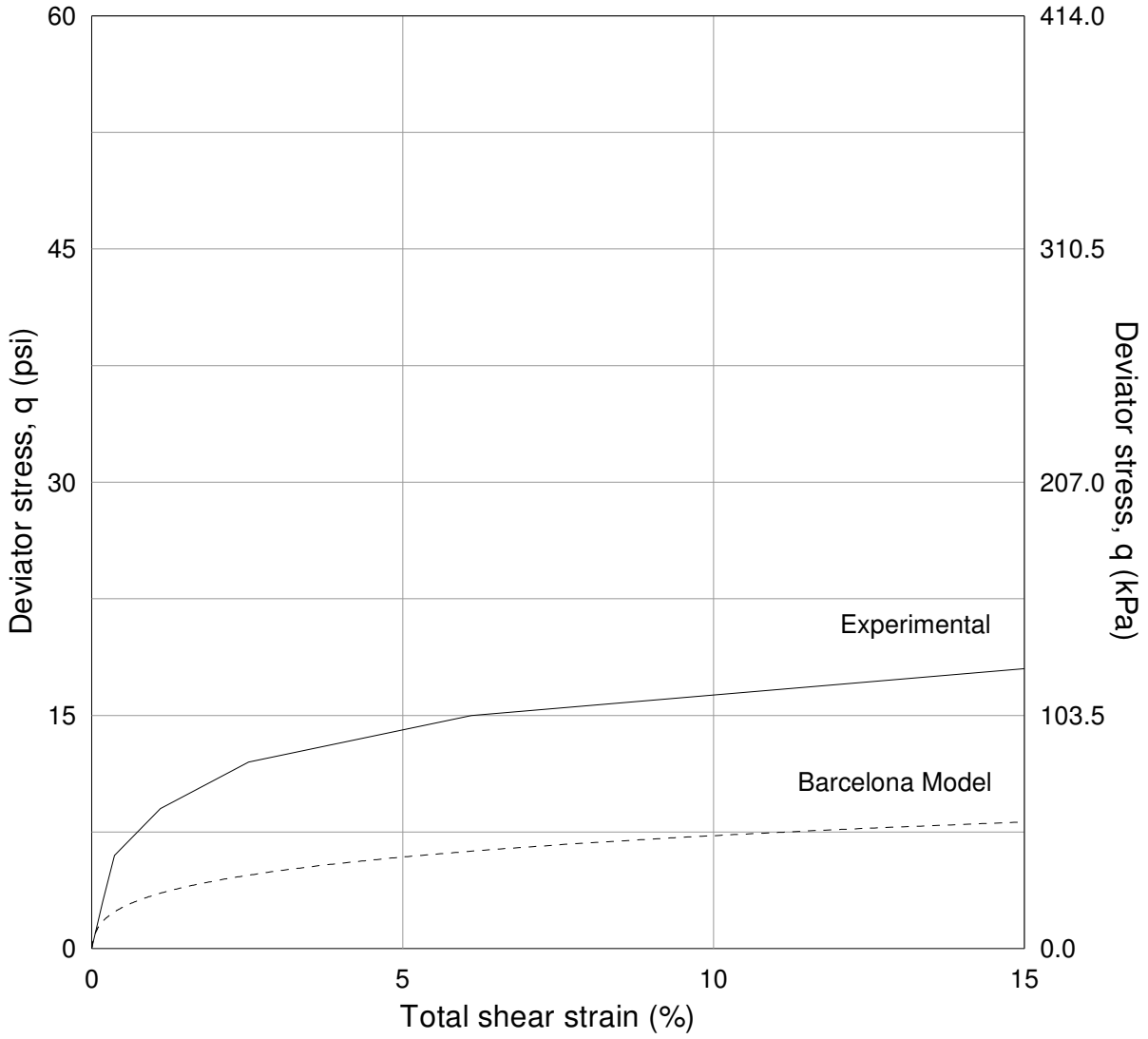

Figure 6.23 Experimental and predicted silty sand response for TC test at s = 100 kPa initial p_{net} = 50 kPa

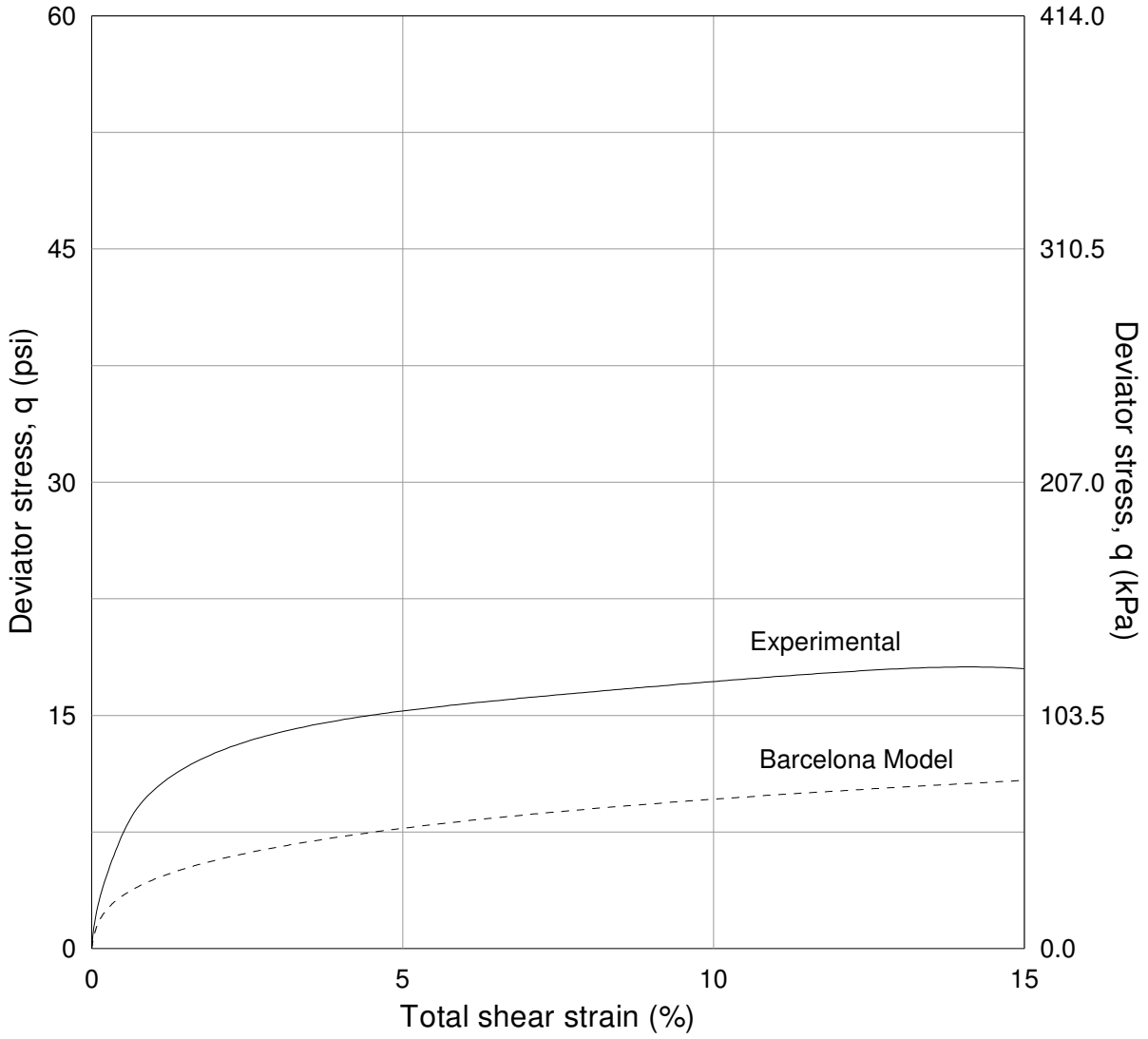

Figure 6.24 Experimental and predicted silty sand response for TC test at s = 200 kPa initial p_{net} = 50 kPa

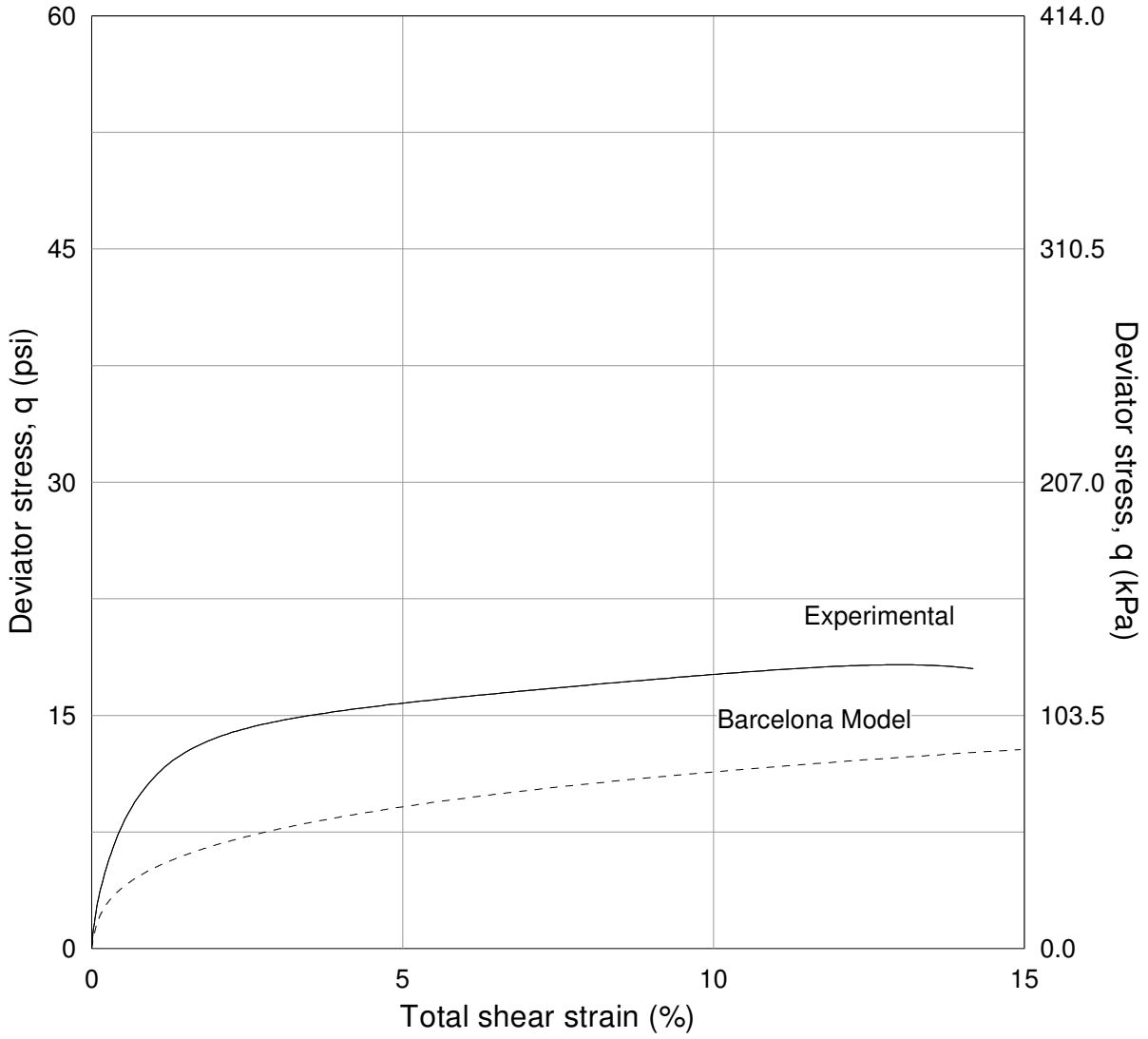

Figure 6.25 Experimental and predicted silty sand response for TC test at s = 300 kPa initial p_{net} = 50 kPa

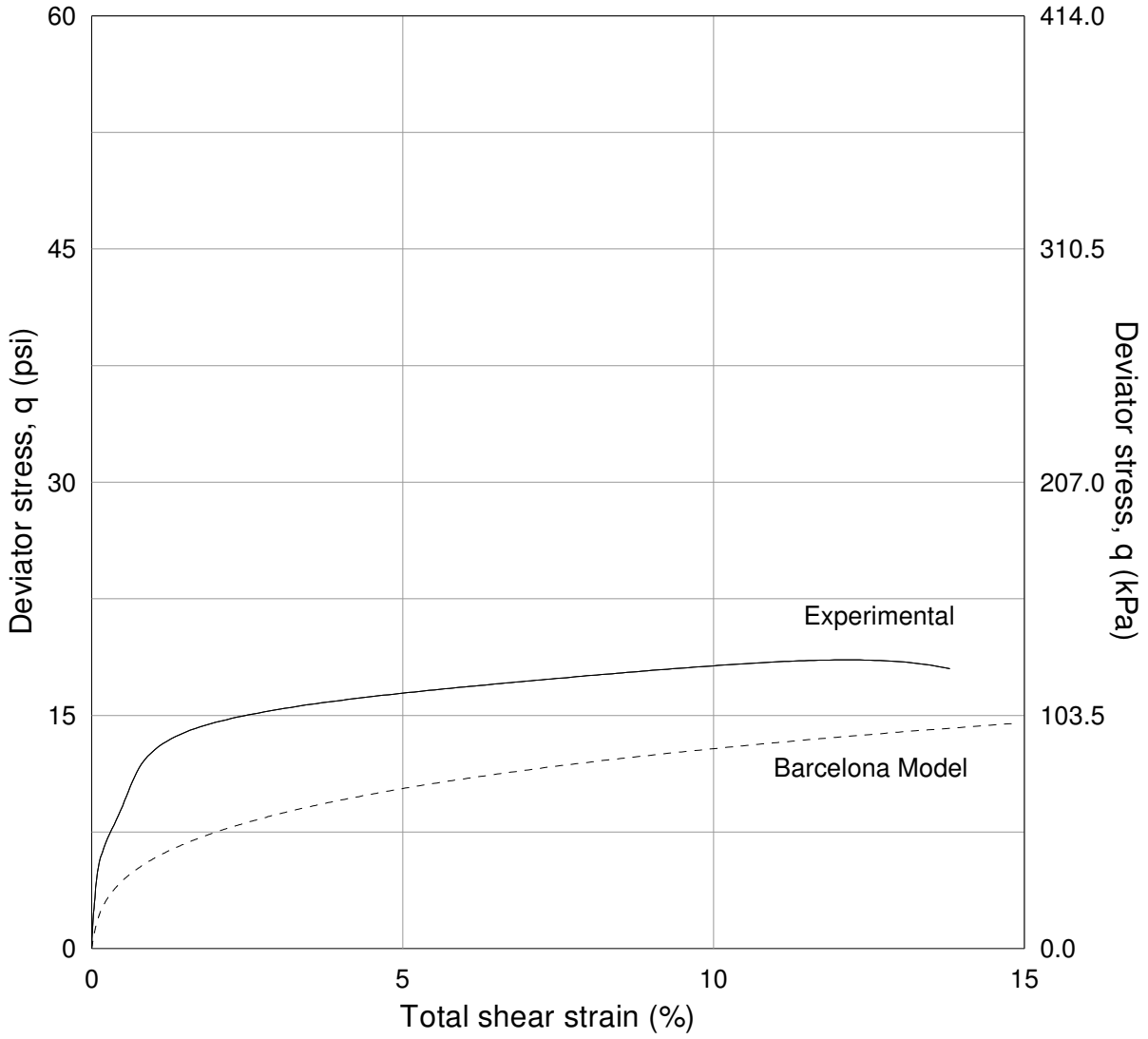

Figure 6.26 Experimental and predicted silty sand response for TC test at s = 400 kPa initial p_{net} = 50 kPa

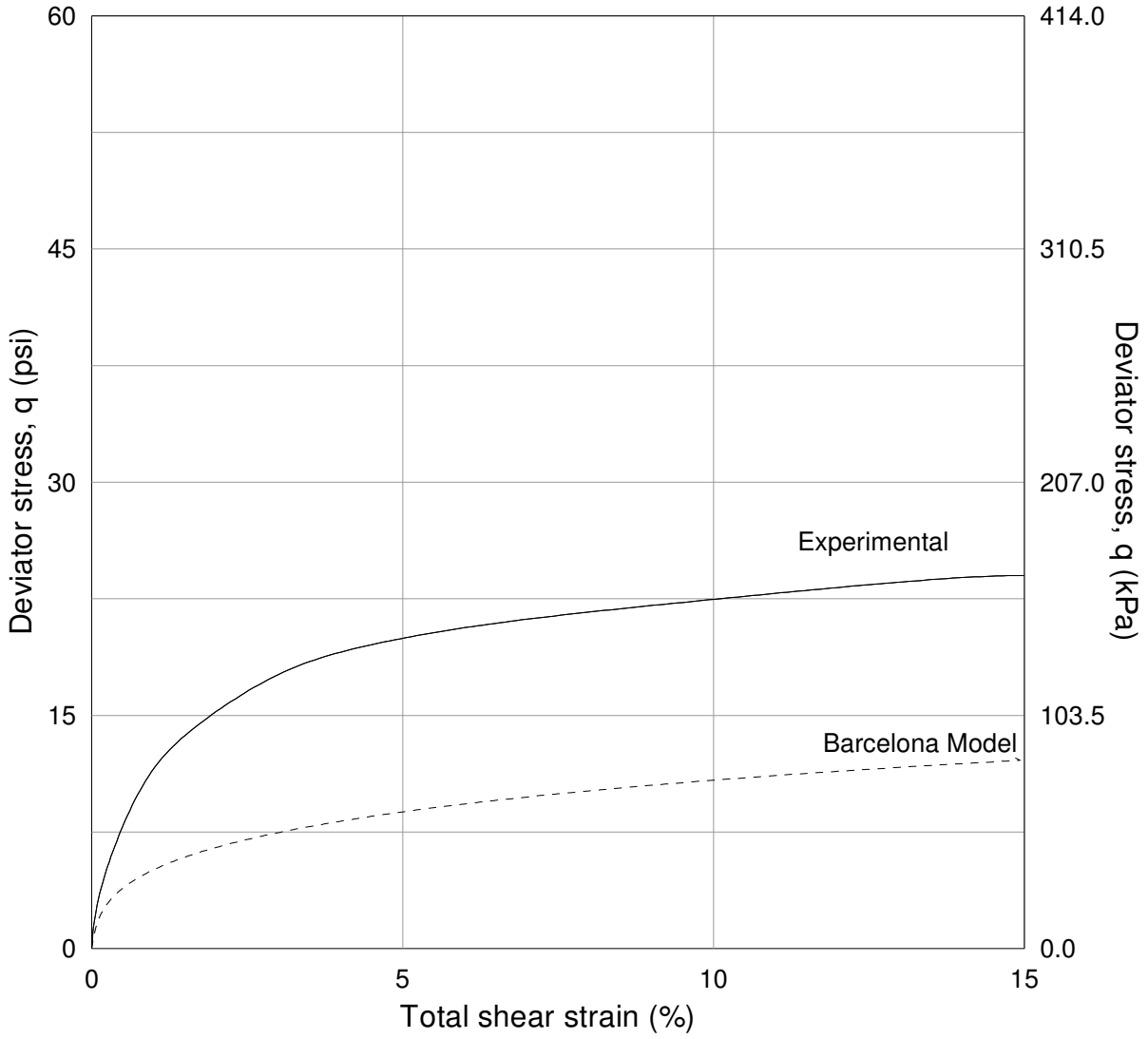

Figure 6.27 Experimental and predicted silty sand response for TC test at s = 50 kPa initial p_{net} = 100 kPa

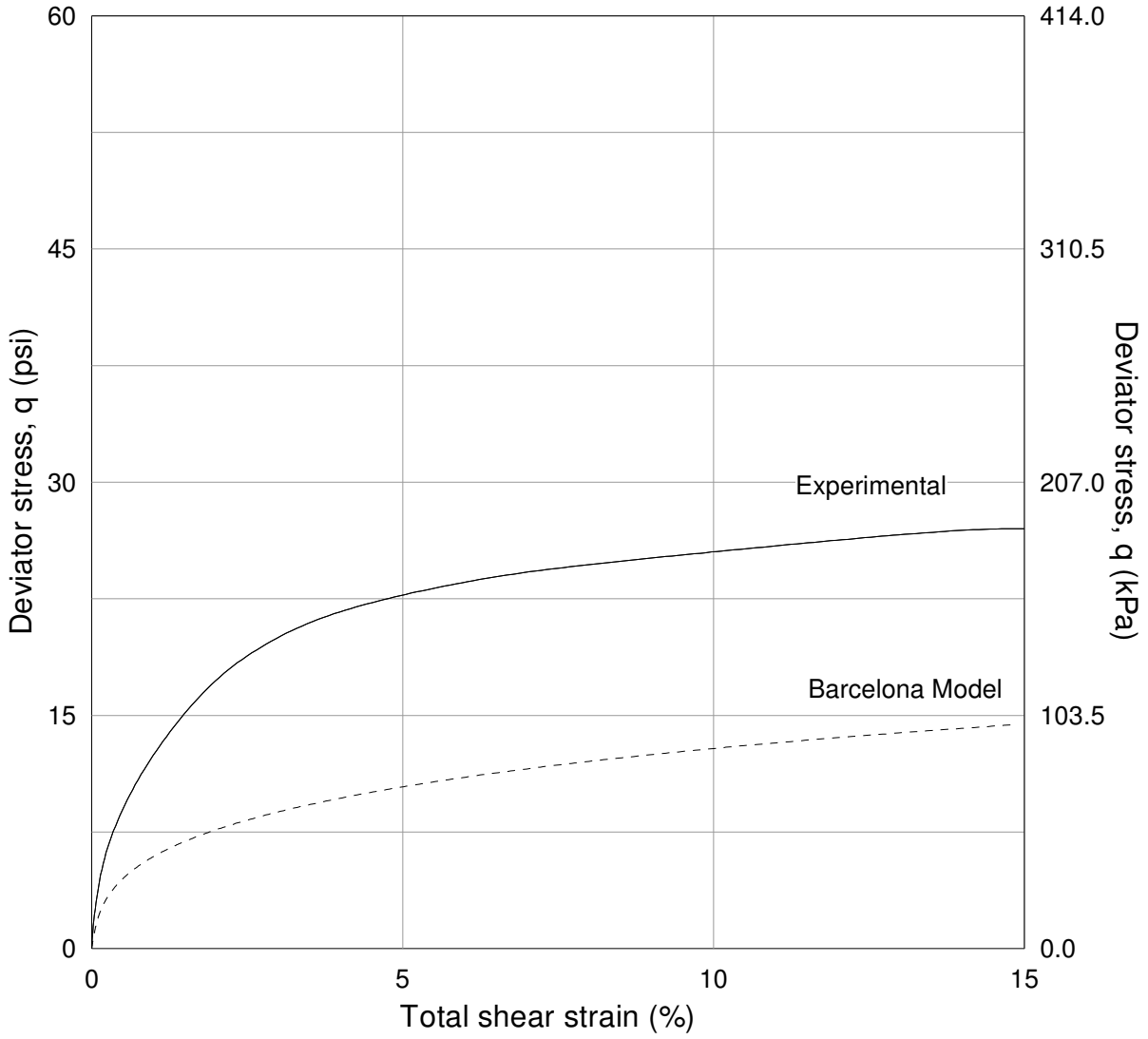

Figure 6.28 Experimental and predicted silty sand response for TC test at s = 100 kPa initial p_{net} = 100 kPa

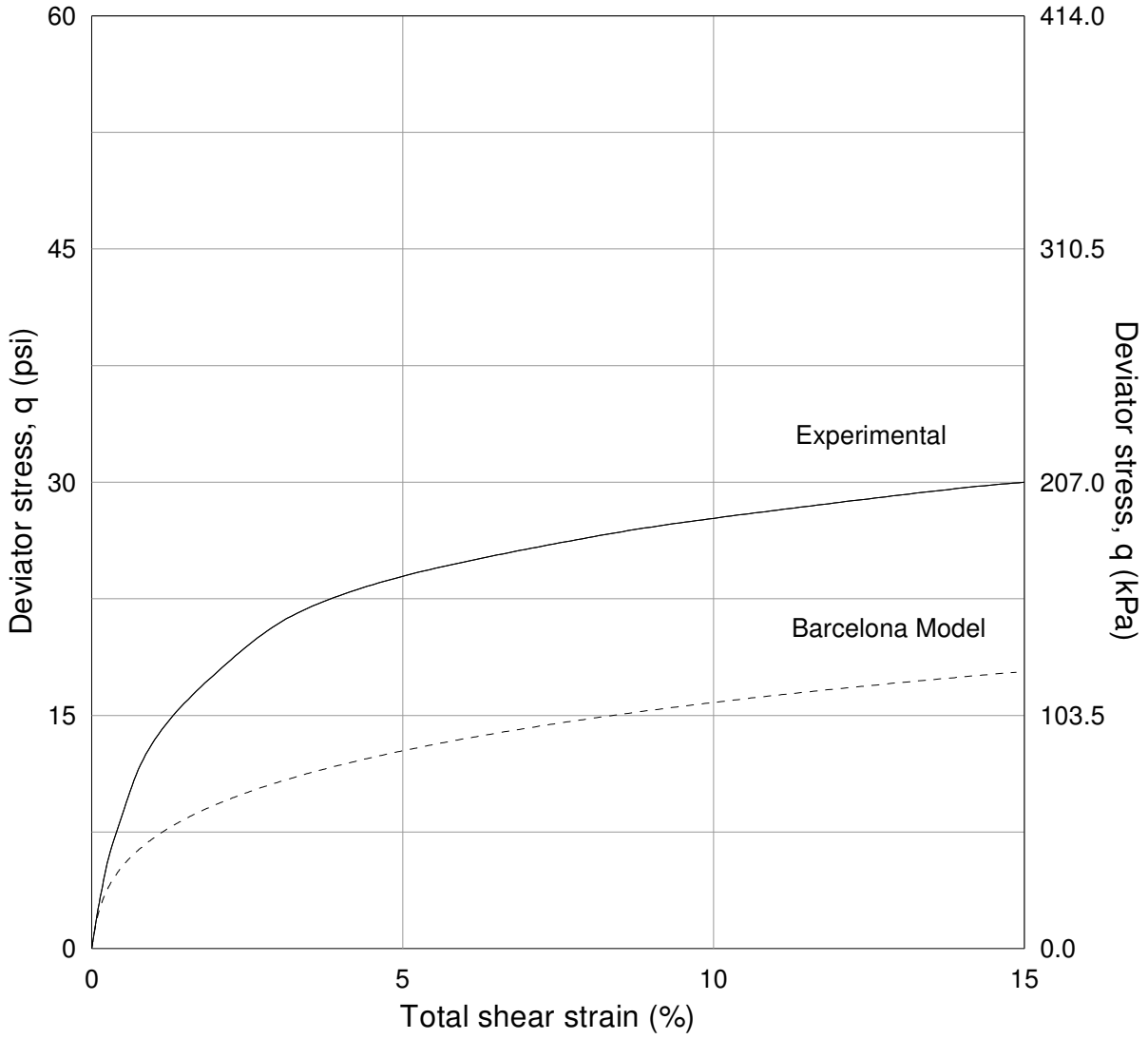

Figure 6.29 Experimental and predicted silty sand response for TC test at s = 200 kPa initial p_{net} = 100 kPa

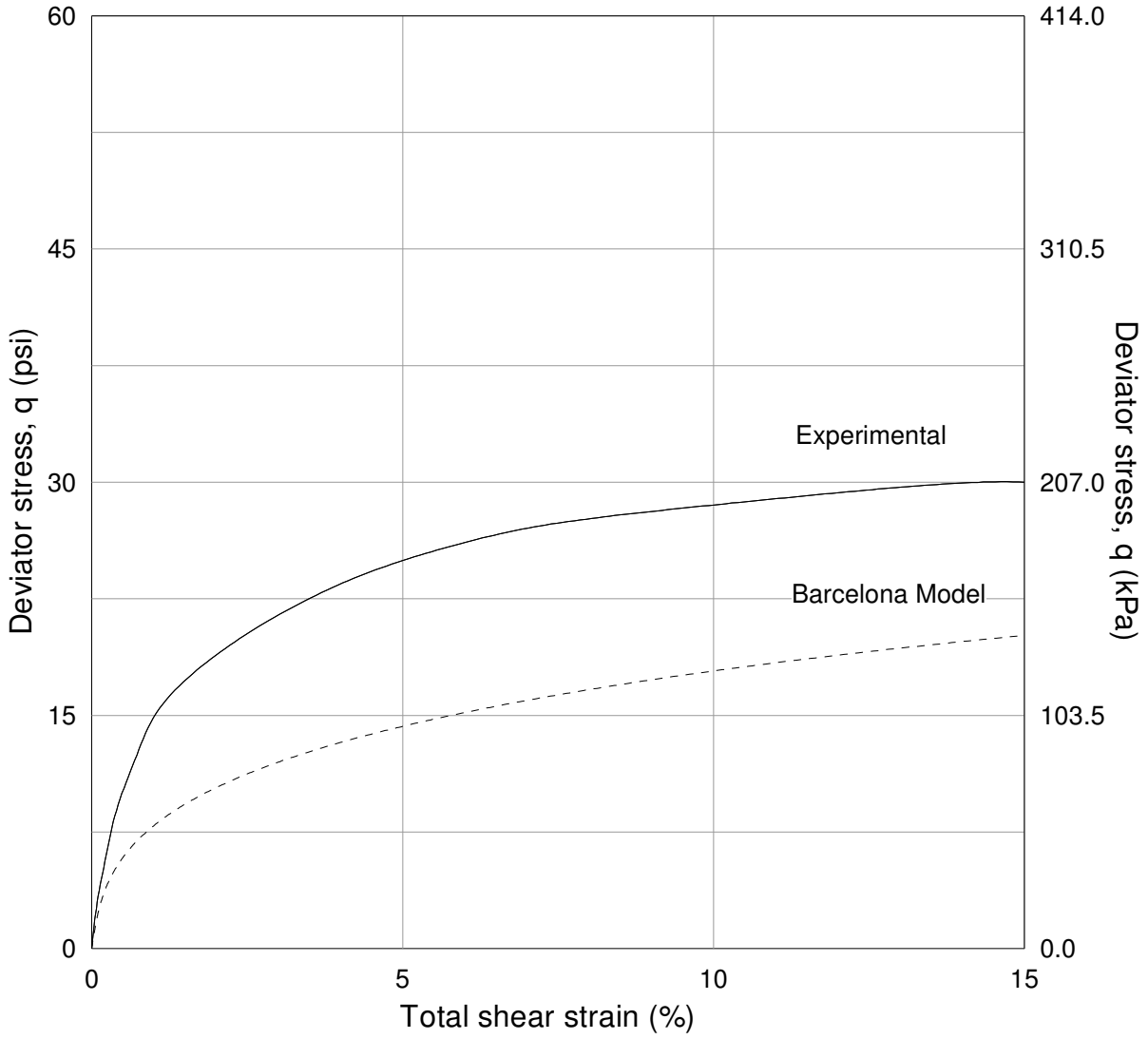

Figure 6.30 Experimental and predicted silty sand response for TC test at s = 300 kPa initial p_{net} = 100 kPa

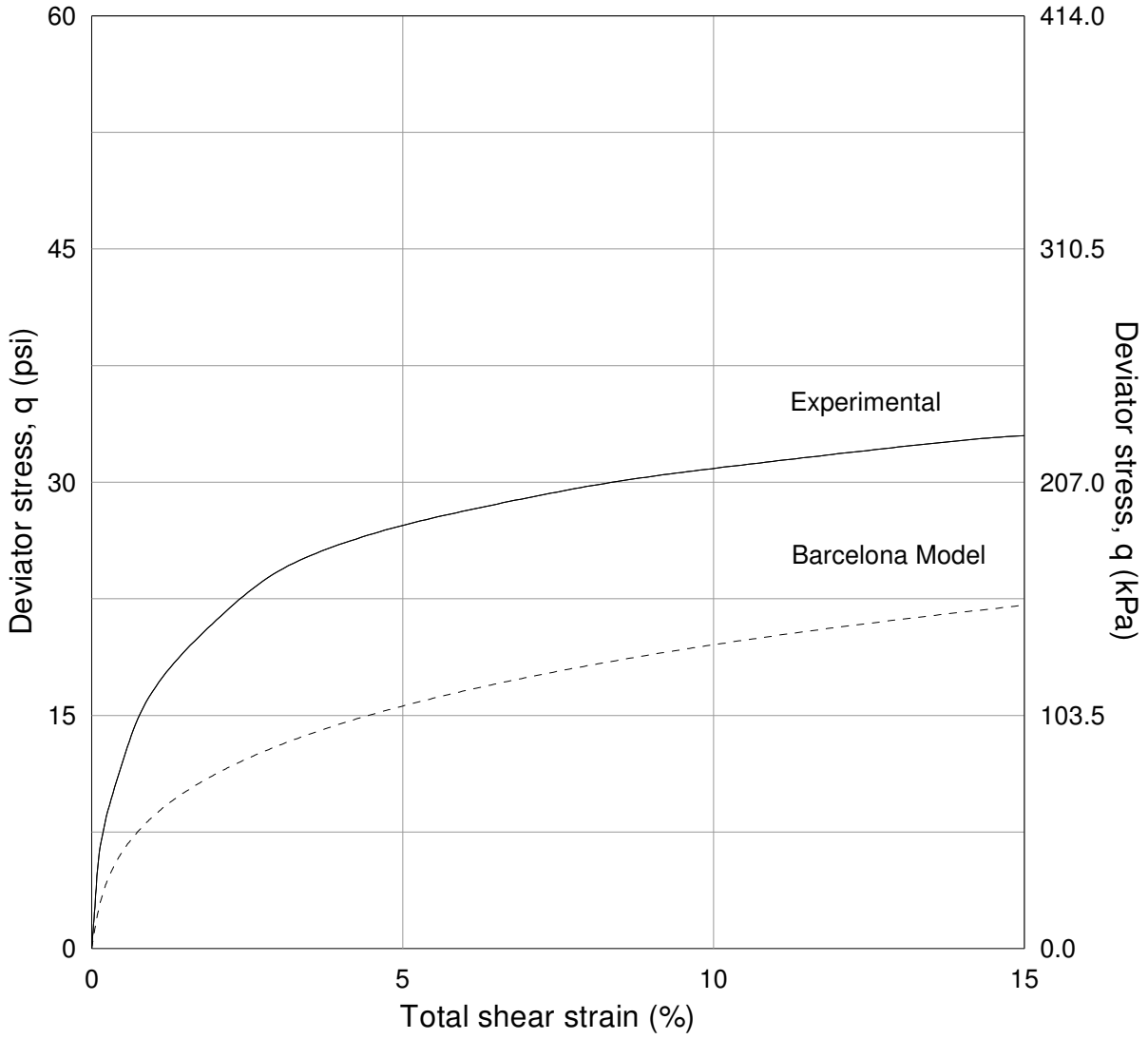

Figure 6.31 Experimental and predicted silty sand response for TC test at s = 400 kPa initial p_{net} = 100 kPa

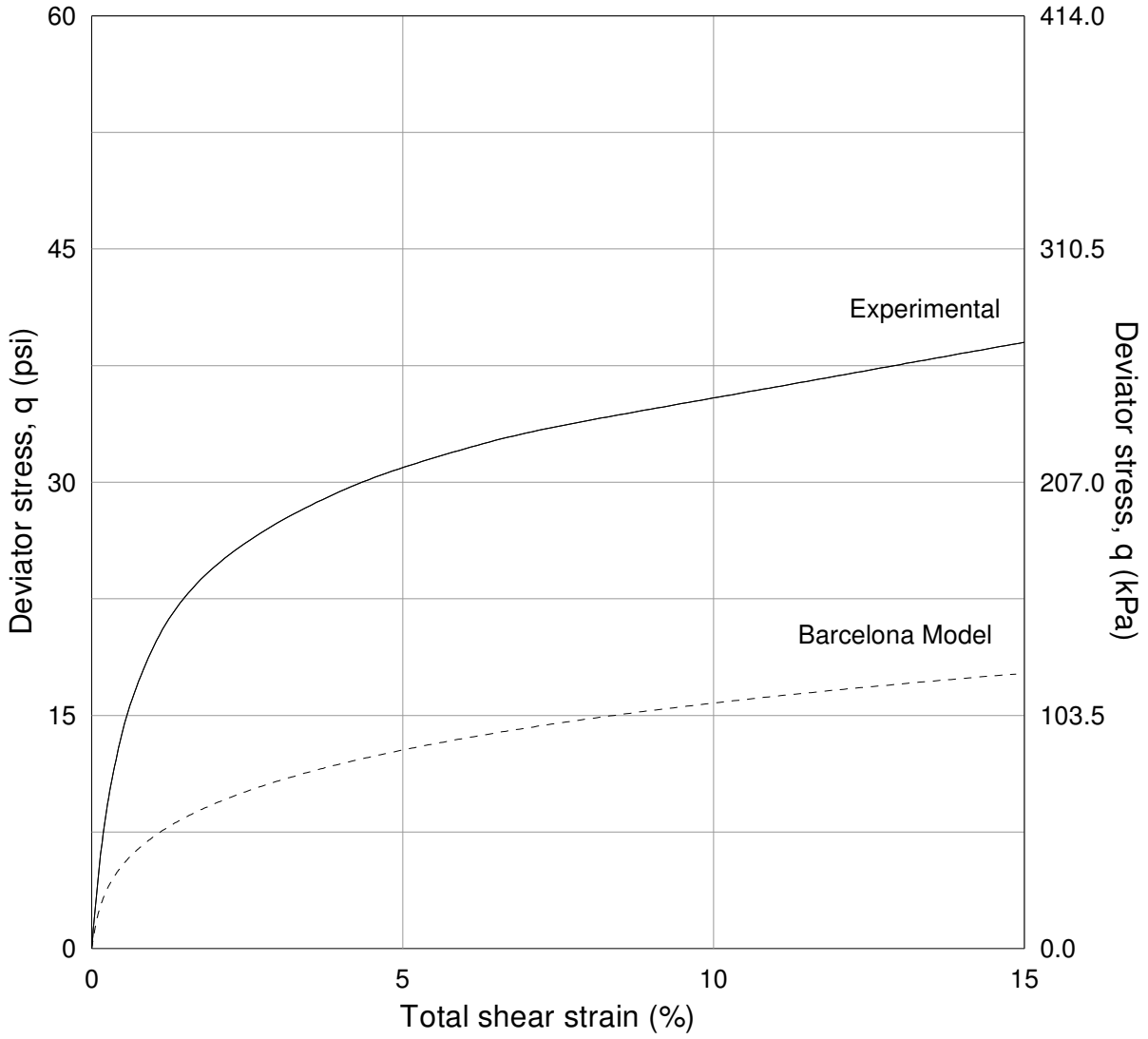

Figure 6.32 Experimental and predicted silty sand response for TC test at s = 50 kPa initial p_{net} = 150 kPa

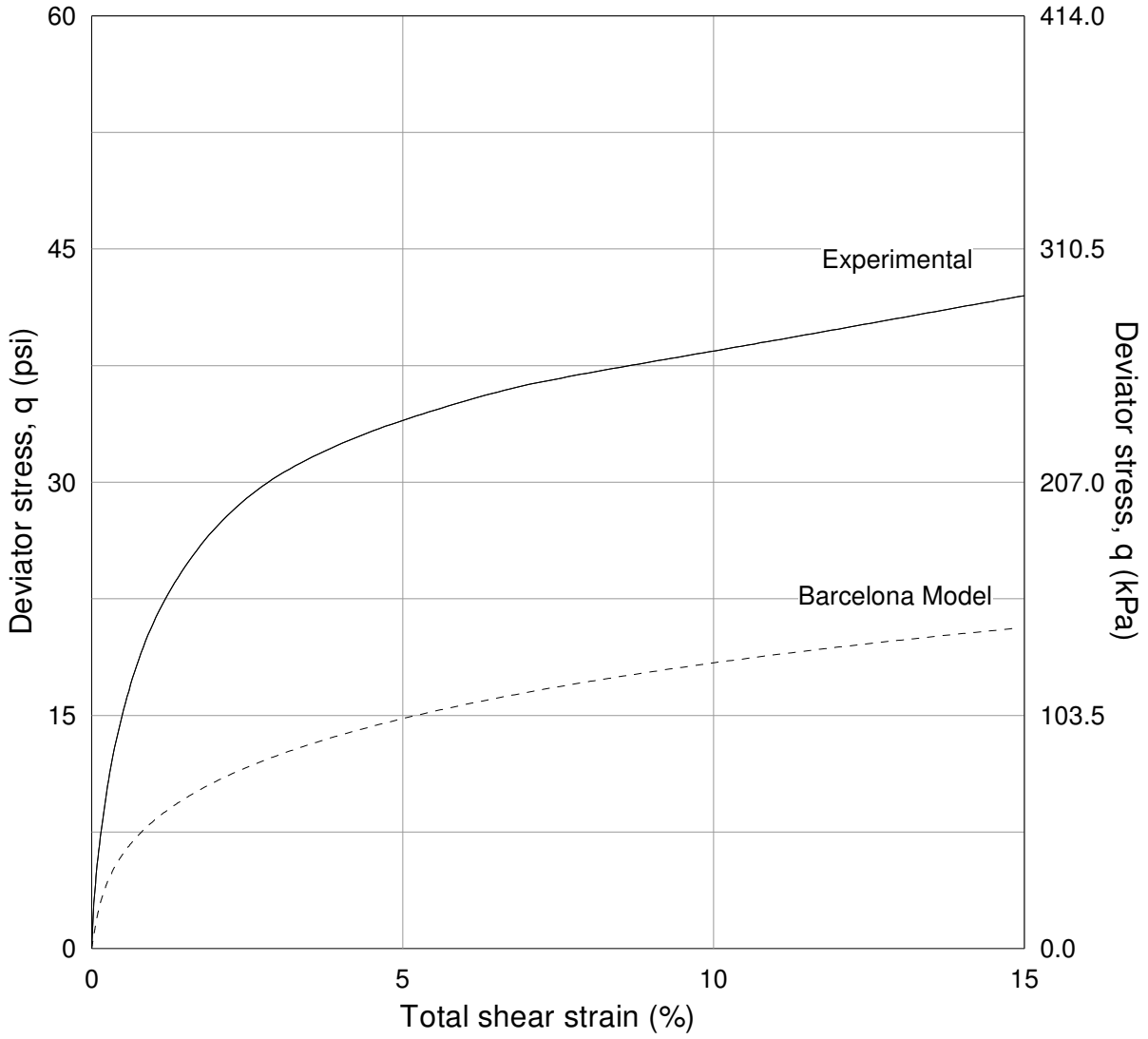

Figure 6.33 Experimental and predicted silty sand response for TC test at s = 100 kPa initial p_{net} = 150 kPa

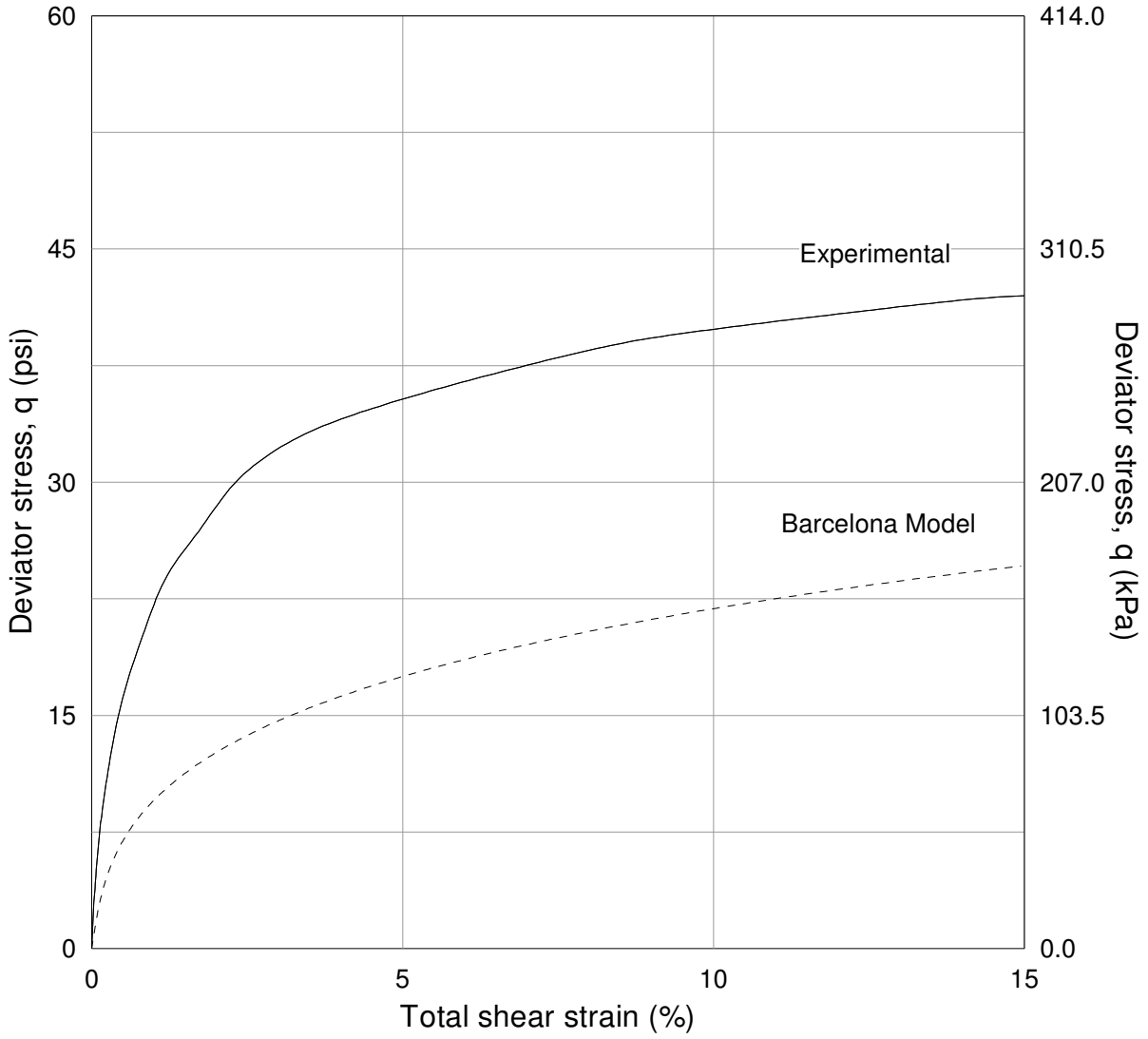

Figure 6.34 Experimental and predicted silty sand response for TC test at s = 200 kPa initial p_{net} = 150 kPa

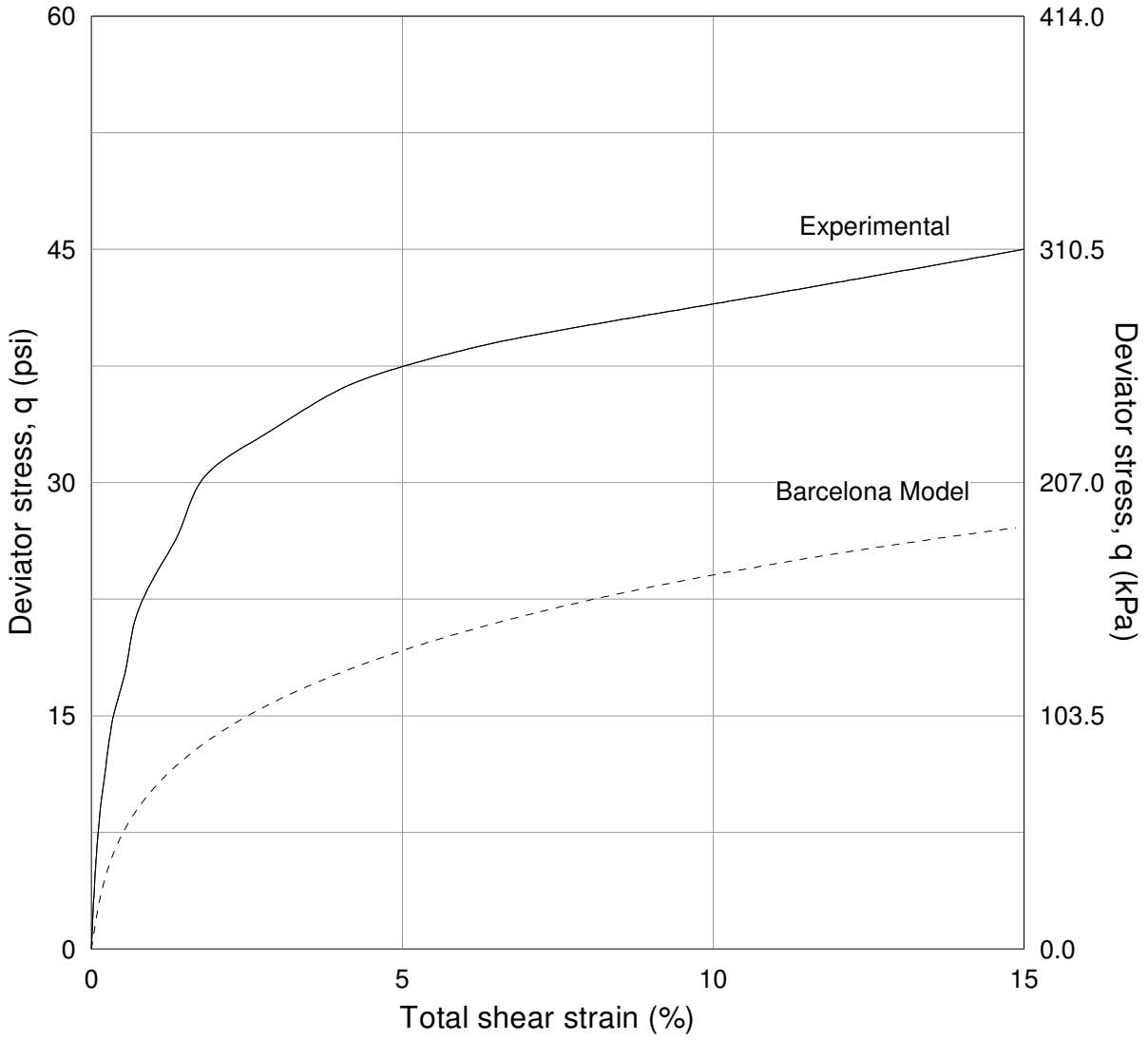

Figure 6.35 Experimental and predicted silty sand response for TC test at s = 300 kPa initial p_{net} = 150 kPa

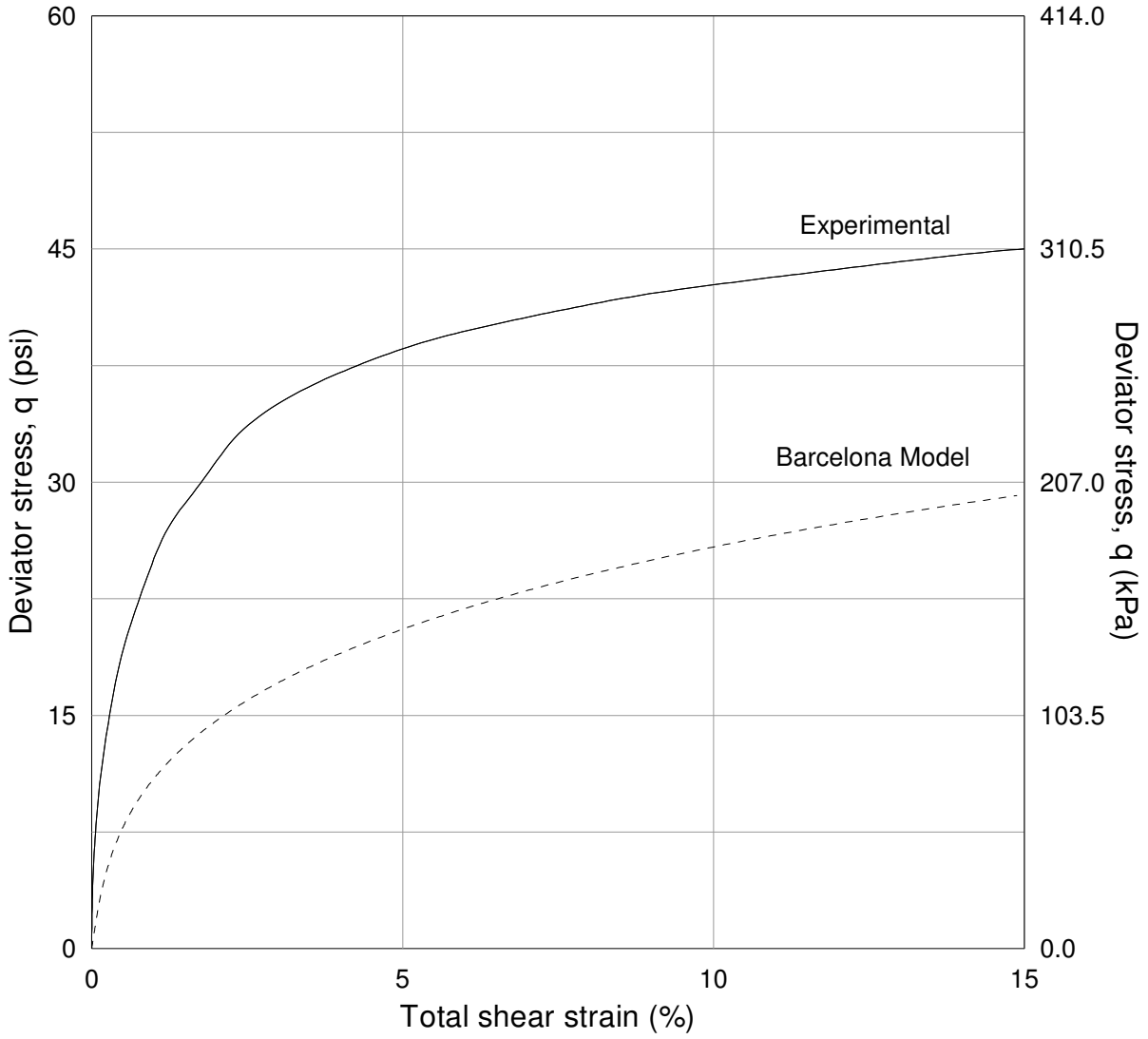

Figure 6.36 Experimental and predicted silty sand response for TC test at s = 400 kPa initial p_{net} = 150 kPa

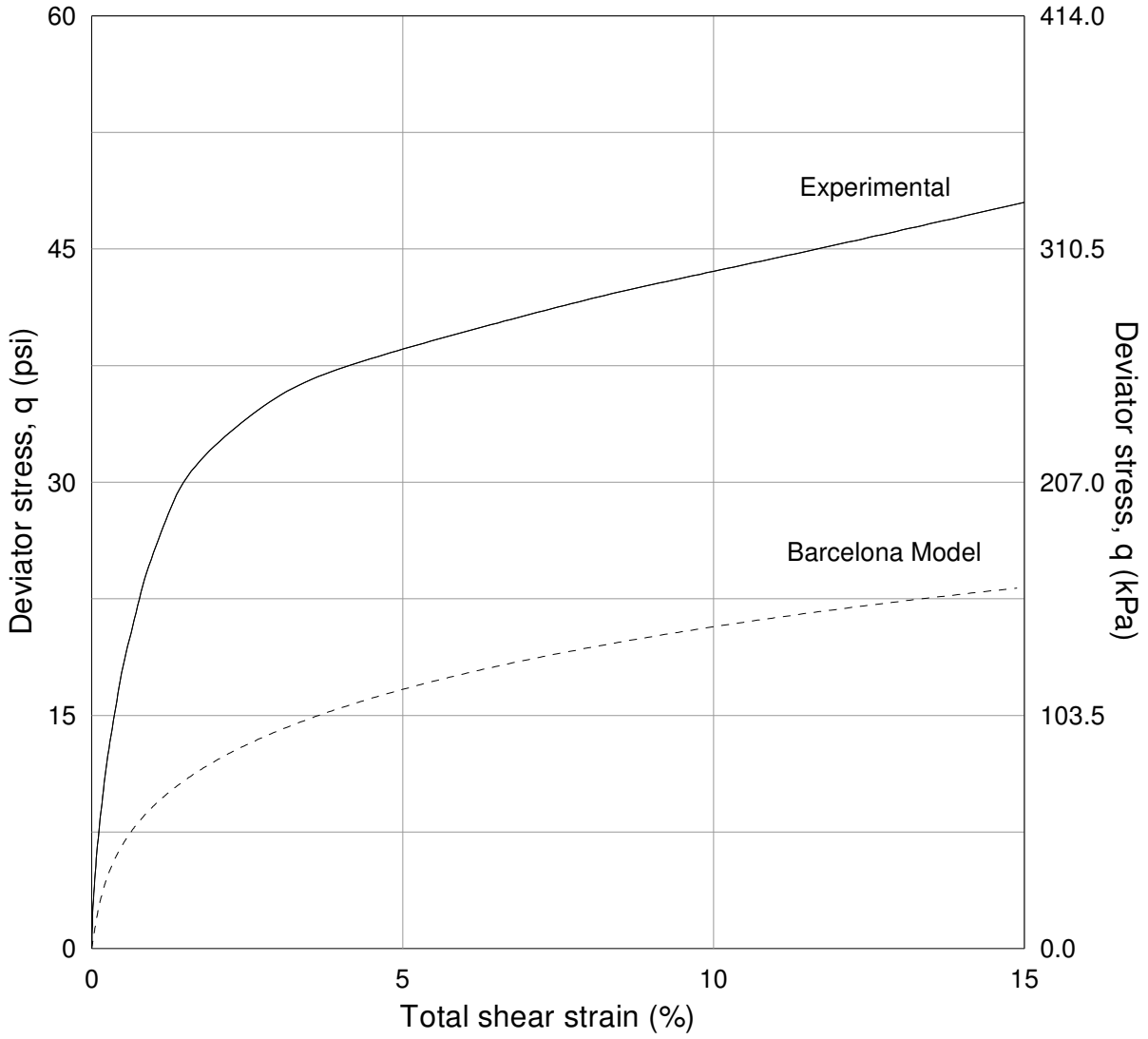

Figure 6.37 Experimental and predicted silty sand response for TC test at s = 50 kPa initial p_{net} = 200 kPa

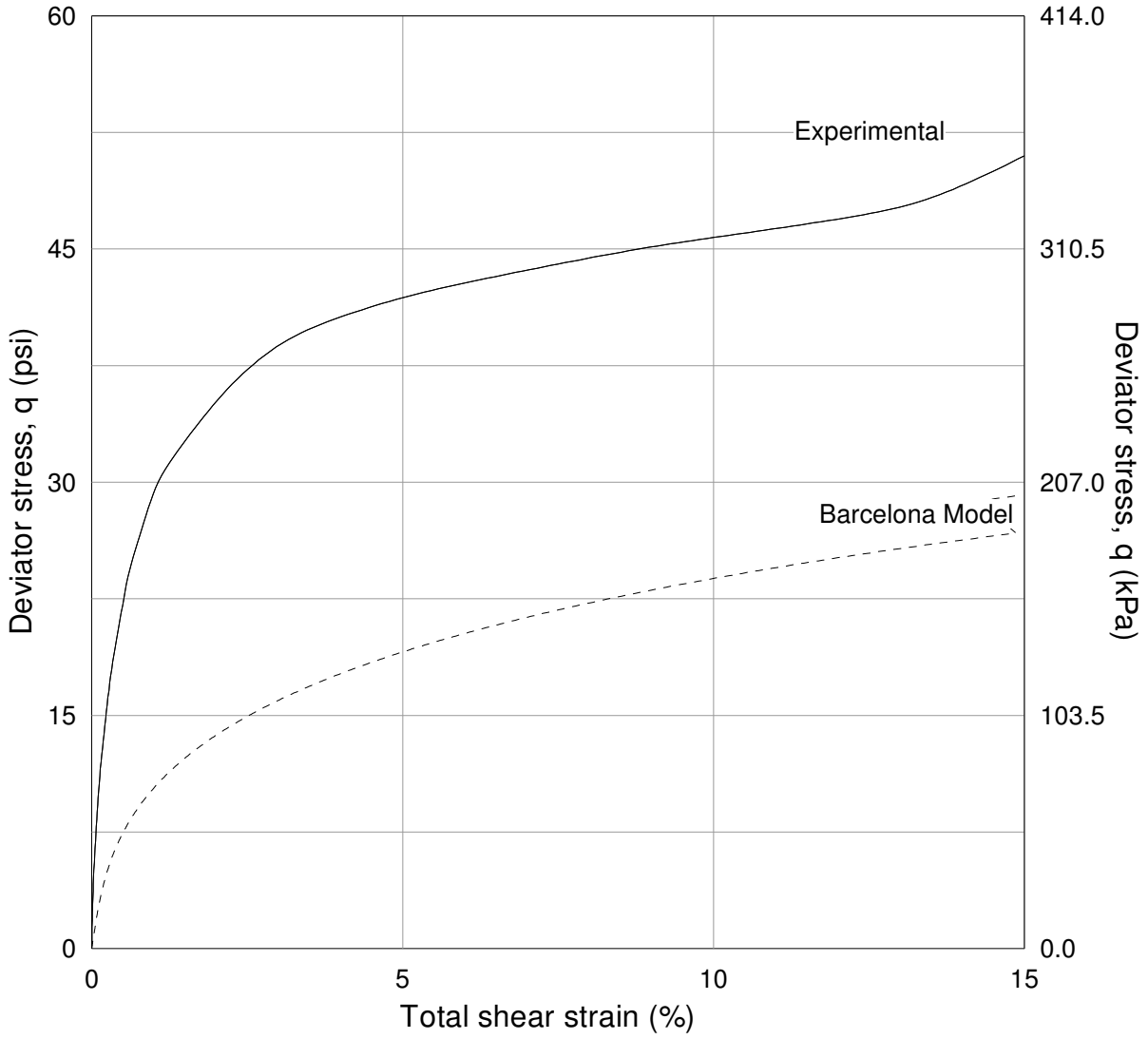

Figure 6.38 Experimental and predicted silty sand response for TC test at s = 100 kPa initial p_{net} = 200 kPa

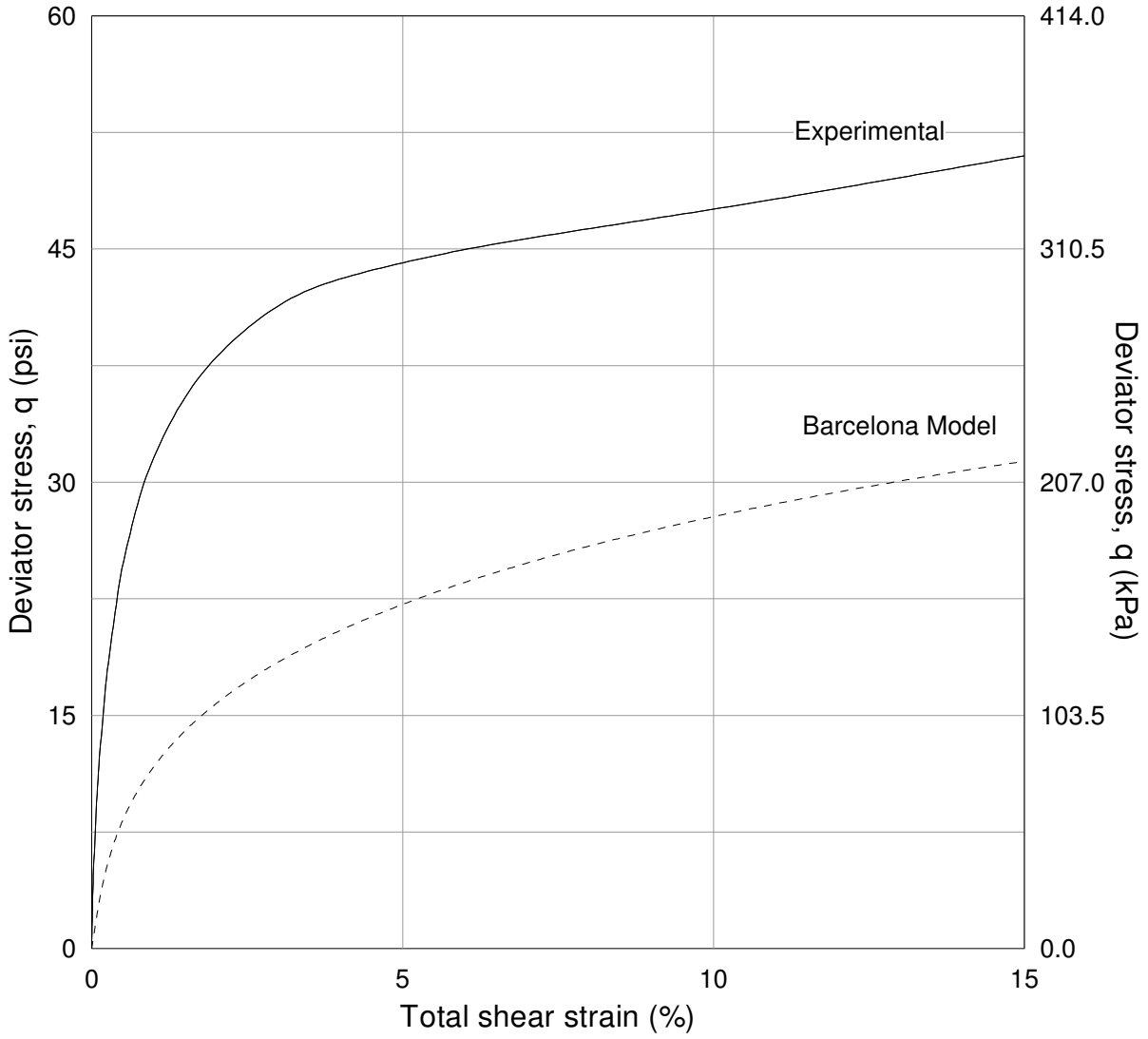

Figure 6.39 Experimental and predicted silty sand response for TC test at s = 200 kPa initial p_{net} = 200 kPa

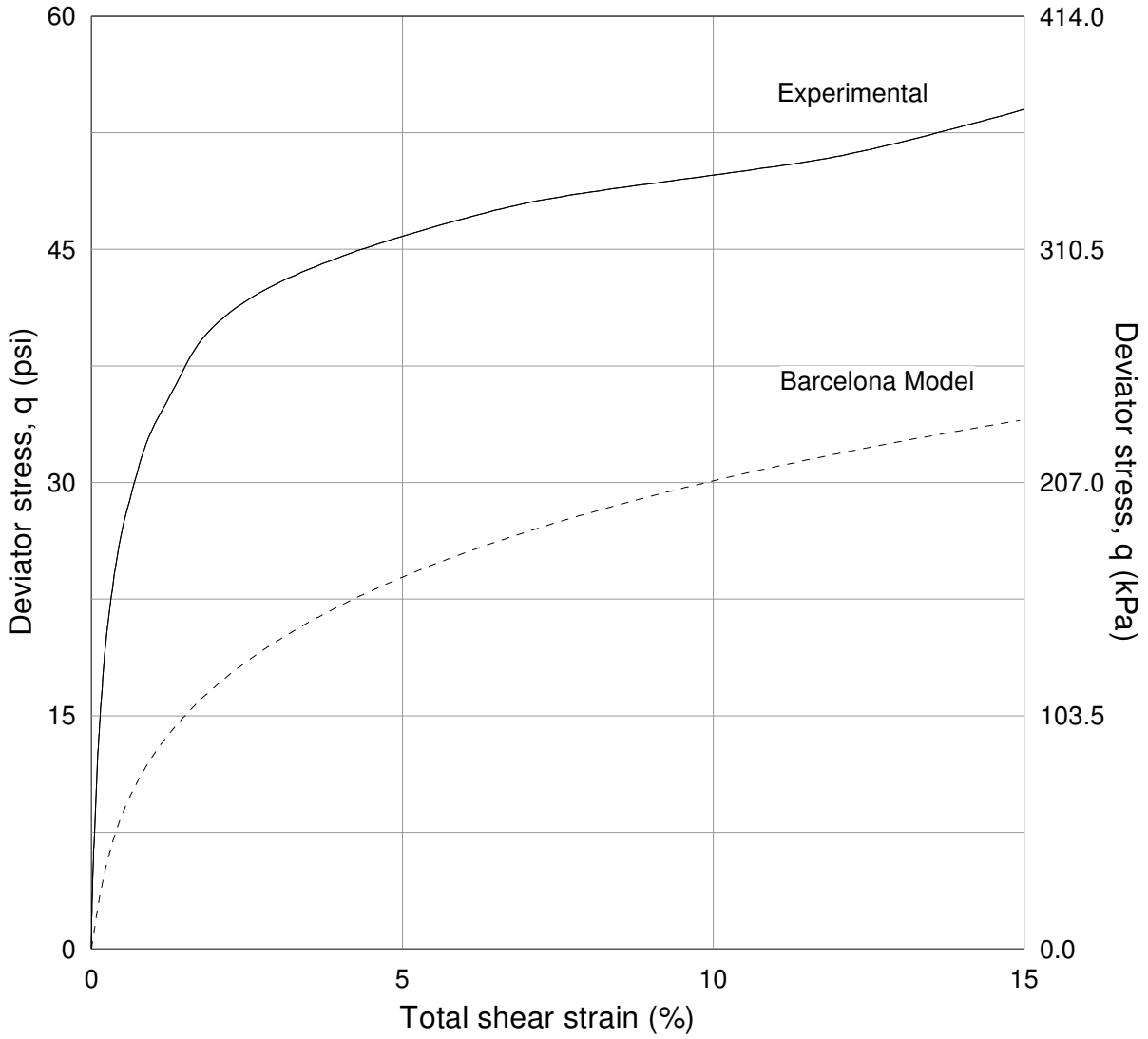

Figure 6.40 Experimental and predicted silty sand response for TC test at s = 300 kPa initial p_{net} = 200 kPa

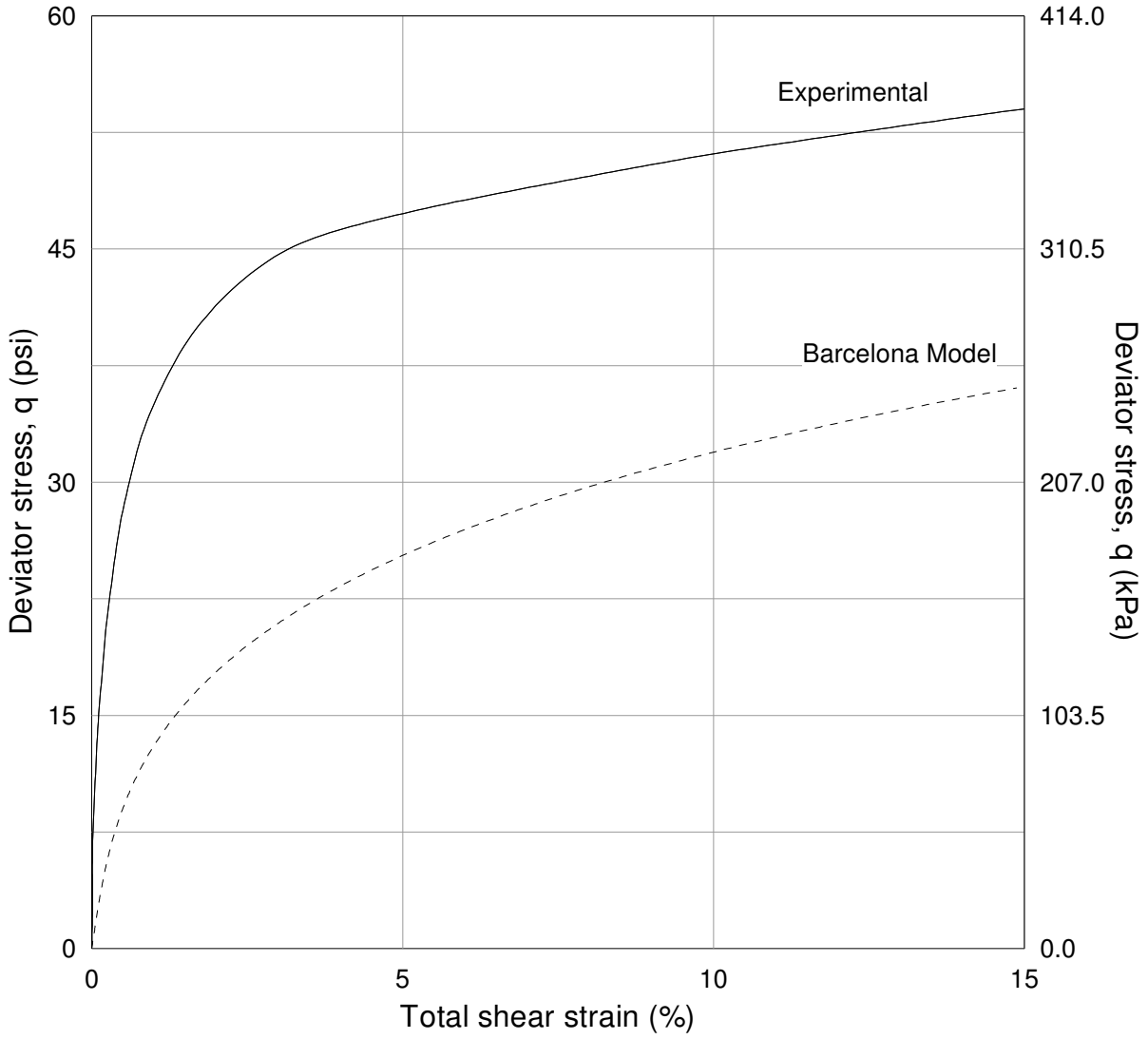

Figure 6.41 Experimental and predicted silty sand response for TC test at s = 400 kPa initial p_{net} = 200 kPa

CHAPTER 7

SUMMARY, CONCLUSIONS AND RECOMMENDATIONS

7.1 Summary

A computer-based, mixed-boundary type, suction-controlled true triaxial (cubical) testing device has been developed to test unsaturated soils under general stress states and controlled matric suction states. The cubical apparatus was found suitable testing unsaturated soils using the axis-translation technique. A comprehensive series of drained (constant-suction), suction-controlled HC, CTC, TC, and TE tests were conducted on 3-in per side, cubical silty sand specimens compacted via a combined pluviation-tamping technique. Test data were also presented in the octahedral stress plane to study the influence of matric suction on the size and position of the failure envelopes of unsaturated soils under general stress states. In all cases, the incipient critical state condition was defined at a total shear strain of approximately10 to 12 %. HC, CTC and TC tests results were also used for validation of the Barcelona model in unsaturated silty sand.

7.2 General Conclusions

7.2.1 Suction-Controlled True Triaxial Device

The presence of the pore-water and pore-air-pressurizing systems units at the bottom wall assembly, was found to have minimal effects on the stress-strain response of cubical soil specimens in terms of the value of deviatoric stress, q, defined at a incipient critical state condition (approximately 12% of total shear strain).

A loading rate of 1 psi/h (10 kPa/h) was found to be appropriate for conducting suction-controlled true triaxial testing on the 3-in per side, cubical silty sand specimens. Proper equalization of the pore-air and pore-water phases was obtained following this loading rate.

The axis-translation technique (Hilf, 1956) was found to be suitable for testing cubical soil specimens in the cubical device under matric suction states above 100 kPa.

7.2.2 Behavior Under Isotropic Stress States

Matric suction exerted a significant influence on the volumetric stiffness of silty sand soil under constant-suction (drained) isotropic loading, with a significant decrease in the volumetric stiffness parameter, $\lambda(s)$, for s = 400 kPa.

A small amount of volumetric collapse was observed in the specimens subjected to a low value (wetting) of matric suction (s = 50 kPa) after confining under a constant net mean stress. The initial loading-collapse (LC) yield curve, induced by the combined pluviation-tamping compaction process, was found to be defined by relatively low values of yield net mean stress, p(s).

Reasonably good agreement was found between the experimental LC yield curve (induced by pluviation-tamping) of silty sand and the one predicted by the constitutive formulation proposed by Alonso et al. (1990) in (p : s : v) space.

7.2.3 Behavior under Axisymmetric Stress States

Matric suction was found to have a significant influence on the shearing resistance of the cubical unsaturated soil specimens, regardless of the stress path that was followed. In all drained, suction-controlled CTC, TC and TE tests, the ultimate deviatoric stress, q, was

identified at an incipient critical state corresponding to, approximately, 12% of total shear strain. The position of the critical state lines in the (p : q) plane was found to be dependent of the level of matric suction, having a significant increase in apparent cohesion (intercept with q axis) for s = 400 kPa. The slopes of the critical state lines were found to be similar to each other, and in agreement with the critical state-based constitutive framework proposed by Alonso et al. (1990) in (p : q : s) space.

The apparent cohesion was found to increase linearly with matric suction, in agreement with the ϕ^b angle in the shear strength equation proposed for unsaturated soils (Fredlund and Rahardjo, 1993).

7.2.4 Validation of Critical State-Based Constitutive Models

The Barcelona model shows reasonably good predictions of silty sand response under CTC stress paths. However, model predictions of silty sand stress-strain response under TC stress paths are rather underestimated.

7.2.5 Behavior under General Stress States

Results from drained (constant-suction), suction-controlled TC and TE tests showed that matric suction exerts a significant influence on the size and position of the failure envelopes in the octahedral plane, with a considerable expansion of the surface for s = 400 kPa. A small value of tensile strength in the silty sand specimens was found to increase with matric suction, $s = (u_a - u_w)$. In general, all of the experimental results obtained from drained (constant-suction) testing, along with the numerical analyses, validated the suitability of the suction-controlled cubical device developed in this study for testing unsaturated soils under general stress states and varying matric suction conditions.

7.3 Key Recommendations for Future Work

Further suction-controlled simple shear (SS) tests should be performed in the cubical device to fully describe the shape of the failure surface on principal and octahedral stress planes for varying matric suction conditions and different values of the octahedral normal stress. A series of SS tests is currently being undertaken by this research supervisor, Dr. Laureano Hoyos.

The device is currently being upgraded for simultaneously strain-controlled and suction-controlled testing via the PCP-5000-UNSAT panel.

REFERENCES

Aitchison, G. D. (1967). "Separate Roles of Site Investigation, Quantification of Soil Properties, and Selection of Operational Environment in the Determination of Foundation Design on Expansive Soils," Proc., 3rd Asian Reg. Conf. Soil Mech. and Found. Engrg., Haifa, Israel, Vol. 3, 72-77.

Aitchison, G. D. (1973). "The Quantitative Description of the Stress - Deformation Behavior of Expensive Soils-Preface to Set of Papers," Proc., 3rd Int. Conf. on Expansive Soils, Haifa, Israel, Vol. 2, 79-82.

Aitchison, G. D.; and Woodburn, J. A. (1969). "Soil Suction in Foundation Design," Proc., 7th Int. Conf. Soil Mech. and Found. Engrg., Mexico, Vol. 2, 1-8.

Alonso, E. E.; Gens, A.; and Hight, D. W. (1987). "Special Problem Soils. General Report," Proc., 9th Eur. Conf. on Soil Mech. and Found. Engrg., Dublin, Vol. 3, 1087-1146.

Alonso, E. E.; Gens, A.; and Josa, A. (1990). "A Constitutive Model for Partially Saturated Soils," Geotechnique, 40(3), 405-430.

Arthur, J. R. F. (1988). "Cubical Devices: Versatility and Constrains," Advanced Triaxial Testing of Soil and Rock, STP 977, ASTM, Philadelphia, 743-765.

Atkinson, R. H. (1972). "A Cubical Test Cell for Multiaxial Testing of Materials," Ph.D. dissertation, University of Colorado at Boulder, Boulder, CO.

Barbour, S.L. and Fredlund, D.G. (1989). "Mechanisms of osmotic flow and volume change in clay," Canadian Geotechnical Journal, 26:551-562.

Barden, L.; Madedor, A. O.; and Sides, G. R. (1969). "Volume Change Characteristics of Unsaturated Clay," ASCE J. Soil Mech. Found. Div., 95(SM1).

Brady, N.C. (1974). "The nature and properties of soil," MacMaillan Publishing Co., Inc., New York.

Bear, J. (1979). "Hydraulic of Groundwater," McGraw-Hill Series in Water Resources and Environmental Engrg., McGraw-Hill, New York, NY.

Biot, M.A., (1941) "General Theory of Three-Dimensional Consolidation," J.Appl. Phys., vol.12, no.2, pp. 155-164.

Bishop, A. W. (1959). "The Principle of Effective Stress," Lecture delivered in Oslo, Norway, in 1955, published in: Teknisk Ukeblad, 106(39), 859-863.

Bishop, A. W.; and Blight, G. E (1963). "Some Aspects of Effective Stress in Saturated and Unsaturated Soils," Geotechnique, 13(3), 177-197.

Bishop, A. W.; and Donald, I. B. (1961). "The Experimental Study of Partly Saturated Soils in the Triaxial Apparatus," Proc., 5th Int. Conf. on Soil Mech. and Found. Engrg., Paris, France, Vol. 1, 13-21.

Bishop, A. W.; Alpan, I.; Blight, G. E; and Donald, I. B. (1960). "Factors Controlling the Shear Strength of Partly Saturated Cohesive Soils," Proc., ASCE Res. Conf. on Shear Strength of Cohesive Soils, Boulder, CO, 503-532.

Blight, G. E. (1961). "Strength and Consolidation Characteristics of Compacted Soils," Ph.D. Dissertation, University of London, London, England.

Blight, G. E. (1965). “A Study of Effective Stresses for Volume Change,” Proc., Symp. on Moisture Equilibria and Moisture Changes in Soils Beneath Covered Areas, ed. G. D. Aitchison, Australia: Butterworths, 259-269.

Brackley, I. J. A. (1971). “Partial Collapse in Unsaturated Expansive Clay,” Proc., 5th African Reg. Conf. on Soil Mech. and Found. Engrg., South Africa, Vol.1, 23-30.

Brennen, C.E. (1995). “Cavitation and Bubble Dynamics,” Oxford University Press, New York.

Burland, J. B. (1964). Discussion on: “Some Aspects of Effective Stress in Saturated and Unsaturated Soils,” Geotechnique, Vol. 14, 65-68.

Burland, J. B.(1965). “Some Aspects of the Mechanical Behavior of Partly Saturated Soils,” Proc., Symp. on Moisture Equilibria and Moisture Changes in Soils Beneath Covered Areas, ed. G. D. Aitchison, Australia: Butterworths, 270-278.

Callisto, L., and Calabresi, G. (1998). “Mechanical Behavior of a Natural Soft Clay,” Gèotechnique 48 (4), 495-513.

Childs, E. C. (1969). “An Introduction to the Physical Basis of Soil Water Phenomena,” Wiley-Interscience, London, UK.

Coleman, J. D. (1962). “Stress/Strain Relations for Partly Saturated Soils,” Geotechnique, 12(4), 348-350.

Croney, D.; Coleman, J. D.; and Black, W. P. M. (1958). “Movement and Distribution of Water in Soil in Relation to Highway Design and Performance” Water and Its Conduction in Soils, Highway Research Board, Special Report, Washington, DC, No. 40, 226-252.

Donald, I. B. (1961). "The Mechanical Properties of Saturated and Partly Saturated Soils with Special Reference to Negative Pore Water Pressure," Ph.D. Dissertation, University of London, London, England.

Fredlund, D. G. (1973). "Volume Change Behavior of Unsaturated Soils," Ph.D. Dissertation, University of Alberta, Edmonton, Alta., Canada.

Fredlund, D.G. (1989). "Soil suction monitoring for roads and airfields," Symposium on the State-of-the Art of Pavement Response Monitoring Systems for Road and Airfields, sponsored by US. Army Corps of Engineers, Hanover , NH, March 6-9, 1989.

Fredlund, D. G. (1991). "How Negative Can Pore-Water Pressure Get ?," Geotechnical News, Canadian Geotech. Soc., 9(3), 44-46.

Fredlund, D.G. (1995). "The scope of unsaturated soil mechanics: an overview, 1st. Int. Conf. on Unsaturated soils," Paris, (1995), 215-222, eds. E.E.Alonso and P.Delage, publ. Balkema, Rotterdam.

Fredlund, D. G.; and Morgenstern, N. R. (1977). "Stress State Variables for Unsaturated Soils," ASCE J. Geotech. Engrg. Div., 103(GT5), 447-466.

Fredlund, D. G., & Rahardjo, H. (1993). Soil Mechanics for Unsaturated Soils. Wiley, New York.

Fredlund,D.G. and Xing, A. (1994). "Equations for the soil water characteristic curve. Canadiain Geotechnical Journal," 31:521-532.

Fredlund, D. G.; Morgenstern, N. R.; and Widger, R. A. (1978). "The Shear Strength of Unsaturated Soils," Canadian Geotech. J., 15(3), 313-321.

Fung, Y.C. (1965). “Foundations of solid Mechanics,” Prentice Hall, Englewood Cliffs, NJ.

Gens, A.; and Alonso, E. E. (1992). “A Framework for the Behavior of Unsaturated Expansive Clays,” Canadian Geotech. J., Vol. 29, 1013-1032.

Gibbs, H. J.; and Coffey, C. T. (1969). “Techniques for Pore Pressure Measurements and Shear Testing of Soils,” Proc., 7th Int. Conf. on Soil Mech. and Found. Engrg., Mexico, Vol. 1, 151-157.

Graham, J., Saadat, F., Gray, M.N.,Dixon, D.A. and Zhang, Q.Y. (1988). “Strength and volume change behavior of sand-bentonite mixture,” Canadian Geotechnical Journal, 26:292-305.

Hilf, J. W. (1948). “Estimating Construction Pore Pressures In Rolled Earth Dams,” Proc., 2nd Int. Conf. on Soil Mech. and Found. Engrg., Rotterdam,Vol. III, 234-240.

Hilf, J. W. (1956). “An Investigation of Pore-Water Pressure in Compacted Cohesive Soils,” Tech. Memo. No. 654, U.S. Dep. of the Interior, Bureau of Reclamation, Design and Construction Div., Denver, CO.

Ho, D. Y. F.; and Fredlund, D. G. (1982a). “Increase in Shear Strength due to Soil Suction for Two Hong Kong Soils,” Proc., ASCE Geotech. Conf. on Engrg. and Const. in Tropical and Residual Soils, Honolulu, HI, 263-295.

Hoyos, L.R., (1998). “Experimental and Computational Modeling of Unsaturated Soil Behavior under True Triaxial Stress States,” PhD dissertation, Georgia Institute of Technology, Atlanta, Georgia, 358 pp.

Hoyos L.R. and Macari E.J., (2001). “Development of a Stress/Suction-Controlled True Triaxial Testing Device for Unsaturated Soils”. Geotechnical Testing Journal, 24(1), 5-13.

Jennings, J. E. (1961). “A Revised Effective Stress Law for Use in the Prediction of the Behavior of Unsaturated Soils,” Proc., Pore Pressure and Suction in Soils Conf., London, England: Butterworths, 26-30.

Jennings, J. E.; and Burland, J. B. (1962). “Limitations to the Use of Effective Stresses in Partly Saturated Soils,” Geotechnique, 12(2), 125-144.

Kaye,G.W.C. and laby, T.H., (1993). “Tables of Physical and Chemical Constants,” Longman, Boston.

Kjellman, W. (1936). “Report on an Apparatus for Consummate Investigation of the Mechanical Properties of Soils,” Proc., 1st Int. Conf. on Soil Mechanics and Foundation Engineering, 2, 16-20.

Ko, H. Y., & Scott, R. F. (1967). “A New Soil Testing Apparatus. Geotechniuque,” 17 (1), 40-57.

Krahn, J.; and Fredlund, D. G. (1972). “On Total, Matric and Osmotic Suction,” J. Soil Sci., 114(5), 339-348.

Kumar,S., and Malik, R.S. (1990). “Verification of quick capillary rise approach for determining pore geometrical characteristics in soils of varying texture,” Soil Science, 150(6), 83-888.

Lade, P. V., & Ducan, J. M. (1973). “Cubical Triaxial Tests on Cohesionless Soil,” Journal of the Soil Mechanic Foundation Division, ASCE, 99 (10), 793-812.

Lambe, T. W. (1967). “Stress Path Method,” ASCE J. Soil Mech. Found. Engrg. Div., 93(SM6), 309-331.

Lambe, T. W.; and Whitman, R. V. (1979). “Soil Mechanics,” John Wiley and Sons, Inc., New York, NY.

Lane, K.S., and Washburn, S.E. (1946). “Capillary tests by capillarimeters and by soil filled tubes,” Proceedings of Highway Research Borad, 26,460-473

Laplace, P.S. (1806) “Mecanique Celeste,” suppl. 10^{th} vol. English Translation reprinted by Chelsea, New York (1966).

Lu, N., and Likos W. J. (2004). “Unsaturated Soil Mechanics,” John Wiley & Sons, New York.

Macari, E.J., Weihe, S., Arduino, P., (1997). “Implicit integration of elasto-plastic constitutive Models for frictional materials with highly non-linear hardening functions,” Journal of Mechanics of Cohesive-Frictional Materials 2, 1–29.

Macari, E.J., Hoyos, L.R.., Arduino, P., (2003). “Constitutive Modeling of Unsaturated Soil Behavior under Axisymmetric Stress States using a Stress/Suction-Controlled Cubical Test Cell,” Int. Journal of Plasticity, 19(2003), 1481-1515.

Malik, R.S., Kumar, S., and Malik, R.K. (1989). “Maximal capillary rise flux as a function of height from the water table,” Soil Science, 148(5), 322-326.

Matsuoka, H., Sun, D.A., Kogane, A., Fukuzawa, N., and Ichihara, W. (2002). “Stress-strain behavior of unsaturated soil in true triaxial tests,” Canadian Geotechnical Journal, 39: 608-619.

Matyas, E. L.; and Radhakrishna, H. S. (1968). “Volume Change Characteristics of Partially Saturated Soils,” Geotechnique, 18(4), 432-448.

McQueen, I.S., and Miller, R.F. (1974) “Approximating soil moisture characteristics from limited data: Empirical evidence and tentative model,” Water Resources Research, 10(3), 521-527.

Mitchell, J.K. (1976). “Fundametals of soil behavior,” J.Wiley & Sons Publishers.

Morgenstern, N. R. (1979). “Properties of Compacted Soils,” Proc., 6th Panam. Conf. on Soil Mech. and Found. Engrg., Lima, Peru, Vol. 3, 349-354.

Oberg, A. L. (1997). “Matrix Suction in Silt and Sand Slopes: Significance and Practical Use in Stability Analysis.” Ph.D. Dissertation, Chalmers University of Technology, Goteborg, Sweden.

Park J.H. (2005). “Performance and Check-out Verification Testing of a New True Triaxial apparatus Using Partially Saturated Silty Sand,” M.Sc. thesis, University of Texas at Arlington, Arlington, TX.

Pyo, S.C. (2006). “General Response of Partially Saturated Silty Sand under Drained and Undrained True Triaxial Testing,” M.Sc. thesis, University of Texas at Arlington, Arlington, TX.

Reddy, K.R., Saxena, S.K., and Budiman, J. (1992). "Development of a True Triaxial Testing Apparatus," Geotechnical Testing Journal, GTJODJ, 15(2), 89-105.

Richards, B. G. (1966). “The Significance of Moisture Flow and Equilibrium in Unsaturated Soils in Relation to the Design of Engineering Structures Built on Shallow

Foundations in Australia," Proc., Symp. on Permeability and Capillary, Amer. Soc. Testing Materials, Atlantic City, NJ.

Richards, B.G. (1974). "Behavior of unsaturated soil, in soil mechanics—new horizons," I.K. Lee ed. New York: American Elsevier, 112-157.

Robinson, R.A. and Stoke, R.H. (1968). "Electrolyte solutions," 2nd ed. Butterworths London, United Kingdom.

Sivakumar, V., (1993). "A Critical State Framework for Unsaturated Soils," PhD dissertation, University of Sheffield, England, 236 pp.

Skempton, A. W. (1961). "Effective Stress in Soils, Concrete and Rocks," Proc., Conf. on Pore Pressure, London: Butterworths, UK, 4-16.

Soilmoisture Equipment Corporation (SEC) 2003, "Commercial Publications," SEC, Santa Barbara, CA.

Sture, S., & Desai, C. S. (1979). "Fluid Cushion Truly Triaxial or Multiaxial Testing Device," Geotechnical Testing Journal, 2(1), 20-33.

Sture, S. (1979). "Development of Multiaxial Cubical Test Device with Pore Water Pressure Monitoring Facilities," Report No. VPI-E-79.18, Department of Civil Engineering, Virginia Polytechnic Institute and State University, Blacksburg, VA.

Terzaghi, K. (1936). "The Shear Resistance of Saturated Soils," Proc., 1st Int. Conf. Soil Mech. and Found. Engrg., Harvard University, Cambridge, MA,Vol. 1, 54-56.

Terzaghi, K. (1936). "The Shearing Resistance of Saturated Soils and the Angle between the Planes of Shear," Proceedings 1st International Conference on Soil Mechanics and Foundation Engineering, 1, 54-56.

Toll, D. G. (1990). “A Framework for Unsaturated Soil Behavior,” Geotechnique, 40(1), 31-44.

Vaunat, J., Cante, J.C., Ledesma, A., Gens, A., (2000). “A stress point algorithm for an elastoplastic model in unsaturated soils,” International Journal of Plasticity 16 (2), 121–141.

Wan, A.W. L., Gray, M.M., and Graham, J. (1995). “On the relations of suction, moisture content, and soil structure in compacted clays,” Proc of 1st. Int. Conf. on Unsaturated soils, Paris, (1995), 215-222, eds. E.E.Alonso and P.Delage, publ. Balkema, Rotterdam.

Weast, R.C., Astle, M.J., and Beyer, W.H., (1981). “CRC Handbook of Chemistry and Physics,” 65th ed., Boca Raton, FL.

Wheeler, S.J., Sivakumar, V., (1995). “An elasto-plastic critical state framework for unsaturated soils,” Geotechnique 45 (1), 35–53.

Yamada, Y., & Ishihara, K. (1982). “Yielding of Loose Sand in Three-Dimensional Stress Conditions,” Japanese Society of Soil Mechanics and Foundation Engineering, 22 (3), 16-31.

Young, T. (1805). “Philosophical Transactions of the Royal Society”, 95, 65.

BIOGRAPHICAL INFORMATION

Arthit Laikram was born on October 2, 1978, at the City of Bangkok, Thailand. He received his bachelor's degree in Civil Engineering from King Mongkut's University of Technology, Thonburi, Thailand, in October 2000. During his undergraduate school years, he had the opportunity to be trained as a civil engineer at the Bangna-Bangpakong Expressway project in Thailand for 3 months. After graduation with B.S. degree, he decided to pursue graduate studies majoring in geotechnical engineering at The University of Texas at Arlington in 2002. During his graduate studies, he had the opportunity to work as a graduate research and teaching assistant under supervision of Dr. Laureano R. Hoyos in the area of soil improvement. He received his Master of Science degree in Civil Engineering from The University of Texas at Arlington in December 2003. In 2004, he decided to continue his graduate education into the PhD program at the University of Texas at Arlington also under direct supervision of Dr. Laureano R. Hoyos in the area of unsaturated soil mechanics. His doctoral research work and dissertation were sponsored by the US National Science Foundation under grant No. 0216545. He received his Doctor of Philosophy degree in Civil Engineering from The University of Texas at Arlington in December 2007.